A consistent coupled-channels description of Feshbach resonances through two- three- and many-body systems

Braun, Denise J.M.

Award date:
2018

A consistent coupled-channels description of Feshbach resonances through two- three- and many-body systems

D.J.M. Braun

August 2018

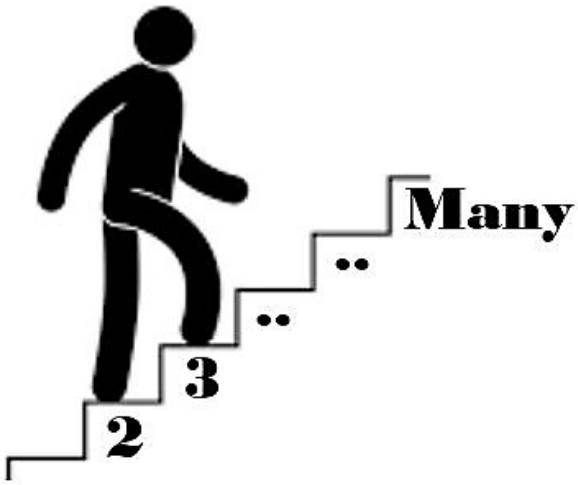

Master thesis

Supervisors:
dr.ir.S.J.J.M.F. Kokkelmans
P.M.A. Mestrom , MSc.
S.Musolino , MSc.

Department of Applied Physics
Coherence and Quantum Technology

Eindhoven University of Technology

Abstract

The achievement of the formation of a Bose-Einstein condensate in an ultra cold, dilute gas, in the year 1995 [1] has sparked the interest in research into systems in which atomic interactions take the central stage. As Bose-Einstein condensates exist at ultra low temperatures, the quantum nature of the matter becomes apparent and it has even been shown that the wave like characteristics of atoms can be observed from the interference pattern between two Bose-Einstein condensates [2]. This apparentness of the quantum nature of the condensate, and the possibility to form a superfluidic state in Bose-Einstein condensate gives some indication of the interest of the analysis of these condensates [3].

In this thesis, we study the dynamical evolution of a Bose-Einstein condensate and we investigate the effect of the resonance width on the observed evolution of the condensate. However, before moving on to the analysis of a many-body system, two-body and three-body systems are investigated. By analysing the underlying two-body physics, it is possible to extract a value for the momentum-space cut-off of the potential such that elaborate full-coupled channels results for the dimer energy can be reproduced. In doing so, it is possible to use physically realistic input data for the many-body simulations. Furthermore, by studying the three-body interactions, the effect of the resonance width on Efimov trimers can be investigated. We find a similar dependency of the three-body parameter as presented in the work of D.S. Petrov and R. Sanjukta [4, 5]. This indicates the capability of the model to accurately describe both broad- and narrow Feshbach resonances. Furthermore, the many-body analysis could be extended in further research to include three-body correlations. This would make it possible to study the effect of the presence of a background gas on the observed Efimov trimers.

After analysing the underlying two-body physics and eveluating a three-body system, the many-body system is investigated. This many-body system is used in order to study the dynamical evolution of the Bose-Einstein condensate. Simulations reveal the quantum depletion of the condensate and the dynamical evolution of the embedded dimer energy towards more deeply bound states for an increased simulation time of the Bose-Einstein condensate. This has been observed in other research [6] and is a result of the Bose enhancement of the interaction between excited state atoms which are expelled from the condensate. The usage of a coupled-channels model makes it possible to include the formation of a molecular condensate in the analysis. The simulations of the many-body system reveal that a decrease in the resonance width results in an increase in the population of this molecular condensate. This is in accordance with the increased importance of the molecular bound state, which lives in the closed channel subspace, for increasingly narrow resonances [7]. As the molecular condensate population fraction increases for a decrease in the resonance width, the excited state population that is obtained from the depletion of the Bose-Einstein condensate is decreased. This results in a decrease of the Bose enhancement of the excited atom interactions and therefore a decrease in the amount with which the embedded dimer is pushed towards more deeply bound energies as a function of the simulation time. The dependency of the dimer energy on the resonance width indicates the importance of the usage of a coupled-channels model in the description of many-body systems which involve narrow Feshbach resonances.

The model as presented in this thesis effectively presents a first step in the development of a coupled-channels model that can be used in many-body simulations in order to study both broad *and* narrow Feshbach resonances.

Contents

Chapter 1

Introduction

Whereas first theorized in the year 1925 [8], the experimental formation of a Bose-Einstein condensate was only realized in 1995 [1]. Since then, it has become a *cool* topic, due to its relation to the remarkable phenomenon of superfluidity [3, 9]. However, on a more fundamental level, the Bose-Einstein condensate, which is more commonly referred to as the *fifth state of matter* [10], also sparks the possibility of interesting physics, due to the apparentness of the quantum effects at ultra-low temperatures. Suggestions to harness this macroscopic quantum state as robust qubits highlight the importance of the analysis of this novel state of matter [11, 12, 13].

In this report, the dynamical evolution of a Bose-Einstein condensate will be studied. Furthermore, the effect of the resonance width on the evolution of the condensate will be analysed. However, before jumping to the analysis of such a condensate, which consist of many particles, the underlying two-and three-body physics which govern the interactions between identical bosons will be studied. This effectively provides a bottom-up approach which makes it possible to obtain a more detailed understanding of the few-body interactions which take place in many-body systems [14, 15], such as Bose-Einstein condensates.

Motivated by their experimental tunability [16], the two-and three-body interactions that will be analysed in this report are in the form of coupled-channels interactions. These type of interactions can result in tunable *Feshbach resonances*. Once such a resonance occurs, the scattering length of the two-particle interaction diverges and two-body scattering cross section becomes much larger than the potential interaction range. This regime, which is known as the *unitary regime* [17] will be thoroughly analysed in this report. Especially on the three-body interaction level interesting physics occur in this regime, as universal *Efimov* trimers pop-up in this limit [18, 19]. By studying the interesting physics of these coupled-channels systems on the two-and three-body level, a foundation to understand many-particle system dynamics can be formed.

As an example of the usefulness of following this bottom-up approach, the investigation of two-body interactions makes it possible to quantify a potential interaction range which properly matches more evolved theoretical studies [20]. This interaction range can be implemented in the many-body analysis, effectively getting rid of the usual application of contact-interactions in many-body physics and getting one step closer to modelling more physically realistic potential interactions. Furthermore, the analysis of two-body interactions before analysing many-body interactions makes it possible to explicitly pin-point the effects of a background gas on two-particle interactions. Therefore, the effect of moving from a vacuum system to an embedded system can be understood in more detail [21].

Apart from focussing on extracting a suitable range to properly represent evolved theoretical models, the two-and three-body analysis which will be carried out in this report will also focus on the effect of the *resonance width* of the interactions. As previously investigated, it turns out that *broad* Feshbach resonances don't require the more elaborate and complex usage of a coupled-channels system [22, 23], whereas *narrow* resonances are expected to require a coupled- channels approach [4, 7].

The effect of the resonance width will be thoroughly analysed, not only on the two- and three-body level, but also on the many-body level. The goal of this analysis is to quantify the importance of the usage of a coupled-channels system approach to represent narrow Feshbach resonances as compared to previously studied, less complex, single channel models. Whereas these single channel approaches have proven useful in the analysis of atomic species which have a *broad* resonance character, such as Rubidium-85 [22], the application of a coupled-channels model to study many-particle interactions in gases which have a narrow resonances, such as some resonances in Sodium-23 [16], is expected to be crucial in the possibility to derive a proper description of the many-particle system.

Using the more elaborate coupled-channels system, the analysis as presented in this report will hopefully bring us one step closer in the accurate modelling of the dynamics of a Bose-Einstein condensate. However, in order to get one step closer to a more realistic description of the dynamics in a Bose Einstein condensate, the picture on the cover reveals that many steps on the stairs to a description of a many-body physics system have to be taken. Whereas the two-particle physics will be already actively implemented in the many-body equations which govern the Bose-Einstein condensate in this report, the three-body physics and, more interestingly, the Efimov effect which is observed in three-body physics still need to be implemented in the model. Therefore, whereas a beginning in climbing the stairs to a good many-body physics model has been completed, many steps still need to be taken. Using the stairs as an indication throughout the entire report, the pictogram will be added at the beginning of each chapter in order to clarify how many particles are being investigated. However, before moving on to these chapters, some concepts which have been introduced in this section, such as Feshbach resonances and the Efimov effect, will be discussed in more detail.

1.1 Feshbach resonances

As outlined in the previous section, this thesis will use a coupled-channels system in order to study two- three- and many-particle systems. The advantage of using such a coupled-channels approach over having a single channel model resides in the fact that the coupled-channels resonances, better known as a Feshbach resonances, are magnetically tunable [15]. Therefore, contrary to their single channel counterparts, being potential resonances, they offer an experimental tunability of the interaction through the application of an external magnetic field. This magnetic tunability is a result of the existence of multiple different coupled spin configurations of two interacting particles[1]. The resulting channels correspond to different hyperfine configurations with distinctive magnetic momenta. Due to this difference in the magnetic momenta of the two interaction channels, it is possible to alter the relative asymptotic energy difference between the channels through the application of an external magnetic field. Through the tuning of this magnetic field, it is possible to obtain a resonant interaction between the scattering particles for which, as briefly mentioned in the previous section, the scattering length will diverge. In order to clarify the structure of the coupled-channels which support the formation of a magnetic tunable Feshbach resonance, a schematic representation of the system is provided in figure 1.1.

[1] In fact, more than two interaction potentials exist [16]. However, if the asymptotic energy thresholds are sufficiently far removed from the entrance energy, these channels can be neglected as a first approximation. MSc. Secker is currently analysing the effect of incorporation of additional interaction channels into the model.

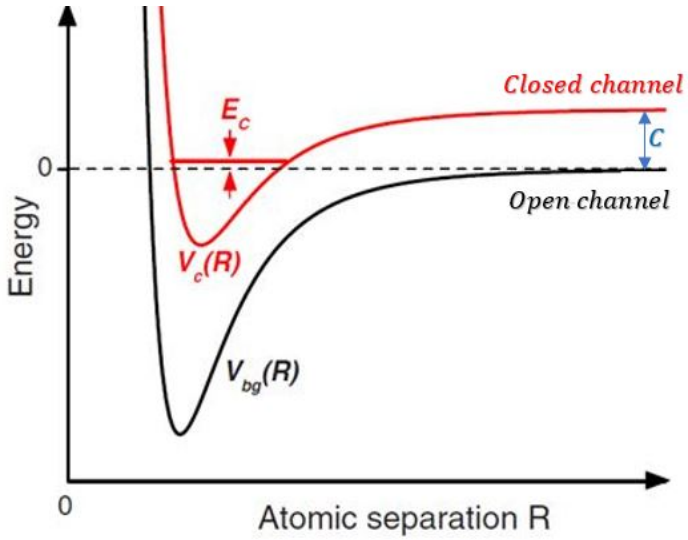

Figure 1.1: Schematic representation of a coupled-channels system

As can be seen upon inspection of figure 1.1 two different potential interaction channels exist which have different asymptotic energy levels. For the channel represented by the black line, the asymptotic energy level, which is set to a value of zero, is lower than- or equal to the entrance energy of the scattered particle[2]. Therefore, the particle can both enter and exit in this potential channel [24]. As a result of this property, this channel is more commonly referred to as an *open channel*. The second channel on the other hand, which is represented by the red line, has an asymptotic energy level which surpasses the entrance energy. Therefore, the particle can interact in this channel for distances smaller than a range R[3], but cannot exit in this channel [25]. As a result of this property, this second channel is more commonly referred to as a *closed channel*.

Throughout this report, it will be assumed that a single bound state with energy E_c[4] exists in the closed channel subspace and no bound states exist in the open channel subspace [24, 26] [5]. By changing the asymptotic energy difference between the two channels, which is indicated by the symbol C in figure 1.1, it is possible to create a Feshbach resonance. Such a resonance occurs once the entrance energy equals the bound state energy E_c [15, 24]. Having already disclosed that a Feshbach resonance can be controlled through the application of an external magnetic field, the following subsection will focus on the effect of the magnetic field in more detail.

1.1.1 Details of magnetic tunability

Despite the fact that the addition of a second potential interaction channel to the two particle scattering process might seem to complicate the scattering analysis, the effect of the second channel on the scattering length as controlled by an external magnetic field is rather mathematically

[2]In section 2.2 it will be proven that the scattering of two particles can be modelled by the scattering of a single reduced mass particle of a two-particle interaction potential

[3]The value of this range will be discussed in more detail in section 3.1.

[4]This energy E_c is measured with respect to the open channel asymptote

[5]It is possible to include the presence of a bound state in the open channel. The effect of having this additional bound state will be discussed in chapter 5

straightforward as presented by the following equation [25]

$$a_s = a_{bg}\left(1 - \frac{\delta\mu\Delta B}{B - B_0}\right). \tag{1.1}$$

In the previous equation, the symbol a_{bg} has been introduced. This symbol represents the obtained scattering length as a result of the scattering interaction with the open channel without the influence of the closed channel. This scattering length is referred to as the *background* scattering length and the open channel can analogously also be referred to as the *background channel*. The symbol a_s on the left hand side of the equation represents the total scattering length of the interaction. It includes both background channel effects and effects as a result of the coupling of the open channel to the closed channel. In order to clarify the structure of equation 1.1, the following figure can be used:

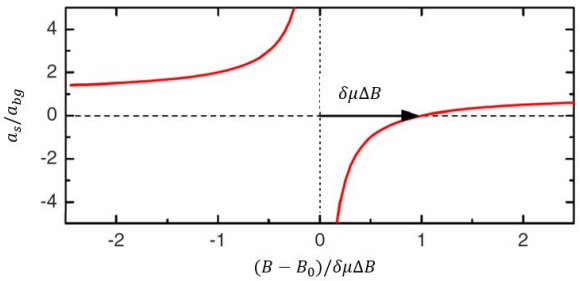

Figure 1.2: The scattering length a_s as a function of the magnetic field B. The figure is adapted from reference [16].

Through the analysis of figure 1.2, the meaning of the factors B_0 and $\delta\mu\Delta B$ become more insightful. First of all, B_0 represents the location of the resonance, which is fixed for different atomic species [27, 16]. As can be seen upon inspection of both equation 1.1 and the previous figure, once the magnetic field B equals the value of B_0, a resonance occurs and the scattering length diverges. Furthermore, the figure indicates that the width of this resonance is governed by the factor $\delta\mu\Delta B$. The factor $\delta\mu$ represents the differential magnetic moment between the two interaction channels of the investigated atomic species [16], whereas the factor ΔB represents the width of the resonance. Similarly to the factor B_0, the width of the resonance ΔB is a constant for different atomic species[6] [27, 16]. The value of this constant depends on the interaction strength between the open and the closed channel [24]. As will be discussed in chapter 6, narrow resonances correspond to weakly coupled-channels whereas broad resonances correspond to strongly coupled-channels. Repeating what has been previously stated in the beginning of this introduction, the more precise effect of the width of the resonance on the physics of the interactions between particles will be analysed in detail in this report, on both a few-particle and a many-particle level. The goal of this analysis is to establish the importance of the coupled-channels treatment of the interactions in order to properly describe systems with narrow Feshbach resonances.

1.2 The modelled potential

As mentioned at the beginning of the introduction, one of the advantages of applying a bottom up approach to the treatment of scattering interactions resides in the possibility to implement few-body physics quantities on a many-body level, such as the range of the potential interaction. In order to implement a range into the analysis, whilst keeping the complexity of the model at a minimum, the modelled potential is a *separable* potential [28]. A potential showing this characteristic is the delta

[6] A single atomic species can have multiple resonances, and therefore multiple, fixed, values for the resonance width ΔB and the resonant field strength B_0.

function potential. Whereas other potentials such as the van der Waals potential might be more physically realistic in the representation of atomic interactions, a trade-off has been made in order to keep the complexity of the modelled potential, which will be applied in the many-body analysis, at a minimum. However, in order to be able to incorporate a finite range to the modelled potential, the potential is assigned a finite cut-off in momentum space. Effectively this means that, after using the separable form of the delta function potential, the model is altered to have a finite range. In doing so, the simplicity of the incorporation of the model is used whereas the introduction of a finite range offers the possibility to match the modelled potential with more evolved theoretical models of a full-coupled channels system [20]. The calibration of the finite range using the data of more evolved models makes it possible to investigate interactions between particles with realistic input parameters.

Furthermore, the interactions which will be analysed in this thesis only correspond to s-wave interactions. Whereas the non-zero angular momentum components vanish for the delta function potential [14], this is generally not the case. At ultra low temperatures, the s-wave interaction is dominant over the other contributions [17], but more elaborate studies such as presented in reference [14] show that the higher order terms cannot be neglected in general. This once more shows that the model which is used in this thesis could be extended to more elaborate forms and should merely be regarded as a model with reduced complexity in order to simplify its implementation in many-body systems.

1.3 The Efimov effect

Using the coupled-channels approach as outlined in section 1.1 and implementing the modelled potential as described in section 1.2, it is possible to describe two body interactions. Next, upon adding a third particle to the system, interesting universal physics occurs. As theoretically predicted by Vitaly Efimov in the early 70's [18] and experimentally observed at the University of Innsbruck in 2006 [23] [7], it is possible to form an infinite number of three-body bound states even in a regime of scattering lengths ($a < 0$) where the formation of two-body bound states is not possible. This regime is more commonly referred to as the *Borromean ring* region [4], as schematically represented by figure 1.3.

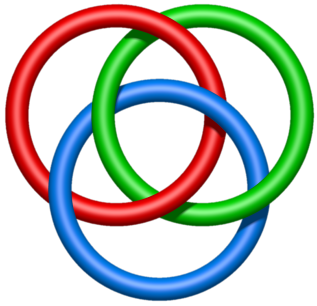

Figure 1.3: A schematic representation of Borromean rings. The figure is adapted from reference [30].

As indicated in figure 1.3, the three rings can be bound together, but break apart as soon as a single ring is removed. This perfect analogy between the rings and the three-body bound states, which are

[7] Experimental observations of this effect amount to recording peaks in the three-body recombination rate for negative scattering lengths where Efimov trimers emerge from the scattering continuum and observing dips in the three-body recombination rate for positive scattering lengths for which the Efimov trimers disappear into the particle scattering continuum [27]. More details of these experimental observations can be found in reference [29].

referred to as *Efimov trimers*, indicates the striking character of the trimer states. Adding to the striking character of this effect is the universal scaling that exists between the subsequent three-body bound states [18, 4]. Effectively, this implies that the entire Efimov spectrum of three-body bound states can be fixed upon knowing the value of a single parameter. The parameter which is used to fix the spectrum is more commonly referred to as the *three body parameter* [31]. In order to understand the meaning of this parameter and the observed universal scaling laws in more detail, the figure as presented below can be investigated.

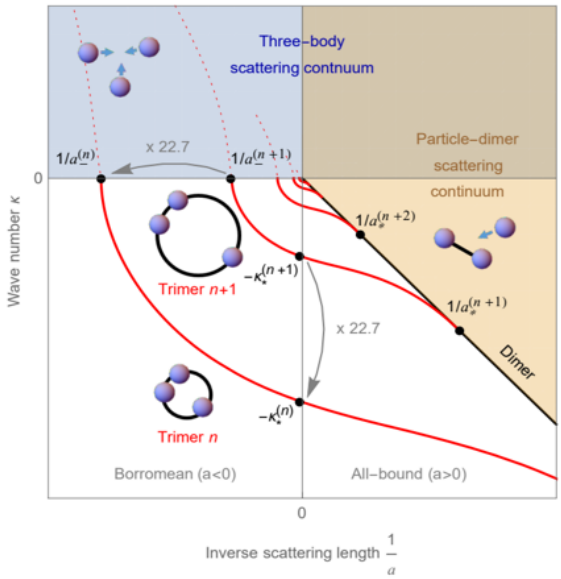

Figure 1.4: Schematic representation of an Efimov spectrum. In this figure, the wave number κ is plotted as a function of the inverse scattering length $1/a_s$. The blue shaded region represents the three-body scattering continuum, whereas the orange region represents the particle-dimer scattering continuum. This orange region is bounded by a black line which represents the two-body dimer energy. Red lines are used in order to indicate the consecutive Efimov trimers. The presented spectrum is valid for particles with equal mass m in the zero-range theory. The figure is adapted from reference [4].

Figure 1.4 presents an energy spectrum of a three-body system in zero-range theory [8]. As indicated in the figure, the Efimov trimers accumulate at $1/a \to 0$. This regime, where the scattering length diverges and the underlying two-body interactions become resonant, is known as the *unitary* regime [4]. In this regime, the value of the scattering length $|a|$ is much larger than the typical two-body interaction range r_0. As a result of this inequality, the short range details of the modelled potential do not alter the Efimov spectrum [23], indicating that Efimov spectra can be obtained regardless of the short range details of the potential. It is this *unitary* regime in which the many-body interactions in this report will be investigated. However, it is important to include the side-note that the lowest lying Efimov trimers can be affected by the short range details of the interaction, as these trimers exist at smaller values of the scattering length [15, 14]. The effect of incorporating a range in the Efimov spectrum will be discussed in more detail in the next subsection.

Coming back to the topic of universal scaling in the Efimov spectrum, several points can be extracted from figure 1.4 in order to show this universal character. First of all, the universality of the spectrum is observed in the scaling of the trimer binding energies $E^*_{3b,n}$ at unitarity. The subsequent

[8] This will be discussed in more detail in subsection 1.3.1.

trimer energies can be related to each other through the following expression:

$$E^*_{3b,n+1} = e^{-2\pi/s_0} E^*_{3b,n}. \tag{1.2}$$

The parameter s_0 which has been introduced in the previous equation equals a value of $s_0 = 1.00624$ for identical bosons [32]. In figure 1.4, the wave number κ has been plotted on the y-axis instead of the energy E. However, these two parameters are related as follows:

$$\kappa = \text{sign}(E)\sqrt{\frac{m|E|}{\hbar^2}}. \tag{1.3}$$

Using the previous relation in combination with equation 1.2, the values of the wave numbers κ^* at unitarity of the subsequent Efimov trimers are related by the following universal scaling law:

$$\kappa^*_{n+1} = e^{-\pi/s_0}\kappa^*_n \approx \kappa^*_n/22.7. \tag{1.4}$$

The same scaling law can be found upon inspection of the values of the subsequent scattering lengths a_+ where the Efimov trimers hit the particle-dimer scattering continuum. This particle-dimer scattering continuum is bounded by a black line in figure 1.4 which represents the dimer binding energy. For large value of the scattering length a, this dimer energy can be approximated by [16]

$$E_{2b} = \frac{-\hbar^2}{ma^2}. \tag{1.5}$$

where m represents the mass of each boson. The previous expression is exact for zero-range potentials and, more generally, correctly describes the dimer binding energy for potentials in a regime where the scattering length a is much larger than the range of the potential r_0, meaning that $|a| >> r_0$. The derivation of this expression is presented in appendix F. The exact relation between the dimer energy and the scattering length for the two-body interactions modelled in this thesis will be discussed in more detail in chapter 6.

Apart from the universality observed in the scattering length a_+ for which consecutive Efimiov trimers hit the particle-dimer scattering continuum and the universal scaling law observed for the wave numbers κ^* at unitarity for consecutive Efimov trimers, it is possible to distinguish even more universal scaling laws. As indicated in figure 1.4, the same scaling law as presented in equation 1.4 can be used in order to describe the relation amongst the values of the scattering length a_- for which subsequent Efimov trimers merge with the three-body scattering continuum.

Taking the universality of the spectrum even one step further, it can additionally be proven that universal relations also exist between the parameters κ^*, a_* and a_- [32, 33]. These relations are presented below:

$$a_{*,n}\kappa^*_n = 0.0707645, \tag{1.6}$$

$$a_{-,n}\kappa^*_n = -1.50763. \tag{1.7}$$

The rich collection of universal scaling laws that exists for Efimov trimers will be used in order to verify the occurrence of universal scaling behaviour for the modelled potential as presented in section 1.2. The usage of a coupled-channels approach as outlined in section 1.1 is advantageous in this analysis, as it offers the possibility to alter the scattering length and even to create a Feshbach resonance through the variation of an externally applied magnetic field.

1.3.1 The three-body parameter

As mentioned in the previous section, the occurrence of universal scaling in the Efimov spectrum offers the possibility to fix the whole spectrum through the calculation of a single point. Whereas the choice of this point, known as the three-body parameter, is not unique, throughout this thesis, the point which will be used is the characterized by the parameter a_-^0, which represents the scattering length for which the lowest lying Efimov trimer hits the three-body scattering continuum. Apart from using this point in order to fix the Efimov spectrum, this three-body parameter will furthermore be used in order to inspect the effect of the resonance width on the three-body spectrum. As explained in section 1.2, the modelled potential has a finite cut-off in momentum space. This means that the interaction between particles is not zero-range. Due to the presence of this finite range, the lowest lying Efimov states can be affected [15, 14]. However, upon increasing the scattering length and propagating towards less deeply bound Efimov trimers, the universal character which was observed for zero range potentials as indicated of 1.4 is recovered, as the inequality $|a| >> r_0$ once more prevails. Whereas the inclusion of a finite range to the potential might affect the universal scaling for deeper lying bound states, it does have an important advantage over not including a range, as it fixes the Efimov spectrum from below [14, 31]. This means that there is a clear deepest lying Efimov trimer below which no other trimers can be formed. If such a range would not be implemented, it would not be possible to fix the spectrum from below. This highlights the importance of including a finite range in the inspection of the Efimov spectrum.

Using the modelled potential with the momentum-space cut-off, the three-body parameter a_-^0 is investigated for both broad- and narrow resonances. Whereas it was first expected that the three-body parameter would be the only parameter in the Efimov spectrum to be influenced by non-universal physics [18, 32], it has been recently observed that there seems to exist a strong correlation between the three-body parameter and the atomic interaction range [4, 34]. Using the van der Waals length l_{vdw} in order to quantify the interaction range, the following relation between the three-body parameter a_- and the van der Waals length has been observed:

$$a_- = -(8.9 \pm 1.8) l_{vdw}, \tag{1.8}$$

$$\text{with} \quad l_{vdw} = \frac{1}{2}\left(2\mu C_6/\hbar^2\right)^{1/4}. \tag{1.9}$$

The factor μ which has been introduced in the previous equation represents the reduced mass of two neutral atoms and the factor C_6 represents the van der Waals coefficient. As indicated in figure 1.5 the existence of the relation as presented in equation 1.8 has been experimentally verified for various atomic species.

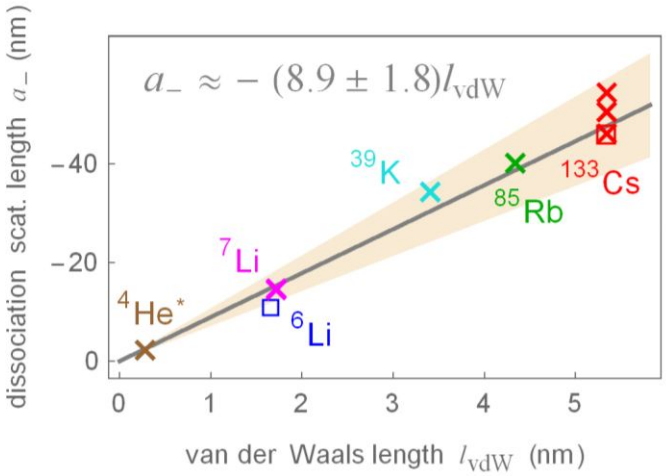

Figure 1.5: Relation between the three-body parameter a_- as a function of the van der Waals length l_{vdw} as experimentally observed for various atomic species. Crosses indicated results for the ground state three-body parameter a_-^0 and squares indicate results for the parameter a_-^1 which indicate the point where the first excited state Efimov trimer emerges from the three-body scattering continuum. This figure has been adapted from reference [4].

More detailed studies, in which thermal corrections have been incorporated, indicate that within an error of 20%, the three-body parameter is universally determined by the van der Waals length, with $a_- \approx -9 l_{vdw}$ [4]. The explanation of this universal behaviour is the topic of recent theoretical studies and it is suggested that it is caused by the sharp drop in the two-body interaction potential at a distance in the order of the van der Waals radius[9]. This drop results in an effective barrier in the three-body potential at distances in the order of the van der Waals radius R_{vdw} **??**. This barrier prevents the three particles from approaching each other sufficiently close in order to reveal non universal features of short range interactions [7]. As non universal features are suppressed, the three-body parameter shows universal behaviour.

However, the observation of this universal behaviour is limited to broad resonances. As broad resonances correspond to resonances where the interaction strength between the closed channel and the open channel is large, the bound state can be effectively described to *live* in the open channel subspace and the two-channel system is said to be dominated by the open channel. Effectively, this amounts to the possibility to reduce the coupled-channels system to a single channel systems. As the calculations carried out to obtain the universal behaviour of the three-body parameters rely on the usage of this single channel approach, the results cannot be extended to narrow Feshbach resonances. Contrary to broad resonances, narrow Feshbach resonances are dominated by the closed channel. Theoretical observations indicate that these resonances are influenced by an additional length scale, being the resonance strength parameter R^* [5, 7]. This parameter is inversely related to the resonance width ΔB. Therefore, upon reducing the resonance width ΔB, the resonance strength parameter R^* increases in value. Due to the dependency of the three body parameter on this additional length scale, experimental observations of the three-body parameters start to deviate from the theoretically expected behaviour. This discrepancy between theory and experiment is indicated in figure 1.6.

[9]The vdWaals radius is used instead of the vdWaals length l_{vdw} in other literature references [16], but is equivalent to the definition as presented in equation 1.9.

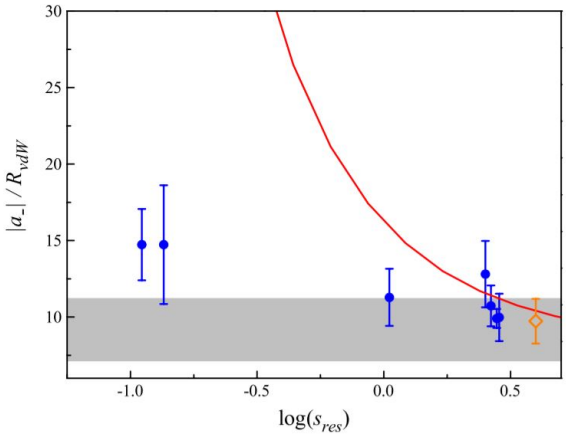

Figure 1.6: Figure indicating the three body parameter a_- rescaled with the van der Waals radius R_{vdw} as a function of the logarithm of s_{res}, with $s_{res} = 0.956 R_{vdw}/R^*$. Blue circles indicate the experimentally obtained results from reference [7], whereas open diamond corresponds to predictions for $s_{res} >> 1$ [31] and the red line corresponds to predictions for generic s_{res} [35]. The gray region indicates the scatter in in experimental data for $|a_-|/R_{vdw}$ as measured in other atomic species. This figure has been adapted from reference [7].

The previous figure indicates the discrepancy between theoretical expectations and experimental observations and therefore highlights the interest to use a coupled-channels approach to study narrow Feshbach resonances. The analysis of the effect of the variation of resonance strength parameter R^* on the observed three-body parameter will be presented in chapter 9.

1.4 Bose-Einstein condensation

As mentioned at the beginning of the introduction, the dynamical evolution of a Bose-Einstein condensate will be investigated in the many-body part of this thesis. These condensates form at ultra low temperatures[10]. In order to achieve this low temperature regime, sub-Doppler -cooling and evaporative-cooling techniques have to be applied [36, 37]. In order to avoid the formation of solids during the cooling process, the gaseous condensates are dilute systems [38]. This means that the interparticle separation is much larger than the scattering length a_s, resulting in the following condition for the formation a Bose-Einstein condensate [39]:

$$n^{1/3}|a_s| << 1. \tag{1.10}$$

The parameter n which has been introduced in the previous equation indicates the particle density. Assuming the previous condition is abided by, the temperature of the gas can be lowered to a point where the *critical* temperature T_c is reached. This critical temperature signifies the point where the chemical potential of the system becomes equal to a value of zero [40]. Once the temperature is decreased even further, the particles have to drop out of the thermal distribution in order to avoid obtaining a non-physical positive chemical potential for a Bose gas [41]. The particles dropping out of the thermal distribution accumulate in the ground state of the system. The macroscopic occupation of this ground state is what is known as a Bose-Einstein condensate. An analysis of the Bose-Einstein distribution for a zero value of the chemical potential reveals that the critical temperature T_c for which this formation of a Bose-Einstein condensate is initiated can be calcualted

[10]The critical temperature for the formation of a Bose-Einstein condensate can be calculated from equation 1.11.

as follows [40]:

$$T_c = \frac{3.31}{g^{2/3}} \frac{\hbar^2}{m k_b} \left(\frac{N}{V} \right)^{2/3}. \tag{1.11}$$

The previous equation indicates the dependency of the critical formation on the particle density (N/V), the particle mass m and the degeneracy of each single-particle momentum state g. The interesting quantum effects that occur in a Bose-Einstein can be understood upon inspecting the thermal de Broglie wave length as presented below [41]:

$$\lambda_{TH} = \frac{h}{\sqrt{2\pi m k_b T}}. \tag{1.12}$$

As indicated in the previous equation, a decrease in the temperature results in an increase in the de Broglie wavelength. This means that the wave-like character of the atoms become more apparent once low temperatures are reached. This is schematically represented in the figure 1.7.

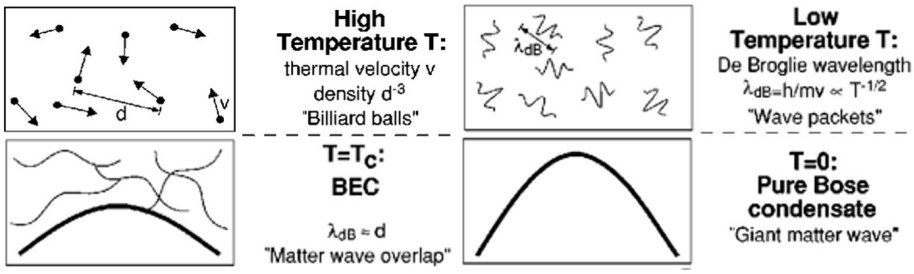

Figure 1.7: Schematic representation of the de Broglie wave length as a function of the temperature. The picutre is adapted from reference [42].

As indicated in figure 1.7, Bose-Einstein condensates behave as giant matter waves. This wave-like behaviour has been experimentally observed in interference experiments between condensates [2]. This explains the statement made at the beginning of the introduction, being that Bose-Einstein condensates clearly exhibit quantum effects. It is also the formation of a giant matter wave which facilitates the existence of superfluity in an interacting Bose-Einstein condensate [3].

1.4.1 Coupled-channels analysis of a Bose-Einstein condensate

Now that the physical foundation of Bose-Einstein condensates has been discussed in some more detail, it is possible to combine the idea of having a coupled channel system with the idea of having a Bose-Einstein condensate. Effectively, the presence of a closed channel potential as presented in section 1.1 could facilitate the coupling of an atomic Bose-Einstein condensate to a bound state living in the closed channel subspace. This bound state could support the existence of a condensed molecule which could be formed by two condensate atoms or, alternatively, could break apart to create two condensate atoms.

As previously mentioned at the beginning of the introduction, the goal is to inspect the dynamical evolution of a Bose-Einstein condensate. Whereas it is important to start with a system in the weakly interacting regime as specified by equation 1.10 in order to form the Bose-Einstein condensate, it is possible to move to a strongly interacting regime once the Bose-Einstein condition has been formed [6]. Experimentally, this can be achieved by changing the strength of the externally applied magnetic field, such that a Feshbach resonance as described in section 1.1 occurs. Once the system is at resonance, the scattering length diverges and the system exists in the *unitary* regime as previously introduced in section 1.3. By inspecting the many-particle system at unitarity, the

scattering length effectively drops out of the system as a length scale, as it diverges to infinity. The only natural length scale remaining in the system is the density of the particles n [43]. It has been observed that this causes the three-body losses that exist in the system to be limited [44]. This will be discussed in more detail in section 13.3. The decrease in the loss rate effectively means that the inspection of the Bose gas at unitarity offers the possibility to study a strongly-interacting system whilst keeping the three-body losses to a minimum.

Due to the strong interactions which occur in the unitary regime, atoms can be excited from the Bose-Einstein condensate [21, 6]. These excited state atoms can collide with each other to redistribute their momenta or even drop back into the atomic condensate. Apart from this, the atoms can alternatively form a molecular bound state due to the presence of a bound state in the closed channel subspace. Of course, the opposite processes can also occur, meaning that the molecule can break apart into two condensate atoms or into two excited state atoms. Chapter 13 will focus on the analysis of the dynamical evolution of the population in the molecular condensate, the atomic condensate and the excited state atoms. In all of the presented many-body results, the system is set to start out with all population in the atomic Bose-Einstein condensate. By starting out in this situation, it is possible to clearly distinguish the processes which lead to the depletion of the condensate and to get an indication of the speed with which this depletion occurs.

Furthermore, the binding energy of the condensed molecular state will be investigated. This analysis will focus on the differences between the dimer energy as obtained in the two-body analysis and the dimer energy that is obtained in the many-body model. In making this comparison, it is possible to pin-point the effect of a background gas on the two-body interactions, meaning that pure many-body effects can be distinguished and analysed. As previously mentioned, we also wish to investigate the effect of the resonance width on the dynamics of the many-body system. In order to analyse this effect, the embedded dimer energy is calculated for various values of the resonance width. Particularly, the differences between broad- and narrow resonances will be investigated in order to quantify the importance of the usage of a coupled-channels approach instead of a less complicated single channels approach in the analysis of the many-body system.

1.5 Outline

In this thesis, the goal is to use a bottom up approach in order to analyse the dynamical evolution of a Bose-Einstein condensate. Furthermore, in carrying out this analysis, the effect of the resonance width $\delta\mu\Delta B$ will be investigated on both a few-body and a many-body level. Using this bottom up-approach as a guideline, the thesis has been divided into three parts.

The first part of this thesis will focus on two-body interactions. In **Chapter** 2, some basic two-body scattering theory will be reviewed. Concepts such as the scattering length and the transition matrix will be introduced. Furthermore, the Feshbach formalism will be discussed in detail such that the introduced concepts, such as the transition matrix, can be applied to analyse coupled-channels system. The analysis of the uncoupled-channels part of the transition matrix will be carried out in **Chapter** 3, before moving on to the more complicated analysis of the coupled-channels part of the transition matrix in **Chapter** 4. Using the expressions as derived in Chapters 3 and 4, **Chapter** 5 will focus on the analysis of the relations between the system parameters used to describe the modelled potential and the physical parameters as presented in section 2.7 in order to get a clear overview of the association between experimental observables and the parameters used to describe the modelled system. Using the derived relations between the system parameters and the experimentally observable parameters, the first

part of **Chapter** 6 will focus on the analysis of the dimer energy. Having obtained an expression for the dimer energy as a function of the scattering length, input data from more elaborate coupled-channels models [45] will be used in order to calibrate the momentum space cut-off Λ.

Having completed the analysis of two-particle systems, the second part of the thesis will focus on three-body systems. Similarly to the discussion of the two-particle system, the analysis of the three-particle system will commence with a Chapter that reviews basic three-particle scattering theory. This includes the revision of the Faddeev equation for three-body bound states [46], which effectively describes the combination of the underlying two-body interactions that collectively describe the dynamics of the three-particle system. Furthermore, it will be proven in this Chapter that the two-body transition matrix which has been derived in **Chapter** 4 can be used in the analysis of the three-particle system upon altering the value of the evaluation energy. Using this information, **Chapter** 8 will present an outline of the procedure which has been used in the numerical implementation of the analysis of the three-particle system. Following this description, the results which have been obtained through the application of the numerical model will be presented in **Chapter** 9. Amongst these results is an Efimov spectrum. This spectrum will be investigated in order to verify the occurrence of the universal scaling laws which have been introduced in section 1.3. Furthermore, results indicating the dependency of the three-body parameter $a_{-,0}$ on the resonance width will be presented and discussed and the correspondence of these results with the behaviour as described in subsection 1.3.1 will be analysed.

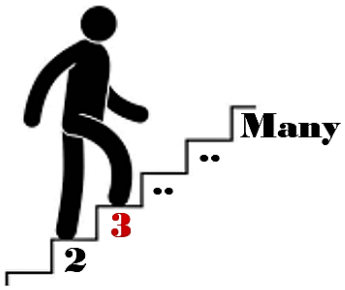

Having analysed the two- and three-body systems, the final part of this thesis will focus on the inspection of a many-body system. Once more, this analysis commences with a Chapter in the underlying physical properties of many-body are discussed. Amongst others, this Chapter will focus on the introduction of a many-body Hamiltonian which properly describes the many-body systems. Subsequently, this many-body Hamiltonian will be used in order to derive the equations of motion which describe the dynamical evolution of the many-body system which starts out as a pure Bose-Einstein condensate. In order to verify the correspondence between the derived many-body equations of motion and the open- and closed channel wave functions which have been derived in the first part of this thesis, **Chapter** 11 will inspect the vacuum limit of the many-body equations. In this limit, the background gas does not exist and the many-body equations should reduce to the previously derived expressions for a two-body system. After establishing the correspondence, **Chapter** 12 will continue with the theoretical analysis of the many-body equivalents of the transition matrix and the dimer energy. Using the derived expressions, **Chapter** 13 will present some results of many-body simulations. These results will be analysed in order to gain an insight into the dynamical evolution of a Bose-Einstein condensate at unitarity and to furthermore analyse the effect of the background gas on the dimer energy. Similarly to the three-particle system analysis, the resonance width will be altered in order to inspect the effect that this parameter has on the many-body system. More particularly, the change in the embedded dimer energy as a function of the resonance width will be inspected.

After having discussed two- three and many-body systems, a conclusion will be presented in **Chapter** 14 in which the most important findings will be summarized and suggestions for further research will be presented.

Part I

Two-body systems

Chapter 2

Two-body scattering theory

This chapter will review some general two-body scattering theory with the goal to understand the basic physics which forms the foundation of the two-body interaction analysis which will be presented in chapters 3 and 4. The theory which is discussed in this chapter is an adaptation of general textbook physics [47].

2.1 Quantum scattering

In quantum theory, a scattering process between two or more particles can be understood from the analysis of the form of a scattered wave function with respect to the form of an incoming wave function. How the incoming wave is altered to its scattered form is indicated in the following figure:

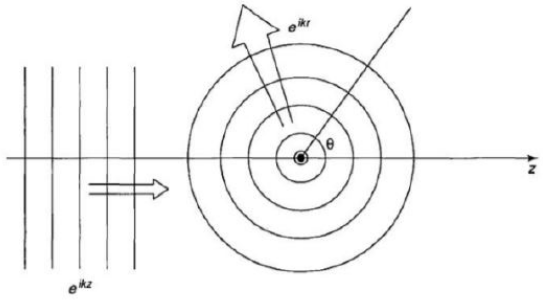

Figure 2.1: An incoming plane wave scattering of a potential. This figure is adapted from D.J. Griffiths [48].

As can be seen in figure 2.1, an incoming wave which is moving in the z-direction is scattered of a spherically symmetric potential[1]. Due to the interaction with the potential, the outgoing wave is no longer solely moving in the z-direction. Instead, the scattered part of the incoming wave[2] is propagating as a spherical wave. Of course, both the incoming and the outgoing wave need to obey the Schrödinger equation. Analysing the radial part of Schrödinger equation for the system as indicated in figure 2.1, whilst only considering s-wave scattering[3] and applying the

[1] As will be shown in section 2.2, the scattering between two particles can be modelled as the scattering of a single particle with an altered mass of a potential

[2] There is always a part of the incoming wave which is not scattered by the potential.

[3] As explained in the introduction, the zero momentum contribution to the overall scattering process is dominant for ultra cold systems

boundary condition that in the limit $r \to \pm\infty$ the wave function is not influenced by the scattering potential, it is possible to find the following general solutions for the incoming and the outgoing wave functions:

$$\psi_{in}(r) = A\sin(kr), \tag{2.1}$$
$$\psi_{out}(r) = A\sin(kr+\delta). \tag{2.2}$$

The previous two equations indicate that, upon applying the correct boundary conditions and using the radial Schrödinger equation, it can be deduced that the scattering between a particle and a potential or, analogously, the scattering between two particles, only induces a phase shift in the outgoing wave with respect to the incoming wave. This indicates the importance of finding the phase shift in a scattering process. How this phase shift is usually computed will be discussed in more detail in section 2.4. However, in order to be able to properly understand this computation procedure, another quantity, being the scattering operator, has to be introduced. This operator, which forms an important ingredient in quantum scattering theory, will be discussed in section 2.3. Furthermore, the implied analogy between the scattering of a single particle of a potential and the scattering of two particles will be discussed in the following section.

2.2 Two-body interactions in the relative momentum frame

In order to describe spinless two-particle interactions, for which the potential interaction is assumed to solely depend on the inter-particle separation distance, the following form of the two-body Hamiltonian can be used:

$$H = \frac{p_1^2}{2m_1} + \frac{p_2^2}{2m_2} + V(|\mathbf{r}_1 - \mathbf{r}_2|). \tag{2.3}$$

The sub-indices 1 and 2 which have been introduced in the previous equation refer to the two different particles which are interacting. As the interaction potential only depends on the relative distance between the particles, and the kinetic energy operators exist in two different single particle subspaces, it is possible to move to a center-of-mass frame through the application of the following set of center-of-mass frame coordinates:

$$\mathbf{R} = \frac{m_1\mathbf{r}_1 + m_2\mathbf{r}_2}{m_1+m_2}, \tag{2.4}$$
$$\mathbf{r} = \mathbf{r}_1 - \mathbf{r}_2. \tag{2.5}$$

Using this new set of coordinates, it is possible to work in the following Hilbert space $H = H_r \otimes H_R$, with the wave-function $|\psi\rangle = |\psi_\mathbf{r}\rangle \otimes |\psi_\mathbf{R}\rangle$. As the potential $V(\mathbf{r})$ only depends on the relative distance between the particles, the full potential is contained in the relative coordinate part of the Hilbert space H_r. Using this information, the two different Hilbert space components of the combined Hilbert space wave-function $|\psi\rangle$ can be expressed as follows:

$$-\frac{\hbar^2}{2M}\frac{d^2}{dr^2}|\psi_\mathbf{R}\rangle = E_\mathbf{R},|\psi_\mathbf{R}\rangle \tag{2.6}$$
$$\left[-\frac{\hbar^2}{2\mu}\frac{d^2}{dr^2} + V(\mathbf{r})\right]|\psi_\mathbf{r}\rangle = E_\mathbf{r}\,|\psi_\mathbf{r}\rangle\,. \tag{2.7}$$

The mass M which has been introduced in equation 2.6 corresponds to the total mass of the two particles, whereas the mass μ which has been introduced in equation 2.7 corresponds to the reduced mass of the two scattering partners, which is defined as follows:

$$\mu = \frac{m_1 m_2}{m_1+m_2}. \tag{2.8}$$

Throughout the analysis carried out in this thesis, the interacting particles are assumed to be identical. Therefore, the reduced mass as defined by equation 2.8 can be expressed in terms of the single particle mass m as $\mu = \frac{1}{2}m$. This relation between the single particle mass m and the reduced mass μ will be used throughout the remainder of the report. Furthermore, as the full character of the interaction potential is contained in the Schrödinger equation for the relative position wave-function $|\psi_{\mathbf{r}}\rangle$ and the Hilbert space can be decoupled into a part solely depending on the relative position $\mathbf{r}$ and a part solely depending on the center of mass position $\mathbf{R}$, it is possible to analyse the scattering of two particles by only considering the relative part of the total wave-function $|\psi\rangle$, keeping in mind that the center of mass contribution can be incorporated into the analysis by adding the kinetic energy term related to the center of mass motion. For the sake of notational and computational convenience, the remainder of this report will only focus on the relative position part. Starting from equation 2.3, the initial two-body Hamiltonian has now effectively been reduced to a single particle Hamiltonian of a particle with a mass μ scattering from a potential $V(\mathbf{r})$, as can be described by the following Hamiltonian:

$$\hat{H} = -\frac{\hbar^2}{2\mu}\frac{d^2}{dr^2} + \hat{V}(\mathbf{r}). \tag{2.9}$$

2.3 The scattering operator

Using the Hamiltonian operator as introduced in equation 2.9, the time-development of the wave-function $\psi(t)$ of two identical particles can be analysed. This wave-function satisfies the time-dependent Schrödinger equation and, as the Hamiltonian governing the time development of the wave-function is independent of time, the general solution to this equation can be expressed as follows:

$$|\psi(t)\rangle = \hat{U}(t)\,|\psi\rangle = e^{-i\hat{H}t}\,|\psi\rangle\,. \tag{2.10}$$

Assuming that the potential $V(r)$ drops off sufficiently fast [4] as $\mathbf{r} \to \infty$, the wave-function as presented by the previous equation should reduce to a free-wave long before and long after the interaction with the potential has taken place. Formally, this means that equation 2.10 has to satisfy the following conditions:

$$\lim_{t\to-\infty} \hat{U}(t)\,|\psi\rangle = e^{-i\hat{H}^0 t}\,|\psi_{in}\rangle = \hat{U}^0(t)\,|\psi_{in}\rangle\,, \tag{2.11}$$

$$\lim_{t\to\infty} U(t)\,|\psi\rangle = e^{-iH^0 t}\,|\psi_{out}\rangle = U^0(t)\,|\psi_{out}\rangle\,. \tag{2.12}$$

The wave-functions $|\psi_{in}\rangle$ and $|\psi_{out}\rangle$ are more commonly referred to as the in- and out-asymptotes of the wave-function. The solutions of these asymptotes correspond to eigenstates of the free-evolution Hamiltonian H^0, which solely contains the kinetic energy term. Exploiting the unitarity of the evolution operator $\hat{U}(t)$, it is possible to use equations 2.11 and 2.12 in order to rewrite equation 2.10 in terms of the in- or out-asymptote:

$$|\psi(t)\rangle = \lim_{t\to-\infty} \hat{U}^\dagger(t)\hat{U}^0(t)\,|\psi_{in}\rangle = \hat{\Omega}_+\,|\psi_{in}\rangle\,, \tag{2.13}$$

$$|\psi(t)\rangle = \lim_{t\to\infty} \hat{U}^\dagger(t)\hat{U}^0(t)\,|\psi_{out}\rangle = \hat{\Omega}_-\,|\psi_{out}\rangle\,. \tag{2.14}$$

The two operators $\hat{\Omega}_\pm$ which have been introduced in the previous equations are named the *Møller wave operators*. As these operators are isometric, meaning that they are linear and preserve the norm, it is possible to introduce the following relation between the in- and the out-asymptote:

$$|\psi_{out}\rangle = \hat{\Omega}_-^\dagger\hat{\Omega}_+\,|\psi_{in}\rangle\,. \tag{2.15}$$

[4] The exact conditions are presented on page 27 of reference [47].

Using this equation, it is possible to describe the change of the incoming wave-function $|\psi_{in}\rangle$ into an outgoing wave-function $|\psi_{out}\rangle$ as a result of a scattering process. The combination of the Møller operators as presented in the previous expression can be related to a new operator $\hat{S}$ as follows:

$$\hat{S} = \hat{\Omega}_-^\dagger \hat{\Omega}_+. \tag{2.16}$$

This newly introduced operator is known as the *scattering operator*, or S-operator for short, and is of vital importance in scattering theory, as it effectively contains all information of experimental interest in a scattering process. Furthermore, it follows directly from the isometry of the Møller operators, that the scattering operator $\hat{S}$ is unitary. This means that, for every normalized in-asymptote $|\psi_{in}\rangle$ there exists a *unique* normalized out-asymptote $|\psi_{out}\rangle$ and vice-versa. The significance of this property and the scattering operator $\hat{S}$ in general will be discussed in more detail in the following sections.

2.4 The scattering matrix and the scattering phase shift

As indicated in the previous section, the problem of understanding the physics underlying a scattering process is reduced to finding the scattering operator describing the process. In order to conveniently analyse the scattering process using the scattering operator, the momentum basis spanned by the momentum states $|\mathbf{p}\rangle$ is often employed. These momentum states obey the following normalization condition:

$$\langle \mathbf{p}'|\mathbf{p}\rangle = \delta(\mathbf{p}' - \mathbf{p}). \tag{2.17}$$

The convenience of using the momentum basis follows from the property that the S-matrix commutes with the free-evolution operator H^0 [47]. As the momentum states $|\mathbf{p}\rangle$ are (improper) eigenvectors of the free-evolution operator H^0, these vectors satisfy the following relation:

$$\hat{H}^0 |\mathbf{p}\rangle = E_p |\mathbf{p}\rangle . \tag{2.18}$$

Using the commutation relation between the S-operator and the free evolution Hamiltonian and exploiting the unitary character of the S-operator, which has been discussed in the previous section, the scattering relation between an incoming momentum state $|\mathbf{p}'\rangle$ and an outgoing momentum state $|\mathbf{p}\rangle$ can be expressed as follows:

$$\langle \mathbf{p}'|\hat{S}|\mathbf{p}\rangle = \delta(E_{p'} - E_p) \cdot \text{remainder}. \tag{2.19}$$

Equation 2.19 effectively implies the conservation of the total energy during the scattering process. Furthermore, the remainder that is present in equation 2.19 can be analysed in more detail by using the knowledge that the scattering operator reduces to the identity operator in the absence of a potential $V(\mathbf{r})$. Splitting the previous equation up into a part which describes the absence of the scattering potential and into a part which describes the effect of the interaction potential on the momentum state, it can be proven that it is possible to rewrite equation 2.19 into the following form [47]

$$\langle \mathbf{p}|\hat{S}|\mathbf{p}'\rangle = \delta(\mathbf{p}' - \mathbf{p}) - 2\pi i \langle \mathbf{p}|\hat{T}|\mathbf{p}'\rangle \delta(E_{p'} - E_p). \tag{2.20}$$

The matrix element $\langle \mathbf{p}|\hat{T}|\mathbf{p}'\rangle$ which has been introduced in the previous equation corresponds to the part of the scattering matrix S which describes the occurrence of a scattering process. Therefore, the matrix containing elements of the form $\langle \mathbf{p}|\hat{T}|\mathbf{p}'\rangle$ is named the *transition matrix*. This matrix, and its corresponding operator form, which is named the T-operator, will be discussed in more detail in section 2.6. However, before moving on to the discussion of this newly introduced matrix, more interesting details of the scattering matrix can be discovered. In order to reveal these additional

characteristics, the momentum basis is transformed to the spherical wave-basis [49, 15].

It can be proven that, apart from the commutation with the free Hamiltonian H^0, the S-matrix also commutes with the angular momentum operators $\mathbf{L}_z$ and L^2 [47]. Due to these commutation relations, the scattering matrix is diagonal in the spherical basis. Therefore, the S-matrix in this basis can be written as follows:

$$\langle E, l, m|\hat{S}|E', l', m'\rangle = S_l(E)\delta_{l,l'}\delta_{m,m'}\delta(E - E'). \tag{2.21}$$

The factor $S_l(E)$ that has been introduced in the previous equation is related to the probability of the occurrence of a scattering process for particles with an energy E and an angular momentum quantum number l. The exact form of this element can be obtained by considering the following two previously introduced characteristics of the scattering operator and the scattering wave function:

1. The scattering matrix S is unitary.
2. The scattering of a wave of a potential induces a phase shift.

Using these two characteristics, the element $S_l(E)$ can be expressed in terms of the phase shift $\delta_l(E)$ as follows:

$$S_l(E) = e^{2i\delta_l(E)}. \tag{2.22}$$

Equation 2.22 indicates the relation between the (real) scattering phase shift and the scattering matrix. Furthermore, this equation indicates the dependency of the phase shift on the angular momentum l and the energy E of the particle scattering of a potential. Using the fact that the energy E and the wave number k are related by $E = \frac{\hbar^2 k^2}{2\mu}$, it is possible to expand the phase shift in terms of the wave number k [5], yielding the following result, which is known as the *effective range expansion* [50, 51]:

$$k^{2l+1}\cot(\delta_l(k)) = -\frac{1}{a_l} + \frac{R_e}{2}k^2 + O(k^4). \tag{2.23}$$

Considering only zero momenta contributions and keeping only the first term of the expansion, the following relation between the scattering length a_0 and the phase shift $\delta_0(k)$ can be derived:

$$k\cot(\delta_0(k)) = -\frac{1}{a_0}. \tag{2.24}$$

As presented in appendix F, retaining only the first term in the effective range expansion as presented in the previous equation, the quadratic relation between the dimer energy E_{2b} and the scattering length which has been previously introduced in section 1.3 can be obtained. However, upon increasing the wave number k, or upon increasing the value of the parameter R_e, which is known as the effective range of the potential [50], the dimer energy starts to deviate from this quadratic relation. Without going into detail in this thesis, be proven that the effective range coefficient is dependent on the resonance width ΔB [25]. Therefore, observations of deviations from the quadratic relation between the dimer energy and the scattering length as presented in equation 1.5 are expected to depend on the resonance width. This will be analysed in more detail in chapter 6.

2.5 Stationary scattering states

As discussed in the previous section, the momentum space basis offers a convenient basis for scattering physics, as the momentum states $|\mathbf{p}\rangle$ represent improper eigenstates of the free-evolution operator

[5] Throughout this entire report extremely cold collisions are being investigated. This means that the wave number will approach a value of zero

H^0. Using the convenience of this basis as a motivation, the following two improper eigenvectors $|\mathbf{p}\pm\rangle$ are introduced:

$$|\mathbf{p}\pm\rangle = \hat{\Omega}_{\pm} |\mathbf{p}\rangle . \tag{2.25}$$

The Møller operators in the previous expression indicate that the states $|\mathbf{p}\pm\rangle$ represent the in- and out-asymptotes of the plane wave state $|\mathbf{p}\rangle$. Comparing this relation to equations 2.13 and 2.14, and expanding the states $|\psi_{in}\rangle$[6] and $|\psi\rangle$ in terms of of plane waves $|\mathbf{p}\rangle$, the following relations can be obtained:

$$|\psi_{in}\rangle = \int \psi_{in}(\mathbf{p}) |\mathbf{p}\rangle \, d\mathbf{p}, \tag{2.26}$$

$$|\psi\rangle = \hat{\Omega}_{+} |\psi_{in}\rangle = \int \psi(\mathbf{p}) \hat{\Omega}_{+} |\mathbf{p}\rangle \, d\mathbf{p} = \int \psi(\mathbf{p}) |\mathbf{p}+\rangle \, d\mathbf{p}. \tag{2.27}$$

The previous two expressions indicate that the state $|\psi\rangle$ has the same expansion in terms of $|\mathbf{p}+\rangle$ as does its asymptote $|\psi\rangle$ in terms of $|\mathbf{p}\rangle$ [47]. Therefore, despite being improper vectors[7], the momentum states $|\mathbf{p}\rangle$ and $|\mathbf{p}+\rangle$ can be used in order to gain an insight into the actual states $|\psi\rangle$ and $|\psi_{in}\rangle$. In fact, it is possible to express the state $|\mathbf{p}+\rangle$ in terms of its in asymptote $|\mathbf{p}\rangle$. In order to obtain this relation, we need to use the fact that the vectors $|\mathbf{p}\pm\rangle$ are eigenvectors of the Hamiltonian $H = H^0 + V$[8]. Using this information it can be proven that the states $|\mathbf{p}\pm\rangle$ are related to the $t = 0$ states $|\mathbf{p}\rangle$ by:

$$|\mathbf{p}\pm\rangle = |\mathbf{p}\rangle + \frac{1}{E_p - \hat{H} \pm i0} \hat{V} |\mathbf{p}\rangle . \tag{2.28}$$

In the denominator of the previous equation, an infinitesimally small complex component has been added in order to avoid having a vanishing denominator for $E_p |\mathbf{p}\rangle = \hat{H} |\mathbf{p}\rangle$. For notational convenience, the previous equation can be rewritten into the following form:

$$|\mathbf{p}\pm\rangle = |\mathbf{p}\rangle + \hat{G}(E_p \pm i0)\hat{V} |\mathbf{p}\rangle . \tag{2.29}$$

The previous expression is known as the *Lipmann-Schwinger* equation [52]. Furthermore, the operator $\hat{G}(E_p \pm i0)$ that has been introduced in the previous equation is better known as a *Green's operator* and is defined as $\hat{G}(E_p \pm i0) = (E_p - \hat{H} \pm i0)^{-1}$ [47].
Upon defining another Green's operator as $\hat{G}^0(E_p \pm i0) = (E - \hat{H}^0 \pm i0)^{-1}$, the following analogous equation to expression 2.29 can be obtained:

$$|\mathbf{p}\pm\rangle = |\mathbf{p}\rangle + \hat{G}^0(E_p \pm i0)\hat{V} |\mathbf{p}\pm\rangle . \tag{2.30}$$

Both equations 2.29 and 2.30 make it possible to gain an insight into the characteristics of the physical state $|\psi\rangle$. As described in section 2.1, this physical state can obtain a phase shift as a result of a scattering process. This phase shift has subsequently been related to the scattering matrix in section 2.4. In order to complete the full circle, the states $|\mathbf{p}\pm\rangle$ will now in turn be related to the part of the S-matrix which describes the occurrence of a scattering process. As discussed in section 2.4, this part is described by the transition operator $\hat{T}$. This operator will be analysed in more detail in the following section.

[6] A similar expansion could be made for the out asymptote $|\psi_{out}\rangle$

[7] This means that they don't satisfy equations 2.11 and 2.12

[8] This follows from the application of the intertwining relation as presented on page 40 of the book written by J.R. Taylor [47].

2.6 The transition operator

The transition operator $\hat{T}$ has been briefly introduced in section 2.4 and is defined as follows [47]:

$$\hat{T}(z) = \hat{V} + \hat{V}\hat{G}(z)\hat{V}. \tag{2.31}$$

The operator $\hat{G}(z)$ corresponds to the Green's operator which has been introduced in the previous section. It can be proven that, by using the definition of the Green's operators $\hat{G}(z)$ and $\hat{G}^0(z)$, this previous expression can be rewritten into the following form [47]:

$$\hat{T}(z) = \hat{V} + \hat{V}\hat{G}^0(z)\hat{T}(z). \tag{2.32}$$

Both equations 2.31 and 2.32 will prove to be useful in the analysis of a scattering procedure and will be used throughout the entire report. Before moving on to other important properties of the T-operator, it is important to notice that instead of using the energy E_p as an input argument for the T-operator, the T-operator is defined as a function of the input argument z. This argument z can, but doesn't necessarily have to, equal the energy. For z unequal to the energy E_p, the transition operator is referred to as the *off-shell T-operator* [14, 15] contrary to the *on-shell T-operator*, for which the input argument z equals the energy E_p. The projection of the on-shell version of the T-operator onto a momentum state $|\mathbf{p}\rangle$, yields the following outcome:

$$\hat{T}(E_p \pm i0)\,|\mathbf{p}\rangle = \left[\hat{V} + \hat{V}\hat{G}(E_p \pm i0)\hat{V}\right]|\mathbf{p}\rangle = \hat{V}\left[1 + \hat{G}(E_p \pm i0)\hat{V}\right]|\mathbf{p}\rangle\,. \tag{2.33}$$

Comparing the previous expression to equation 2.29, the following relation can be obtained:

$$\hat{T}(E_p \pm i0)\,|\mathbf{p}\rangle = \hat{V}\,|\mathbf{p}\pm\rangle\,. \tag{2.34}$$

Whereas at first sight this equation might seem trivial, it in fact represents a valuable relation which will be applied in many calculations throughout the report. In essence the previous equation relates the asymptotic states $|\psi_{in}\rangle$ and $|\psi_{out}\rangle$ to the state $|\psi\rangle$ at $t = 0$ through the application of the T-operator. By projecting the previous equation onto an incoming momentum state $|\mathbf{p}'\rangle$, it is possible to compute the probability of the occurrence of a scattering process with an incoming (relative) momentum $|\mathbf{p}\rangle$ and a outgoing (relative) momentum $|\mathbf{p}'\rangle$.

2.7 The Feshbach formalism

Now that the scattering operator and the transition operator have been introduced, it is possible to apply the information as presented in the previous sections in order to analyse the Feshbach resonances that occur in the coupled-channels system as described in section 1.1. The theory outlined in this section closely follows the approach as followed by S.Kokkelmans [25].

In order to study the effect of Feshbach resonances on a level such that they can be related to interesting scattering physics quantities such as the transition matrix, it should be realized that the total Hilbert space $\mathcal{H}$ now consists of two subspaces $\mathcal{P}$ and $\mathcal{Q}$, where $\mathcal{P}$ represents the open channel subspace and $\mathcal{Q}$ represents the closed channel subspace. One could construct two orthogonal operators $\hat{P}$ and $\hat{Q}$ which project onto the subspaces $\mathcal{P}$ and $\mathcal{Q}$ respectively. Through the application of these operators, the Schrödinger equation for the total system $(E - \hat{H})\,|\psi\rangle = 0$ can be split up into the following two components:

$$(E - \hat{H}_{PP})\,|\psi_P\rangle = \hat{H}_{PQ}\,|\psi_Q\rangle\,, \tag{2.35}$$

$$(E - \hat{H}_{QQ})\,|\psi_Q\rangle = \hat{H}_{QP}\,|\psi_P\rangle\,. \tag{2.36}$$

In the previous two equations, the following notation has been used: $|\psi_P\rangle = \hat{P}|\psi\rangle$, $|\psi_Q\rangle = \hat{Q}|\psi\rangle$, $\hat{H}_{PP} = \hat{P}\hat{H}\hat{P}$, $\hat{H}_{PQ} = \hat{P}\hat{H}\hat{Q}$, $\hat{H}_{QP} = \hat{Q}\hat{H}\hat{P}$ and $\hat{H}_{QQ} = \hat{Q}\hat{H}\hat{Q}$. This notation will be used throughout the entire report. Using equation 2.36, it is possible to obtain the following expression for the closed channel component of the wave function $|\psi_Q\rangle$:

$$|\psi_Q\rangle = \frac{1}{E + i0 - \hat{H}_{QQ}} \hat{H}_{QP} |\psi_P\rangle . \tag{2.37}$$

Similarly to what has been discussed in section 2.5, an infinitesimally small complex component has been added to the denominator of the previous equation in order to avoid the presence of any singularities in the system. As equations 2.35 and 2.36 form a coupled set of equations, it is possible to substitute equation 2.37 into expression 2.35 in order to eliminate $|\psi_Q\rangle$ from equation 2.35, resulting in the following outcome [25]:

$$E|\psi_P\rangle = \left(\hat{H}_{PP} + \hat{H}_{PQ} \frac{1}{E + i0 - \hat{H}_{QQ}} \hat{H}_{QP} \right) |\psi_P\rangle . \tag{2.38}$$

Upon inspection of the right hand side of the previous equation, two different contributions to the development of the open channel wave function $|\psi_P\rangle$ can be distinguished. First of all, the term $\hat{H}_{PP}$ can be recognized. This term is fully contained in the open channel subspace and represents the effect of the background channel, without any coupling effects to the closed channel. The second term on the right hand side however represents the coupling to the closed channel. Here, we can recognize the closed channel equivalent of the Green's operator $\hat{G}(E_p \pm i0)$ which has been introduced in section 2.5 flanked by the coupling terms $\hat{H}_{PQ}$ and $\hat{H}_{QP}$. In the absence of any coupling, this second term would disappear and the open channel subspace would correspond to the total Hilbert space of the process. Having distinguished different contributions to the development of the open channel wave function, the Green's operator $\hat{G}(E + i0)$ which is present in the previous equation is now expanded in terms of bound states $|\phi_{Q,n}\rangle$ and continuous states $|\phi_Q(E)\rangle$ in order to be able to compute an expression for the open channel wave function [25]. The expansion is presented below [9]:

$$\frac{1}{E + i0 - \hat{H}_{QQ}} = \sum_n \frac{|\phi_{Q,n}\rangle \langle\phi_{Q,n}|}{E - \epsilon_{Q,n}} + \int \frac{|\phi_Q(E)\rangle \langle\phi_Q(E)|}{E + i0 - \epsilon} d\epsilon. \tag{2.39}$$

The factors $\epsilon_{Q,n}$ and ϵ which have been introduced in the previous equation correspond to the eigenvalues of $\hat{H}_{QQ}$ for the different considered states. It should be noted that, contrary to the energy E_c which has been introduced in figure 1.1, these energies are measured with respect to the closed channel asymptote. As we want to measure the energy of the system with respect to the open channel asymptote, the bound state energy ϵ_Q as measured with respect to the closed channel subspace has to be transformed to the value E_C which is measured with respect to the open channel subspace. The inspection of figure 1.1 reveals that these two energies are related as follows:

$$E_C = \epsilon_Q + C. \tag{2.40}$$

Next, as ultra cold collisions are being considered, the energy E of the scattered particle will be located just slightly above the open channel asymptotic threshold and therefore simultaneously far away from the closed channel asymptotic threshold. Motivated by this property, the continuum states are neglected in the Feshbach formalism [26, 53]. Furthermore, the spacing between the n bound states is typically large enough such that only a single bound state close in value to the entrance energy E significantly affects the scattering process [25, 15]. Therefore, in the Feshbach formalism, the summation over n bound states as presented in equation 2.39 is replaced by a single

[9] The states $|\phi_Q, n\rangle$ and $|\phi_Q(E)\rangle$ have to be normalized in order to be able to use this expansion. The normalization procedure and the obtained normalization constant X are presented in appendix B.

bound state term. This approximation of having a single bound state in the closed channel has previously been used in figure 1.1. Now, upon applying these approximations to equation 2.39, the following new expression can be obtained [25]:

$$\frac{1}{E + i0 - \hat{H}_{QQ}} = \frac{|\phi_{Q,n}\rangle \langle \phi_{Q,n}|}{E - (\epsilon_Q + C)}. \tag{2.41}$$

Upon substituting the previous expression into equation 2.38 and collecting the effect of $\hat{H}_{PP}$ on the left hand side of the expression, the following new equation can be found:

$$(E - \hat{H}_{PP}) |\psi_P\rangle = \hat{H}_{PQ} \frac{|\phi_{Q,n}\rangle \langle \phi_{Q,n}|}{E - (\epsilon_Q + C)} \hat{H}_{QP} |\psi_P\rangle . \tag{2.42}$$

In order to formally solve the previous expression for the open channel wave function $|\psi_P\rangle$ the following boundary conditions have to be considered [52, 15]:

1. In the absence of any coupling to the closed channel, the solution to $|\psi_P\rangle$ should reduce to satisfy the homogeneous part of equation 2.35. This solution is represented by the scattering state $|\phi_P^+\rangle$.
2. In the absence of both the coupling to the closed channel and the open channel potential, the scattering state $|\phi_P^+\rangle$ should reduce to the unscattered plane wave state $|\chi\rangle$.

Taking the previous two boundary conditions into consideration, equation 2.42 can be solved, yielding the following expression:

$$|\psi_P^+\rangle = |\phi_P^+\rangle + \frac{1}{E + i0 - \hat{H}_{PP}} H_{PQ} \frac{|\phi_Q\rangle \langle \phi_Q|}{E - (\epsilon_Q + C)} \hat{H}_{QP} |\psi_P^+\rangle , \tag{2.43}$$

$$\text{with} \quad |\phi_P^\pm\rangle = |\chi\rangle + \frac{1}{E \pm i0 - \hat{H}_{PP}} \hat{V}_{PP} |\chi\rangle . \tag{2.44}$$

Having obtained an expression for $|\psi_P^+\rangle$, we now wish to find the transition matrix related to this coupled-channels system. In order to find this matrix, equation 2.43 is multiplied from the left hand side by the factor $\langle \chi_{out}| \hat{V}_{eff}$. The newly introduced operator $\hat{V}_{eff}$ represents the combined effect of the uncoupled-channels part of the interaction and the coupled-channels part of the interaction. The inspection of equations 2.43 and 2.44 reveals that this *effective* potential operator $\hat{V}_{eff}$ can be defined as follows:

$$\hat{V}_{eff} = \hat{V}_{PP} + \hat{H}_{PQ} \frac{1}{E - \hat{H}_{QQ}} \hat{H}_{QP}. \tag{2.45}$$

As we know the relation between the transition matrix and the potential interaction from equation 2.34, the effective potential as defined in the previous expression can be used in order to obtain the expression for the coupled-channels transition matrix as presented below:

$$\langle \chi_{out}|\hat{T}(E)|\chi_{in}\rangle = \langle \chi_{out}|\hat{V}_{eff}|\psi_P^+\rangle = \langle \chi_{out}|\hat{V}_{PP}|\psi_P^+\rangle + \langle \chi_{out}| \hat{H}_{PQ} \frac{|\phi_Q\rangle \langle \phi_Q|}{E - (\epsilon_Q + C)} \hat{H}_{QP} |\psi_P^+\rangle . \tag{2.46}$$

In the previous expression, the shorthand notation E^+ has been used in order to express $E + i0$. The straightforward but tedious derivation as presented in appendix A reveals that the previous expression can be cast into the following analogous form:

$$\langle \chi_{out}|\hat{T}(E)|\chi_{in}\rangle = \langle \chi_{out}|\hat{T}_{uncoupled}(E)|\chi_{in}\rangle + \langle \phi_P^-| \hat{H}_{PQ} \frac{|\phi_Q\rangle \langle \phi_Q|}{E - (\epsilon_Q + C)} \hat{H}_{QP} |\psi_P^+\rangle . \tag{2.47}$$

Whereas it seems like an expression for the T-matrix has been obtained, the equation presented above still explicitly depends on the unknown state $|\psi_P^+\rangle$. In order to get rid of this explicit dependence,

equation 2.43 is multiplied by the factor $\langle\phi_Q|\,\hat{H}_{QP}$ from the left side and solved for $\langle\phi_Q|\hat{H}_{QP}|\psi_P^+\rangle$, resulting in the following outcome:

$$\langle\phi_Q|\hat{H}_{QP}|\psi_P^+\rangle = \frac{(E-\epsilon_Q)\,\langle\phi_Q|\hat{H}_{QP}|\phi_P^+\rangle}{E-(\epsilon_Q+C)-\langle\phi_Q|\hat{H}_{QP}\frac{1}{E^+-\hat{H}_{PP}}\hat{H}_{PQ}|\phi_Q\rangle}. \tag{2.48}$$

Substituting the previous equation into expression 2.47, the equation for the T-matrix as presented below can be found:

$$\langle\chi_{out}|\hat{T}(E)|\chi_{in}\rangle = \langle\chi_{out}|\hat{T}_{uncoupled}(E)|\chi_{in}\rangle + \frac{\langle\phi_P^-|\hat{H}_{PQ}|\phi_Q\rangle\,\langle\phi_Q|\hat{H}_{QP}|\phi_P^+\rangle}{E-\epsilon_Q-\langle\phi_Q|\hat{H}_{QP}\frac{1}{E^+-\hat{H}_{PP}}\hat{H}_{PQ}|\phi_Q\rangle}. \tag{2.49}$$

It should be noted that the previous equation is a function of the energy E. However, as explained in section 2.6 it is also possible to define an off-shell T-matrix with an input argument z unequal to the energy E. In terms of the previous equation, this means that the argument E has to be replaced with the arbitrary argument z in order to obtain the off-shell form of the previous expression.

Having obtained the coupled channel T-matrix, it is possible to obtain the coupled- channels S-matrix through the application of equation 2.20. This results in the following outcome:

$$S = S_p\left(1-8\pi^2\mu i\hbar k\frac{\langle\phi_P^-|\hat{H}_{PQ}|\phi_Q\rangle\,\langle\phi_Q|\hat{H}_{QP}|\phi_P^+\rangle}{E-(\epsilon_Q+C)-\langle\phi_Q|\hat{H}_{QP}\frac{1}{E^+-\hat{H}_{PP}}\hat{H}_{PQ}|\phi_Q\rangle}\right). \tag{2.50}$$

In the previous expression, the states $|\phi_P\rangle$ are set to be momentum normalized. Using this normalization, the uncoupled channels part of the scattering matrix, named S_P, can be expressed as:

$$S_P = 1-2\pi i T_P. \tag{2.51}$$

with T_P the uncoupled channels part of the transition matrix.

2.8 Conclusion

In the first part of this chapter, new concepts such as the transition operator and the scattering operator have been introduced. These concepts will prove to be important instruments throughout the entire report, including the three-body part and many-body part. With the help of these operators, it is possible to extract information regarding the effective range of the potential, the scattering length of the interaction and the phase shift of the wave function. As we have reduced the two-particle interaction to a single particle interaction with a potential, it is sufficient to known the transition matrix or the scattering matrix describing the interaction with the potential in order to unveil all the interesting physics of the scattering process. In the second part of the chapter, the concepts which have been introduced in the first part have been used in order to obtain the transition matrix and the scattering matrix which describe a Feshbach resonance. In order to obtain these expressions, the Feshbach formalism has been applied. This formalism relies on the assumption that there is only a single bound state in the closed channel subspace that affects the scattering process. Furthermore, the continuum states in this closed channel have been neglected. Keeping these approximations in mind in the inspection of the validity of a derivation and simulation, the next step is to specify the form of the transition matrix for the separable interaction potential that has been introduced in section 1.2. The derivation of this specific format of the coupled-channels transition matrix will be the main topic of the next chapters. To be more specific, the following chapter will focus on the uncoupled part of the transition matrix as presented in equation 2.49, whereas chapter 4 will focus on the analysis of the coupled-channels contribution to the total coupled-channels transition matrix as presented in equation 2.49.

Chapter 3

The uncoupled transition matrix

In the previous chapter, it has become clear how to extract the important physical character of two particle scattering interactions for both single channel interactions and coupled channel interactions. In order to break down the complicated process of calculating the introduced coupled-channels transition matrix, this chapter will focus on the analysis of the uncoupled part of the transition matrix as presented in equation 2.49, before moving on to the more complicated analysis of the coupled-channels contribution to the total transition matrix as presented in equation 2.49 in the next chapter. The obtained expression for the uncoupled part of the transition matrix will be used in the final part of this chapter in order to inspect some important single channel quantities, being the background scattering length and the bound state energy.

3.1 The delta function potential in momentum space

In order to be able to obtain an expression for the uncoupled transition matrix, the first term on the right-hand side of equation 2.31 indicates that the expression for the potential needs to be specified. As discussed in the introduction, the potential that will be analysed in this thesis takes the form of a delta function. This effectively means that two particles will only interact with each other when they completely overlap in space. The strength of this interaction is characterized by the quantity λ. Using this strength as an input parameter, it is possible to characterize the potential as follows:

$$\hat{V}(\mathbf{r}) = -\lambda \cdot \delta(\mathbf{r}). \tag{3.1}$$

As previously discussed in chapter 2 the momentum space basis offers a convenient basis for the analysis of a scattering process. Fortunately, similarly the delta function potential is conveniently analysed in this basis. In order to move from the position space representation of the potential to this useful momentum space representation, the potential has to be Fourier transformed, as presented below:

$$\langle \mathbf{p}'|\hat{V}|\mathbf{p}\rangle = \iint \langle \mathbf{p}'|\mathbf{r}'\rangle \langle \mathbf{r}'|\hat{V}(\mathbf{r})|\mathbf{r}\rangle \langle \mathbf{r}|\mathbf{p}\rangle \, d(\mathbf{r})d(\mathbf{r}), \tag{3.2}$$

$$\langle \mathbf{p}'|\hat{V}|\mathbf{p}\rangle = \frac{1}{(2\pi\hbar)^3} \iint \exp[-i\mathbf{p}' \cdot \mathbf{r}'] \left(-\lambda\delta(\mathbf{r})\delta(\mathbf{r}-\mathbf{r}')\right) \exp[i\mathbf{p} \cdot \mathbf{r}] d\mathbf{r}d\mathbf{r}', \tag{3.3}$$

$$\langle \mathbf{p}'|\hat{V}|\mathbf{p}\rangle = -\frac{\lambda}{(2\pi\hbar)^3}. \tag{3.4}$$

As can be understood upon inspection of equation 3.4, the delta-function potential in position space has been transformed to a potential with a constant effective strength of $\frac{\lambda}{(2\pi\hbar)^3}$ in momentum space. In order to simplify notation, the following momentum space potential strength is introduced

$$\eta = \frac{\lambda}{(2\pi\hbar)^3}. \tag{3.5}$$

In order to be able to include interesting finite range effects in the scattering interactions, a finite momentum space cut-off Λ will be introduced to the potential. This cut-off effectively sets the potential interaction strength η to a value of zero if the relative momentum between two scattering partners exceeds a particular value $|\mathbf{p}|$. The value of this cut-off can be tuned in order to match multi-channel calculations of different atomic species, effectively increasing the physical relevance of any numerical and analytical analysis [20]. The tuning process of the cut-off Λ will be discussed in more detail in chapter 6. In order to implement the finite cut-off in the definition of the potential, the form factor $|g\rangle$ can be introduced. A projection of a relative momentum $\langle\mathbf{p}|$ onto this form factor will yield a value of one for $|\mathbf{p}| \leq \Lambda$ and a value of zero for $|\mathbf{p}| > \Lambda$. Upon using these form factors, the potential operator $\hat{V}$ in momentum space can be defined as follows:

$$\hat{V} = -\eta \left|g\right\rangle \left\langle g\right|, \quad \text{with} \quad \begin{cases} g(\mathbf{p}) = 1 & |\mathbf{p}| < \Lambda \\ g(\mathbf{p}) = 0 & |\mathbf{p}| \geq \Lambda \end{cases} \tag{3.6}$$

3.2 The two-body T-matrix in momentum space

Having obtained a specific form for the interaction potential as presented in expression 3.6, using the definition of the Green's operator $\hat{G}^0(z)$ and using equation 2.32, it is possible to obtain the following relation for the transition matrix:

$$\langle\mathbf{p}'|\hat{T}(z)|\mathbf{p}\rangle = \langle\mathbf{p}'|\hat{V}|\mathbf{p}\rangle + \langle\mathbf{p}'|\hat{V}\hat{G}^0(z)\hat{T}(z)|\mathbf{p}\rangle\,, \tag{3.7}$$

$$\langle\mathbf{p}'|\hat{T}(z)|\mathbf{p}\rangle = \langle\mathbf{p}'|\hat{V}|\mathbf{p}\rangle + \int \langle\mathbf{p}'|\hat{V}|\mathbf{p}"\rangle \frac{1}{z - \frac{p"^2}{2\mu}} \langle\mathbf{p}"|\hat{T}(z)|\mathbf{p}\rangle\, d\mathbf{p}". \tag{3.8}$$

In the previous equation, the fact that the free evolution Hamiltonian H^0 has an eigenvalue of $p^2/2\mu$ in the momentum basis has been implemented. Next, in order to simplify the solving procedure of the previous equation, the separable characteristic of the potential is once more used, as upon inspection of the previous equation, we expect to have a similar separable form for the transition matrix. Using this information, the transition matrix can be written as follows: $\langle\mathbf{p}'|\hat{T}(z)|\mathbf{p}\rangle = -\tau(z)g(\mathbf{p})g(\mathbf{p}')$, where $\tau(z)$ represents the magnitude of the transition matrix element as a function of the input argument z. Applying this form of the transition matrix, equation 3.8 can be rewritten into the following form:

$$-\tau(z)g(\mathbf{p})g(\mathbf{p}') = -\eta g(\mathbf{p})g(\mathbf{p}') + 4\pi\eta\tau(z)g(\mathbf{p})g(\mathbf{p}') \int_0^\Lambda \frac{p"^2}{z - \frac{p"^2}{2\mu}} dp". \tag{3.9}$$

Whereas the task of finding an expression for the uncoupled T-matrix seems to be completed, the integral that is present in the previous equation should be analysed with care, as the integrand contains a pole for $\frac{\Lambda^2}{2\mu} \geq z \geq 0$. Avoiding the presence of a pole in a denominator has been discussed before. The solution that was presented constituted the addition of an infinitesimally small complex component such that no singularity exists in the analysis. Therefore, if z falls within the regime where a pole exists, a small complex component is added to the denominator. After doing so, the integral can be solved using complex function theory [54]. Without going into detail, this effectively means that the integral needs to be split up into a principal value part and a residue. These two components are then added together to give the total solution of the integral. If, on the other hand,

z doesn't fall within the regime in which a pole exists, the equation can be integrated without using complex function analysis. Considering both possible regimes for the value z, the following set of solutions to the integral that is present in equation 3.9 can be obtained:

$$\begin{cases} \xi(z) = \displaystyle\int_0^\Lambda \frac{p"^2}{z - \frac{p"^2}{2\mu}} dp" = \sqrt{z}(2\mu)^{3/2} \operatorname{arctanh}\left[\frac{\Lambda}{\sqrt{2\mu z}}\right] - 2\mu\Lambda \qquad z \geq \dfrac{\Lambda^2}{2\mu} \vee z \leq 0, & (3.10) \\ \zeta(z) = \displaystyle\int_0^\Lambda \frac{p"^2}{z - \frac{p"^2}{2\mu}} dp" = \sqrt{z}(2\mu)^{3/2} \operatorname{arccoth}\left[\frac{\Lambda}{\sqrt{2\mu z}}\right] - 2\mu\Lambda - \pi i\sqrt{2z}\mu^{3/2} \quad 0 \leq z \leq \dfrac{\Lambda^2}{2\mu}. & (3.11) \end{cases}$$

The two different solutions to the integral as presented in equation 3.9 have been named $\xi(z)$ and $\zeta(z)$ for notational convenience and will be used throughout the remainder of the report. Using these newly defined functions, the following two solution branches for the uncoupled T-matrix can be recovered:

$$\begin{cases} T_{uncoupled}(z, \mathbf{p}, \mathbf{p}') = g(\mathbf{p})g(\mathbf{p}')\dfrac{-\eta}{1 + 4\pi\eta\xi(z)} \qquad z \geq \dfrac{\Lambda^2}{2\mu}, \vee z \leq 0 & (3.12) \\ T_{uncoupled}(z, \mathbf{p}, \mathbf{p}') = g(\mathbf{p})g(\mathbf{p}')\dfrac{-\eta}{1 + 4\pi\eta\zeta(z)} \qquad 0 \leq z \leq \dfrac{\Lambda^2}{2\mu}. & (3.13) \end{cases}$$

3.3 The potential strength and the scattering length

Having obtained the uncoupled T-matrix in the previous section, it is now possible to use this matrix in order to derive some other interesting physical quantities, such as the scattering length. As later on we wish to use the derived T-matrix as the uncoupled part of the total T-matrix as defined in equation 2.49, we suggestively name the scattering length related to the uncoupled channel scattering process a_{bg}, similarly to the notation which has been used in equation 1.1. In order to find the expression for the scattering length, the relation between the scattering matrix and the transition matrix as presented by equation 2.20 can be used in combination with the relation between the scattering matrix and the phase shift as presented by equation 2.22 on the one hand, and the relation between the scattering length and the phase shift as presented by equation 2.24 on the other hand, resulting in the outcome as presented below [15]:

$$T_{uncoupled}(E \to 0) = \frac{a_{bg}}{4\pi^2\mu\hbar}. \tag{3.14}$$

Now that a simple relation between the scattering length and the zero energy limit of the on-shell T-matrix has been established, it is possible to relate the scattering length to the potential strength η. The usefulness of such a relation resides in the fact that this makes it possible to relate a system parameter, being the strength of the potential, to a physical parameter that can be analysed experimentally. This means that the relation provides a link which makes it possible to carry out an analysis whilst keeping its physical implications in mind. Having motivated the usefulness of the relation, the zero energy limit [1] of equation 3.12 or 3.13 and expression 3.14 can be used in order to find the following expression for the potential strength η in terms of the scattering length a_{bg}:

$$\eta = \frac{a_{bg}}{8\pi\mu\Lambda a_{bg} - 4\pi^2\mu\hbar}. \tag{3.15}$$

[1] In this limit, it follows from equations 3.10 and 3.11 that $\zeta(0) = \xi(0) = -2\mu\Lambda$

3.4 The energy of a bound state

Having both studied the T-matrix and the relation between the scattering length and the potential strength, it seems like the analysis of the uncoupled scattering process is a closed book. However, more information can be extracted from this model in regard of the presence of a bound state in an uncoupled potential[2]. This is useful due to the fact that the coupled channel problem that will be analysed in the next chapter constitutes the presence of a single bound state in the closed channel subspace. In order to calculate the binding energy of this bound state, the previously computed uncoupled T-matrix can be used. In order to see how the energy of a bound state is related to the T-matrix, the following general expression for a bound state wave function $|\psi_B\rangle$, which following from the Schrödinger equation, needs to be analysed [47]:

$$|\psi_B\rangle = \frac{1}{E - \hat{H}^0}\hat{V}\,|\psi_B\rangle = \hat{G}^0(E)\hat{V}\,|\psi_B\rangle\,. \tag{3.16}$$

Multiplying the previous equation from the left side by the potential V and introducing the state $|\alpha\rangle = \hat{V}\,|\psi_B\rangle$, the following expression is found:

$$|\alpha\rangle = \hat{V}\hat{G}^0(E)\,|\alpha\rangle\,. \tag{3.17}$$

Solving the previous equation for the state $|\alpha\rangle$ then yields the result as presented below:

$$\Big(1 - \hat{V}\hat{G}^0(E)\Big)\,|\alpha\rangle = 0. \tag{3.18}$$

Whereas the previous result might seem insignificant, its importance becomes clear once equation 2.32 is solved for the on-shell T-matrix, resulting in the following outcome:

$$\hat{T}(E) = \Big(1 - \hat{V}\hat{G}^0(E)\Big)^{-1}\hat{V}. \tag{3.19}$$

Comparing the previous equation to expression 3.18, it is now clear that the bound state energy E_B can be found from the pole of the T-matrix.

Inspecting the pole of the transition matrix as presented in equation 3.12, the bound state energy E_B can be extracted upon solving the equation as displayed below:

$$1 + 4\pi\eta\xi(E_B) = 0. \tag{3.20}$$

Explicitly writing out the function $\xi(E_B)$ using equation 3.10 and collecting all terms depending on the energy E_B on the left hand side results in the following outcome:

$$\sqrt{E_B}(2\mu)^{3/2}\,\mathrm{arctanh}\left[\frac{\Lambda}{\sqrt{2\mu E_B}}\right] = -\frac{1}{4\pi\eta} + 2\mu\Lambda. \tag{3.21}$$

The previous equation indicates that once the cut-off Λ, the reduced mass μ and the potential strength η are known, the bound state energy can be determined.

[2]Note that the derivation in this section is valid for both closed channels and open channels. Therefore, at a later stage, the theory derived in this section can straightforwardly be applied to a bound state in the closed channel subspace by simply using the potential strength of the closed channel in the computation of the bound state energy.

3.5 Conclusion

In this chapter, the uncoupled two particle scattering problem has been analysed. The potential which has been used in this analysis corresponds to a delta potential, which was later contributed a finite range in momentum space named Λ. In order to implement this cut-off, constant form factors $|g\rangle$ were introduced to the potential. Using this form of the potential, the uncoupled T-matrix has been obtained. This transition matrix corresponds to the first term on the right hand side of equation 2.49. The obtained expression for this matrix has subsequently be used in order to derive relations for the background scattering length and the bound state energy. These equations will later be implemented in the full coupled-channels analysis of two particle scattering interactions.

Chapter 4

The coupled transition matrix

Having analysed the uncoupled transition matrix in the previous chapter, this chapter will focus on the effect of the coupling between two channels on the transition matrix as presented in equation 2.49. In doing so, the total model specific version of the coupled-channels T-matrix can be obtained. This T-matrix will then be used in further chapters in order to derive other important properties such as the scattering phase shift.

4.1 The coupled-channels potentials

As previously discussed in section 2.7, the coupled channel system consists of subspaces $\mathcal{P}$ and $\mathcal{Q}$. Combining these two subspaces, the total Hamiltonian can be written into the following matrix form:

$$\begin{pmatrix} \hat{H}_{PP} & \hat{H}_{PQ} \\ \hat{H}_{QP} & \hat{H}_{QQ} \end{pmatrix} = \begin{pmatrix} -\eta \left|g\right\rangle \left\langle g\right| + \hat{H}^0 & -\beta \left|g\right\rangle \left\langle g\right| \\ -\beta \left|g\right\rangle \left\langle g\right| & -\kappa \left|g\right\rangle \left\langle g\right| + C\mathbb{1} + \hat{H}^0 \end{pmatrix} \tag{4.1}$$

In the matrix equation as presented above, the separable form of the potential terms, which has been discussed in the introduction and the previous chapter, has been exploited. Furthermore, the factors η and κ have been used in order to indicate the strength of the open- and closed channels respectively, similarly to the notation which has been used in chapter 3. Apart from these factors, a strength β has been introduced in order to quantify the coupling strength between the two different channels.

Using the previously defined matrix, it is now possible to determine the full coupled T-matrix as defined by equation 2.49. In order to carefully study this matrix, the analysis of the different components of the T-matrix will be discussed in individual sections. In order to specify this division, the equation for the transition matrix is once more presented below:

$$\langle \chi_{out}|\hat{T}(E)|\chi_{in}\rangle = \langle \chi_{out}|\hat{T}_{uncoupled}(E)|\chi_{in}\rangle + \frac{\langle \phi_P^-|\hat{H}_{PQ}|\phi_Q\rangle \langle \phi_Q|\hat{H}_{QP}|\phi_P^+\rangle}{E - (\epsilon_Q + C) - \langle \phi_Q|\hat{H}_{QP}\frac{1}{E^+ - \hat{H}_{PP}}\hat{H}_{PQ}|\phi_Q\rangle}. \tag{4.2}$$

The purple part of equation 4.2 has been calculated in the previous chapter and represents the uncoupled part of the total coupled-channels T-matrix. In the next section, the orange part of the previous equation will be analysed. Then, the blue part will be discussed in section 4.3. After having analysed these two components, the outcome will be combined and used in section 4.4 in order to obtain the final expression for the coupled-channels T-matrix.

4.2 Finding an expression for $\langle \phi_p^- | \hat{H}_{PQ} | \phi_Q \rangle \langle \phi_Q | \hat{H}_{QP} | \phi_p^+ \rangle$

In this section, the orange term as presented in equation 4.2 is investigated. However, it is possible to simplify this analysis by realizing that the two different components correspond to[1] $\langle \phi_Q | \hat{H}_{QP} | \phi_P^+ \rangle^2$, as the operator $\hat{H}_{QP}$ equals the operator $\hat{H}_{PQ}$. Using this information, it suffices to solely analyse the term $\langle \phi_Q | \hat{H}_{QP} | \phi_P^+ \rangle$ instead of the whole orange component as presented in equation 4.2. In order to compute this component, it is projected onto a momentum space basis, resulting in the following integral equation:

$$\langle \phi_Q | \hat{H}_{QP} | \phi_P^+ \rangle = \iint \langle \phi_Q | \mathbf{p} \rangle \langle \mathbf{p} | \hat{H}_{QP} | \mathbf{p}' \rangle \langle \mathbf{p}' | \Psi_{\mathbf{p}",z} \rangle \, d\mathbf{p} d\mathbf{p}'. \tag{4.3}$$

Substituting the expression for $\hat{H}_{QP}$ as presented in equation 4.1 into the previous integral equation and realizing that $\hat{H}_{PQ}$ produces an eigenstate in the momentum space basis, the following equivalent equation can be obtained:

$$\langle \phi_Q | \hat{H}_{QP} | \phi_P^+ \rangle = -\beta \iint \langle \phi_Q | \mathbf{p} \rangle \langle \mathbf{p} | g \rangle \langle g | \mathbf{p}' \rangle \langle \mathbf{p}' | \phi_P^+ \rangle \, d\mathbf{p} d\mathbf{p}'. \tag{4.4}$$

In order to compute the previous integral equation, the factors $\langle \phi_Q | \mathbf{p} \rangle$ and $\langle \mathbf{p}' | \phi_P^+ \rangle$ have to be analysed first.

The first of these factors, being $\langle \phi_Q | \mathbf{p} \rangle$ can be computed rather straightforward through the usage of equations B.1 and 3.17, as the state $|\phi_Q\rangle$ represents a bound state in the closed channel subspace. Using this equation, the factor $\langle \phi_Q | \mathbf{p} \rangle$ reduces to the following form:

$$\langle \phi_Q | \mathbf{p} \rangle = \langle g | X \frac{1}{\epsilon_Q - \hat{H}_0} | \mathbf{p} \rangle \, . \tag{4.5}$$

The factor X that is introduced in the previous equation corresponds to the normalization factor used in order to normalize the state $|\phi_Q\rangle$. This normalization factor is derived in appendix B. Apart from this, the energy ϵ_Q, which has been previously introduced in section 2.7 is used in order to describe the value bound state energy measured with respect to the closed channel asymptotic energy threshold.

The second term that needs to be analysed in more detail, being $\langle \mathbf{p}' | \phi_P^+ \rangle$ needs some special attention, as its analysis is not as straightforward as the investigation of the previous term. As a first step, we use equation 2.44 to represent the state $|\phi_p^+\rangle$. However, the denominator in this equation includes the term $\hat{H}_{PP}$, which both contains a kinetic energy component and a potential. In order to get rid of this potential term in the denominator, the equation has to be rewritten into a different form. In order to do so, the following relations have to be implemented:

1. $\hat{T}_{uncoupled} \, |\mathbf{p}\rangle = \hat{V}_P \, |\phi_P^+\rangle \, .$
2. $\hat{\Omega}(z) \, |\mathbf{p}\rangle = |\phi_P^+\rangle.$
3. $(z - \hat{H}_{PP}) \hat{\Omega}(z) = (z - \hat{H}_{PP}^0).$

Whereas the first two relations have been discussed in chapter 2, the third relation has been adapted from D.R. Levine [55]. Using these relations, the following derivation of the state $|\phi_P^+\rangle$ can be

[1] This equality only holds for real functions. All functions in these terms are real for negative energy values.

obtained:

$$\begin{aligned}(z-\hat{H}_{PP})\hat{\Omega}(z)\,|\mathbf{p}\rangle &= (z-\hat{H}^0_{PP})\,|\mathbf{p}\rangle\,,\\ (z-\hat{H}_{PP})\,|\phi^+_P\rangle &= (z-\hat{H}^0_{PP})\,|\mathbf{p}\rangle\,,\\ (z-\hat{H}^0_{PP}-\hat{V})\,|\phi^+_P\rangle &= (z-\hat{H}^0_{PP})\,|\mathbf{p}\rangle\,,\\ (z-\hat{H}^0_{PP})\,|\phi^+_P\rangle - \hat{T}_{uncoupled}(z)\,|\mathbf{p}\rangle &= (z-\hat{H}^0_{PP})\,|\mathbf{p}\rangle\,.\end{aligned} \tag{4.6}$$

Rearranging the last line, the following expression for $|\phi^+_P\rangle$ is found:

$$|\phi^+_P\rangle = |\mathbf{p}\rangle - \frac{1}{z-\hat{H}^0_{PP}}\tau(z)\,|g\rangle\,\langle g|\mathbf{p}\rangle\,. \tag{4.7}$$

In the previous equation, the separable form of the uncoupled T-matrix, which was introduced in section 3.2, has been implemented. In order to calculate the component $\langle\mathbf{p}|\phi^+_P\rangle$ the previous expression can straightforwardly be projected onto a momentum state $|\mathbf{p}\rangle$.

Now that the expressions for the factors $\langle\phi_Q|\mathbf{p}\rangle$ and $\langle\mathbf{p}|\phi^+_P\rangle$ have been analysed, it is possible to rewrite equation 4.4 into the following form:

$$\langle\phi_Q|\hat{H}_{QP}|\phi^+_P\rangle = -\beta\iint\langle g|X\frac{1}{\epsilon_Q-\frac{p^2}{2\mu}}|\mathbf{p}\rangle\,\langle\mathbf{p}|g\rangle\,\langle g|\mathbf{p}'\rangle\left[\langle\mathbf{p}'|\mathbf{p}"\rangle - \langle\mathbf{p}'|\frac{1}{z-\hat{H}^0_{PP}}\tau(z)|g\rangle\,\langle g|\mathbf{p}"\rangle\right]d\mathbf{p}d\mathbf{p}'. \tag{4.8}$$

Explicitly working out the integral form on the right-hand side of the previous equation results in the following equivalent expression:

$$\begin{aligned}\langle\phi_Q|\hat{H}_{QP}|\phi^+_P\rangle &= -\beta(4\pi)^2X\int_0^\Lambda\frac{p^2}{\epsilon_Q-\frac{p^2}{2\mu}}dp\left[\int_0^\Lambda\frac{\delta(p"-p')}{4\pi p"^2}g(\mathbf{p}")p'^2dp' - \int_0^\Lambda\frac{\tau(z)}{z-\frac{p'^2}{2\mu}}g(\mathbf{p}")p'^2dp'\right],\\ &= -\beta(4\pi)^2X\xi(\epsilon_Q)\left[\frac{g(\mathbf{p}")}{4\pi}-\tau(z)\int_0^\Lambda\frac{p'^2}{z-\frac{p'^2}{2\mu}}g(\mathbf{p}")dp'\right].\end{aligned} \tag{4.9}$$

The integral that remains in the previous equation corresponds to the same integral that has been analysed in section 3.2. Therefore, analogously to the analysis which has been carried out previously, equation 4.9 can be solved to yield the following set of equations:

$$\begin{cases}\langle\phi_Q|\hat{H}_{QP}|\phi^+_P\rangle = -\beta(4\pi)^2X\xi(\epsilon_Q)g(\mathbf{p})\left[\dfrac{1}{4\pi}-\tau(z)\xi(z)\right] & z\geq\dfrac{\Lambda^2}{2\mu}\vee z\leq 0, \qquad (4.10)\\ \langle\phi_Q|\hat{H}_{QP}|\phi^+_P\rangle = -\beta(4\pi)^2X\xi(\epsilon_Q)g(\mathbf{p})\left[\dfrac{1}{4\pi}-\tau(z)\zeta(z)\right] & 0\leq z\leq\dfrac{\Lambda^2}{2\mu}. \qquad (4.11)\end{cases}$$

The set of equations presented above can now be substituted into equation 4.2 and be used in any subsequent analysis.

4.3 Finding an expression for $\langle \phi_Q | \hat{H}_{QP} \frac{1}{z - \hat{H}_{pp}} \hat{H}_{PQ} | \phi_Q \rangle$

Now that the orange part of equation 4.2 has been analysed, this section will focus on the analysis of the blue part as presented in section 4.2. However, the analysis of this element entails the rather complicated factor $\frac{1}{E^+ - \hat{H}_{PP}}$. Similar difficulties were faced in the previous section in the analysis of the factor $\langle p | \phi_P^+ \rangle$. In that case however, no additional coupling terms $\hat{H}_{PQ}$ or $\hat{H}_{QP}$ were present in the matrix element. Due to this difference in form, an alternative approach will be used in this section with the goal to get rid of the denominator which includes the factor $\hat{H}_{PP}$. In order to apply this new approach, the following states are introduced:

$$|\chi\rangle = \hat{H}_{PQ} |\Psi_B\rangle , \tag{4.12}$$

$$|\tilde{\psi}\rangle = \frac{1}{z - \hat{H}_{PP}} |\chi\rangle , \tag{4.13}$$

$$|\tilde{g}\rangle = \hat{V}_{PP} |\tilde{\psi}\rangle . \tag{4.14}$$

Using the previous three expressions, it is possible to relate the states $|\chi\rangle$ and $|\tilde{\psi}\rangle$ as follows:

$$|\chi\rangle = (z - \hat{H}_{PP}) |\tilde{\psi}\rangle , \tag{4.15}$$

$$|\chi\rangle = (z - \hat{H}^0_{PP} - \hat{V}_{PP}) |\tilde{\psi}\rangle . \tag{4.16}$$

Applying the definition of the state $|\tilde{g}\rangle$ it is then possible to rewrite the previous expression as:

$$|\chi\rangle = (z - H^0_{PP}) |\tilde{\psi}\rangle - |\tilde{g}\rangle . \tag{4.17}$$

Next, solving equation 4.17 for $|\tilde{\psi}\rangle$ yields:

$$|\tilde{\psi}\rangle = \frac{1}{z - \hat{H}^0_{PP}} |\chi\rangle + \frac{1}{z - \hat{H}^0_{PP}} |\tilde{g}\rangle . \tag{4.18}$$

Upon multiplying the previous expression by a factor V_{PP}, using the definition of the T-matrix as presented by equation 2.31 and solving the previous equation for $|\tilde{g}\rangle$ it is then possible to obtain the next useful relation:

$$|\tilde{g}\rangle = \hat{T}_{uncoupled}(z) \frac{1}{z - \hat{H}^0_{PP}} |\chi\rangle . \tag{4.19}$$

After having carried out all previous steps, it is now possible to substitute expression 4.19 into equation 4.18, meaning that the denominator $(z - \hat{H}_{PP})^{-1}$ has successfully been eliminated from the initial equation and that the following final result has been obtained:

$$|\tilde{\psi}\rangle = \frac{1}{z - \hat{H}^0_{PP}} |\chi\rangle + \frac{1}{z - \hat{H}^0_{PP}} \hat{T}_{uncoupled}(z) \frac{1}{z - \hat{H}^0_{PP}} |\chi\rangle . \tag{4.20}$$

Comparing this expression to the definition of $|\tilde{\psi}\rangle$ as presented in equation 4.13 it then becomes clear that the denominator of the T-matrix as presented by the blue part of equation 4.2 can be successfully rewritten as:

$$\langle \phi_Q | \hat{H}_{QP} \left[\frac{1}{z - \hat{H}^0_{PP}} + \frac{1}{z - \hat{H}^0_{PP}} \hat{T}_{uncoupled}(z) \frac{1}{z - \hat{H}^0_{PP}} \right] \hat{H}_{PQ} | \phi_Q \rangle . \tag{4.21}$$

Whereas at first sight the previous equation might seem more complicated than the initial form of the denominator of the T-matrix, in reality the complexity has decreased, as equation 4.21 only

contains factors which have been analysed previously. Implementing this information, meaning that the separable form of the uncoupled T-matrix as presented in section 3.2 is applied, the closed channel bound state wave function $|\phi_Q\rangle$ as analysed in section 3.4 is used and the form of the coupling terms $\hat{H}_{PQ}$ and $\hat{H}_{QP}$ as defined by equation 12.3 is implemented, equation 4.21 can be written as:

$$\langle g|\frac{-\beta X}{\epsilon_Q - \hat{H}^0_{PP}}|g\rangle \left(\langle g|\frac{-\beta}{z-\hat{H}^0_{PP}}|g\rangle \langle g|\frac{X}{\epsilon_Q - \hat{H}^0_{PP}}|g\rangle - \langle g|\frac{\tau(z)}{z-\hat{H}^0_{PP}}|g\rangle \langle g|\frac{-\beta}{z-\hat{H}^0_{PP}}|g\rangle \langle g|\frac{X}{\epsilon_Q - \hat{H}^0_{PP}}|g\rangle \right). \tag{4.22}$$

Projecting the previous equation onto a momentum space basis and once more implementing the definitions of the functions $\xi(z)$ and $\zeta(z)$ as introduced in equations 3.10 and 3.11, the following final solution branches for the factor $\langle \phi_Q|\hat{H}_{QP}\frac{1}{z-\hat{H}_{pp}}\hat{H}_{PQ}|\phi_Q\rangle$ can be found:

$$\begin{cases} \langle \phi_Q|\hat{H}_{QP}\dfrac{1}{z-\hat{H}_{pp}}\hat{H}_{PQ}|\phi_Q\rangle = (4\pi)^3\beta^2X^2\xi(\epsilon_Q)^2\xi(z)\left[1-4\pi\xi(z)\tau(z)\right] & z \geq \dfrac{\Lambda^2}{2\mu} \vee z \leq 0, \quad (4.23) \\ \langle \phi_Q|\hat{H}_{QP}\dfrac{1}{z-\hat{H}_{pp}}\hat{H}_{PQ}|\phi_Q\rangle = (4\pi)^3\beta^2X^2\xi(\epsilon_Q)^2\zeta(z)\left[1-4\pi\zeta(z)\tau(z)\right] & 0 \leq z \leq \dfrac{\Lambda^2}{2\mu}. \quad (4.24) \end{cases}$$

4.4 The expression for the coupled-channels T-matrix

Having analysed all relevant terms of equation 4.2 in both this chapter and the previous chapter, it is now finally possible to combine the results in order to obtain the following set of equations for the coupled-channels T-matrix:

$$\begin{cases} T_{coupled}(z,\mathbf{p},\mathbf{p}') = T^{first}_{uncoupled}(z,\mathbf{p},\mathbf{p}') + \dfrac{g(\mathbf{p})g(\mathbf{p}')(4\pi)^4\beta^2X^2\xi(\epsilon_Q)^2\left(\frac{1}{4\pi}-\tau(z)\xi(z)\right)^2}{z-(\epsilon_Q+C)-(4\pi)^3\beta^2X^2\xi(\epsilon_Q)^2\left(\xi(z)-4\pi\tau(z)\xi(z)^2\right)} & (4.25) \\ \qquad\qquad z \geq \dfrac{\Lambda^2}{2\mu} \vee z \leq 0, & \\ T_{coupled}(z,\mathbf{p},\mathbf{p}') = T^{second}_{uncoupled}(z,\mathbf{p},\mathbf{p}') + \dfrac{g(\mathbf{p})g(\mathbf{p}')(4\pi)^4\beta^2X^2\xi(\epsilon_Q)^2\left(\frac{1}{4\pi}-\tau(z)\zeta(z)\right)^2}{z-(\epsilon_Q+C)-(4\pi)^3\beta^2X^2\xi(\epsilon_Q)^2\left(\zeta(z)-4\pi\tau(z)\zeta(z)^2\right)} & (4.26) \\ \qquad\qquad 0 \leq z \leq \dfrac{\Lambda^2}{2\mu}. & \end{cases}$$

The term $T^{first}_{uncoupled}(z,\mathbf{p},\mathbf{p}')$ which is present in equation 4.25 corresponds to the uncoupled T-matrix as expressed by equation 3.12 whereas the term $T^{second}_{uncoupled}(z,\mathbf{p},\mathbf{p}')$ that is present in expression 4.26 corresponds to the uncoupled T-matrix as expressed by equation 3.13. From now on, the superscripts *first* and *second* will be omitted. It should however always be remembered that the proper solution branch has to be chosen based upon the value of the input parameter z. An inspection of the previous equation reveals that the usage of separable potentials has resulted in the formation of a separable expression for the coupled-channels transition matrix. Using this separable transition matrix, it is possible to inspect interesting properties of the two-particle interaction processes, such as the scattering length of an interaction and the dressed bound state energy of the coupled-channels system.

4.5 Conclusion

Through the separate analysis of the various terms of the coupled-channels T-matrix as presented by equation 4.2, it has become possible to find an expression for this matrix which describes the coupled-channels scattering problem using separable potentials with a finite cut-off Λ. This expression will be used throughout the rest of the report. It should be noted that the derived coupled-channels T-matrix is subjected to approximations which have been used in the Feshbach formalism. These approximations, which have been introduced in section 2.7 should always be kept in mind and be regarded as possible limitations of the model.

Chapter 5

Physical quantities and system parameters

Whereas the previous chapter has focussed on the derivation of the transition matrix, which effectively makes it possible to analyse scattering processes, the variables which have been used to obtain this expression have not yet been related to physical quantities. This chapter will focus on the relation of the thus far used system parameters to the relevant physical parameters. These physical parameters have been previously introduced in 1.1.1 and effectively describe the resonance position $\delta\mu B_0$, the resonance width $\delta\mu\Delta B$ and the background scattering length a_{bg} of the scattering process. In order to relate the system parameters such as the interaction strength κ and the potential strength η to these physical parameters, the approach as presented by S.Kokkelmans [25] will be closely followed in this chapter. Having derived the relation between the two parameter sets, the second part of this chapter will focus on the analysis of another relevant quantity, being the resonance strength parameter R^*, which can be derived using the introduced physical parameters. Before moving on to a new topic, the final part of this chapter will focus on the comparison of the phase shift which can be obtained using the newly derived physical parameter set and the phase shift which can be acquired using the expressions as derived in reference [25]. In this comparison, both scattering processes excluding and including an open channel resonance will be analysed.

5.1 The scattering matrix and physical quantities

In subsection 1.1.1 , the general behaviour of the scattering length for a coupled channel system has been presented in terms of the background scattering length a_{bg} and the magnetic field parameters B_0, B, and ΔB. As the scattering matrix is related to the scattering length as described in section 2.4, it is similarly possible to express the coupled-channels scattering matrix as presented by equation 2.50 in terms of these parameters. Subsequently, the obtained expression can be compared to the S-matrix which follows from the transition matrix as presented in section 4.4 and is expressed in terms of system parameters. Through carrying out this comparison, it should then be possible to relate the system parameters to the relevant physical parameters.

A previously stated, the first step in the comparison process is to rewrite the scattering matrix as presented by equation 2.50 in terms of physical parameters. However, in the process of carrying out this mapping, it is crucial to understand the physical effect of all different relevant terms that are present in equation 2.50. In order to gain this physical insight, the term $\langle\phi_Q|\hat{H}_{QP}(E^+ - \hat{H}_{PP})^{-1}\hat{H}_{PQ}|\phi_Q\rangle$ which is present in the denominator of equation 2.50 is inspected in some more detail. Instead of

getting rid of the term $(E^+ - \hat{H}_{PP})^{-1}$ that is present in this denominator, as was discussed in section 4.3, this factor is now expanded in terms of continuum states $|\phi_P^+(\epsilon)\rangle$ and bound states $|\phi_{P,n}\rangle$, similarly to the approach which has been followed to expand the factor $(E^+ - \hat{H}_{QQ})^{-1}$ in section 2.7. Carrying out this expansion results in the following outcome [56, 25]:

$$\frac{1}{E^+ - \hat{H}_{PP}} = \sum_n \frac{|\phi_{P,n}\rangle \langle\phi_{P,n}|}{E - \epsilon_{P,n}} + \int_{\epsilon_{threshold}}^{\infty} \frac{|\phi_P^+(\epsilon)\rangle \langle\phi_P^+(\epsilon)|}{E^+ - \epsilon} d\epsilon. \tag{5.1}$$

Contrary to the method that has been used to simplify the term $(E^+ - \hat{H}_{QQ})^{-1}$ in section 2.7, it is now not possible to neglect the continuum states that are present in the previous equation, as the threshold energy $\epsilon_{threshold}$, which corresponds to the asymptotic energy value of the open channel, is not sufficiently large compared to the scattering energy [56]. Due to the presence of this integral over the continuum states, there will be a value of the integral for which the denominator diverges. Similarly to the approach followed in section 3.2, this diverging character is avoided by integrating over the pole in the complex plane. This method effectively means that the integral is split up in an imaginary component which is calculated using complex function theorem and a principal value part named $\mathbb{P}$ which is real [54]. Combining the real parts of equation 5.1, the real part of the factor $\langle\phi_Q|\hat{H}_{QP}(E^+ - \hat{H}_{PP})^{-1}\hat{H}_{PQ}|\phi_Q\rangle$, which is named $\Delta_{res}(E)$ analogously to the notation in chapter four of reference [25], can be expressed as follows:

$$\Delta_{res}(E) = \sum_n \frac{\left|\langle\phi_Q|\hat{H}_{QP}|\phi_{P,n}\rangle\right|^2}{E - \epsilon_{P,n}} + \mathbb{P}\int_{\epsilon_{threshold}}^{\infty} \frac{\left|\langle\phi_Q|\hat{H}_{QP}|\phi_P^+(E)\rangle\right|^2}{E - \epsilon} d\epsilon. \tag{5.2}$$

Equation 5.2 effectively describes the amount with which the energy $\epsilon_Q + C$ [1] is shifted. This term will be analysed in the low energy regime in more detail later on in this section.

Having analysed the real part of equation 5.1, it is also possible to analyse the complex part of equation 5.1, which is named $\Gamma(E)$ analogously to the definition used in reference [25], resulting in the following outcome:

$$\Gamma(E) = 2\pi\left|\langle\phi_Q|\hat{H}_{QP}|\phi_P^+(E)\rangle\right|^2. \tag{5.3}$$

The previous equation can effectively be interpreted to add a width to the resonance. This width can be related to magnetic field properties in the low energy limit. However, before discussing this relation, it is important to notice the similarity in the form between equations 5.3 and the numerator in equation 2.50. Using this correspondence in form, it is possible to rewrite equation 2.50 as follows:

$$S(k) = S_P\left(1 - \frac{i\Gamma(E)}{E - (\epsilon_Q + C) - \Delta_{res}(E) + \frac{i}{2}\Gamma(E)}\right). \tag{5.4}$$

The previous equation shows the structure of the coupled channel resonance and can qualitatively be compared to the Feshbach resonance structure as presented by figure 1.2 in order to establish the following relations between the physical parameters and the system parameters:

$$\begin{aligned} \Gamma(E) &\sim \delta\mu\Delta B \\ \epsilon_Q + C + \Delta_{res}(E) &\sim \delta\mu(B - B_0) \end{aligned} \tag{5.5}$$

In order to find the exact relations corresponding to the previous two qualitative relations, equation 5.4 is analysed in more detail for both non-resonant open channel interactions and resonant open channel interactions in the following sections.

[1] Remember that the factor C was added to the bound state energy ϵ_Q in order to measure the energy with respect to the open channel threshold instead of the closed channel threshold

5.2 Non-resonant open channel interactions

With the goal to reduce the complexity of finding the relation between system parameters and physical parameters for the coupled channel system with a separable finite range interaction potential, as a first step the open channel subspace is assumed to be non-resonant. This means that the background scattering length a_{bg} will not diverge for specific values of the wave number k.

Due to the unitary character of the S-matrix, which has been discussed in section 2.4, and the absence of a resonance in the open channel, it is possible to express the uncoupled part of the scattering matrix as presented by the term S_P in equation 5.4 as:

$$S = e^{-2ika_{bg}}. \tag{5.6}$$

In order to verify the correctness of the previously introduced expression, it can be seen that its definition is consistent with the definition of the scattering matrix in terms of the phase shift as presented in equation 2.22 and the effective range expansion of the phase shift in terms of the scattering length as presented by equation 2.24.

Substituting this expression for the uncoupled scattering matrix component S_P into equation 5.4, it is then possible to obtain the following expression for the total coupled-channels S-matrix:

$$S(k) = e^{-2ika_{bg}} \left(1 - \frac{4\pi\mu i\hbar k\Gamma(E)}{E - (\epsilon_Q + C) - \Delta_{res}(E) + \frac{i}{2}\Gamma(E)} \right). \tag{5.7}$$

Now, in the case of non-resonant open channel interactions, the resonant shift $\Delta_{res}(E)$ that is present in the previous equation is approximately constant[2] [25]. In that case, upon the inspection of the denominator of the previous equation, it can be deduced that the resonance energy shift, named ϵ_{res}, can be written as follows:

$$\epsilon_{res} = E - (\epsilon_Q + C) - \Delta_{res}. \tag{5.8}$$

Upon rewriting the energy E, which represents the kinetic energy of the incoming particle with a (relative) wave number k, in terms of this wave number, the following equivalent expression can be obtained:

$$\epsilon_{res} = \frac{\hbar^2 k^2}{2\mu} - (\epsilon_Q + C) - \Delta_{res}. \tag{5.9}$$

Equation 5.9 indicates how the resonance energy is dependent on a kinetic energy contribution and a contribution related to the shifted bound state energy ϵ_Q. It is this second contribution that can be varied through the variation of the external magnetic field strength. Since the asymptotic energy shift C is approximately linear in the magnetic field around the resonance position [57] and the bound state energy ϵ_Q and the resonance energy shift Δ_{res} are constant, it can be deduced that the previous equation can be rewritten into the following form:

$$\epsilon_{res} = \frac{\hbar^2 k^2}{2\mu} - \delta\mu(B - B_0). \tag{5.10}$$

The previous equation indicates that the combination of the resonance energy shift Δ_{res} and the closed channel bound state energy $\epsilon_Q + C$ measured with respect to the open channel threshold describe the energy shift [3] which is caused by the variation of the applied external magnetic field.

[2] The exact energy dependency of this term for the modelled system can be extracted from the real part of equation 4.21. In the ultra cold regime, where $k \to 0$, a Taylor series reveals that the zeroth order term in this series corresponds to the energy independent form as presented by the second term on the right hand side of equation 5.12.

[3] The term $\delta_m u(B - B_0)$ expresses an energy.

At zero interaction energies, the value of the external magnetic field $B = B_0$ corresponds to the occurrence of a resonance of the system. Furthermore, the differential magnetic moment $\delta\mu$, which has first been introduced in subsection 1.1.1, effectively characterizes the linear dependence of the asymptotic energy shift C in the system. Comparing the two alternative expressions for the resonance energy ϵ_{res}, the following relation can be deduced:

$$\delta\mu(B - B_0) = (\epsilon_Q + C) + \mathrm{Re}\left[\langle\phi_Q|H_{QP}\frac{1}{E^+ - H_{PP}}H_{PQ}|\phi_Q\rangle\right]. \tag{5.11}$$

Substituting the zero energy limit ($k \to 0$) [4] of equation 4.23 into the previous expression the previous equation reduces to the following analogous form:

$$\delta\mu(B - B_0) = (\epsilon_Q + C) - 2\mu\Lambda\left((4\pi)^3\beta^2X^2\xi(\epsilon_Q)^2\left[1 - \frac{2a_{bg}\Lambda}{\pi\hbar}\right]\right). \tag{5.12}$$

The importance of the previous equation should not be underestimated as it offers a handle between the tuning of system parameters and its effect on the experimentally used external magnetic field. The previous expression indicates that the open channel scattering length a_{bg}, the coupling strength β, the closed channel bound state energy ϵ_Q and the momentum space cut-off Λ all influence the position of the Feshbach resonance and the variation in the magnetic field can be simulated through the variation in the input parameter C. The effect of the coupling strength β on the character of the Feshbach resonance and the proper tuning of the momentum space cut-off Λ in order to reproduce experimentally relevant systems will be discussed in detail in chapter 6.

Knowing how the magnetic field is related to the system at hand, the next step is to determine how the resonance width $\delta\mu\Delta B$, which is indicated in figure 1.2 is related to the previously introduced parameter $\Gamma(E)$. In the zero energy limit and in the absence of open channel resonances, it can be proven that this term is constant [5]. Naming this constant $\tilde{C}$ and using equation 5.11, it is possible to rewrite equation 5.9 into the following form:

$$S(k) = e^{-2ika_{bg}}\left(1 - \frac{2i\tilde{C}k}{E - \delta\mu(B - B_0) + i\tilde{C}k}\right), \tag{5.13}$$

$$\text{with} \quad \tilde{C} = 2\pi\mu\hbar\Gamma(E) = 4\pi^2\mu\hbar\left|\langle\phi_Q|H_{QP}|\phi_P^+\rangle\right|^2. \tag{5.14}$$

Using equations 2.22 and 2.24 in order to calculate the scattering length a_s corresponding to the scattering matrix as presented by the previous equation, the following expression is obtained:

$$a_s = a_{bg} - \frac{\tilde{C}}{\delta\mu(B - B_0)}. \tag{5.15}$$

Comparing this expression for the scattering matrix to the form as presented by equation 1.1 then makes it possible to relate the parameter $\tilde{C}$ to the resonance width $\delta\mu\Delta B$, yielding the following result:

$$\tilde{C} = a_{bg}\delta\mu\Delta B. \tag{5.16}$$

Comparing equation 5.14 to the previous equation, the following relation can be established:

$$a_{bg}\delta\mu\Delta B = 4\pi^2\mu\hbar\left|\langle\phi_Q|H_{QP}|\phi_P^+\rangle\right|^2. \tag{5.17}$$

[4] As ultra cold collisions are being considered in the entire report, the wave number approaches a value of zero. A zeroth order approximation of this limit is used in this section in order to relate the system parameters to the physical parameters

[5] In reference [25], this parameter is said to be linear in k [57]. However, in the current situation, a momentum normalization has been used instead of a energy normalization. This difference in normalization results in a difference of the momentum dependency of the term Γ

Substituting equation 4.11 into the previous equation, it is possible to relate the system parameters to the physical parameters $a_{bg}\delta\mu\Delta B$, yielding the following outcome:

$$a_{bg}\delta\mu\Delta B = 4\pi^2\mu\hbar\cdot\beta^2(4\pi)^2X^2\xi^2(\epsilon_Q)\left[1-\frac{2\Lambda a_{bg}}{\pi\hbar}\right]^2. \tag{5.18}$$

Similarly to equation 5.12, equation 5.18 will prove to be of vital importance in the remainder of the report as it offers a handle to relate the system parameters to the experimental parameters.

In order to investigate the correctness of the previously found relations between system- and physical parameters, section 5.5 will focus on the comparison of the phase shift that can be obtained from equation 2.50 and equation 5.7, with the system parameter relations substituted in this second equation. However, before moving on to this analysis, the next section will focus on the inclusion of an open channel resonance in the scattering matrix in order to investigate how this alters the relations between system- and physical parameters.

5.3 Resonant open channel interactions

Whereas the previous section focussed on the specific case of Feshbach resonances where no resonant open channel interactions are present, this section will focus on the more general case where there is the possibility of having a bound state in the open channel with energy $\epsilon_P = -\frac{\hbar^2\kappa^2}{2\mu}$. For the sake of complexity, only a single bound state in the open channel will be considered to significantly affect the scattering process. Due to the presence of this bound state, it is no longer possible to express the uncoupled part of the S-matrix S_P as presented in equation 5.6. Instead, following J.J.Sakurai [49], the S-matrix with a pole at $k=\kappa$ can be expressed as follows:

$$S_P(k) = e^{-2ikr_0}\frac{\kappa-ik}{\kappa+ik}. \tag{5.19}$$

Similarly to equation 5.6, the parameter r_0 represents the non-resonant part of the background scattering length. The resonant contribution to the background scattering length on the other hand, is related to the position of the pole through the relation $a_P = 1/\kappa$. The total background scattering length a_{bg} related to this process corresponds to the sum of the non-resonant contribution r_0 and the resonant contribution a_P.

In order to compare the investigated system to the case of having a resonant open channel contribution, equation 3.15 is solved for the background scattering length, yielding the following result:

$$a_{bg} = \frac{4\pi^2\mu\hbar\eta}{8\pi\eta\mu\Lambda-1}. \tag{5.20}$$

The previous equation can subsequently be rewritten into a the following more suggestive form:

$$a_{bg} = \frac{\pi\hbar}{2\Lambda}\left[1+\frac{1}{8\pi\mu\eta\Lambda-1}\right]. \tag{5.21}$$

Whereas the first term in equation 5.21 cannot diverge, the second term in equation 5.21 will diverge for particular values of the parameters μ,Λ and η. Therefore, using this equation and using the knowledge that the total background scattering length is equal to the sum of the non-resonant contribution r_0 and the resonant contribution a_P, the following two expressions for these different

contributions can be obtained:

$$r_0 = \frac{\pi\hbar}{2\Lambda}, \tag{5.22}$$

$$a_p = \frac{\pi\hbar}{2\Lambda\left(8\pi\mu\Lambda\eta - 1\right)}. \tag{5.23}$$

Without going into the details, it can be proven that, using the introduced terms r_0 and a_P, it is possible to express the total coupled-channels scattering length a_s as: [25]

$$a_s = r_0 + a_p\left(1 - \frac{\delta\mu\Delta B_{res}}{\delta\mu(B - B_0)}\right). \tag{5.24}$$

Notice the presence of the term ΔB_{res} in the previous expression instead of the priorly used term ΔB. These two terms are related as follows:

$$\Delta B_{res} = \Delta B\frac{a_{bg}}{a_P}. \tag{5.25}$$

The reason for this new definition of the width ΔB is related to the definition of the resonance strength parameter R^* which will be discussed in the next section. Apart from this new definition, the relation between the system parameters and the physical parameters as represented by equations 5.12 and 5.18 remain unchanged. However, the presence of the open channel resonance will alter the scattering process, as the uncoupled part S_P of the total scattering matrix as represented by equation 5.4 is no longer expressed by equation 5.6 but instead needs to be expressed through the application of equation 5.19. The effect of the inclusion of this resonant pole on the phase shift will be investigated in more detail in section 5.5.

5.4 The resonance strength parameter R^*

An important parameter which will be used throughout the remainder of this report in order to characterize the interaction strength is the so-called resonance strength parameter R^*. The definition of this parameter in the case of non-resonant open channel interactions can be deduced from equation 5.13, which can be rewritten as follows:

$$S(k) = e^{-2ika_{bg}}\left(1 - \frac{2ik}{R^*k^2 - \frac{\delta\mu(B-B_0)}{\bar{C}} + ik}\right), \tag{5.26}$$

$$\text{with} \quad R^* = \frac{\hbar^2}{2\mu\delta\mu\Delta B a_{bg}}. \tag{5.27}$$

Upon inspection of 5.26 it can be seen that the resonance strength length-scale parameter R^* effectively quantifies the strength of the k^2 term in equation 5.26. Furthermore, using equation 5.27 and 1.1, it can be deduced that a small value of this parameter R^* corresponds to a *broad* resonance, whereas a large value of this parameter R^* corresponds to a *narrow* resonance. The effect of changing the value of this parameter on scattering interactions, both on a three-body and a many-body level, will be investigated in later chapters of this thesis. Without going into detail in this report, it

can be proven that the strength of the k^2 term in the scattering matrix including an open channel resonance can be quantified by the following new definition of the resonance strength parameter [5]:

$$R^*_{resonant} = \frac{\hbar^2}{2\mu\delta\mu\Delta B a_P}. \tag{5.28}$$

Comparing equation 5.28 to equation 5.27, it can be deduced that the parameters R^* and $R^*_{resonant}$ are related as follows:

$$R^* = \frac{a_P}{a_{bg}} R^*_{resonant}. \tag{5.29}$$

As it is desired to only use a single resonance strength parameter R^*, it is possible to, instead of redefining the resonance strength parameter for systems with an open channel resonance, redefine the magnetic field width ΔB as $\Delta B_{res} = \Delta B \frac{a_{bg}}{a_P}$. This definition has previously been used in equation 5.24 and will be subsequently be used in the analysis of the phase shift for a system which contains an open channel resonance.

5.5 The scattering phase shift δ_0

Whereas the scattering matrix that follows from the transition matrix as presented in section 4.4 has been derived without making any assumptions regarding the presence of bound states in the open channel, the scattering matrices which have been derived in this chapter have been derived with assumptions regarding the open channel structure. The goal of this section is to study the effect of these assumptions on the scattering matrix and to check the validity of the derived relations between the physical parameters and the system parameters through the comparison of phase shift expressions which can be obtained from the different expressions for the scattering matrix which have been derived in this chapter and the expression for the scattering matrix which can be derived from the transition matrix as presented in section 4.4.

In order to compare the expressions for the S-matrix for both the case where an open channel resonant state is absent and the case where a single open channel resonance is present to the general form of the scattering matrix which follows from the on-shell version of the transition matrix as presented in section 4.4, the solution which is valid in the range $0 \leq E \leq \frac{\Lambda^2}{2\mu}$ needs to be selected from this section and solved in the limit where $k \to 0$, as the low-temperature limit is being investigated. Using this solution and applying the relation between the scattering matrix and the transition matrix as presented by equation 2.20, the following expression can be obtained:

$$S(k) = 1 - 2ik \left(a_{bg} + \frac{4\pi^2(4\pi)^3\mu\hbar\beta^2 X^2 \xi(\epsilon_Q)^2 \left[1 - \frac{2a_{bg}\Lambda}{\pi\hbar}\right]^2}{\epsilon_Q + C - 2\mu\Lambda(4\pi)^3\beta^2 X^2 \xi(\epsilon_Q)^2 \left[1 - \frac{2a_{bg}\Lambda}{\pi\hbar}\right]} \right). \tag{5.30}$$

Using the relation between the scattering matrix and the phase shift as presented by equation 2.22, it is then possible to obtain the following expression for the phase shift:

$$\delta_0(k) = -\frac{i}{2}\ln\left[1 - 2ik \left(a_{bg} + \frac{4\pi^2(4\pi)^3\mu\hbar\beta^2 X^2 \xi(\epsilon_Q)^2 \left[1 - \frac{2a_{bg}\Lambda}{\pi\hbar}\right]^2}{\epsilon_Q + C - 2\mu\Lambda(4\pi)^3\beta^2 X^2 \xi(\epsilon_Q)^2 \left[1 - \frac{2a_{bg}\Lambda}{\pi\hbar}\right]} \right)\right]. \tag{5.31}$$

Similarly, through the application of equation 2.22, it can be proven that the phase shift in the absence of an open channel resonance $\delta_{0,nonres}$ and the phase shift in the presence of a single open

channel resonance $\delta_{0,res}$ can be expressed as follows [25]:

$$\delta_{0,nonres}(k) = -ka_{bg} - \text{Arg}\left[R^*k^2 + \frac{1}{a_s - a_{bg}} + ik\right], \tag{5.32}$$

$$\delta_{0,res}(k) = -kr_0 - \arctan\left[ka_P\right] - \text{Arg}\left[R^*k^2 + \frac{1}{a_s - a_{bg}} + \frac{ik}{1 + ika_P}\right]. \tag{5.33}$$

Using the relations between the system parameters and the physical parameters as presented by equations 5.12 and 5.18 in the previous expressions and rewriting the scattering length through the application of equation 5.24, the previous two equations can be expressed in terms of the system parameters. The resulting equations, which are rather lengthy, are presented in appendix D.

Now that the relevant expressions for the phase shift have been introduced, it is possible to compare the outcome of these expressions. The results which will be here are made dimensionless in terms of the cut-off Λ, as this parameter has not yet been tuned to match experimental values and therefore a suitable value is not yet known. The dimensionless quantities in terms of Λ are indicated by an overhead bar. Furthermore, a list of these dimensionless quantities is presented in appendix E. Using this dimensionless form, the figure below indicates the obtained results for the different expressions of the phase shifts as a function of $\bar{k}$[6] for various values of the background scattering length $\bar{a}_{bg}$.

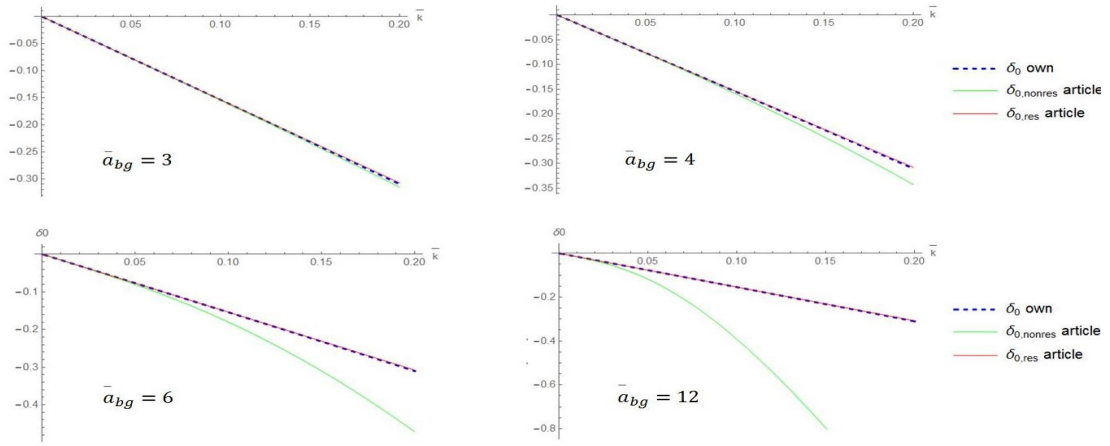

Figure 5.1: Phase shifts δ_0 (blue dashed line), $\delta_{0,res}$ (red solid line) and $\delta_{0,nonres}$ (green solid line) as a function of the wave number $\bar{k}$ for various values of $\bar{a}_{bg}$ for the following set of parameters: $\bar{\mu} = 0.5$, $\bar{\epsilon_Q} = -1$, $\bar{\beta} = 1$, $\bar{C} = 0$

Upon inspection of figure 5.1, it can be seen that, for small values of $\bar{k}$, the derived expression for the phase shift as presented in equation 5.31 matches the expression for the Feshbach resonance including a single open channel resonance contribution as presented in equation 5.33 for both smaller and larger values of the background scattering length a_{bg}, whereas the expression for the phase shift which excludes the presence of an open channel resonance as presented by equation 5.32 starts to deviate from the derived phase shift as presented by equation 5.31 for larger values of the background scattering length. This deviation is expected, as large and eventually diverging values of the background scattering length effectively mean that a (nearly) resonant bound state is present in the open channel subspace. Therefore, equation 5.7 is no longer valid.

The correspondence between all three expressions for small values of $\bar{a}_{bg}$ and the correspondence between the equations for δ_0 and $\delta_{0,res}$ for larger values of $\bar{a}_{bg}$ indicate that the found relations

[6]Remember that the expressions only hold in the limit $k \to 0$. Therefore, only small values of k are considered.

between the system parameters and the physical parameters which have been derived in this chapter correctly describe the expected behaviour of the system. Having found this correspondence, the relations between the system parameters and the physical parameters will be used throughout the remainder of the report.

Whereas the phase shift as presented in the previous figure does not include the presence of any resonance, the asymptotic energy shift $\bar{C}$ can be varied such that a resonance is found. The obtained results for various values of the shift $\bar{C}$ and a fixed value of the background scattering length are presented below:

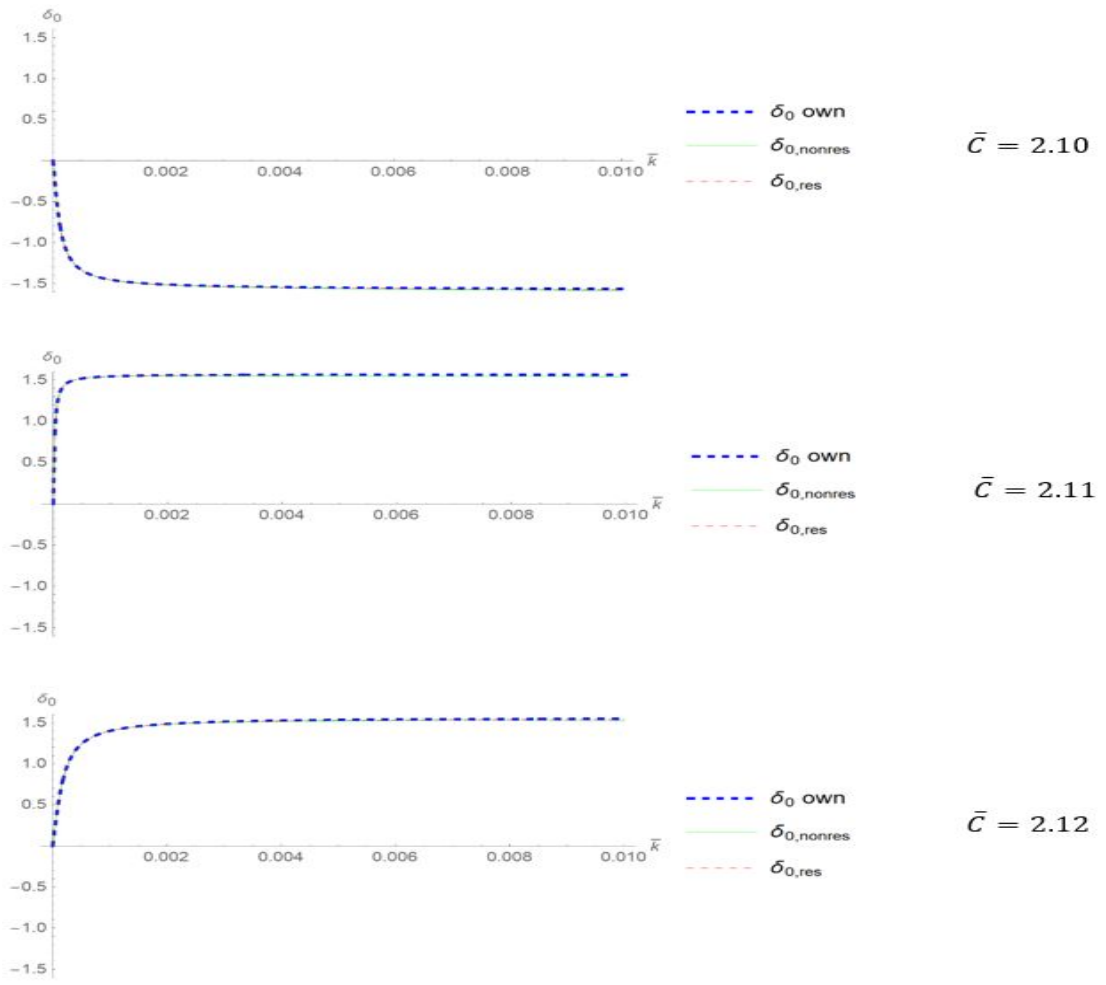

Figure 5.2: Phase shifts δ_0 (blue dashed line), $\delta_{0,res}$ (red solid line) and $\delta_{0,nonres}$ (green solid line) as a function of the wave number $\bar{k}$ for various values of the asymptotic energy shift $\bar{C}$ for the following set of parameters: $\bar{\mu} = 0.5$, $\bar{a}_{bg} = 3$, $\bar{\epsilon}_Q = -50$, $\bar{\beta} = 1$

As can be seen upon inspection of the results that are presented in figure 5.2, the presence of a resonance results in the phase shift decreasing to a value of $-\frac{\pi}{2}$ before a jump in the phase shift of a value of π occurs [7]. Substituting the value of $-\frac{\pi}{2}$ into equation 2.24, the equation reveals that, for this value of δ_0, the scattering length diverges to a value of $\pm\infty$. The sign of the divergence is related to the direction from which the value of $-\frac{\pi}{2}$ is approached. Upon inspection of figure 5.2 it can be

[7] This jump is a result of the domain of the cotangent function in mathematica. In mathematica, the function is defined on the domain $-\frac{\pi}{2} \leq \delta \leq \frac{\pi}{2}$

seen that the value of $-\frac{\pi}{2}$ is approached from above, meaning that, upon inspection of equation 2.24, the scattering length diverges to $+\infty$. Passing through the resonance crossing to the other side, the phase shift flips sign and starts to decrease from a value of $\frac{\pi}{2}$ to slightly smaller values. Substituting such a slightly smaller value than the value $\frac{\pi}{2}$ into equation 2.24 indicates that the scattering length diverges to $-\infty$. Comparing this diverging behaviour to figure 1.2 indicates that the observed behaviour of the phase shift corresponds to the expected behaviour of the scattering length for a Feshbach resonance. The previous figure therefore indicates, once more, that the obtained relations between the system parameters and the physical parameters are suitable to describe the physically expected behaviour of a coupled-channels system [8].

5.6 Conclusion

In this chapter, the system parameters which were used to describe the model in the previous chapters have been related to physical parameters. The values of these physical parameters can be extracted from experimental data [16]. This means that it is now almost possible to carry out simulations of the investigated model using physically relevant input data. All that remains is to calibrate the momentum space cut-off Λ in such a way that the expected atomic species specific behaviour is reproduced. This calibration will be investigated in the next chapter. As the relations between the two sets of parameters that have been derived in this chapter will be applied in the next chapter to obtain expressions for the scattering length and the bound state energy, an overview of the most important derived relations is presented in this section. Note that these relations only present suggestively rewritten versions of previously introduced equations and do not include any novel physics.

1. First of all, as previously introduced in chapter 3, the open channel potential strength η can be expressed as follows:

$$\eta = \frac{a_{bg}}{8\pi\mu\Lambda a_{bg} - 4\pi^2\mu\hbar}. \tag{5.34}$$

2. Next, using equations 5.27 and 5.18, the coupling strength β can be re-written in terms of the resonance strength parameter R^*, the background scattering length a_{bg} and the bare state closed channel binding energy ϵ_Q:

$$\beta = \sqrt{\frac{\hbar}{8\pi^2\mu^2(4\pi)^2X^2\xi(\epsilon_Q)^2\left[1-\frac{2\Lambda a_{bg}}{\pi\hbar}\right]^2 R^*}}. \tag{5.35}$$

3. Furthermore, as presented by equation 5.12 it is possible to identify a relation between the bound state energy $\epsilon_Q + C$ as measured with respect to the open channel asymptote on the one hand and the energy shift from the resonance position $\delta\mu(B - B_0)$ on the other hand:

$$\epsilon_Q + C = \delta\mu(B - B_0) + 2\mu\Lambda\left((4\pi)^3\beta^2X^2\xi(\epsilon_Q)^2\left[1-\frac{2a_{bg}\Lambda}{\pi\hbar}\right]\right). \tag{5.36}$$

   Substituting the expression for the parameter β as presented in equation 5.35 into equation 5.36, the following, equivalent, relation can be obtained:

$$\epsilon_Q + C = \delta\mu(B - B_0) + \frac{\hbar\Lambda}{\pi\mu R^*\left[1-\frac{2\Lambda a_{bg}}{\pi\hbar}\right]}. \tag{5.37}$$

[8] Similarly to before, small differences between the three expressions for the phase shift are related to the fact that the correspondence between the relations only hold in the limit $k \to 0$

Chapter 6

The dimer energy and cut-off calibrations

Having discussed all relevant scattering physics underlying the coupled-channels interactions between two identical particles in the previous chapters, it is now possible to analyse some physical properties of the system, such as the two body bound state energy, or *dimer energy*. As previously stated in section 3.4 it is possible to find bound states energies through the analysis of the pole of the transition matrix. Considering systems in which the open channel does not contain any bound state near the entrance energy, this reduces to investigating the pole of the coupled-channels part of the transition matrix as presented in equation 4.25. Using this transition matrix as an input, the first part of this chapter will focus on the derivation of the dimer energy E_{2b} in terms of both system parameters and physical parameters. Furthermore, the effect of the asymptotic energy shift C and the channel coupling strength β on the dimer binding energy will be discussed. Applying the derived relations for the dimer binding energy, it is then possible to express the scattering length a_s of the modelled system in terms of physical parameters.

Using the derived expressions for the scattering length and the dimer binding energy, the second part of this chapter will use these expressions in order to calibrate the momentum space cut-off Λ such that the expected physical behaviour which follows from full-coupled-channels calculations can be obtained. In this thesis, the cut-off calibration will be carried out for both Potassium-39 and Rubidium-85, as these atomic species will later be used in the many-body interaction analysis in chapter 13. The input parameters and the data points which are used in this chapter have been supplied by T.M.Secker [45]. In his work, the full coupled channel problem has been analysed, meaning that the Feshbach formalism has not been used and the closed channel continuum states have not been neglected. In the analysis carried out in this chapter, an approximative method is used in order to extract a constant value for the momentum space cut-off Λ. The reason for using this approximative method is the fact that using a constant value for Λ will greatly simplify the many-body analysis that will be carried out in chapter 13.

6.1 The dimer energy: System parameters

Having previously derived the coupled-channels transition matrix as presented in section 4.4, it is rather straightforward to find the pole of the coupled-channels part of this transition matrix. Selecting the solution branch corresponding to negative energies, the energy E_{2b} for which a pole is found and therefore a bound state is formed can be expressed as follows:

$$E_{2b} = (\epsilon_Q + C) + (4\pi)^3 \beta^2 X^2 \xi(\epsilon_Q)^2 \left(\xi(E_{2b}) - 4\pi\tau(E_{2b})\xi(E_{2b})^2\right). \tag{6.1}$$

Using the definition of the term $\tau(z)$, being $\tau(z) = -T_{uncoupled}/g(p)g(p')$ and substituting equation 3.12 into this relation, the previous expression can be rewritten into the following form:

$$E_{2b} = (\epsilon_Q + C) + (4\pi)^3\beta^2 X^2 \xi(\epsilon_Q)^2 \left(\xi(E_{2b}) + \frac{4\pi\eta\xi(E_{2b})^2}{1 + 4\pi\eta\xi(E_{2b})}\right). \tag{6.2}$$

Whereas the previous equation has been obtained without much difficulty, it is not yet sufficient to calculate the binding energy E_{2b} as a closer inspection of equation 6.2 reveals that the right hand side of the equation explicitly depends on the binding energy E_{2b}. Therefore, an alternative solving method has to be implemented in order to compute the binding energy.

As the previous equation contains the free parameter C, which can be tuned through the variation of the externally applied magnetic field, this parameter seems to be a logical choice to be used to find the dimer binding energy E_{2b}. Using this knowledge, a Matlab script has been written in which a grid with various negative values for the binding energies E_{2b} has been used as an input. Next, these energies are substituted in the previous equation and the value of C is calibrated such that the previous equation is satisfied. This calibration of C amounts to solving the previous expression for C, resulting in the following outcome:

$$C = E_{2b} - \epsilon_Q - (4\pi)^3\beta^2 X^2 \xi(\epsilon_Q)^2 \xi(E_{2b}) \left(1 + \frac{4\pi\eta\xi(E_{2b})}{1 + 4\pi\eta\xi(E_{2b})}\right). \tag{6.3}$$

Fixing the values for the potential strength η [1] and the bare closed channel bound state ϵ_Q whilst varying the dimer binding energy E_{2b} it is possible to obtain the following figure, in which the bound state energy has been plotted as a function of the asymptotic energy shift C for various values of the interaction strength β:

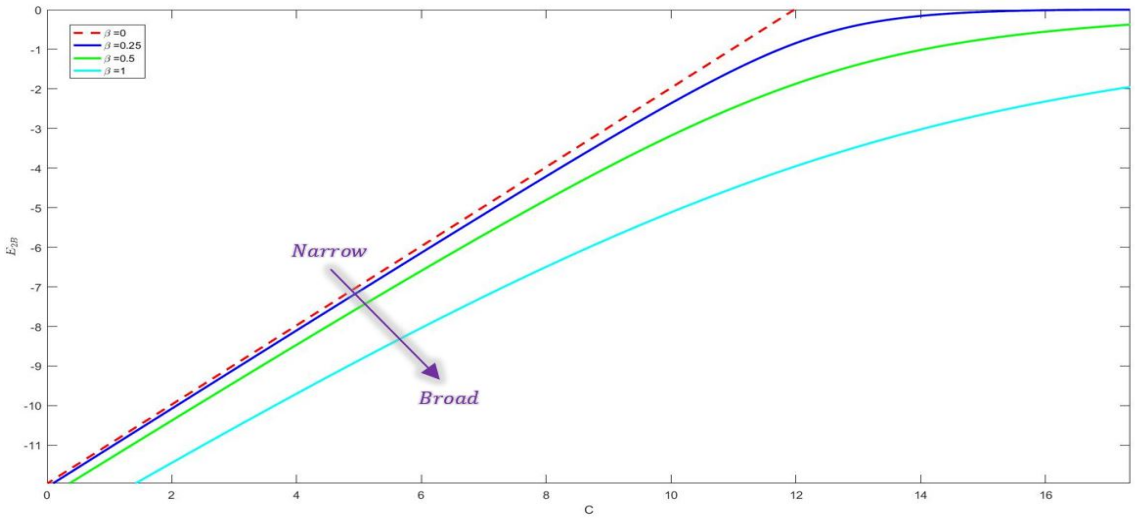

Figure 6.1: Dimer binding energy $\bar{E}_{2b}$ as a function of the asymptotic energy shift $\bar{C}$ for various values of the coupling strength $\bar{\beta}$ and the following set of parameters: $\bar{\mu} = 0.5$, $\bar{a}_{bg} = -1$, $\bar{\epsilon}_Q = -11.97$

As can be seen upon inspection of figure 6.1, an increase in the coupling strength β results in the bound state energy E_{2b} being pushed towards more negative values for a zero value of the asymptotic energy shift C. This is a result of the fact that an increase in the coupling strength β corresponds to an increase in the dressing of the binding energy E_{2b}. Therefore, the bound state, which now has a

[1] The value of the potential strength $\bar{\eta}$ follows from the value of $\bar{a}_{bg}$ through the application of equation 3.15

closed-channel *and* an open-channel contribution, is effectively pushed down towards deeper bound values.

Furthermore, upon increasing the value of the asymptotic energy shift C towards values where the dimer energy E_{2b} comes close to hitting the two-body scattering continuum, the relation between the asymptotic energy shift C and the dimer energy E_{2b} starts to deviate from its linear character. The point at which this deviation from the linear trajectory starts to occur decreases to smaller values of the asymptotic energy shift C for an increasingly large coupling strength β. In order to understand this increasingly large deviation, the relation between the coupling strength β and the width of the resonance ΔB as presented by equation 5.18 can be investigated. As indicated in this equation, the increase of the coupling strength β corresponds to an increase in the resonance width ΔB. This means that increasing the coupling strength β results in the formation of an increasingly *broad* resonance. This is indicated by the purple arrow in figure 6.1. Apart from this, an inspection of equation 6.2 reveals that the dimer energy E_{2b} reduces to the factor $\delta\mu(B - B_0)$ in the zero energy limit ($k \to 0$). Using this equivalence on one hand, and the equivalence between the coupling strength β and the resonance width ΔB on the other hand, it can be understood that the deviation of the curves in figure 6.1 from their linear trajectories for various values of the coupling strength reflects the increase of the resonance width analogously to the behaviour as observed in the behaviour of the scattering length as presented in figure 1.2 [2]. The equivalence between the behaviour observed in figures 1.2 and 6.1 is a first indication of the fact that the model is applicable in the investigation of the effect of the resonance width on the observed interactions. A more detailed investigation of the effect of the resonance width on three- and many-body interactions will be presented in chapters 9 and 13.

6.2 The dimer energy: physical parameters

Having analysed the dimer energy as a function of the system parameters, it is similarly possible to express the dimer energy in terms of physical parameters. Employing the relations between the system parameters and the physical parameters as presented in chapter 5 and using equation 6.2, it is possible to obtain the following expression for the dimer energy in terms of physical parameters:

$$\begin{aligned} E_{2b} =& -\frac{\hbar^2}{(a_s - a_{bg})mR^*} + \frac{2\hbar\Lambda}{\left(1 - \frac{2\Lambda a_{bg}}{\pi\hbar}\right) R^*\pi m} \\ &+ \frac{2\hbar\xi(E_{2b})}{\pi m^2 \left(1 - \frac{2\Lambda a_{bg}}{\pi\hbar}\right)^2 R^*} \left(1 - \frac{\xi(E_{2b})a_{bg}}{m\Lambda a_{bg} - \pi m\hbar/2 + a_{bg}\xi(E_{2b})}\right). \end{aligned} \tag{6.4}$$

Having expressed the dimer energy in terms of the scattering length a_s, it is straightforward to rewrite the previous expression such that the scattering length can be expressed in terms of the dimer energy, yielding the outcome as presented below:

$$\begin{aligned} a_s =& a_{bg} + \frac{\hbar^2}{mR^*} \left(-E_{2b} + \frac{2\hbar\Lambda}{\left(1 - \frac{2\Lambda a_{bg}}{\pi\hbar}\right) R^*\pi m} \right. \\ &\left. + \frac{2\hbar\xi(E_{2b})}{\pi m^2 \left(1 - \frac{2\Lambda a_{bg}}{\pi\hbar}\right)^2 R^*} \left(1 - \frac{\xi(E_{2b})a_{bg}}{m\Lambda a_{bg} - \pi m\hbar/2 + a_{bg}\xi(E_{2b})}\right) \right)^{-1}. \end{aligned} \tag{6.5}$$

[2] The scattering length diverges for $B = B_0$, or analogously, for $E_{2b} = 0$.

Now that the expressions for the dimer energy and the scattering length in terms of physical parameters have been obtained, it is possible to calibrate the cut-off Λ, such that the input of a dimer energy E_{2b} in equation 6.5 yields a value of the scattering length a_s which is consistent with theoretically expected values derived for a full coupled-channels model [20]. The calibration procedure which is applied in this analysis will be discussed in more detail in the next section.

6.3 Calibration method

As the many-body analysis is carried out near and at unitarity, only scattering lengths in the range $0 \leq \bar{a}/a_s \leq 0.1$, with $\bar{a} \approx 0.956 R_{vdw}$ [58] and R_{vdw} the van der Waals range are considered in finding a fixed value of the cut-off. In order to find this fixed value which results in the best correspondence with equation 6.5 in this regime, the expression for the scattering length is expanded up to the second order around $\hbar k \to 0$. This limit effectively corresponds to inspecting the low-energy regime of the scattering interactions, which is the limit we are interested in, as ultra-cold collisions are being investigated. Furthermore, equation 2.24 reveals that the scattering length is defined in this limit.

Applying the expansion $\hbar k \to 0$ to equation 6.5, the following expression for the inverse of the scattering length a_s can be obtained:

$$\frac{1}{a_s} = k + \left(\frac{R^*}{\hbar^2} - \frac{2}{\pi \Lambda \hbar} \right) \hbar^2 k^2. \tag{6.6}$$

As the wave number k is related to the energy E according to the relation $k = \frac{\sqrt{mE}}{\hbar}$, it is possible to use the supplied input data for E_{2b} in order to calculate the scattering length as presented by equation 6.6 for various values of the cut-off Λ. Next, through the comparison of the outcome of this equation to the supplied data points [45], it is possible to select the value of the cut-off which best resembles the input data for the scattering length. This analysis is carried out for both Potassium-39 and Rubidium-85 as presented in the following two subsections.

6.3.1 Cut-off calibration for Potassium-39

In order to calibrate the cut-off for Potassium-39, the following values have been used in the analysis:

Parameter	**Value**	**Unit**
R_{vdw}	64.61	a_0
$\bar{a}$	61.77	a_0
a_{bg}	-29	a_0
m	38.9637	u
R^*	29.41	a_0

Table 6.1: Values of the relevant system parameters for Potassium-39. The parameters are expressed in units of the Bohr radius a_0, with $a_0 = 5.29 \cdot 10^{-11}$m and in units of the atomic mass-unit, with $u = 1.6605402 \cdot 10^{-27}$kg. The parameters R_{vdw} and $\bar{a}$ have been added to the table as these parameters will be used to re-scale the axes in the figures which will be presented in this section.

Upon implementing the values as presented in the table above into equation 6.6, the following figure can be obtained:

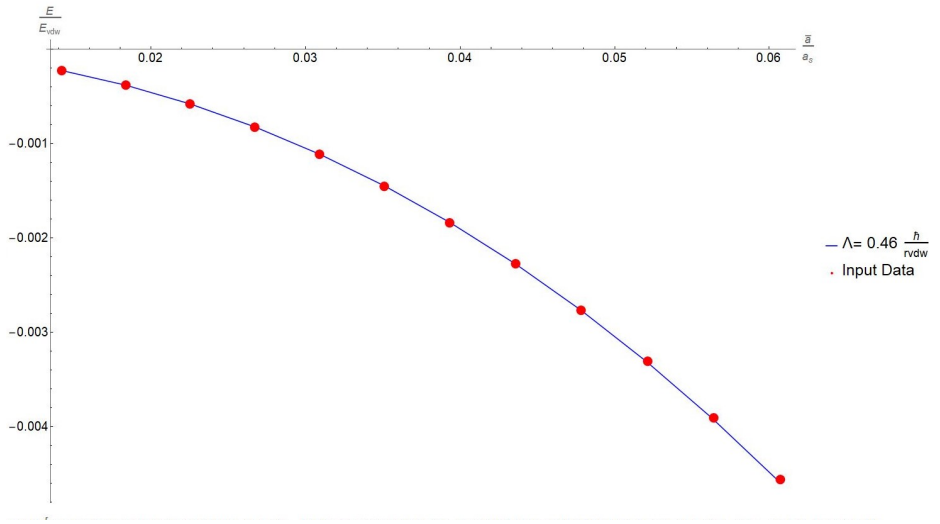

Figure 6.2: The rescaled dimer energy E_{2b}/E_{vdw}, with $E_{vdw} = \hbar^2/(mR_{vdw}^2)$, as a function of the rescaled inverse scattering length $\bar{a}/a_s$ following from the input data (red dots) and following from equation 6.6 (blue line)

As can be seen in the previous figure, the usage of a constant value of the cut-off Λ equal to $\Lambda = 0.46\hbar/R_{vdw}$ results in a good correspondence with the used input data points. As can be seen in appendix G.1, using this value of the cut-off, the difference between the input data points and the calibrated values does not surpass a relative difference of 0.4%. Motivated by this small relative difference, the constant value of $\Lambda = 0.46\hbar/R_{vdw}$ will be used in the many body simulations for Potassium-39.

6.3.2 Cut-off calibration for Rubidium-85

Completely analogous to the method which has been applied in the previous subsection, it is possible to carry out a cut-off calibration for Rubidium-85. In the analysis of this atomic species, the following input parameter values have been used:

Parameter	**Value**	**Unit**
R_{vdw}	82.1	a_0
$\bar{a}$	78.41	a_0
a_{bg}	-443	a_0
m	84.9	u
R^*	2.80	a_0

Table 6.2: Values of the relevant system parameters for Rubidium-85. The parameters are expressed in units of the Bohr radius a_0, with $a_0 = 5.29 \cdot 10^{-11}$m and in units of the atomic mass-unit, with $u = 1.6605402 \cdot 10^{-27}$kg.

Using the input data as presented in the previous table and implementing the calibration method as outlined in section 6.3, the following results can be obtained:

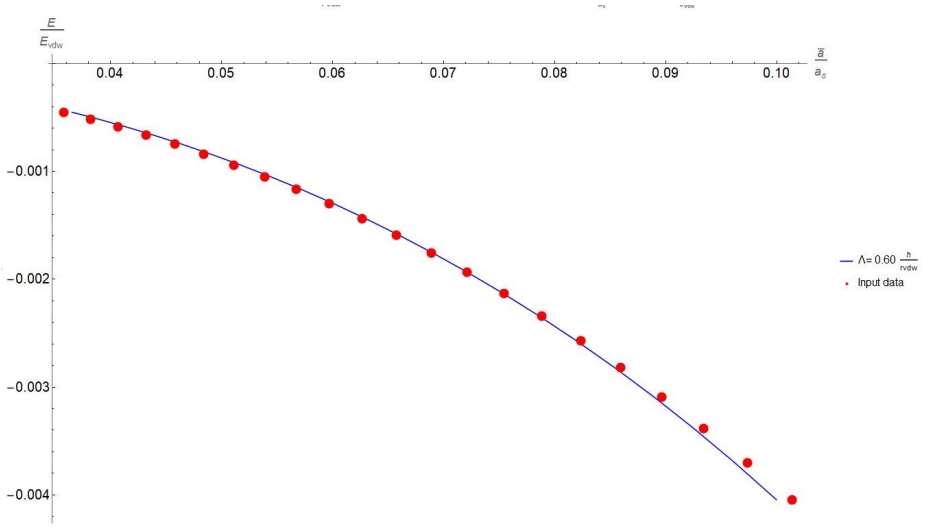

Figure 6.3: The rescaled dimer energy E_{2b}/E_{vdw} as a function of the rescaled inverse scattering length $\bar{a}/a_s$ following from the input data (green dots) and following from equation 6.6 (full lines) for various values of the cut-off Λ

Whereas a usage of a constant value of the cut-off still results in a good correspondence with the input data points, the comparison between the previous figure and figure 6.2 shows that the degree of correspondence has decreased. This is a result of the fact that the calibration for Potassium-39 has been carried out in the smaller regime $0 \leq \bar{a}/a_s \leq 0.06$, whereas the calibration for Rubidium-85 has been carried out in the regime $0 \leq \bar{a}/a_s \leq 0.1$. This difference in the regime size is a result of the fact that no input data point beyond $\bar{a}/a_s$ were supplied for Potassium-39, whereas these data points for Rubidium-85 were available. Despite the slightly less good correspondence, it is shown in appendix G.2 that the use of a cut-off value of $\Lambda = 0.6\hbar/R_{vdw}$, still agrees with the data points up to a maximum error between the calibrated value and the data points of $2,2\%$.

An interesting comparison with the calibrated value of the cut-off as presented by V.E.Colussi [21] and the cut-off value as calculated for Rubidium-85 can be made upon realizing that, as previously mentioned in section 1.1, increasingly broad resonances can be effectively modelled as a single channel system. Therefore, as the resonance that is investigated for Rubidium-85 is rather broad, also compared to the Potassium-39 resonance, which is also already quite broad[3], the calculated value of the cut-off starts to approach the expected value of the cut-off as derived from a single-channel analysis. As presented by V.E. [21], the single channel analysis yields a cut-off value of $\Lambda = \frac{2}{\pi}\hbar/\bar{a} \approx 0.6659\hbar/R_{vdw}$. Upon investigating even more broad resonances than the resonance of Rubidium-85, the cut-off is expected to asymptotically approach the single-channel cut-off value.

[3]The broadness of the Potassium-39 and the Rubidium-85 resonances will be discussed in more detail in chapter 9.

6.4 Conclusion

In this chapter, the dimer energy has been analysed in terms of both system parameters and physical parameters. During the analysis of the dimer energy in terms of system parameters, the effect of the asymptotic energy shift C and the coupling strength β has been investigated. This analysis revealed that an increase of the interaction strength results in the dimer energy being shifted towards more negative values. Furthermore, it was observed that an increase in the interaction strength results in an increased deviation from the linear relation between the dimer energy and the asymptotic energy shift. After having analysed these effects and having related them to the expected effect of the resonance width ΔB as introduced in section 1.1, the second part of the chapter focussed on the calibration of the cut-off Λ for Potassium-39 and Rubidium-85. In order to carry out these calibrations, the expression for the dimer energy in terms of physical parameters and the equation for the scattering length a_s have been applied. In the used calibration method, a constant value for the cut-off has been extracted. As the inspection of equation 6.5 reveals that the cut-off in fact varies as a function of the scattering length and the dimer energy, the calibrated constant value of the cut-off can only be used over a small range of scattering lengths. As the many-body simulations will be carried out near or at unitarity, the regime of investigated scattering lengths remains small. Therefore, the usage of a fixed value of the cut-off does not pose an issue and effectively simplifies the many-body analysis.

Part II

Three-body systems

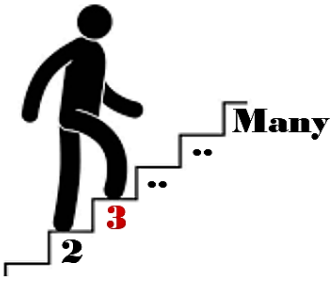

Chapter 7

Three-particle scattering theory

Having discussed the relevant two particle physics, a third particle will now be introduced to the analysis. In this chapter, the effect of the addition of this extra particle to the general scattering physics will be discussed. Fortunately, it is not necessary to start from scratch, as it will turn out that a large part of the theory which applies to two particle scattering can be adjusted to include a third particle. The theory that will be presented in this chapter will later be used in chapter 9 in order to obtain an Efimov spectrum, which have been previously discussed in the introduction. Furthermore, the three-body effects can be incorporated in the many-body analysis, meaning that three particle correlations can be included in the simulations, resulting in more physically realistic results. It should be noted that this chapter will only focus on the analysis of three-body bound states. The analysis could however be extended to include atom-dimer scattering states. However, this discussion is beyond the scope of this report and is thoroughly analysed in reference [14].

7.1 The Faddeev equation for three-body bound states

In order to find an expression for the three-body bound state,the three-body Schrödinger equation, which is defined as follows, has to be solved:

$$(\hat{H}^0 + \hat{V})\Psi = E\Psi. \tag{7.1}$$

Assuming that the three bosons are identical and only interact by pairwise forces, the potential operator $\hat{V}$ can be expressed as the sum of three different two-body interactions, meaning that $\hat{V}$ can be written as: $\hat{V} = \hat{V}_{12} + \hat{V}_{23} + \hat{V}_{31}$. The sub indices in this expression characterise the interactions in the different two-body subsystems. Using the explicit definition of V consisting of three different contributions and using the definition for the Green's function $\hat{G}^0(E) = (E - \hat{H}^0)^{-1}$, the three-body Schrödinger equation can be rewritten as follows:

$$\Psi = \hat{G}^0 \sum_{i=1}^{3} \hat{V}_i \Psi. \tag{7.2}$$

The index i in equation 7.2 refers to the particle which is absent in the two-particle sub system. Explicitly writing out the summation term in equation 7.2 results in the following expression:

$$\Psi = \underbrace{\hat{G}^0 \hat{V}_1 \Psi}_{\psi_1} + \underbrace{\hat{G}^0 \hat{V}_2 \Psi}_{\psi_2} + \underbrace{\hat{G}^0 \hat{V}_3 \Psi}_{\psi_3}. \tag{7.3}$$

The terms $\psi_{1,2,3}$ which have been introduced in the previous equations can be expressed in terms of Ψ, resulting in the following relations:

$$\begin{aligned}
\psi_i &= \hat{G}^0 \hat{V}_i \Psi, \\
&= \hat{G}^0 \hat{V}_i \sum_{i=1}^{3} \psi_i, \\
&= \hat{G}^0 \hat{V}_i \psi_i + \hat{G}^0 \hat{V}_i \sum_{i \neq j} \psi_j, \\
(1 - \hat{G}^0 \hat{V}_i)\psi_i &= \hat{G}^0 \hat{V}_i \sum_{i \neq j} \psi_j.
\end{aligned}$$

Upon introducing the operator $\hat{T}_i = (1 - \hat{V}_i \hat{G}^0)^{-1} \hat{V}_i$, the wave-function ψ_i can be expressed as follows:

$$\psi_i = \hat{G}^0 \hat{T}_i \sum_{i \neq j} \psi_j. \tag{7.4}$$

An analogous approach could be used in order to find expressions of the form of equation 7.4 for the other two-body subsystem component wave functions ψ_j and ψ_k. Expressing the relations for these three components in a matrix form then results in the following representation [46]:

$$\begin{pmatrix} \psi_1 \\ \psi_2 \\ \psi_3 \end{pmatrix} = \hat{G}^0(E) \begin{pmatrix} 0 & \hat{T}_1 & \hat{T}_1 \\ \hat{T}_2 & 0 & \hat{T}_2 \\ \hat{T}_3 & \hat{T}_3 & 0 \end{pmatrix} \begin{pmatrix} \psi_1 \\ \psi_2 \\ \psi_3 \end{pmatrix} \tag{7.5}$$

Upon inspection of the previous matrix system, it can be seen that the each individual component ψ_i depends on the other wave function components ψ_j and ψ_k. In order to get rid of this cross-dependency it is possible to use the symmetry of the wave functions, which follows from the fact that identical bosons are being considered. Exploiting the symmetry, the following permutation operators can be introduced:

$$\hat{P}_+ = \hat{P}_{ik} \hat{P}_{jk}, \tag{7.6}$$

$$\hat{P}_- = \hat{P}_{ij} \hat{P}_{jk}. \tag{7.7}$$

Using these permutation operators, it can be proven that each component ψ_i can be written as a function of itself as expressed below [59]:

$$\psi_i = \hat{G}^0(E) \hat{T}_i \left(\hat{P}_+ + \hat{P}_- \right) \psi_i. \tag{7.8}$$

Equation 7.8 is known as the *Faddeev equation* for three body bound states [46]. By projecting this function onto a momentum space basis, it is possible to extract information regarding the bound state wave function. The momentum space basis which is used in this analysis will be discussed in the next section.

7.2 The Jacobi coordinate system

Whereas the two-particle scattering system could be reduced to a relative momentum frame in which the single coordinate $\mathbf{p}$ fully quantified the system, this coordinate no longer suffices to describe the whole system once a third particle is added to the configuration. In order to describe the position of the third particle with respect to the center of mass of the two-particle subsystem, the additional coordinate $\mathbf{q}$ has to be introduced. The set of coordinates $\mathbf{p}$ and $\mathbf{q}$ now fully quantifies the three-particle system in momentum space. This set of coordinates is known as the momentum space *Jacobi* coordinate system and can be related to the single particle momenta $\mathbf{k}_i$ as follows[1][59]:

$$\mathbf{p}_i = \frac{1}{2}\left(\mathbf{k}_j - \mathbf{k}_k\right), \tag{7.9}$$

$$\mathbf{q}_i = \frac{2}{3}\left(\mathbf{k}_i - \frac{1}{2}\left(\mathbf{k}_j + \mathbf{k}_k\right)\right). \tag{7.10}$$

The usage of the dummy indices i, j and k in the previous equations signifies that three equivalent basis sets $|\mathbf{p}_1, \mathbf{q}_1\rangle_1$, $|\mathbf{p}_2, \mathbf{q}_2\rangle_2$ and $|\mathbf{p}_3, \mathbf{q}_3\rangle_3$ can be used in order to quantify the three-body system. These different basis sets are schematically represented in the following figure:

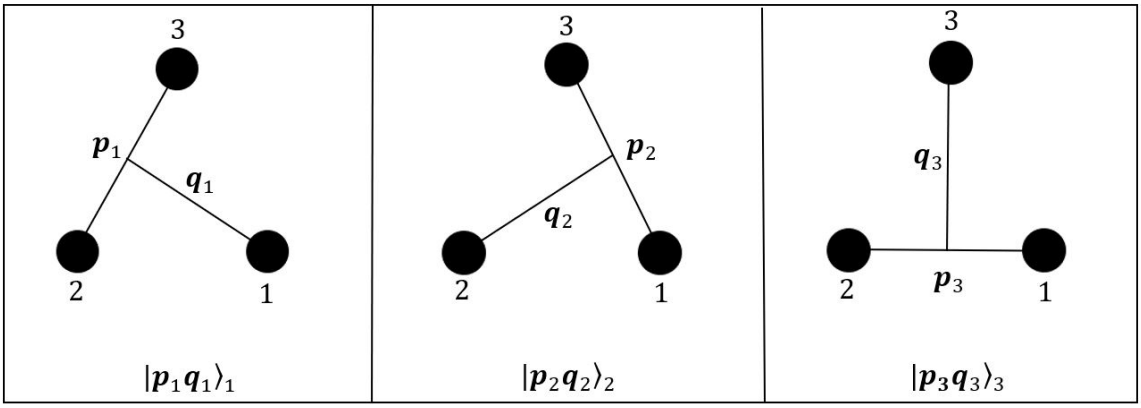

Figure 7.1: Schematic representation of the three different possible Jacobi coordinate systems.

As the three momentum states $|\mathbf{p}_1, \mathbf{q}_1\rangle_1$, $|\mathbf{p}_2, \mathbf{q}_2\rangle_2$ and $|\mathbf{p}_3, \mathbf{q}_3\rangle_3$ are equivalent, it suffices to use one of these states to quantify the momentum of the system. Therefore, the sub-indices used to define the momentum components can be omitted and we can define a momentum basis using the notation $|\mathbf{p}, \mathbf{q}\rangle = |\mathbf{p}, \mathbf{q}\rangle_i$. A full analysis of the Jacobi coordinate system is presented in appendix E.4 of the Master thesis of P.M.A. Mestrom [14].

[1]The expressions as presented below are valid for three-particle systems in which the three particles all have an equal mass.

7.3 Momentum space projection of the Faddeev equation

As equation 7.8 is equivalent for all three wave function components ψ_1, ψ_2 and ψ_3, it suffices to study a single component ψ_i and to extend the obtained result to all three wave function components. In this section, a general outline of the momentum projection of a single wave function component ψ_i will be discussed. More details of this projection procedure can be found in references [14, 59].

Projecting equation 7.8 onto a basis state $|\mathbf{p},\mathbf{q}\rangle$ as introduced in the previous section, the following expression can be obtained:

$$\begin{aligned}\langle \mathbf{p},\mathbf{q}|\psi_i\rangle &= \langle \mathbf{p},\mathbf{q}|\hat{G}^0(E)\hat{T}_i\left(\hat{P}_+ + \hat{P}_-\right)|\psi_i\rangle\,, \\ &= \int .. \int \langle \mathbf{p},\mathbf{q}|\hat{G}^0(E)|\mathbf{p}',\mathbf{q}'\rangle \langle \mathbf{p}',\mathbf{q}'|\hat{T}_i|\mathbf{p}'',\mathbf{q}''\rangle \langle \mathbf{p}'',\mathbf{q}''|\hat{P}|\mathbf{p}''',\mathbf{q}'''\rangle \\ &\qquad \langle \mathbf{p}''',\mathbf{q}'''|\psi_i\rangle\, d\mathbf{p}' d\mathbf{q}' d\mathbf{p}'' d\mathbf{q}'' d\mathbf{p}''' d\mathbf{q}.''' \end{aligned} \tag{7.11}$$

The previous equation can be solved through the usage of the following properties of the Green's operator $\hat{G}^0(E)$, the transition operator $\hat{T}_i$ and the perturbation operator $\hat{P} = \hat{P}_+ + \hat{P}_-$:

1. The projection of the Green's function $\hat{G}^0(E)$ onto the momentum basis spanned by states $|\mathbf{p}'\rangle$ and $|\mathbf{q}'\rangle$ yields the eigenvalues of the free evolution Hamiltonian H^0, as the Green's operator is diagonal in the momentum basis and the states $|\mathbf{p}'\rangle$ and $|\mathbf{q}'\rangle$ are eigenstates of the free evolution operator $\hat{H}^0$.

2. The transition operator T_i represents the two-body operator in the presence of a third particle i. Due to the presence of this third particle, the value z at which the system needs to be evaluated equals $z = E - \frac{3}{4m}q^2$. This can be understood from the new eigenvalue of the free evolution Hamiltonian operator $\hat{H}^0$ projected onto the momentum state $|\mathbf{p}'',\mathbf{q}''\rangle$ as presented below:

$$\hat{H}^0\,|\mathbf{p}'',\mathbf{q}''\rangle = E_{p'',q''}\,|\mathbf{p}'',\mathbf{q}''\rangle \tag{7.12}$$

   The energy $E_{p'',q''}$ can be expressed in terms of the coordinates $\mathbf{p}''$ and $\mathbf{q}''$. Upon using figure 7.1 and the analysis of the Jacobi coordinates as presented by P.M.A. Mestrom [14], the following result can be obtained:

$$\begin{aligned} E_{p'',q''} &= \frac{1}{2m}\sum_{i=1}^{3}\mathbf{P}_i = \frac{1}{2m}\left(|\mathbf{q}''|^2 + \left|\mathbf{p}'' - \frac{1}{2}\mathbf{q}''\right|^2 + \left|-\mathbf{p}'' - \frac{1}{2}\mathbf{q}''\right|^2\right), \\ &= \frac{1}{2m}\left(\frac{3}{2}q''^2 + 2p''^2\right). \end{aligned} \tag{7.13}$$

   Equation 7.13 indicates that the eigenvalue equation $\hat{H}^0\,|\mathbf{p}\rangle = \frac{p''^2}{2\mu}\,|\mathbf{p}''\rangle$ which was valid for the two-body analysis has been replaced with the eigenvalue equation $\hat{H}^0\,|\mathbf{p}'',\mathbf{q}''\rangle = \frac{1}{2\mu}\left(\frac{3}{4}q''^2 + p''^2\right)|\mathbf{p}'',\mathbf{q}''\rangle$. Therefore, in order to be able to still use the two-body coupled-channels T-matrix as presented in section 4.4, it is required to use a value of $z = E - \frac{3}{4}q^2$ as the evaluation point. This highlights the importance of having obtained the off-shell form of the T-matrix, as the three body analysis can now straightforwardly use this two-body off-shell T-matrix without having to re-derive a new transition matrix for the three-body analysis.

3. The application of the perturbation operator $\hat{P}$ onto a basis state $|\mathbf{p}'',\mathbf{q}''\rangle$ effectively results in a rotation of the particle indices as presented in figure 7.1. The exact effect of the application of the permutation operator on the Jacobi momentum states is well documented and can be found in, amongst others, references [14, 59]. The results as presented in these reference will be used in order to rewrite equation 7.11.

Using the properties of the Green's function $G^0(E)$, the transition operator $\hat{T}_i$ and the perturbation operator $\hat{P}$ as presented above, it can be proven that equation 7.11 can be expressed as follows [14]:

$$\langle \mathbf{p}, \mathbf{q} | \psi_i(E) \rangle = \int \frac{t_s \left(\mathbf{p}, \frac{1}{2}\mathbf{q} + \mathbf{q}''', E - \frac{3}{8\mu} q^2 \right)}{E - \frac{1}{2\mu} \left(q^2 + \mathbf{q} \cdot \mathbf{q}''' + q'''^2 \right)} \langle \mathbf{q} + \frac{1}{2}\mathbf{q}''', \mathbf{q}''' | \psi_i(E) \rangle \, d\mathbf{q}.''' \tag{7.14}$$

The factor $t_s \left(\mathbf{p}, \frac{1}{2}\mathbf{q} + \mathbf{q}', E - \frac{3}{8\mu}\mathbf{q}^2 \right)$ that has been introduced in the previous equation corresponds to the symmetrized two-body T-matrix and is defined as follows [14]:

$$t_s(\mathbf{p}, \mathbf{p}''', E) = \langle \mathbf{p} | T(E) | \mathbf{p}''' \rangle + \langle \mathbf{p} | T(E) | - \mathbf{p}''' \rangle = 2 \sum_{l=0, even}^{\infty} (2l+1) P_l(\hat{p}''' \cdot \hat{p}) t_l(\mathbf{p}, \mathbf{p}''', E). \tag{7.15}$$

The orbital angular momentum l which has been introduced in the previous equation corresponds to the momentum of the two-particle system with $r_{23} = r_2 - r_3$ and $\hat{l} = -i\hbar r_{23} \times \nabla_{23}$. In this thesis, we are looking for solutions where the total angular momentum $\vec{L}$ of the three-particle system equals a value of zero. The definition of this angular momentum $\vec{L}$ and the expansion of the function $\langle \mathbf{p}, \mathbf{q} | \psi_i(E) \rangle$ in terms of the relevant angular momentum states has been thoroughly analysed in reference [14]. Without going into the details of this derivation, the expansion of the function $\langle \mathbf{p}, \mathbf{q} | \psi_i(E) \rangle$ in terms of the two-particle angular momentum l is presented below:

$$\langle \mathbf{p}, \mathbf{q} | \psi_i(E) \rangle = \sum_{l=0}^{\infty} \sum_{m_l=-l}^{l} (-1)^l Y_l^{m_l}(\hat{p}) \bar{Y}_l^{m_l}(\hat{q}) \tilde{\psi}_l(p, q, E). \tag{7.16}$$

Considering ultra-cold collisions, the s-wave interactions which exist between the two particles will dominate the scattering process. In order to obtain a simple model representing the two body interactions, only these s-wave terms will be considered in this thesis. Whereas neglecting the higher order angular momenta terms is an approximation, in the case of a delta function potential only the s-wave scattering terms have a non-zero contribution to the scattering process. This can be understood upon the expansion of equation 3.2 in terms of spherical harmonics. However, it is important to note that in general the higher order angular momentum components cannot be neglected [14]. Nonetheless, as only s-wave interactions are considered in this thesis in order to obtain a simple model, equation 7.16 reduces to the following form:

$$\langle \mathbf{p}, \mathbf{q} | \psi_i(E) \rangle = \frac{1}{4\pi} \tilde{\psi}_0(p, q, E). \tag{7.17}$$

Next, upon using the fact that the only dependency of the function $\langle \mathbf{p}, \mathbf{q} | \psi_i(E) \rangle$ on the momentum $\mathbf{p}$ is contained in the constant form factor $g(p)$ which has previously been introduced in chapter 3, it is possible to express the factor $\tilde{\psi}_0(p, q, E)$ as $\tilde{\psi}_0(p, q, E) = g(p)\tilde{\psi}_0(q, E)$. Using this information and applying equations 7.17 and 7.14, the following expression can be obtained:

$$\tilde{\psi}_0(q, E) = - \int \frac{2\tau_{coupled}(E - \frac{3}{8\mu}q^2)}{E - \frac{1}{2\mu}(q^2 + \mathbf{q} \cdot \mathbf{q}' + q'^2)} g\left(\left| \frac{1}{2}\mathbf{q} + \mathbf{q}' \right| \right) g\left(\left| \mathbf{q} + \frac{1}{2}\mathbf{q}' \right| \right) \tilde{\psi}_0(q', E) d\mathbf{q}.' \tag{7.18}$$

The factor $\tau_{coupled}(E - \frac{3}{8\mu}q^2)$ which has been introduced in the previous equation is related to the coupled-channels T-matrix as $T_{coupled}(p, p', z) = -\tau_{coupled}(z) g(p) g(p')$, similarly to the definition of $\tau(E)$ which was introduced in chapter 3. Utilizing the connection between the previous equation and the two-body off-shell T-matrix as presented in section 4.4, equation 7.18 can be solved. In doing so, the three body bound states can be found. However, it should be noted that this solving procedure is not trivial. Instead, the equation needs to be numerically evaluated. The method followed to numerically analyse the previous expression is presented in the next chapter.

7.4 Conclusion

As presented in the previous section, it is possible to use the two-body T-matrix in the three-body analysis. This effectively means that it is not necessary to derive any new quantities and the previously introduced two-body relations provide sufficient information to analyse three-body bound states and to be able to generate the desired Efimov spectra. Therefore, without having to introduce any new theory, equation 7.14 can straightforwardly be implemented in Matlab. The numerical procedure followed to obtain the desired results is presented in the next chapter.

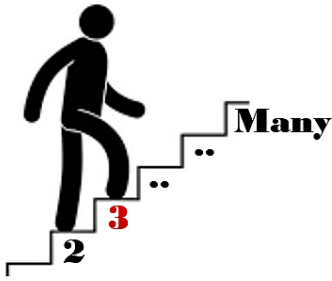

Chapter 8

Numerical model set-up

Using the theory which has been outlined in the previous chapter as a starting point, this chapter will focus on the numerical implementation method which is used in order to obtain the desired results. It should be noted that the numerical method as outlined in this chapter focusses on the analysis of non-resonant open channel interactions. This means that systems with large positive background scattering lengths cannot be investigated with the currently used code [1]. This is a result of the fact that systems with large background scattering lengths will have a pole in the uncoupled-channels part of the transition matrix. In the currently used code, this pole is not included and only the two-body bound state which has been analysed in chapter 6 is assumed to exist in the coupled-channels system. For the atomic species which we desire to evaluate, being Potassium-39 and Rubidium-85, the exclusion of the possibility to examine resonant open channel interactions does not present a problem, as both species have a negative background scattering length and therefore don't contain a bound state in the background channel.

8.1 The Nyström method and the Kernel

As mentioned in the previous chapter, it is sufficient to solve equation 7.18 in order to be able to analyse thee-body bound states. However, the solving procedure of this equation is not straightforward, as the right-hand side of equation 7.18 contains an integral which is explicitly dependent on the unknown function $\tilde{\psi}_0(q', E)$. In order to still be able to numerically analyse this integral equation, the Nyström method can be applied. This method involves the introduction of grids for the momenta variables q' and q with grid positions chosen according to a quadrature rule. Applying this method, it is possible to approximate the integral as a sum of the integrand values evaluated at the positions of the grid points q_i, weighed with a grid-point dependent weight w_i. This means that the integral can be approximated as follows:

$$\int_a^b f(q)dq = \sum_{i=1}^{N_q} w_i f(q_i). \tag{8.1}$$

The method which has been used in the previous expression to rewrite the integral in terms of a weighed sum is known as the *Nyström* method. The parameter N_q that has been introduced in this method represents the number of grid points and will be used as an input parameter in the numerical implementation such that an increase in the value of N_q corresponds to an increase in the accuracy of the calculations. As the form factors $g\left(\left|\frac{1}{2}q + q'\right|\right)$ and $g\left(\left|q + \frac{1}{2}q'\right|\right)$ which are present in equation 7.18 yield a value of zero for values of the momenta q and q' which surpass the cut-off Λ,

[1] The extension of the code to include resonant open channel interactions is beyond the scope of this report.

the grid does not need to include any point beyond this cut-off value. Furthermore, if it is desired to study higher Efimov states, which are located at smaller values of the momenta, the grid needs to be allocated an increased number of points for small momenta in order to be sufficiently sensitive. Motivated by the book of W.H. Press [60], a Gauss-Legendre quadrature is used in order to distribute the grid-points q_i and in order to determine their grid-position dependent weights. The grid-points q_i are set equal to the roots of the Legendre polynomial P_{N_q}, whereas their corresponding weights w_i are determined as follows [60, 15]:

$$w_i = \frac{2}{(1-q_i^2)(P_{N_q}(q_i))^2}. \tag{8.2}$$

It should be noted that the used Legendre polynomial P_{N_q} is defined on the domain $[-1, 1]$, whereas the integral equation which has to be solved is defined on the domain $[0, \infty)$. Therefore, the expressions for the grid points q_i and their weights w_i have to be transformed as follows:

$$q_{i,new} = \alpha \left(\frac{2}{q_i + 1} - 1 \right), \tag{8.3}$$

$$w_{i,new} = \frac{2\alpha w_i}{(q_i+1)^2}. \tag{8.4}$$

The parameter α which has been introduced in the previous two equations determines the spacing and the position of the quadrature points. This introduction of this parameter means that there are now two grid specific parameters which can be altered in order to change the grid, being the parameters α and N_q. These parameters can be tuned such that the calculations have converged. Following the suggestions made by R.M. Kroeze [15], the following values will be used as a default values [2]: $N_q = 400$ and $\alpha = 7 \cdot 10^{-3}$.

Having specified the used grid, and using the Nyström method as presented in equation 8.1, the integral equations for $\tilde{\psi}_0(\mathbf{q}, E)$ as introduced in the previous chapter can be expressed as follows:

$$\tilde{\psi}_0(q_i, E) = \sum_j K(q_i, q_j) w_{j,new} \tilde{\psi}_0(q_j, E). \tag{8.5}$$

Absorbing the weights $w_{j,new}$ into the newly defined matrix $\tilde{K}(q_i, q_j) = K(q_i, q_j) w_{j,new}$, the previous equation can be rewritten as follows:

$$\tilde{\psi}_0(q_i, E) = \sum_j \tilde{K}(q_i, q_j) \tilde{\psi}_0(q_j, E). \tag{8.6}$$

The introduction of the new matrix $\tilde{K}(q_i, q_j)$ has paid off, as the previous expression corresponds to an eigenvalue equation for the three-body bound state with an eigenvalue of 1. This means that non-trivial solutions to the previous equation can be obtained straightforwardly by solving the following expression:

$$\det\left(I - \tilde{K}\right) = 0. \tag{8.7}$$

The matrix $\tilde{K}(q_i, q_j)$ which has been introduced in order to find solutions for the three-body equation is more commonly referred to as the *Kernel* of the system. In order to find the expression for the Kernel, equation 7.18 will be rewritten in a form in which the angular integration over the polar angle ϕ has been carried out and the new variable $u = \cos(\hat{\mathbf{q}} \cdot \hat{\mathbf{q}}')$ has been used to rewrite the equation. The procedure of carrying out the angular integration and transforming to the new variable u is

[2] The convergence of the results using these parameter values has been verified

reported in appendix H and the final result is presented below:

$$\tilde{\psi}_0(q,E) = -4\pi \iint dq' du \frac{q'^2 \tau_{coupled}\left(E - \frac{3}{4m}q^2\right)}{E - \frac{1}{m}\left(q^2 + qq'u + q'^2\right)} g\left(\sqrt{\frac{1}{4}q^2 + q'^2 + uqq'}\right) g\left(\sqrt{\frac{1}{4}q'^2 + q^2 + uqq'}\right) \tilde{\psi}_0(q',E). \tag{8.8}$$

Replacing the integration over the variable u with a Riemann summation over $N_u = 2/du$ steps with step size du, the previous equation reduces to the following form:

$$\tilde{\psi}_0(q,E) = -4\pi du \int dq' \sum_{n=1}^{N_u} \frac{q'^2 \tau_{coupled}\left(E - \frac{3}{4m}q^2\right)}{E - \frac{1}{m}\left(q^2 + qq'u_n + q'^2\right)} g\left(\sqrt{\frac{1}{4}q^2 + q'^2 + u_n qq'}\right) g\left(\sqrt{\frac{1}{4}q'^2 + q^2 + u_n qq'}\right) \tilde{\psi}_0(q',E). \tag{8.9}$$

Next, by using the Nyström method as previously outlined and comparing equation 8.9 to equation 8.6, it can be deduced that the Kernel matrix element $\tilde{K}(q_i, q_j)$ is defined as follows [14]

$$\tilde{K}(q_i,q_j) = -4\pi du \sum_{n=1}^{N_u} \frac{q_j^2 dq_j}{E - \frac{1}{2\mu}(q_i^2 + q_i q_j u_n + q_j^2)} \tau_{coupled}\left(E - \frac{3}{8\mu}q_i^2\right) g\left(\sqrt{\frac{1}{4}q_i^2 + q_j^2 + u_n q_i q_j}\right) g\left(\sqrt{\frac{1}{4}q_j^2 + q_i^2 + u_n q_i q_j}\right). \tag{8.10}$$

Identifying the factors dq_j with the weights $w_{j,new}$, all ingredients which are required to find a solution to equation 8.7 are now known. This means that it is possible to calculate three-body bound states solutions and to obtain an Efimov spectrum. Some more details of the steps followed to obtain these results are presented in the following section.

8.2 Overview of the used numerical approach

In order to clarify the procedure which has been used in order to numerically obtain the desired three-body results, the following schematic overview which presents the main computational steps which need to be taken is presented below:

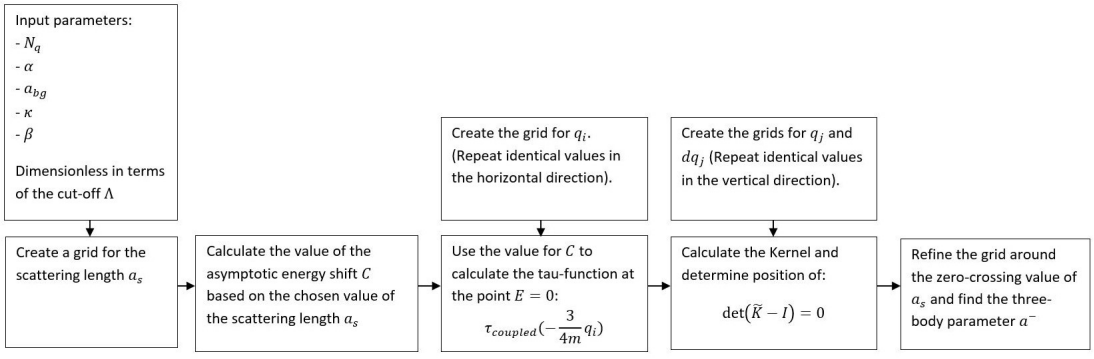

Figure 8.1: Schemtatic representation indicating the numerical procedure followed in order to obtain the value for the three body parameter a^-, which is the point where the three-body bound state hits the continuum.

As can be seen upon inspection of figure 8.1, the $\tau_{coupled}$ function which is present in the Kernel is evaluated around the point $E = 0$. This means that the point where the three-body bound state hits the three-body continuum is calculated if the method as described in the previous figure is followed. This point will from now on be referred to as the three-body parameter a^-. In order to obtain the entire Efimov spectrum, a similar procedure can be followed for different values of the energy. By calculating the three-body parameter a^- before calculating the entire spectrum however, it is possible to set a minimum value for a_s, as the values for the scattering length away from $E = 0$ needs to be larger than the value of the three-body parameter a^-. Furthermore, by calculating the dimer energy E_{2b} as a function of the scattering length a_s through the usage of equation 6.1, it is possible to also set a maximum value of the scattering length that needs to be investigated, as for larger values of the scattering length, a dimer state will form. By looking for multiple zero-crossings of equation 8.7 is possible to repeat the same procedure in order to obtain the spectra for higher Efimov states.

8.3 Conclusion

Using the theory as presented in this chapter, it is now possible to numerically investigate three-body bound states and to obtain an Efimov spectrum. A Gauss-Legendre grid has been used in order to numerically solve the integral equation as presented in expression 7.14. In order to refine the used grid, it is possible to vary the parameters α and N_q, which determine the grid spacing and the number of grid points respectively. However, the refining of the grid comes at a computational cost. Other numerical input parameters include the background scattering length a_{bg}, the closed channel potential strength κ and the coupling strength β. Using the mapping from system parameters to physical parameters as presented in chapter 5, the system could analogously be expressed in terms of physical parameters. The next two chapters will use the knowledge obtained in this chapter in order to analyse an Efimov spectrum and in order to investigate the effect of the width of a Feshbach resonance on the the three-body scattering physics.

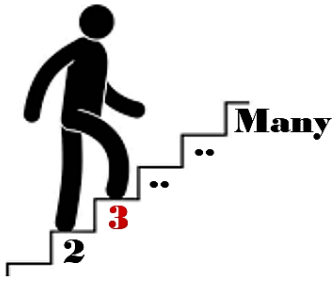

Chapter 9

Three-body results

Using the numerical method as described in the previous chapter it is possible to obtain Efimov spectra. In the first part of this chapter, a single Efimov spectrum will be analysed in detail. Other spectra could be obtained through the variation of the input parameters as mentioned in figure 8.1. The spectrum discussed in this chapter is set to have a negative background scattering length $\bar{a}_{bg}$, as the atomic species which we wish to analyse in the many-body code also have negative values for the background scattering length. Furthermore, by choosing negative values (or small positive values), it is possible to avoid any open channel resonance contributions, which cannot be properly analysed with the currently used code. For the sake of completeness, an additional Efimov spectrum with a small positive scattering length $\bar{a}_{bg}$ has been presented in appendix I in order to verify the applicability of the code for small positive background scattering lengths. After the analysis of the Efimov spectrum has been completed, the second part of this chapter will focus on the analysis of the effect of the resonance width on the observed three-body physics. In order to analyse this effect, the three-body parameter $\bar{a}_0^-$, which quantifies the point where the ground state Efimov trimer hits the three-body scattering continuum, is calculated for various values of the resonance strength parameter $\bar{R}^*$. The two different limits to this width parameter R^*, which describe narrow- and broad resonances, will be analysed in detail with the goal to understand if any universal relations between the three-body parameter and the resonance strength parameter exist. However, before being able to obtain the desired results and to interpret these results, the numerical method which has been applied in order to obtain the results will be discussed.

9.1 Analysis of an Efimov spectrum

Similarly to the two-body bound state analysis which has been presented in chapter 5, the results which will be presented in this section are dimensionless in terms of the cut-off Λ and the mass m. In the case of the Efimov spectrum which is presented in figure 9.1, the following set of input parameters has been used:

Parameter	Value
$\bar{a}_{bg}$	-1
$\bar{\epsilon}_Q$	-32.9
β	0.5

Table 9.1: Input parameters used to obtain the Efimov spectrum as presented in figure 9.1

Using equation 5.35 and implementing the parameter values as presented in the previous table, the resonance strength parameter $\bar{R}^*$ can be found to equal a value of $\bar{R}^* = 0.0181$. The effect of

the variation of this parameter will be discussed in more detail in the second part of this chapter. Upon using resonance strength parameter value as stated above and applying the values of the parameters as presented in table 9.1, it is possible to obtain an Efimov spectrum. In order to limit the computational cost, only the first five Efimov states have been calculated. The results of this computation are presented below:

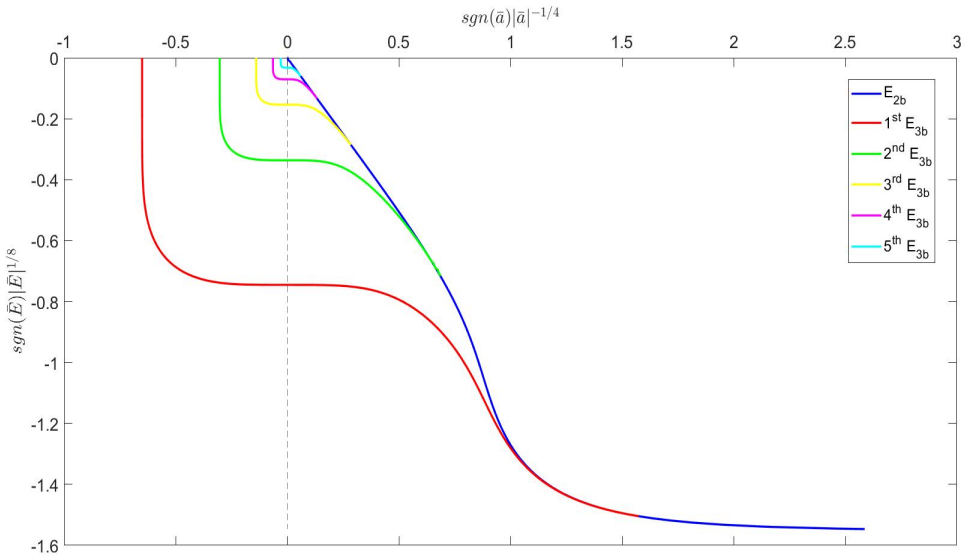

Figure 9.1: The first five Efimov states following from the set of input parameters as presented in table 9.1. The dark blue line corresponds to the dimer energy as calculated with the help of equation 6.2

Upon qualitatively inspecting figure 9.1, the results seem to show a correspondence with the expected behaviour of Efimov trimers as presented in section 1.3. The five Efimov trimers all emerge from the three-body continuum and live in the Borromean ring region, which was previously discussed in the introduction. Crossing from this region to the regime in which the scattering length is positive, the trimers eventually hit the particle-dimer scattering continuum. The dimer energy has been previously analysed in chapter 6. Motivated by the qualitative agreement between the expected Efimov spectrum and the obtained spectrum, it is possible to investigate the three-body parameters in order to establish a quantitative agreement. As these three-body parameters are expected to display universal scaling, as presented in section 1.3, they offer a good possibility to unveil any possible discrepancies between the expected an the obtained results. Using the spectrum as presented in figure 9.1, the three body parameters $\bar{a}^-$ and $\bar{\kappa}^*$, which have been introduced in section 1.3 have been extracted, yielding the following outcome:

Efimov state n	$\bar{\mathbf{a}}^-_{\mathbf{n}}$	$\bar{\kappa}^*_{\mathbf{n}}$	$\bar{\mathbf{a}}^-_{\mathbf{n+1}}/\bar{\mathbf{a}}^-_{\mathbf{n}}$	$\bar{\mathbf{a}}^-_{\mathbf{n}} \cdot \bar{\kappa}^*_{\mathbf{n}}$
0	-5.604	$0.30855 \pm 1.5 \cdot 10^{-4}$	21.32	-1.729
1	$-1.20 \cdot 10^2$	0.0128	22.39	-1.536
2	$-2.68 \cdot 10^3$	$5.6391 \cdot 10^{-4}$	22.67	-1.511
3	$-6.07 \cdot 10^4$	$2.4844 \cdot 10^{-5}$	22.69	-1.508
4	$-1.38 \cdot 10^6$	$1.0885 \cdot 10^{-6}$	–	-1.502

Table 9.2: Values of the extracted three-body parameters $\bar{a}^-_n$ and $\bar{\kappa}^*_n$ from the spectrum as presented in figure 9.1 and additional derived scalings

The third and the fourth columns in table 9.2 indicate that the expected universal scaling as pre-

sented in the introduction is observed for the higher Efimov states, whereas the ground-, and to a lesser extend, the first excited Efimov state show a deviation from the expected behaviour. This deviation can be contributed to the fact that the potential which has been used to obtain the spectrum is not truly zero-range [4]. As the universal scaling laws rely on the condition that the inequality $|a| >> r_0$ holds, as explained in the introduction, the theory breaks down for the ground state Efimov trimer and the first excited state trimer, as this condition is no longer abided by. For these trimers, the finite range effects of the potential are sufficiently strong to cause a break with the universal scaling law. Similar deviations from this universal scaling have been found and analysed extensively in literature [35, 61].

9.2 Analysis of the effect of the resonance width

Having obtained an Efimov spectrum and having verified the occurrence universal scaling in this spectrum, the second part of this chapter will focus on the analysis of the effect of the resonance width on the obtained Efimov spectrum. This effect is studied through the variation of the resonance strength parameter R^*, which is related to the resonance width as outlined in equation 5.27. As the value of this parameter is varied, the change in the value of the three-body parameter $\bar{a}_0^-$ is registered. The results of this analysis will be presented in the next section.

However, before moving on to the discussion of these results, the used numerical approach has to be analysed in more detail. Whereas all relevant equations needed to transform from system parameters to physical parameters have been previously analysed in chapter 5, a problem arises once we desire to analyse broad resonances. This problem becomes clear upon inspection of figure 6.1. As can be seen in this figure, an increase in the value of the interaction strength parameter β results in the value of the asymptotic energy shift C being pushed towards larger values before the bound state dimer hits the continuum. As an increasing value of the coupling strength parameter β corresponds to a decreasing resonance strength parameter R^* and an increasingly broad resonance, this means that the value of the asymptotic energy shift C can reach non-physically large values before the dimer energy hits the continuum. In order to avoid this problem, the system can be re-parametrised such that the asymptotic energy shift assumes a constant value C_0.

The re-parametrization procedure relies on the fact that the point where the two-body bound state hits the continuum corresponds to a divergence in the scattering length, which can be understood upon inspection of figure 6.1. Equation 1.1 reveals a similar divergence for a magnetic field value $B = B_0$. Applying this information to equation 5.37, the following expression for the value C_0 can be derived:

$$C_0 = -\epsilon_Q + \frac{\Lambda\hbar}{\pi\mu\left[1 - \frac{2\Lambda a_{bg}}{\pi\hbar}\right]^2 R^*}. \tag{9.1}$$

As can be understood upon inspection of equation 9.1, a changing value of the resonance strength parameter R^* for fixed values of the background scattering length a_{bg} needs to be compensated by a changing value of the closed channel bound state energy ϵ_Q such that C_0 remains constant. For the sake of clarity, the effect of the re-parametrisation on figure 6.1, in which the dimer energy was plotted as a function of the asymptotic energy shift C, is presented in figure 9.2.

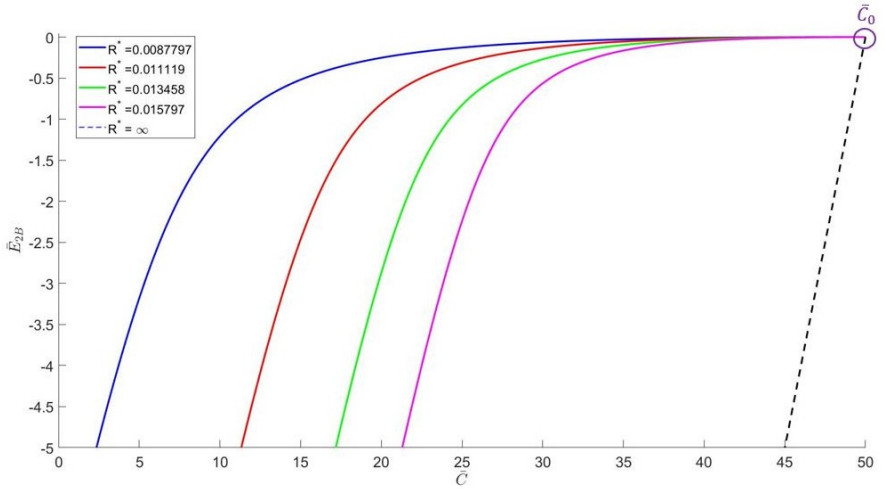

Figure 9.2: The dimer binding energy $\bar{E}_{2b}$ as a function of $\bar{C}$ for various values of $\bar{R}^*$ and fixed background scattering length $\bar{a}_{bg} = -1$. The bound state energy $\bar{\epsilon}_Q$ is altered in order to keep the parameter $\bar{C}_0$ as introduced in equation 9.1 constant.

Figure 9.2 indicates that the desired effect of the re-parametrisation procedure has been achieved. Using this novel approach, it is now possible to investigate the effect of the variation of the resonance strength parameter on the three-body parameter $\bar{a}_0^-$.

9.3 Results indicating the resonance width effect

Applying the method as outlined in the previous section, it is possible to calculate the value of the three-body parameter $\bar{a}_0^-$ for various values of the resonance strength parameter, resulting in the output as presented in figure 9.3.

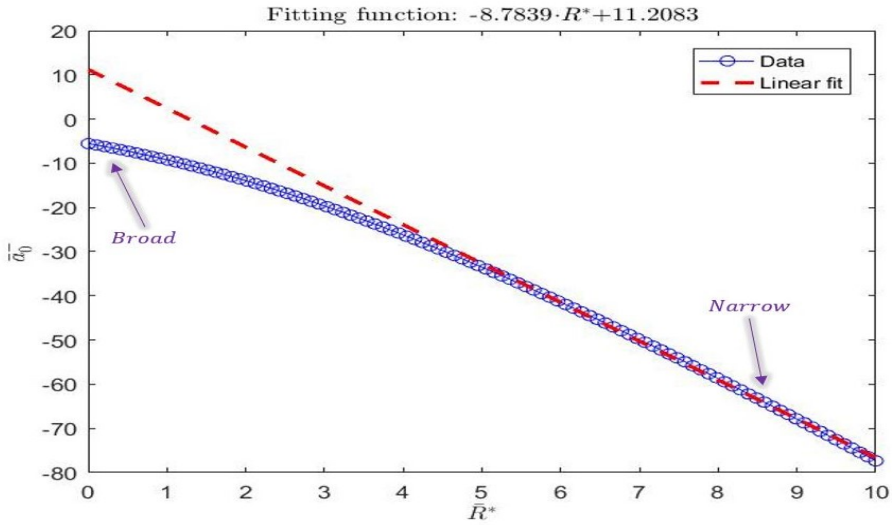

Figure 9.3: The three body parameter $\bar{a}_0^-$ as a function of the resonance strength parameter $\bar{R}^*$, for $\bar{a}_{bg} = -1$ and $\bar{C}_0 = 100$. A linear fit (red dashed line) has been added to the figure in order to indicate the linear dependency of the results for large values of $\bar{R}^*$.

Figure 9.3 indicates the existence of a linear relation between the resonance strength parameter R^* and the three body parameter $\bar{a}_0^-$ for narrow resonances. Upon decreasing the value of the resonance strength parameter R^*, meaning that the resonance width is increased, the curve starts to flatten out. In order to understand this relation in more detail, the dependency of the two-body T-matrix on the resonance strength parameter can be inspected, as this is the only part of the Kernel as presented by equation 8.9 which is a function of R^*. Therefore, once the relation between the T-matrix and the resonance strength parameter is known, the relation between the three body parameter and the resonance strength parameter $\bar{R}^*$ will also be known.

9.3.1 The coupled-channels T-matrix as a function of the resonance strength parameter

Using the expression for the coupled-channel T-matrix as presented in section 4.4, and using the relations between the system parameters and the physical parameters as presented in chapter 5, it is possible to obtain the following expression for the coupled-channels T-matrix:

$$T_{coupled}(E,\mathbf{p},\mathbf{p}') = T_{uncoupled}(E,\mathbf{p},\mathbf{p}') + \frac{g(\mathbf{p})g(\mathbf{p}')\frac{\hbar}{2\pi^2 m^2\left[1-\frac{2\Lambda a_{bg}}{\pi\hbar}\right]^2 R^*}\left(1-\frac{4\pi a_{bg}\xi(E)}{4\pi a_{bg}m\Lambda-2\pi^2 m\hbar+4\pi a_{bg}\xi(E)}\right)^2}{E+\frac{\hbar^2}{(a_s-a_{bg})mR^*}-\frac{\hbar\Lambda}{\left[1-\frac{2\Lambda a_{bg}}{\pi\hbar}\right]R^*\pi m/2}}$$

$$-\frac{g(\mathbf{p})g(\mathbf{p}')\frac{\hbar}{2\pi^2 m^2\left[1-\frac{2\Lambda a_{bg}}{\pi\hbar}\right]^2 R^*}\left(1-\frac{4\pi a_{bg}\xi(E)}{4\pi a_{bg}m\Lambda-2\pi^2 m\hbar+4\pi a_{bg}\xi(E)}\right)^2}{\frac{2\hbar\xi(E)}{\pi m^2\left[1-\frac{2\Lambda a_{bg}}{\pi\hbar}\right]^2 R^*}\left(1-\frac{4\pi a_{bg}\xi(E)}{4\pi a_{bg}m\Lambda-2\pi^2 m\hbar+4\pi a_{bg}\xi(E)}\right)}. \tag{9.2}$$

For small values of R^*, the terms in the previous equation that scale with $1/R^*$ will start to dominate over terms which are independent of R^*. Upon inspection of the previous equation, this means that the factor E which is present in the denominator of the second fraction can be neglected. After having neglected this term, it can be seen that all other terms in the second denominator scale with the same fraction $1/R^*$. Therefore, this factor will be cancelled out upon simplifying the fraction. This effectively means that the coupled T-matrix can then be viewed as independent of R^* for small values of R^*. As previously stated, the only factor that can possibly be dependent on the resonance strength parameter R^* in the Kernel is the two-body coupled T-matrix. Therefore, due to the fact that the T-matrix is independent of R^* for small values of R^*, the Kernel is also independent of R^* for small values of R^*. This explains the deviation from the linear trajectory in figure 9.3 for small values of R^*. Approaching the limit $R \to 0$, the slope of the curve will decrease towards a value of zero.[1]

In the case of large values of R^*, the analysis of the T-matrix becomes more complicated. This is a result of the fact that, despite R^* becoming large, factors that scale with $1/R^*$ can still have a large contribution to the overall T-matrix, as these terms also depend on other factors such as a_s, a_{bg} and the energy E. Therefore, it is not safe to neglect terms which scale with $1/R^*$ without considering the values of the other input parameters. However, in order to gain insight into the apparent linear relation between the three body parameter and the resonance strength parameter for large values of R^* , the transition matrix can be made dimensionless in terms of the resonance strength parameter R^* and plotted against the wave-number $\tilde{k}$ where the $\sim$ symbol indicates the usage of a wave number which is dimensionless in terms of R^*. So far, simulations have been carried out where the parameters were dimensionless in terms of Λ, which was indicated with the overhead

[1]The minimum value of R^* that is plotted in figure 9.3 is $R^* = 3.9 \cdot 10^{-3}$. Smaller values of R^* are excluded as these values would yield positive values for the bound state energy ϵ_Q, which can be understood upon inspection of equation 9.1.

bar symbol. In order to go from this dimensionless system to a system which is dimensionless in terms of R^*, the following relations can be applied:

$$\tilde{\tau} = \bar{\tau}\frac{\hbar}{\Lambda R^*}, \tag{9.3}$$

$$\tilde{k} = \bar{k}\frac{\Lambda R^*}{\hbar}. \tag{9.4}$$

Plotting $\tilde{\tau}$ as a function of $\tilde{k}$ for various values of R^*, the following figure can be obtained:

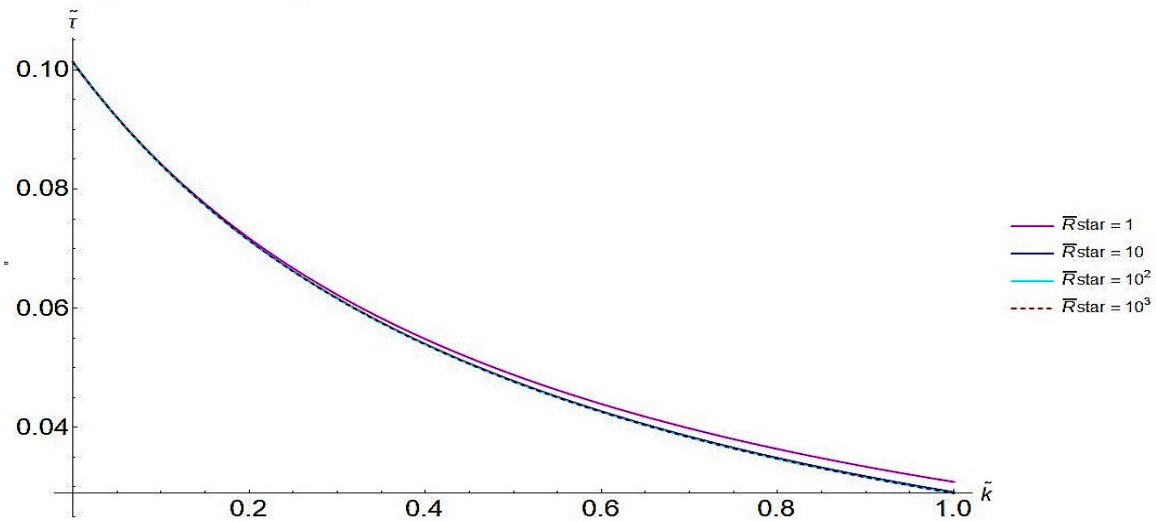

Figure 9.4: $\tilde{\tau}$ as a function of $\tilde{k}$ for various values of R^*. The following values were used: $\Lambda = 4$, $\hbar = 1$ and $\bar{a}_s = \frac{-2R^*\Lambda}{\hbar}$, $\bar{a}_{bg} = -1$

Figure 9.4 indicates that the $\tilde{\tau}$-function can be made independent of the resonance strength parameter for larger values of R^*. Upon inspection of figure 9.4, it becomes clear that this statement is already quite accurate for $R^* = 10$, as it can be seen that a change of R^* from a value of $R^* = 10$ to a value of $R^* = 100$ only results in a slight change in $\tilde{\tau}$. Using the information that $\tilde{\tau}$ becomes independent of R^* for larger values of R^* means that $\bar{\tau}$, which is related to $\tilde{\tau}$ according to the relation as described by equation 9.3, is linear in R^* for larger values of R^*. As previously stated, $\bar{\tau}$, and therefore the transition matrix, is the only part of the Kernel that depends on R^*. Therefore, a linear relation between $\bar{\tau}$ and R^* for large values of R^* indicates a linear relation between the three-body parameter $\bar{a}^-$ and R^* for large values of R^*. This is in correspondence with the results that have been presented in figure 9.3.

9.3.2 Interpretation of the results

Now that the relation between the three-body parameter and the resonance strength parameter has been investigated, it is possible to compare the obtained results with the expected behaviour of the three-body parameter dependency on the resonance width as presented in subsection 1.3.1. Similarly to the behaviour outlined in subsection 1.3.1, the three-body parameter as obtained through the numerical implementation of the coupled-channels model is independent of the resonance strength parameter R^* for small values of R^*. As small values of R^* correspond to broad resonances, these results are in correspondence with the single channel approach as presented in subsection 1.3.1 for which van der Waals universality was observed for the three-body parameter for broad resonances

[4]. As the modelled system does not involve a van der Waals type potential, the analogy in the correspondence should be taken only to the point that the interaction is universal in the range of the potential. This follows from figure 9.3 upon realizing that the three-body parameter has been made dimensionless in terms of the momentum space cut-off Λ. Therefore, using the relation between the dimensionless form of the scattering length and the cut-off as presented in appendix E, it follows that the three-body parameter derived in this thesis is universal in terms of the range of the potential, quantified by the value of the cut-off Λ.

Analogously to the process described in subsection 1.3.1, the universality of the three-body parameter in terms of the range is lost for increasingly narrow resonances. For these resonances, which correspond to large values of the resonance strength parameter R^*, the three-body parameter gains a linear dependency on the extra length scale R^*. Effectively, this parameter has replaced the potential range as the dependent length scale. Similar linear relations between the three-body parameter and the resonance strength parameter have been observed in references [4] and [5]. The correspondence with these articles indicates that the used coupled-channels model is capable of reproducing the expected behaviour of the three-particle system for broad- as well as narrow resonances.

9.4 Conclusion

In this chapter, it has been proven that the used coupled-channels model is capable of reproducing an Efimov spectrum which shows the expected universal behaviour as outlined in subsection 1.3.1. Furthermore, upon analysing the effect of the resonance width on the three-body parameter $\bar{a}_0^-$, it has been shown that the expected universal behaviour was observed for broad resonances. Apart from this, the model also showed the expected deviation of this universal behaviour for increasingly narrow resonances. Similar relations between the resonance strength parameter R^* and the three-body parameter as observed in other studies could be obtained with the used coupled-channels model. This indicates the usefulness of the coupled-channels approach for the analysis of scattering physics over a large range of resonance widths.

Part III

Many-body systems

Chapter 10

Many-body scattering physics

Knowing how to analyse two-and three-body scattering interactions, it is time to take a 'quantum' leap and move to the analysis of many particle systems. The goal of the first part of this chapter is to review the basic physics and analyse the used approximations which are necessary in order to gain an insight into the many-body system. The theory used in this chapter will prove to be quite different from the two- and three-particle scattering theory which has been discussed thus far. Mainly, this is a result of the lack of the possibility to unveil the many-body wave function, which will extend to large proportions and complexity for an increasing number of particles. Concepts such as the usage of second quantization and quantum field operators will be introduced in this chapter in order to tackle the many body scattering problem. All the introduced concepts are defined to describe a system which consists of indistinguishable bosons and exists at ultra-low temperatures such that the ground state is macroscopically occupied and a Bose-Einstein condensate exists.

Applying the introduced physical concepts, which are well documented in literature [62], the second part of this chapter will focus on the introduction of a many-body Hamiltonian that describes the coupled-channels interactions in an embedded environment. In the description of this many-body Hamiltonian, the second quantization format which has been described in the first part of the chapter will be applied. Furthermore, the Hamiltonian will be expressed in momentum space, using relative momentum coordinates reminiscent of the coordinates which have been used in the two- and three-body analysis.

Having specified the Hamiltonian, it will then be used in order to obtain the many-body equations of motion for a coupled-channels system consisting of an atomic condensate and excited state atoms that live in the open channel subspace and a molecular condensate that lives in the closed channel subspace. The equations of motion of these components, together with the equation of motion describing the correlation between excited state atoms, will then be used in the next chapter in order to verify whether the expressions which have been derived in this chapter are consistent with the previously derived two-body interaction equations.

10.1 Second quantization

Since the many-particle system that is considered in this report consists of identical bosons, the information which particle occupies a particular state is not relevant. Instead, it is more suited to quantify how many particles occupy a particular state. In other words: the relevant property of the many-particle system is contained in the occupation number n_i of a state i. Therefore, it is a logical choice to use an occupation number basis, or *Second quantization* representation in order to

describe a many-particle state, resulting in the following notation:

$$|\Psi\rangle = |n_1, n_2, ..n_a\rangle \,. \tag{10.1}$$

The space presented in the previous equation corresponds to the *Fock space* basis and will be used to describe the many-body state in the remainder of this report. Similarly to the textbook harmonic-oscillator problem, it is possible to introduce creation- and annihilation operators $\hat{a}_i^\dagger$ and $\hat{a}_i$ in order to describe a change in the occupation number of a Fock basis state i. Using these creation- and annihilation operators, it is also possible to introduce the number operator $\hat{n}_i = \hat{a}_i^\dagger \hat{a}_i$ which, as the name implies, returns the number of particles that exists in a state i once applied to a Fock state. Furthermore, the introduced operators can be used to express single-particle and two-particle operators in a second quantized form. The method followed in order to define these operators in this representation is presented in appendix K and the final results are presented below:

$$\hat{F} = \sum_{\alpha,\beta} \langle \beta | F | \alpha \rangle \, \hat{a}_\beta^\dagger \hat{a}_\alpha, \tag{10.2}$$

$$\hat{V} = \frac{1}{2} \sum_{\alpha,\beta,\gamma,\delta} \hat{a}_\alpha^\dagger \hat{a}_\beta^\dagger \, \langle \alpha\beta | V | \gamma\delta \rangle \, \hat{a}_\delta \hat{a}_\gamma. \tag{10.3}$$

The operator $\hat{F}$ that has been introduced in equation 10.2 corresponds to a single-particle operator such as the kinetic energy operator, whereas the operator $\hat{V}$ that has been introduced in equation 10.3 corresponds to a two-particle operator such as a two-body potential interaction. The descriptions of these operators in second quantized form will be applied in equation 10.34 in order to define the many-body Hamiltonian.

10.2 The quantum field operator and the Bogoliubov approximation

Using the second quantization representation that has been introduced in the previous section, it is possible to work in the momentum space representation similarly to the basis which has been used in the two- and three-particle analysis [62]. In doing so, it is possible to identify different number states with states that have different discrete momenta k. Subsequently, it is possible to apply a Fourier transformation in order to move from the momentum space representation in which the operators $\hat{a}^\dagger(\mathbf{k})$ and $\hat{a}(\mathbf{k})$ are defined to a position space representation. This results in the introduction of the *field operators* which are defined as follows [63, 62]:

$$\hat{\Psi}(\mathbf{r}) = \frac{1}{\sqrt{V}} \sum_{\mathbf{k}} e^{i\mathbf{k}\cdot\mathbf{r}} \hat{a}_{\mathbf{k}}, \tag{10.4}$$

$$\hat{\Psi}^\dagger(\mathbf{r}) = \frac{1}{\sqrt{V}} \sum_{\mathbf{k}} e^{-i\mathbf{k}\cdot\mathbf{r}} \hat{a}_{\mathbf{k}}^\dagger. \tag{10.5}$$

The factor V which has been introduced in the previous equations corresponds to the quantization volume. Both equations 10.4 and 10.5 effectively correspond to the product of a normalized single-particle wave function $\phi_k(\mathbf{r})$ multiplied by a annihilation- or creation operator. If the ground state of the system is a Bose-Einstein condensate living in the state with $k = 0$, the single-particle wave function simply reduces to the form $\phi_0 = 1/\sqrt{V}$ [64]. Using the fact that the macroscopic majority of all particles fall into this ground state, meaning that the number of particles in the ground state N_0 approaches the total number of particles N, it proves to be convenient to re-write the field operator

$\hat{\Psi}(\mathbf{r})$ [1] into the following form:

$$\hat{\Psi}(\mathbf{r}) = \phi_0 \hat{a}_0 + \frac{1}{\sqrt{V}} \sum_{k \neq 0} e^{i\mathbf{k}\cdot\mathbf{r}} \hat{a}_{\mathbf{k}}. \tag{10.6}$$

In order to simplify the previously introduced equation, we now apply the *Bogoliubov approximation* [65]. This approximation amounts to stating that the difference between the number of bosons in the ground state being N_0 and $N_0 - 1$ is negligible due to the macroscopic occupation number of this state. Therefore, the creation- and annihilation operators can effectively be replaced with the real number $\sqrt{N_0}$ as follows:

$$\hat{a}_0 |N_0, ..\rangle \approx \sqrt{N_0} |N_0, ..\rangle \rightarrow \hat{a}_0 = \sqrt{N_0}, \tag{10.7}$$

$$\hat{a}_0^\dagger |N_0, ..\rangle \approx \sqrt{N_0} |N_0, ..\rangle \rightarrow \hat{a}_0^\dagger = \sqrt{N_0}. \tag{10.8}$$

Using the previous two relations, equation 10.6 can be rewritten into the following form:

$$\hat{\Psi}(\mathbf{r}) = \sqrt{N_0}\phi_0 + \frac{1}{\sqrt{V}} \sum_{k \neq 0} e^{i\mathbf{k}\cdot\mathbf{r}} \hat{a}_{\mathbf{k}}. \tag{10.9}$$

Upon inspection of the previous equation, it can be seen that the first term on the right-hand side represents the wave function of the condensate, being $\Phi_0 = \sqrt{N_0}\phi_0$ which has an amplitude of $|\Phi_0|^2 = N_0$, with N_0 the number of particles in the condensate. Furthermore, the second term on the right hand side of this same equation can be regarded as a mere quantum fluctuation to the condensate wave function. This is a result of the fact that almost all particles exist in the ground state and therefore the term describing the excited state field operator contribution only slightly influences the overall outcome. Using this information, we now make another approximation, known as the *coherent state* approximation [66]. In order to understand the impact of this approximation, the expectation value of the previous equation is computed:

$$\langle \hat{\Psi}(\mathbf{r}) \rangle = \langle \Phi_0 \rangle + \left\langle \frac{1}{\sqrt{V}} \sum_{k \neq 0} e^{i\mathbf{k}\cdot\mathbf{r}} \hat{a}_{\mathbf{k}} \right\rangle. \tag{10.10}$$

The implementation of the coherent state approximation on the previous equation effectively amounts to neglecting the second term on the right hand side. This means that the quantum fluctuations around the condensate wave function are set to equal a zero value such that $\langle \hat{\Psi}(\mathbf{r}) \rangle = \langle \Phi_0 \rangle$.

10.3 Cumulant theory

Having applied the Bogoliubov approximation and the coherent state approximation to the field operator in the previous equation, it is now effectively possible to compute the wave function of the condensate through the calculation of the expectation value of the annihilation operator $\hat{a}_0$.

However, the coherent state approximation which has been used in the previous section only amounts to neglecting the expectation value of the excited state annihilation operator. This means that whereas the single particle expectation value $\langle \hat{a}_{\mathbf{k}\neq 0} \rangle$ is equal to zero, the expectation values of the two particle correlations $\langle \hat{a}_{\mathbf{k}\neq 0} \hat{a}_{-\mathbf{k}} \rangle_c$ and $\langle \hat{a}^\dagger_{\mathbf{k}\neq 0} \hat{a}_{\mathbf{k}} \rangle$ are non-zero [2]. The subscript c has been added to the previous expression in order to signify that only the expectation value of the correlation between the particles is computed, without calculating the product of the single particle expectation

[1] An analogous method can be used in order to express the creation field operator $\hat{\Psi}(\mathbf{r})^\dagger$

[2] Note that the expectation values are only non-zero for expressions in which the total momentum is conserved

values. Neglecting third- and higher order correlations, the following expressions for the correlation expectation values can be derived [66]:

$$\langle \hat{a}_0 \rangle_c = \langle \hat{a}_0 \rangle , \tag{10.11}$$

$$\langle \hat{a}_{\mathbf{k}\neq 0} \rangle_c = \langle \hat{a}_{\mathbf{k}\neq 0} \rangle = 0, \tag{10.12}$$

$$\langle \hat{a}_0 \hat{a}_0 \rangle_c = \langle \hat{a}_0 \hat{a}_0 \rangle - \langle \hat{a}_0 \rangle \langle \hat{a}_0 \rangle = 0, \tag{10.13}$$

$$\langle \hat{a}_{\mathbf{k}\neq 0} \hat{a}_{-\mathbf{k}} \rangle_c = \langle \hat{a}_{\mathbf{k}\neq 0} \hat{a}_{-\mathbf{k}} \rangle - \langle \hat{a}_{\mathbf{k}\neq 0} \rangle \langle \hat{a}_{-\mathbf{k}} \rangle = \langle \hat{a}_{\mathbf{k}\neq 0} \hat{a}_{-\mathbf{k}} \rangle , \tag{10.14}$$

$$\langle \hat{a}^\dagger_{\mathbf{k}\neq 0} \hat{a}_{\mathbf{k}} \rangle_c = \langle \hat{a}^\dagger_{\mathbf{k}\neq 0} \hat{a}_{\mathbf{k}} \rangle - \langle \hat{a}^\dagger_{\mathbf{k}\neq 0} \rangle \langle \hat{a}_{\mathbf{k}} \rangle = \langle \hat{a}^\dagger_{\mathbf{k}\neq 0} \hat{a}_{\mathbf{k}} \rangle . \tag{10.15}$$

The previously introduced expressions, which are referred to as the *cumulant* expressions, will prove to be of vital importance in the analysis of the many-body system. Whereas the importance of equation 10.11 in the determination of the condensate wave function has already been explained in the previous section, equations 10.14 and 10.15 will also prove to be useful.

Equation 10.14 describes the probability that two excited state particles with opposite momenta collide. These particles could subsequently redistribute their momenta or even decay to the condensate. Alternatively, two particles in the condensate could be excited to form a pair of two particles with opposite momenta. The physical effect of the term $\langle \hat{a}_{\mathbf{k}\neq 0} \hat{a}_{-\mathbf{k}} \rangle_c$, which is more commonly referred to as the anomalous density term $\kappa_{\mathbf{k}}$, will be studied in subsection 10.6.4 in order to be able to quantitatively describe the dynamics of the excited state particles. Next, equation 10.15 describes the number of excited state particles. This can be understood from the definition of the number operator $\hat{N}_{\mathbf{k}} = \hat{a}^\dagger_{\mathbf{k}} \hat{a}_{\mathbf{k}}$ [67]. Therefore, through the analysis of this term, which is more commonly referred to as the normal density term $\rho_{\mathbf{k}}$, it is possible to extract information regarding the amount of particles that are not in the condensate. It should be noted that in order for the Bogoliubov equation to hold, the value of the normal density term $\rho_{\mathbf{k}}$ should always stay small, such that only the state at $k = 0$ is macroscopically occupied [65].

10.4 Incorporating Feshbach-resonance theory

So far, the many-body system has been described in terms of an atomic condensate represented by the term $\langle \hat{a}_0 \rangle$, a normal density term $\rho_{\mathbf{k}}$ representing the number of excited state particles and an anomalous density term $\kappa_{\mathbf{k}}$ representing the collisions occurring between the excited state particles. However, all these quantities effectively live in a single channel. We have not yet analysed what happens if two particles collide and form a bound state, or what happens if such a bound state decays into two separate particles. This point is where the two-channel description which has been used in the two- and three-particle analysis comes into play. Using the coupled-channels description and once more applying the Feshbach formalism, it is possible to follow the outline as suggested by S.Kokkelmans and M.Holland [68] and to introduce a closed channel to the system which contains a bound state such that molecules can be formed. Similarly to the introduction of creation- and annihilation operators in order to describe the formation or the destruction of atoms, it is possible to introduce operators which either destroy or form a molecule. These molecular operators, represented by the symbols $\hat{b}^\dagger_{\mathbf{k}}$ and $\hat{b}_{\mathbf{k}}$ will be used to describe the creation and the annihilation of molecule respectively. Contrary to the previously introduced atomic creation-and annihilation operators, the molecular operators live in the closed channel subspace. The creation or annihilation of a molecule in this channel corresponds to the annihilation of creation of two atoms in the open channel, such that the total number of particles is conserved.

Similarly to the analysis of the closed channel subspace in section 2.7, only a single bound state is assumed to live in the closed channel subspace. Furthermore, the continuum states in this subspace are neglected. Applying this information and implementing the theory as outlined in the

previous sections, it is possible to obtain information regarding the molecular condensate wave function through the calculation of the expectation value of the molecular annihilation operator $\hat{b}_0$. This molecular condensate wave function represents the bound state in the closed channel subspace. In the model which will be studied in the next sections, and following the approach used in reference [68], the interactions amongst two- or more molecules are neglected. Having included a second channel to the system in which a molecular bound state can be formed, the description of the coupled-channels system in terms of second quantized operators has been completed. Using the theory outlined in this section and the previous sections, the next part of this chapter will focus on the analysis of the coupled-channels many-body Hamiltonian.

10.5 The coupled-channels many-body Hamiltonian

Using a model similar to the system which has been used in the analysis of two- and three-body interactions, we wish to analyse the dynamics of a many-body system which contains an atomic potential and is coupled to a closed channel which supports a molecular bound state. The dynamics of such a gas can be described in terms of a coupled-channels Hamiltonian system similar to the form which has been previously presented in equation 4.1. In this case, the open channel component, named $\hat{H}_a$, includes the atomic free-evolution Hamiltonian $\hat{H}_0$ plus an additional term which describes the interaction between two atoms. Furthermore, the off-diagonal coupling terms are described by an interaction Hamiltonian $\hat{H}_i$ which quantifies the interaction strength between atoms and molecules. Next, the closed channel contribution, named $\hat{H}_m$, consists of the free-evolution Hamiltonian $\hat{H}_0$ of the molecules. Using the definitions as presented above and applying the second quantized form of single-particle and two-particle operators as presented in equations 10.2 and 10.3, the Hamiltonian terms $\hat{H}_a$ and $\hat{H}_m$ can be expressed as follows:

$$\hat{H}_a = \sum_{\mathbf{k}} t^a_{\mathbf{k}} \hat{a}^\dagger_{\mathbf{k}} \hat{a}_{\mathbf{k}} + \frac{1}{2} \sum_{\mathbf{k}_1\mathbf{k}_2\mathbf{k}_3\mathbf{k}_4} V_{\mathbf{k}_1\mathbf{k}_2\mathbf{k}_3\mathbf{k}_4} \hat{a}^\dagger_{\mathbf{k}_1} \hat{a}^\dagger_{\mathbf{k}_2} \hat{a}_{\mathbf{k}_3} \hat{a}_{\mathbf{k}_4}, \tag{10.16}$$

$$\hat{H}_m = \sum_{\mathbf{q}} \left(t^m_{\mathbf{q}} + \nu \right) \hat{b}^\dagger_{\mathbf{q}} \hat{b}_{\mathbf{q}}. \tag{10.17}$$

The term $V_{\mathbf{k}_1\mathbf{k}_2\mathbf{k}_3\mathbf{k}_4}$ which has been introduced in the previous equation describes the interaction strength between two particles with incoming wave numbers $\mathbf{k}_1$ and $\mathbf{k}_2$ and outgoing wave numbers $\mathbf{k}_3$ and $\mathbf{k}_4$. Furthermore, the two terms $t^a_{\mathbf{k}}$ and $t^m_{\mathbf{q}}$ correspond to the momentum space projections of the atomic kinetic energy operator $\hat{t}^a = \frac{\hbar^2\nabla^2}{2m}$ and the molecular kinetic energy operator $\hat{t}^m = \frac{\hbar^2\nabla^2}{4m}$ respectively. Apart from these kinetic energy terms, the molecular Hamiltonian contains an extra term ν in its free evolution part. This factor describes the detuning of the molecular bound state energy with respect to the entrance energy of the atomic potential and is defined according to equation 2.40. Apart from identifying all newly introduced terms, it is important to notice that equation 10.16 is a function of the atomic creation- and annihilation operators $\hat{a}^\dagger_{\mathbf{k}}$ and $\hat{a}_{\mathbf{k}}$, whereas equation 10.17 is a function of the molecular creation- and annihilation operators $\hat{b}^\dagger_{\mathbf{q}}$ and $\hat{b}_{\mathbf{q}}$. These two sets of annihilation- and creation operators that live in different subspaces have been previously analysed in section 10.4. Moreover, the interaction Hamiltonian $\hat{H}_i$ can be expressed in second quantized form as presented below:

$$\hat{H}_i = \frac{1}{2} \sum_{\mathbf{k}_1\mathbf{k}_2\mathbf{q}} \left(g_{\mathbf{k}_1\mathbf{k}_2\mathbf{q}} \hat{b}^\dagger_{\mathbf{q}} \hat{a}_{\mathbf{k}_2} \hat{a}_{\mathbf{k}_1} + \text{H.c} \right). \tag{10.18}$$

The factor $g_{\mathbf{k}_1\mathbf{k}_2\mathbf{q}}$ that has been introduced in the previous equation describes the interaction strength between two atoms with wave numbers $\mathbf{k}_1$ and $\mathbf{k}_2$ and a single molecule with a wave number $\mathbf{q}$. It is this term which couples the open channel subspace to the closed channel subspace. Combining

equation 10.18 with expressions 10.16 and 10.17, the following equation for the total many-body Hamiltonian operator can be obtained:

$$\begin{aligned}\hat{H} = &\sum_{\mathbf{k}} t^a_{\mathbf{k}} \hat{a}^\dagger_{\mathbf{k}} \hat{a}_{\mathbf{k}} + \frac{1}{2} \sum_{p_1 p_2 p_3 p_4} V_{\mathbf{k}_1\mathbf{k}_2\mathbf{k}_3\mathbf{k}_4} \hat{a}^\dagger_{\mathbf{k}_1} \hat{a}^\dagger_{\mathbf{k}_2} \hat{a}_{\mathbf{k}_3} \hat{a}_{\mathbf{k}_4} \\ &+ \sum_{\mathbf{q}} \left(t^m_{\mathbf{q}} + \nu\right) \hat{b}^\dagger_{\mathbf{q}} \hat{b}_{\mathbf{q}} + \frac{1}{2} \sum_{\mathbf{k}_1\mathbf{k}_2\mathbf{q}} \left(g_{\mathbf{k}_1\mathbf{k}_2\mathbf{q}} \hat{b}^\dagger_{\mathbf{q}} \hat{a}_{\mathbf{k}_2} \hat{a}_{\mathbf{k}_1} + \text{H.c}\right). \end{aligned} \tag{10.19}$$

Having obtained an equation for the many-body Hamiltonian, the exact form of the potential terms $V_{\mathbf{k}_1\mathbf{k}_2\mathbf{k}_3\mathbf{k}_4}$ and $g_{\mathbf{k}_1\mathbf{k}_2\mathbf{q}}$ need to be specified. Similarly to the procedure which has been applied in the study of two-body and three-body interactions, the potential operator $\hat{V}$ that describes the interaction between two atoms and the interaction operator $\hat{g}$ that represents the interaction between two atoms and a molecule will be described by a separable potential form which has a fixed strength and a finite wave number cut-off $K = \Lambda/\hbar$, with Λ the momentum space cut-off which has been previously analysed in chapter 6. Realising that this cut-off acts on the relative wave numbers between particles, the atoms-molecule interaction term $\hat{g}$ and the atom-atom interaction term $\hat{V}$ need to be expressed in terms of a center of mass wave number and a relative wave number contribution. In the case of the matrix element $V_{\mathbf{k}_1\mathbf{k}_2\mathbf{k}_3\mathbf{k}_4}$, this results in the following analogous definition [69]:

$$V_{\mathbf{k}_1\mathbf{k}_2\mathbf{k}_3\mathbf{k}_4} = \langle \mathbf{k}_1| \otimes \langle \mathbf{k}_2|\hat{V}|\mathbf{k}_3\rangle \otimes |\mathbf{k}_4\rangle = \langle \mathbf{k}_{rel}| \otimes \langle \mathbf{K}|\hat{V}|\mathbf{K}'\rangle \otimes |\mathbf{k}'_{rel}\rangle\,. \tag{10.20}$$

The relative wave numbers $\mathbf{k}_{rel}$ and $\mathbf{k}'_{rel}$ and the center of mass wave numbers $\mathbf{K}$ and $\mathbf{K}'$ which have been introduced in the previous equation are related to the wave numbers $\mathbf{k}_1$, $\mathbf{k}_2$, $\mathbf{k}_3$ and $\mathbf{k}_4$ as follows:

$$\mathbf{k}_{rel} = \frac{\mathbf{k}_1 - \mathbf{k}_2}{2}, \tag{10.21}$$

$$\mathbf{K} = \mathbf{k}_1 + \mathbf{k}_2, \tag{10.22}$$

$$\mathbf{K}'_{rel} = \frac{\mathbf{k}_3 - \mathbf{k}_4}{2}, \tag{10.23}$$

$$\mathbf{K}' = \mathbf{k}_3 + \mathbf{k}_4. \tag{10.24}$$

Using these expressions for the center of mass wave numbers and the relative wave numbers and using the separable potential form $\hat{V} = -\tilde{V}\,|g\rangle\,\langle g|$ to describe the interaction between the atoms, equation 10.20 reduces to the following form [69]:

$$V_{\mathbf{k}_1\mathbf{k}_2\mathbf{k}_3\mathbf{k}_4} = -\tilde{V}\delta_{\mathbf{K},\mathbf{K}'}\theta\left(K - |\mathbf{k}_{rel}|\right)\theta\left(K - |\mathbf{k}'_{rel}|\right), \tag{10.25}$$

where $\delta_{\mathbf{K},\mathbf{K}'}$ indicates that the center of mass wave number remains unaltered. Therefore, the interaction can fully be described by the usage of three wave numbers $\mathbf{K}$, $\mathbf{k}'_{rel}$ and $\mathbf{k}_{rel}$ instead of the usage of four different wave numbers $\mathbf{k}_1$, $\mathbf{k}_2$, $\mathbf{k}_3$ and $\mathbf{k}_4$. Using this information, the following new set of coordinates can be introduced:

$$\mathbf{p} = \frac{\mathbf{K}}{2} + \mathbf{K}'_{rel}, \tag{10.26}$$

$$\mathbf{p}' = \frac{\mathbf{K}}{2} - \mathbf{k}'_{rel}, \tag{10.27}$$

$$\mathbf{q} = \mathbf{k}_{rel} - \mathbf{k}'_{rel}. \tag{10.28}$$

Using this new set of parameters and coupling them to the original coordinates $\mathbf{k}_1$, $\mathbf{k}_2$, $\mathbf{k}_3$ and $\mathbf{k}_4$ through the relations as presented in equations 10.21 through 10.24, the atomic part of the Hamiltonian as presented by equation 10.16 can be rewritten as follows:

$$\hat{H}_a = \sum_{\mathbf{k}} t^a_{\mathbf{k}} \hat{a}^\dagger_{\mathbf{k}} \hat{a}_{\mathbf{k}} - \tilde{V} \sum_{\mathbf{p}'\mathbf{p}\mathbf{q}} \theta\left(K - \frac{|\mathbf{p} - \mathbf{p}' + 2\mathbf{q}|}{2}\right) \theta\left(K - \frac{|\mathbf{p} - \mathbf{p}'|}{2}\right) \hat{a}^\dagger_{\mathbf{p}+\mathbf{q}} \hat{a}^\dagger_{\mathbf{p}'-\mathbf{q}} \hat{a}_{\mathbf{p}} \hat{a}_{\mathbf{p}'}. \tag{10.29}$$

A similar approach can be used to rewrite the term $g_{\mathbf{p}_1\mathbf{p}_2\mathbf{q}}$ which describes the coupling between two atoms and the molecules. Completely analogous to the term describing the interaction between two atoms, this interaction term has to conserve total wave number. This means that the wave number $\mathbf{q}$ of the annihilated/created molecule equals the sum of the wave numbers $\mathbf{k}_1$ and $\mathbf{k}_2$ of the created/annihilated atoms. Furthermore, upon expressing the coupling operator $\hat{g}$ as follows: $\hat{g} = -\tilde{G}\,|g\rangle\,\langle g|$, with G the interaction strength, the expression for $g_{\mathbf{k}_1\mathbf{k}_2\mathbf{q}}$ can be rewritten into the form as presented below:

$$g_{\mathbf{k}_1\mathbf{k}_2\mathbf{q}} = -\tilde{G}\theta\left(K - |\mathbf{k}_{rel}|\right). \tag{10.30}$$

The introduced relative wave number $\mathbf{k}_{rel}$ in the previous equation corresponds to the relative wave number of the atoms which has been introduced in equation 10.21. Next, defining the center of mass wave number of the molecule as $\mathbf{q} = \mathbf{K}$ and applying the conservation of the total wave number, the wave numbers $\mathbf{k}_1$ and $\mathbf{k}_2$ of the interacting atoms can be expressed as indicated below:

$$\mathbf{k}_1 = \frac{\mathbf{K}}{2} + \mathbf{k}_{rel}, \tag{10.31}$$

$$\mathbf{p}_2 = \frac{\mathbf{K}}{2} - \mathbf{k}_{rel}. \tag{10.32}$$

Using these expressions, the interaction component of the system Hamiltonian, as defined by equation 10.18, reduces to the following form:

$$\hat{H}_i = -\frac{\tilde{G}}{2}\sum_{\mathbf{k}_{rel},\mathbf{K}} \theta\left(K - |\mathbf{k}_{rel}|\right)\left[\hat{b}^\dagger_{\mathbf{K}}\hat{a}_{\mathbf{K}/2+\mathbf{k}_{rel}}\hat{a}_{\mathbf{K}/2-\mathbf{k}_{rel}} + \text{H.c}\right]. \tag{10.33}$$

Combining the expression for the molecular and the atomic Hamiltonians as presented in equations 10.17 and 10.29 with the expression of the interaction Hamiltonian as presented by equation 10.33, the following final expression for the many-body Hamiltonian operator $\hat{H}$ can be obtained:

$$\begin{aligned}\hat{H} =& \sum_{\mathbf{k}} t^a_{\mathbf{k}}\hat{a}^\dagger_{\mathbf{k}}\hat{a}_{\mathbf{k}} + \sum_{\mathbf{q}}\left(t^m_{\mathbf{q}} + \nu\right)\hat{b}^\dagger_{\mathbf{q}}\hat{b}_{\mathbf{q}} \\ &- \frac{\tilde{V}}{2}\sum_{\mathbf{p}'\mathbf{p}\mathbf{q}} \theta\left(K - \frac{|\mathbf{p} - \mathbf{p}' + 2\mathbf{q}|}{2}\right)\theta\left(K - \frac{|\mathbf{p} - \mathbf{p}'|}{2}\right)\hat{a}^\dagger_{\mathbf{p}+\mathbf{q}}\hat{a}^\dagger_{\mathbf{p}'-\mathbf{q}}\hat{a}_{\mathbf{p}}\hat{a}_{\mathbf{p}'} \\ &- \frac{\tilde{G}}{2}\sum_{\mathbf{k}_{rel},\mathbf{K}} \theta\left(K - |\mathbf{k}_{rel}|\right)\left[\hat{b}^\dagger_{\mathbf{K}}\hat{a}_{\mathbf{K}/2+\mathbf{k}_{rel}}\hat{a}_{\mathbf{K}/2-\mathbf{k}_{rel}} + \text{H.c}\right].\end{aligned} \tag{10.34}$$

Having obtained an expression for the many-body Hamiltonian, it is now possible to analyse the equations of motion for the many-body system, which will be the topic of discussion of the next section.

10.6 Hartree-Fock-Bogoliubov equations of motion

Using the many-body Hamiltonian as presented in equation 10.34, this section will focus on the derivation of the following set of equations of motion:

1. The equation of motion for the atomic condensate ψ_a. As explained in section 10.2, the atomic condensate wave function is related to the excitation value of the atomic ground state annihilation operator $\hat{a}_0$.
2. The equation of motion for the molecular condensate ψ_m. Analogously to the atomic condensate, the molecular condensate wave function is related to the expectation value of the molecular ground state annihilation operator $\hat{b}_0$ which lives in the closed channel subspace.
3. The equation of motion for the atomic excitations as represented by the factor $\rho_{\mathbf{k}}$, with $\mathbf{k} \neq 0$.
4. The equation of motion of the anomalous density term $\kappa_{\mathbf{k}}$ with $\mathbf{k} \neq 0$. As previously discussed in section 10.3, this term quantifies the correlations between excited state atoms.

Each of the four equations which are described above will be derived through the application of the Heisenberg equation of motion [69] and will be discussed in separate sections. All of these equations, which are known as the *Hartree-Fock-Bogoliubov* equations of motion [62], rely on the usage of the approximations which have been introduced in section 10.2 and will be analysed in wave number space or k-space.

10.6.1 Equation of motion of the molecular condensate

Applying the expression for the many-body Hamiltonian as presented by equation 10.34, it is possible to obtain the following expression for the Heisenberg equation of motion for the molecular annihilation operator $\hat{b}_{\mathbf{k}}$:

$$
\begin{aligned}
i\hbar\frac{\partial}{\partial t}\hat{b}_{\mathbf{k}} &= \left[\hat{b}_{\mathbf{k}}, \hat{H}\right], && (10.35)\\
&= \sum_p t_p^a \left[\hat{b}_{\mathbf{k}}, \hat{a}^\dagger_{\mathbf{p}}\hat{a}_{\mathbf{p}}\right] + \sum_{\mathbf{q}} \left(t^m_{\mathbf{q}} + \nu\right)\left[\hat{b}_{\mathbf{k}}, \hat{b}^\dagger_{\mathbf{q}}\hat{b}_{\mathbf{q}}\right] \\
&- \frac{\tilde{V}}{2}\sum_{\mathbf{p'pq}} \theta\left(K - \frac{|\mathbf{p}-\mathbf{p'}+2\mathbf{q}|}{2}\right)\theta\left(K - \frac{|\mathbf{p}-\mathbf{p'}|}{2}\right)\left[\hat{b}_{\mathbf{k}}, \hat{a}^\dagger_{\mathbf{p}+\mathbf{q}}\hat{a}^\dagger_{\mathbf{p'}-\mathbf{q}}\hat{a}_{\mathbf{p}}\hat{a}_{\mathbf{p'}}\right] \\
&- \frac{\tilde{G}}{2}\sum_{\mathbf{pq}} \theta\left(\mathbf{k}-|\mathbf{q}|\right)\left([\hat{b}_{\mathbf{k}}, \hat{b}^\dagger_{2\mathbf{p}}\hat{a}_{\mathbf{p}+\mathbf{q}}\hat{a}_{\mathbf{p}-\mathbf{q}}] + [\hat{b}_{\mathbf{k}}, \hat{b}_{2\mathbf{p}}\hat{a}^\dagger_{\mathbf{p}+\mathbf{q}}\hat{a}^\dagger_{\mathbf{p}-\mathbf{q}}]\right). && (10.36)
\end{aligned}
$$

In order to simplify the previous equation, the bosonic commutation rules as presented below can be applied:

$$
\begin{aligned}
[\hat{a}_i, \hat{a}^\dagger_j] &= \delta_{i,j}, && (10.37)\\
[\hat{a}_i, \hat{a}_j] &= 0, && (10.38)\\
[\hat{a}^\dagger_i, \hat{a}^\dagger_j] &= 0, && (10.39)\\
[A, BC] &= [A, B]C + B[A, C], && (10.40)\\
[A, BCD] &= [A, B]CD + B[A, C]D + BC[A, D]. && (10.41)
\end{aligned}
$$

Equations 10.37 through 10.39 describe the physical commutation rules [48] for bosonic annihilation and creation operators. The relations as presented in equations 10.40 and 10.41 follow directly from these bosonic commutation relations. The same commutation rules hold for the molecular creation- and annihilation operators $\hat{b}^\dagger_{\mathbf{k}}$ and $\hat{b}_{\mathbf{k}}$. Furthermore, as the atomic operators act on a

different subspace than the molecular operators, the commutation between any of these two different operators yields a value of zero. Implementing all of this information, equation 10.36 can be rewritten as follows:

$$i\hbar\frac{\partial}{\partial t}\hat{b}_{\mathbf{k}} = \left(t^m_{\mathbf{k}} + \nu\right)\hat{b}_{\mathbf{k}} - \frac{\tilde{G}}{2}\sum_{\mathbf{q}}\theta\left(K - |\mathbf{q}|\right)\hat{a}_{\mathbf{q}}\hat{a}_{-\mathbf{q}}. \tag{10.42}$$

The intermediate steps which have been taken in order to obtain the result as presented above are recorded in appendix M . As described in section 10.4, it is possible to obtain the equation of motion for the molecular condensate ψ_m through the computation of the expectation value of the operator $\hat{b}_0$. In calculating the expectation value of the previous equation, the cumulant constraints as listed in appendix L have been applied. Using these constraints in the computation of the expectation value of equation 10.42, the following expression for the molecular condensate wave function ψ_m can be obtained:

$$i\hbar\dot{\psi}_m = \nu\psi_m - \frac{\tilde{G}}{2}\psi_a^2 - \frac{\tilde{G}}{2}\sum_{\mathbf{q}}{}'\theta\left(K - |\mathbf{q}|\right)\kappa_{\mathbf{q}}. \tag{10.43}$$

The overhead symbol $'$ which has been introduced in the summation term in the previous equation refers to the exclusion of the zero momentum term $q = 0$ in the summation. Furthermore, in order to obtain the previous equation, the identification of the term $\langle\hat{a}_{\mathbf{q}}\hat{a}_{-\mathbf{q}}\rangle_c$ with the anomalous density term $\kappa_{\mathbf{q}}$ has been implemented and the factor $\langle\hat{a}_0\hat{a}_0\rangle$ has been identified as the square of the atomic condensate wave function ψ_a.

Equation 10.43 represents the form of the equation of motion for the molecular condensate which will be used in the numerical simulations of the many-body system as presented in chapter 13.

10.6.2 Equation of motion of the atomic condensate

In order to obtain equation of motion for the atomic condensate wave-function, the approach as described in the previous section is repeated. However, in this case, the Heisenberg equation of motion is used to analyse the time evolution of the atomic annihilation operator $\hat{a}_{\mathbf{k}}$ instead of the molecular annihilation operator $\hat{b}_{\mathbf{q}}$. This results in the following outcome:

$$\begin{aligned} i\hbar\frac{\partial}{\partial t}\hat{a}_{\mathbf{k}} &= \left[\hat{a}_{\mathbf{k}}, \hat{H}\right], \qquad (10.44)\\ &= \sum_{\mathbf{p}} t^a_{\mathbf{p}}\left[\hat{a}_{\mathbf{k}}, \hat{a}^\dagger_{\mathbf{p}}\hat{a}_{\mathbf{p}}\right] + \sum_{\mathbf{q}}\left(t^m_{\mathbf{q}} + \nu\right)\left[\hat{a}_{\mathbf{k}}, \hat{b}^\dagger_{\mathbf{q}}\hat{b}_{\mathbf{q}}\right]\\ &- \frac{\tilde{V}}{2}\sum_{\mathbf{p'pq}}\theta\left(K - \frac{|\mathbf{p} - \mathbf{p}' + 2\mathbf{q}|}{2}\right)\theta\left(K - \frac{|\mathbf{p} - \mathbf{p}'|}{2}\right)\left[\hat{a}_{\mathbf{k}}, \hat{a}^\dagger_{\mathbf{p}+\mathbf{q}}\hat{a}^\dagger_{\mathbf{p}'-\mathbf{q}}\hat{a}_{\mathbf{p}}\hat{a}_{\mathbf{p}'}\right].\\ &- \frac{\tilde{G}}{2}\sum_{\mathbf{pq}}\theta\left(K - |q|\right)\left(\left[\hat{a}_{\mathbf{k}}, \hat{b}^\dagger_{2\mathbf{p}}\hat{a}_{\mathbf{p}+\mathbf{q}}\hat{a}_{\mathbf{p}-\mathbf{q}}\right] + \left[\hat{a}_{\mathbf{k}}, \hat{b}_{2\mathbf{p}}\hat{a}^\dagger_{\mathbf{p}+\mathbf{q}}\hat{a}^\dagger_{\mathbf{p}-\mathbf{q}}\right]\right) \qquad (10.45)\end{aligned}$$

Applying the commutation relations as presented in the previous section and following the intermediate steps presented in appendix M, equation 10.45 can be reduced to the following form:

$$\begin{aligned} i\hbar\frac{\partial}{\partial t}\hat{a}_{\mathbf{k}} =& t^a_{\mathbf{k}}\hat{a}_{\mathbf{k}} - \tilde{V}\sum_{\mathbf{p'p}}\theta\left(K - \frac{|2\mathbf{k} - \mathbf{p}' - \mathbf{p}|}{2}\right)\theta\left(K - \frac{|\mathbf{p} - \mathbf{p}'|}{2}\right)\hat{a}^\dagger_{\mathbf{p}+\mathbf{p}'-\mathbf{k}}\hat{a}_{\mathbf{p}}\hat{a}_{\mathbf{p}'}\\ &- \tilde{G}\sum_{\mathbf{q}}\theta\left(K - |\mathbf{q}|\right)\hat{b}_{2\mathbf{q}}\hat{a}^\dagger_{2\mathbf{q}}. \end{aligned} \tag{10.46}$$

Analogous to the method followed in the previous section, it is possible to obtain the equation of motion for the atomic condensate ψ_a through the calculation of the expectation value of the previous equation. Applying the cumulant constraints as presented in appendix L to this equation and using the result of the analysis of the term $\langle \hat{a}^\dagger_{\mathbf{p}+\mathbf{p}'} \hat{a}_{\mathbf{p}} \hat{a}_{\mathbf{p}'} \rangle$ as outlined in appendix M, the following expression for the equation of motion of the atomic condensate wave function ψ_a can be obtained:

$$i\hbar\dot{\psi}_a = -\tilde{V}|\psi_a|^2\psi_a - \tilde{V}\sum_{\mathbf{p}}{}' \theta\left(K - \frac{|\mathbf{p}|}{2}\right)\left(2\rho_{\mathbf{p}}\psi_a + \psi_a^*\kappa_{\mathbf{p}}\right) - \tilde{G}\psi_m\psi_a^*. \tag{10.47}$$

Equation 10.47 represents the form of the equation of motion for the atomic condensate which will be used in the numerical analysis of the many-body system as presented in chapter 13.

10.6.3 Equation of motion of the normal density

As previously introduced in section 10.3, the normal density term is defined as $\rho_{\mathbf{k}} \equiv \langle \hat{a}^\dagger_{\mathbf{k}} \hat{a}_{\mathbf{k}} \rangle_{\mathbf{k}\neq 0}$. Using this information and applying the same method as outlined in the previous two subsections, the equation of motion governing the normal density term can be derived through solving the Heisenberg equation of motion as presented below:

$$\begin{aligned}
i\hbar\frac{\partial}{\partial t}\left(\hat{a}^\dagger_{\mathbf{k}}\hat{a}_{\mathbf{k}}\right) &= \left[\hat{a}^\dagger_{\mathbf{k}}\hat{a}_{\mathbf{k}}, \hat{H}\right], \\
&= \sum_{\mathbf{p}} t^a_{\mathbf{p}}\left[\hat{a}^\dagger_{\mathbf{k}}\hat{a}_{\mathbf{k}}, \hat{a}^\dagger_{\mathbf{p}}\hat{a}_{\mathbf{p}}\right] \\
&\quad - \frac{\tilde{V}}{2}\sum_{\mathbf{p}'\mathbf{p}\mathbf{q}} \theta\left(K - \frac{|\mathbf{p}-\mathbf{p}'+2\mathbf{q}|}{2}\right)\theta\left(K - \frac{|\mathbf{p}-\mathbf{p}'|}{2}\right)\left[\hat{a}^\dagger_{\mathbf{k}}\hat{a}_{\mathbf{k}}, \hat{a}^\dagger_{\mathbf{p}+\mathbf{q}}\hat{a}^\dagger_{\mathbf{p}'-\mathbf{q}}\hat{a}_{\mathbf{p}}\hat{a}_{\mathbf{p}'}\right] \\
&\quad - \frac{\tilde{G}}{2}\sum_{\mathbf{p},\mathbf{q}} \theta\left(K - |\mathbf{q}|\right)\left([\hat{a}^\dagger_{\mathbf{k}}\hat{a}_{\mathbf{k}}, \hat{b}^\dagger_{2\mathbf{p}}\hat{a}_{\mathbf{p}+\mathbf{q}}\hat{a}_{\mathbf{p}-\mathbf{q}}] + [\hat{a}^\dagger_{\mathbf{k}}\hat{a}_{\mathbf{k}}, \hat{b}_{2\mathbf{p}}\hat{a}^\dagger_{\mathbf{p}+\mathbf{q}}\hat{a}^\dagger_{\mathbf{p}-\mathbf{q}}]\right).
\end{aligned} \tag{10.48}$$

Following the rather length derivation as outlined in appendix M, the previous expression can be rewritten into the following form:

$$\begin{aligned}
i\hbar\frac{\partial}{\partial t}\left(\hat{a}^\dagger_{\mathbf{k}}\hat{a}_{\mathbf{k}}\right) =& -\tilde{V}\sum_{\mathbf{p}'\mathbf{q}} \theta\left(K - \frac{|\mathbf{k}-\mathbf{p}'+\mathbf{q}|}{2}\right)\theta\left(K - \frac{|\mathbf{k}-\mathbf{p}'-\mathbf{q}|}{2}\right)\left(\hat{a}^\dagger_{\mathbf{k}}\hat{a}^\dagger_{\mathbf{p}'-\mathbf{q}}\hat{a}_{\mathbf{k}-\mathbf{q}}\hat{a}_{\mathbf{p}'}\right) \\
&+ \tilde{V}\sum_{\mathbf{p}'\mathbf{q}} \theta\left(K - \frac{|\mathbf{k}-\mathbf{p}'+2\mathbf{q}|}{2}\right)\theta\left(K - \frac{|\mathbf{k}-\mathbf{p}'|}{2}\right)\left(\hat{a}^\dagger_{\mathbf{k}+\mathbf{q}}\hat{a}^\dagger_{\mathbf{p}'-\mathbf{q}}\hat{a}_{\mathbf{p}'}\hat{a}_{\mathbf{k}}\right). \\
&- \tilde{G}\sum_{q} \theta\left(K - |\mathbf{q}|\right)\left(\hat{b}_{2\mathbf{k}-2\mathbf{q}}\hat{a}^\dagger_{\mathbf{k}}\hat{a}^\dagger_{\mathbf{k}-2\mathbf{q}} - \hat{b}^\dagger_{2\mathbf{k}-2\mathbf{q}}\hat{a}_{\mathbf{k}-2\mathbf{q}}\hat{a}_{\mathbf{k}}\right).
\end{aligned} \tag{10.49}$$

Analogous to the method followed in the previous two subsections, the expectation value of equation 10.49 needs to be calculated in order to obtain the expression for the normal density term. Following the steps as outlined in appendix M, this procedure yields the following outcome for the equation of motion of the normal density term:

$$\begin{aligned}
i\hbar\frac{\partial}{\partial t}\rho_{\mathbf{k}} =& -\tilde{V}\sum_{\mathbf{p}'}{}' \theta\left(K - |\mathbf{k}|\right)\theta\left(K - |\mathbf{p}'|\right)\left[\kappa^*_{\mathbf{k}}\kappa_{\mathbf{p}'} - \kappa_{\mathbf{k}}\kappa^*_{\mathbf{k}'}\right] - \tilde{V}\theta\left(K - |\mathbf{k}|\right)\left[\kappa^*_{\mathbf{k}}\psi_a^2 - \kappa_{\mathbf{k}}\psi_a^{*^2}\right] \\
&- \tilde{G}\theta\left(K - |\mathbf{k}|\right)\left[\kappa^*_{\mathbf{k}}\psi_m - \kappa_{\mathbf{k}}\psi^*_m\right].
\end{aligned} \tag{10.50}$$

The equation of motion for the normal density term $\rho_{\mathbf{k}}$ as presented in the previous expression will be used in the numerical analysis of the many-body system as presented in chapter in order to track the number of excited state atoms as a function of the evaluation time.

10.6.4 Equation of motion of the anomalous density

The fourth, and final, equation of motion which we like to introduce is the equation of motion of the anomalous density term $\kappa_{\mathbf{k}}$. Using the definition of this factor in terms of atomic annihilation operators $\kappa_{\mathbf{k}} \equiv \langle \hat{a}_{-\mathbf{k}} \hat{a}_{\mathbf{k}} \rangle$, the following Heisenberg equation of motion can be obtained:

$$\begin{aligned} i\hbar \frac{\partial}{\partial t} \left(\hat{a}_{-\mathbf{k}} \hat{a}_{\mathbf{k}} \right) &= \left[\hat{a}_{-\mathbf{k}} \hat{a}_{\mathbf{k}}, \hat{H} \right], \\ &= \sum_{\mathbf{p}} t^a_{\mathbf{p}} \left[\hat{a}_{-\mathbf{k}} \hat{a}_{\mathbf{k}}, \hat{a}^\dagger_{\mathbf{p}} \hat{a}_{\mathbf{p}} \right] \\ &\quad - \frac{\tilde{V}}{2} \sum_{\mathbf{p}'\mathbf{p}\mathbf{q}} \theta \left(K - \frac{|\mathbf{p} - \mathbf{p}' + 2\mathbf{q}|}{2} \right) \theta \left(K - \frac{|\mathbf{p} - \mathbf{p}'|}{2} \right) \left[\hat{a}_{-\mathbf{k}} \hat{a}_{\mathbf{k}}, \hat{a}^\dagger_{\mathbf{p}+\mathbf{q}} \hat{a}^\dagger_{\mathbf{p}'-\mathbf{q}} \hat{a}_{\mathbf{p}} \hat{a}_{\mathbf{p}'} \right]. \\ &\quad - \frac{\tilde{G}}{2} \sum_{\mathbf{p},\mathbf{q}} \theta \left(K - |\mathbf{q}| \right) \left([\hat{a}_{-\mathbf{k}} \hat{a}_{\mathbf{k}}, \hat{b}^\dagger_{2\mathbf{p}} \hat{a}_{\mathbf{p}+\mathbf{q}} \hat{a}_{\mathbf{p}-\mathbf{q}}] + [\hat{a}_{-\mathbf{k}} \hat{a}_{\mathbf{k}}, \hat{b}_{2\mathbf{p}} \hat{a}^\dagger_{\mathbf{p}+\mathbf{q}} \hat{a}^\dagger_{\mathbf{p}-\mathbf{q}}] \right) \end{aligned} \tag{10.51}$$

Once more, upon working out the commutator factors that are present in the previous equation as outlined in appendix M, equation 10.51 can be rewritten into the following form:

$$\begin{aligned} i\hbar \frac{\partial}{\partial t} \left(\hat{a}_{-\mathbf{k}} \hat{a}_{\mathbf{k}} \right) &= \left(t^a_{\mathbf{k}} + t^a_{-\mathbf{k}} \right) \hat{a}_{\mathbf{k}} \hat{a}_{-\mathbf{k}} \\ &- \tilde{V} \sum_{\mathbf{p}'\mathbf{q}} \theta \left(K - \frac{|\mathbf{k} - \mathbf{p}' + \mathbf{q}|}{2} \right) \theta \left(K - \frac{|\mathbf{k} - \mathbf{q} - \mathbf{p}'|}{2} \right) \hat{a}_{-\mathbf{k}} \hat{a}^\dagger_{\mathbf{p}'-\mathbf{q}} \hat{a}_{\mathbf{k}-\mathbf{q}} \hat{a}_{\mathbf{p}'} \\ &- \tilde{V} \sum_{\mathbf{p}'\mathbf{q}} \theta \left(K - \frac{|-\mathbf{k} - \mathbf{p}' + \mathbf{q}|}{2} \right) \theta \left(K - \frac{|-\mathbf{k} - \mathbf{q} - \mathbf{p}'|}{2} \right) \hat{a}^\dagger_{\mathbf{p}'-\mathbf{q}} \hat{a}_{\mathbf{k}} \hat{a}_{-\mathbf{k}-\mathbf{q}} \hat{a}_{\mathbf{p}'} \\ &- \tilde{G} \sum_{\mathbf{q}} \theta \left(K - |\mathbf{q}| \right) \left(\hat{b}_{2\mathbf{q}-2\mathbf{k}} \hat{a}^\dagger_{2\mathbf{q}-\mathbf{k}} \hat{a}_{\mathbf{k}} + \hat{b}_{2\mathbf{k}+2\mathbf{q}} \hat{a}_{-\mathbf{k}} \hat{a}^\dagger_{\mathbf{k}+2\mathbf{q}} \right). \end{aligned} \tag{10.52}$$

Upon calculating the expectation value of the previous equation, the following expression for the equation of motion for the anomalous density term $\kappa_{\mathbf{k}}$ can be derived:

$$\begin{aligned} i\hbar \frac{\partial}{\partial t} \kappa_{\mathbf{k}} &= 2t^a_k \kappa_{\mathbf{k}} - 2\tilde{V} \sum_{p'}{}' \left[\theta \left(K - \frac{|k - p'|}{2} \right) + \theta \left(K - \frac{|-k - p'|}{2} \right) \right] \kappa_{\mathbf{k}} \rho_{\mathbf{p}'} \\ &\quad - \tilde{V} \sum_{p'}{}' \theta \left(K - |k| \right) \theta \left(K - |p'| \right) \left[1 + 2\rho_{\mathbf{k}} \right] \kappa_{\mathbf{p}'} \\ &\quad - 4\tilde{V} \theta \left(K - \frac{|k|}{2} \right) \kappa_{\mathbf{k}} |\psi_a|^2 - \tilde{V} \theta \left(K - |k| \right) \psi_a^2 \left[1 + 2\rho_{\mathbf{k}} \right] \\ &\quad - \tilde{G} \theta \left(K - |k| \right) \psi_m \left[1 + 2\rho_{\mathbf{k}} \right]. \end{aligned} \tag{10.53}$$

A closer inspection of the previous equation reveals the presence of the term $(1 + 2\rho_{\mathbf{k}})$. The factor $(1 + \rho_{\mathbf{k}})$ that can be extracted from this term is better known as the *Bose enhancement* factor [66]. As the name implies, this component effectively enhances the dynamics of atomic excitations in wave number modes which are already occupied by other identical bosons [70, 21]. This factor represents a pure many-body effect and is caused by the presence of the background gas that consists of excited state atoms. The result of the presence of this term on the dynamical evolution of the many-body system will be discussed in more detail in chapter 13.

10.7 Conclusion

Having applied the Bogoliubov- and the coherent state approximation, it has been proven in the first part of this chapter that it is possible to inspect the equations of motion for the atomic condensate, the molecular condensate, the normal density term and the anomalous density term through the analysis of the expectation values of creation- and annihilation operators. The used approximations relied on having a macroscopic occupation of the ground state level, implying that the system needs to exist at ultra-cold temperatures [3]. Using these approximations, an expression for the many-body Hamiltonian has been obtained in the second part of the chapter. Similarly to the analysis as presented in chapter 3, the potentials describing the interaction amongst two atoms and the interaction describing the coupling between two atoms in the open channel subspace and a molecule in the closed channel subspace have been defined to be separable and are contributed a finite range cut-off K. The value of the momentum-space analogue of this cut-off has been previously analysed in chapter 6. Using the obtained many-body Hamiltonian, the final part of this chapter has focussed on the derivation of the equations of motion for the molecular condensate, the atomic condensate, the excited state atoms and the anomalous density term. In the derivation of these expressions, only second order correlations between interacting particles have been considered. The obtained expressions correspond to the momentum space analogue of the equations as presented by S.Kokkelmans and M.Holland [68]. In order to verify whether the equations of motion which have been derived in this chapter are consistent with the open- and closed channel wave function as introduced in section 2.7, the vacuum limit of the equations of motion will be inspected in the next chapter.

[3] In the model used in this report, temperature effects have not been included. Meaning that the temperature has been set to an artificial value of absolute zero

Chapter 11

Many-body equations in the vacuum limit

Having obtained the equations of motion for the relevant many-body quantities in the previous chapter, this chapter will focus on the analysis of the vacuum limit of these equations. In this limit, no background gas exists. This means that the quantities $|\psi_a|^2$, $|\psi_m|^2$ and ρ_k, which signify the populations in the atomic condensate, the molecular condensate and the excited state respectively, are set to equal a value of zero. This vacuum limit is interesting as the many-body equations should reduce to the two-body equations for the open channel wave function $|\psi_P\rangle$ and the closed channel wave function $|\psi_Q\rangle$ which have been introduced in section 2.7. Before moving on to the analysis of the vacuum limit of the relevant many-body equations however, the exact relation between the two-body wave functions and the many-body expressions will be discussed in more detail in the following two sections.

11.1 The open channel wave function and the anomalous density

As previously mentioned in section 10.6, the anomalous density term $\kappa_{\mathbf{k}}$ quantifies the correlations between excited state atoms and includes the possibility of the formation of a bound state which, in the case of the many-body system, corresponds to a molecular state which lives in a closed channel. This is similar to the physical interpretation of the non-zero relative moment components[1] of the open channel wave function $|\psi_P\rangle$. However, in order to compare the open channel wave function $|\psi_P\rangle$ to the vacuum limit of the anomalous density term $\kappa_{\mathbf{k}}$, it should be remembered that the two-body scattering analysis has been reduced to the analysis of a single particle interaction with a finite range potential. Therefore, in order to properly compare the anomalous density term with this reduced mass two-body wave function, the mapping between the single particle mass m and the reduced particle mass μ has to be carefully implemented. Taking this mapping into account, the comparison between the open channel wave function $\psi(k)$ and the anomalous density term $\kappa_{\mathbf{k}}$ will be discussed in section 11.3.

[1] The zero relative momentum component is included in the atomic condensate.

11.2 The closed channel wave function and the molecular condensate

In the analysis of the closed channel wave function $|\psi_Q\rangle$ as presented in section 2.7, the closed channel continuum states have been neglected and a single bound state $|\phi_i\rangle$ is defined to live in the closed channel subspace. We can now define an amplitude ϕ_i for the closed channel to be in this bound state as follows:

$$\phi_i = \frac{\langle \phi_i | \psi_Q \rangle}{\sqrt{2}}. \tag{11.1}$$

A similar amplitude function has been introduced by S.Kokkelmans in reference [24]. However, the definition as presented in equation 11.1 is divided by an additional factor $\sqrt{2}$. The difference in the definition of the amplitude follows from the consideration of identical bosons instead of identical fermions with an additional spin degree of freedom, which were analysed in reference [24]. Equation 11.1 indicates the possibility to compare the closed channel wave-function $|\psi_Q\rangle$ to the molecular condensate function ψ_m through the projection of the closed channel wave function onto the bound state ψ_Q. This projection procedure will be analysed in detail in section 11.4.

11.3 The vacuum limit of the anomalous density equation of motion

Having analysed the relation between the anomalous density term and the open channel wave function in section 11.1, the correspondence between these two terms will be analysed in this section. In order to verify this correspondence, the equation of motion of the anomalous density $\kappa_{\mathbf{k}}$ as presented in expression 10.53 needs to be inspected in the vacuum limit. Taking the vacuum limit of this expression amounts to setting the density of the background gas to a value of zero. Implementing this information, equation 10.53 reduces to the following form:

$$i\hbar\dot{\kappa}_{\mathbf{k}} = 2E_{\mathbf{k}}\kappa_{\mathbf{k}} - \tilde{V}\sum_{p'}{}' \theta\left(K - |\mathbf{k}|\right)\theta\left(K - |\mathbf{p}'|\right)\kappa_{\mathbf{p}'} - \tilde{V}\theta\left(K - |\mathbf{k}|\right)\psi_a^2 - \tilde{G}\theta\left(K - |\mathbf{k}|\right)\psi_m, \tag{11.2}$$

where first two terms on the right hand side of equation 11.2 are the *homogeneous* terms, depending on the existence of $\kappa_{\mathbf{k}}$. More specifically, the first term on the right hand side of equation 11.2 describes the kinetic energy of the anomalous density term $E_{\mathbf{k}} = t^a_{\mathbf{k}}$, whereas the second term on the right hand side of the same equation describes the interaction between atoms with initial wave numbers $\mathbf{p}'$ and $-\mathbf{p}'$. These atoms experience an interaction with a strength $-\tilde{V}$ and exit the interaction with wave numbers $\mathbf{k}$ and $-\mathbf{k}$. Contrary to the first two terms on the right hand side of equation 11.2, the third and the fourth term in this same equation represent the *source* terms. The third term on the right hand side of equation 11.2 describes the formation of atoms with non-zero wave numbers $\mathbf{k}$ and $-\mathbf{k}$ as a result of the interaction between atoms in the atomic condensate. The fourth term on the right hand side of equation 11.2 describes a similar procedure. However, in this term, the seeding of $\kappa_{\mathbf{k}}$ is a result of interactions taking place in the molecular condensate, which is coupled to the open channel subspace with an interaction strength $-\tilde{G}$.

In order to be able to compare the vacuum limit of the anomalous density term $\kappa_{\mathbf{k}}$ as presented in equation 11.2 to the open channel wave function $|\psi_P\rangle$, the eigenvalue equation corresponding to equation 11.2 has to be obtained. This is needed due to the fact that the two-body equations are not dynamical. In order to obtain a time independent eigenvalue equation of the anomalous density term, the time-dependent Schrödinger equation has to be solved, yielding the following general

outcome[2]:

$$\kappa(\mathbf{k},t) = \sum_{n=1}^{\infty} c_n \phi_{a,n}(\mathbf{k}) e^{-iE_n t/\hbar}. \tag{11.3}$$

Notice that the subscript a has been used in equation 11.3 in order to express the stationary solutions of the anomalous density term. This subscript has been chosen in order to clarify that the considered solution defines an *atomic* state. Upon substituting equation 11.3 into equation 11.2, the following eigenvalue equation for the atomic state ϕ_a can be obtained[3]:

$$\begin{aligned} E_n \phi_a(\mathbf{k}) =& 2E_{\mathbf{k}} \phi_a(\mathbf{k}) - \tilde{V} {\sum_{\mathbf{p}'}}' \theta\left(K - |\mathbf{k}|\right) \theta\left(K - |\mathbf{p}'|\right) \phi_a(\mathbf{p}') - \tilde{V} \theta\left(K - |\mathbf{k}|\right) \phi_a(0) \\ & - \tilde{G} \theta\left(K - |\mathbf{k}|\right) \phi_m. \end{aligned} \tag{11.4}$$

As can be seen upon inspection of the previous equation, the eigenvalue equation for the atomic state ϕ_a is a function of the eigenvalue equation of the molecular condensate ϕ_m. The means that the eigenvalue equations of these two components ϕ_a and ϕ_m are coupled, similarly to the coupling that exists between the open channel wave function and the closed channel wave function as described in section 2.7. This once more indicates the analogy between the Feshbach formalism which has been described in section 2.7 and the many-body analysis which has been carried out in the previous chapter.

Having obtained the eigenvalue equation as presented above, it is now possible to follow the outline as suggested in section 11.1 in order to establish a correspondence between the two-body wave function $|\psi_P\rangle$ and the vacuum limit of the many-body anomalous density term $\kappa_{\mathbf{k}}$. In carrying out this comparison, the wave number normalized equivalent of the potential terms as present in matrix equation 4.1 will be applied. In order to signify using wave number normalized potential strengths instead of momentum normalized potential strengths, an overhead tilde will be added to the potential strength terms[4], yielding the following outcome: Upon using these newly defined potential terms and applying equations 2.35 and 4.1, the following expression for the open channel wave function $|\psi_P\rangle$ can be obtained:

$$E\left|\psi_P\right\rangle = \hat{H}^0 \left|\psi_P\right\rangle - \tilde{\eta} \left|g\right\rangle \left\langle g\right| - \tilde{\beta} \left|g\right\rangle \left\langle g|\psi_Q\right\rangle \tag{11.5}$$

Projecting the previous equation onto the relative wave number state $|\mathbf{k}\rangle$ results in the following outcome:

$$E\psi_P(\mathbf{k}) = E_{kin}^{red}(\mathbf{k})\psi_P(\mathbf{k}) - \tilde{\eta} \left\langle \mathbf{k}|g\right\rangle \int \left\langle g|\mathbf{k}'\right\rangle \left\langle \mathbf{k}'|\psi_P\right\rangle d\mathbf{k}' - \tilde{\beta} \left\langle \mathbf{k}|g\right\rangle \int \left\langle g|\mathbf{k}'\right\rangle \left\langle \mathbf{k}'|\phi_i\right\rangle \left\langle \phi_i|\psi_Q\right\rangle d\mathbf{k}'. \tag{11.6}$$

In order to calculate the term $-\tilde{\beta} \left\langle \mathbf{k}'|\psi_i\right\rangle$, the following relations can be introduced:

$$-\tilde{\beta} \left\langle \mathbf{k}'|\phi_i\right\rangle = -\frac{\tilde{g}_1(\mathbf{k}')}{\sqrt{2}}, \tag{11.7}$$

$$\text{with} \quad -\int \frac{\tilde{g}_1(\mathbf{k}')}{\sqrt{2}} \theta\left(K - |\mathbf{k}'|\right) d\mathbf{k}' = \frac{\tilde{g}_1}{\sqrt{2}(2\pi)^{3/2}} = -\frac{G_1}{\sqrt{2}}. \tag{11.8}$$

[2]This solution is only valid in the *quasi-stationary* limit. This means that the time dependency of the density term $\rho_{\mathbf{k}}$ and the atomic condensate ψ_A is neglected. This is possible if the dynamics of these terms evolve slower than the dynamics of the anomalous density term.

[3]The eigenvalue equations in this chapter use *right* eigenvector. The significance of this clarification will be discussed in more detail in section 12.1.

[4]The wave number potential strengths $\tilde{\eta}$ and $\tilde{\beta}$ are related to the momentum normalized potential strengths η and β as follows: $\tilde{\eta} = \hbar^3\eta$ and $\tilde{\beta} = \hbar^3\beta$.

The equations as presented above have been inspired by reference [24] and the details of these relations are presented in appendix J. As the set of parameters which is introduced in this appendix greatly simplify the notation of the many-body equations of motion, they will be used throughout the remainder of this report.

Upon applying the newly introduced relations as presented above and utilising expression 11.1 , equation 11.6 reduces to the following form:

$$E\psi_P(\mathbf{k}) = E_{kin}^{red}(\mathbf{k})\psi_P(\mathbf{k}) - \tilde{\eta}\theta\left(K - |\mathbf{k}|\right)\int \theta\left(K - |\mathbf{k}'|\right)\psi_P(\mathbf{k}')d\mathbf{k}' - G_1\phi_i. \tag{11.9}$$

The superscript which has been added to the kinetic energy term in the previous equation refers to the fact that the kinetic energy is measured for a particle with a reduced mass μ. Using this information, it becomes clear that the term $E_{kin}^{red}(\mathbf{k})$ which is present in the previous equation is equivalent to the term $2E_{\mathbf{k}}$ which is present in expression 11.4. Having established the relation between the kinetic energy terms in equations 11.9 and 11.4, the two equations seem to match once identifying the potential strengths $\tilde{\eta}$ and G_1 with the potential strengths $\tilde{V}$ and $\tilde{G}$ respectively[5] Having established a correspondence between the many-body equation for the anomalous density term in the vacuum limit and the open channel wave function, the next section will verify if this correspondence can be extended to link the molecular condensate wave function to the closed channel wave function.

11.4 The vacuum limit of the equation of motion of the molecular condensate ϕ_m

Similarly to the process followed in the previous section, the first step in analysing the correspondence between the molecular condensate wave function and the closed channel wave function $|\psi_Q\rangle$ amounts to inspecting the vacuum limit of the molecular equation of motion. Applying this limit to expression 10.43, the following equation can be obtained:

$$i\hbar\dot{\psi}_m = \nu\psi_m - \frac{\tilde{G}}{2}\sum_{\mathbf{q}}\theta\left(K - |\mathbf{q}|\right)\kappa_{\mathbf{q}}. \tag{11.10}$$

As previously discussed in section 2.7, the first term on the right hand side of equation 11.10 quantifies the detuning of the closed channel bound state with respect to the open channel asymptotic energy and is defined as $\nu = \epsilon_Q + C$. Following the terminology introduced in the previous section, this term could be regarded as the *homogeneous term* of the molecular condensate wave function [66]. Next, the second term on the right hand side of equation 11.10, which can be regarded as a *source term*, describes the seeding of the molecular condensate as a result of the interaction between two atoms with opposite relative wave number q with an interaction strength $\tilde{G}/2$.

Following the same approach as outlined in the previous section, equation 11.10 can be used in order to obtain the following eigenvalue equation:

$$E_n\phi_{m,n} = \nu\phi_{m,n} - \frac{\tilde{G}}{2}\sum_{\mathbf{q}}\theta\left(K - |\mathbf{q}|\right)\phi_a(\mathbf{q}). \tag{11.11}$$

As suggested in section 11.2, the previous equation can be compared to the closed channel wave function projected onto a bound state ϕ_i. Using equation 2.36 and implementing the knowledge that

[5] In the analysis, the fraction $V/(2\pi)^3$ has been set to equal a value of 1, considering the relation $\sum_k \rightarrow \int \frac{V}{(2\pi)^3}d\mathbf{k}$, this means that the summation and the integration terms are interchangeable.

the normalized bound state ϕ_i is the only bound state that exists in the closed channel subspace, the projection of the closed channel wave function onto this bound state results in the expression as presented below:

$$E\left|\phi_i\right\rangle\left\langle\phi_i|\psi_Q\right\rangle = -\tilde{\beta}\left|g\right\rangle\left\langle g|\psi_P\right\rangle + \hat{H}_{QQ}\left|\phi_i\right\rangle\left\langle\phi_i|\psi_Q\right\rangle. \tag{11.12}$$

The function $\hat{H}_{QQ}\left|\phi_i\right\rangle$ has been previously encountered in section 2.7 and simply yields the bound state energy $\nu = \epsilon_Q + C$ as an eigenvalue. Using this knowledge and applying equation 11.1, the previous expression can be rewritten into the following analogous form:

$$\sqrt{2}E\phi_i = -\tilde{\beta}\iint\left\langle\phi_m|\mathbf{k}\right\rangle\left\langle\mathbf{k}|g\right\rangle\left\langle g|\mathbf{k}'\right\rangle\left\langle\mathbf{k}'|\psi_P\right\rangle d\mathbf{k}d\mathbf{k}' + \sqrt{2}\nu\phi_i. \tag{11.13}$$

Implementing the relation as presented by equation 11.8, the previous expression reduces to the following form:

$$E\phi_m = -\frac{G_1}{2}\int\theta\left(K - |\mathbf{k}|\right)\psi_P(\mathbf{k})d\mathbf{k}' + \nu\phi_m. \tag{11.14}$$

Comparing the previous equation to expression 11.10, the correspondence between the two equations can be seen by once more matching the potential strengths $\tilde{V}$ and $\tilde{G}$ to the parameters $\tilde{\eta}$ and G_1.

11.5 Conclusion

In this chapter, the vacuum limit of the many-body equations for the molecular condensate ϕ_m and the anomalous density term $\kappa_{\mathbf{k}}$ have been compared to the two-body wave functions $|\psi_P\rangle$ and $|\psi_Q\rangle$. This comparison revealed a correspondence between the many-body equations in the vacuum limit and the two-body equations. Motivated by the match between two-body and many-body equations, the next chapter will focus on the derivation of the many-body analogue of the coupled-channel T-matrix as analysed in chapter 4 and the many-body equivalent of the dimer energy as analysed in chapter 6.

Chapter 12

The Embedded T-matrix and the embedded dimer energy

The first part of this chapter will focus on the derivation of the many-body analogue of the coupled-channels transition matrix which has been discussed in chapter 4. The steps taken in this derivation match the steps which were taken in the derivation of the two-body transition matrix to a large extend. Therefore, the derivation of the many-body transition matrix, which is referred to as the *embedded* T-matrix [6], does not require an introduction of a new method of analysis. Once the embedded transition matrix has been obtained, the second part of the chapter will focus on the analysis of the embedded dimer energy, which can be extracted from the pole of the embedded transition matrix. In the analysis of this factor, the differences between the dimer energy in a two-body system and the dimer energy in a many-body system will be discussed in detail. This makes it possible to specify the effect of the background gas on the formation of two-body bound states.

12.1 The asymmetric many-body coupled-channels matrix

As the analogy between the many-body equations in the vacuum limit and the two-body coupled-channels equations has been established in chapter 11, it is possible to express the many-body coupled-channels components in a matrix form which is similar to the two-body coupled-channels matrix as presented by equation 4.1. However, unlike the two-body matrix, the many-body coupled-channels matrix is asymmetric. This is a result of the presence of the Bose enhancement term[1] $(1 + 2\rho_{\mathbf{k}})$ in the anomalous density term $\kappa_{\mathbf{k}}$, and the absence of this same term in the molecular condensate term ϕ_m. As previously mentioned in subsection 10.6.4, the Bose enhancement term effectively acts to enhance the dynamics of excitation pairs which are formed in a wave number mode which is already occupied by other identical bosons. The absence of the enhancement term in the equation of motion of the molecular condensate can be understood upon realizing that the molecules have been considered to be non-interacting. The excited atoms as represented by the anomalous density term $\kappa_{\mathbf{k}}$ on the other hand interact with a potential strength $\tilde{V}$ as previously mentioned in section 10.5. In order to represent the effect of Bose-enhancement in operator form, the following operator $\hat{B}$ is introduced [21]

$$\langle \mathbf{k}| \hat{B} = (1 + 2\rho_{\mathbf{k}}) \langle \mathbf{k}| . \tag{12.1}$$

The wave number k which is acted on by the Bose-enhancement operator $\hat{B}$ in the previous equation represents a relative wave number state between two atoms. It should be noted that the

[1] The factor 2 in this term is a result of having reduced the two-particle system to a single particle system with relative momentum k. This means that the two atoms yield the enhancement term: $1 + \rho_{\mathbf{k}} + \rho_{-\mathbf{k}} = 1 + 2\rho_{\mathbf{k}}$.

Bose-enhancement operator is asymmetric, as $\langle k|\hat{B}|k'\rangle \neq \langle k'|\hat{B}|k\rangle$, with $\mathbf{k}, \mathbf{k}' \neq 0$. This asymmetry of the Bose-enhancement operator causes a difference between the left- and right eigenvectors of the coupled-channels system. The relation between these eigenvectors has been studied in appendix O.

In order to further simplify the notation of the many-body coupled-channels system, the approach as outlined by Blaizot and Ripka [62] is used as an inspiration in order to introduce the following reduced particle version of the *Hartree-Fock* Hamiltonian h_{hf} as defined in reference [62]:

$$h_{hf}^{red}(\mathbf{k},t) = E_{kin}^{red}(\mathbf{k}) - 4\tilde{V}\sum_{\mathbf{p}'}{}' \theta\left(K - \frac{|\mathbf{k}-\mathbf{p}'|}{2}\right)\rho_{\mathbf{p}'}(t) - 4\tilde{V}\theta\left(K - \frac{|\mathbf{k}|}{2}\right)|\psi_a(t)|^2. \tag{12.2}$$

Upon using the right eigenvectors of the system and implementing the newly introduced Bose-enhancement operator $\hat{B}$ and the Hartree-Fock Hamiltonian h_{hf}^{red}, it is possible to express the coupled-channels matrix representation of the many-body equations as follows:

$$E\begin{pmatrix}|\psi_P^R\rangle \\ |\psi_Q^R\rangle\end{pmatrix} = \begin{pmatrix}\hat{h}_{hf}^{red}(t) + \hat{B}\hat{V} & \hat{B}\hat{G} \\ \hat{G} & \hat{H}_{QQ}\end{pmatrix}\begin{pmatrix}|\psi_P^R\rangle \\ |\psi_Q^R\rangle\end{pmatrix} \tag{12.3}$$

The eigenvector $|\psi_P^R\rangle$ which has been introduced in the previous matrix equation corresponds to the open channel wave function, which, if projected onto the relative momentum state $|\mathbf{k}\rangle$, yields the embedded analogue of the eigenvalue equation for $\phi_a(\mathbf{k})$ as represented by 11.4. Furthermore, the eigenvector $|\psi_Q^R\rangle$ which has been introduced in the previous equation corresponds to the closed channel wave function, which, if projected onto the bound state $|\phi_i\rangle$ yields the embedded analogue of the eigenvalue equation for ϕ_m as represented by equation 11.12.

The asymmetry in the matrix as presented above disappears in the vacuum limit, as the Bose-enhancement operator $\hat{B}$ reduces to the identity operator in this limit. Furthermore, the difference between the left- and right eigenvectors also disappears in this same limit, as analysed in appendix O. From this point onwards, the superscript R which has been used in equation 12.3 in order to clarify the usage of right eigenvectors instead of left eigenvectors will be omitted and right eigenvectors will be used throughout the remainder of this report.

12.2 The Feshbach formalism and the embedded T-matrix

Using the coupled-channels many-body system as described by equation 12.3 and eliminating the closed-channel dependency of the open-channel wave function $|\psi_P\rangle$, it is possible to extract the expression:

$$E\,|\psi_P\rangle = \hat{h}_{hf}^{red}(t)\,|\psi_P\rangle + \hat{B}\hat{V}\,|\psi_P\rangle + \hat{B}\hat{G}\frac{1}{E-\hat{H}_{QQ}}\hat{G}\,|\psi_P\rangle\,. \tag{12.4}$$

Applying the approach as outlined in section 2.7, the previous equation can be solved in order to obtain the following expression for the open channel wave function $|\psi_P\rangle$:

$$|\psi_P^+\rangle = |\phi_P^+\rangle + \frac{1}{E-\hat{h}_{hf}^{red}(t)-\hat{B}\hat{V}}\hat{B}\hat{G}\frac{1}{E-\hat{H}_{QQ}}\hat{G}\,|\psi_P\rangle\,. \tag{12.5}$$

Analogously to the notation used in the analysis of the two-body coupled channel system as presented in chapter 2, the superscript + has been added to the previous expression in order to signify the addition of a infinitesimally small *positive* imaginary component to the denominators in the previous function in order to avoid the possible existence of singularities for positive scattering energies.

Furthermore, having introduced a similar asymptotic solution in equation 2.44, the solution $|\phi_P^+\rangle$ which is introduced in the previous expression corresponds to the embedded equivalent of equation 2.44 and can be expressed as follows:

$$|\phi_P^+\rangle = |\mathbf{k}\rangle + \hat{G}_P^e(E,t)\hat{B}\hat{V}\,|\mathbf{k}\rangle\,. \tag{12.6}$$

The state $|\mathbf{k}\rangle$ which has been introduced in the previous equation corresponds to an unscattered plane wave state. Furthermore, the newly introduced Green's operator $\hat{G}_P^e(E,t)$ should not be confused with the open channel Green's operator $\hat{G}_P(E)$ which prevails in the denominator of expression 2.44. The operator $\hat{G}_P^e(E)$ represents the *embedded* analogue of the open channel Green's operator $\hat{G}_P(E)$. Upon inspection of the expression 12.3, it can be deduced that this embedded open channel Green's operator is defined as follows:

$$\hat{G}_P^e(E,t) = \left(E - \hat{h}_{hf}^{red}(t) - \hat{B}\hat{V}\right)^{-1}. \tag{12.7}$$

Contrary to the open channel Green's function, the closed channel Green's function $G_Q(E)$ is not affected by the presence of a background gas. Once more, this is the result of the absence of Bose enhancement in the closed channel subspace. Using this knowledge and implementing the definition of the embedded open channel Green's operator, equation 12.5 can be rewritten into the following form:

$$|\psi_P^+\rangle = |\phi_P^+\rangle + \hat{G}_P^e(E,t)\hat{B}\hat{G}\hat{G}_Q(E)\hat{G}\,|\psi_P^+\rangle\,. \tag{12.8}$$

Using the previous equation together with the definition of the asymptotic solution $|\phi_P^+\rangle$ as presented in equation 12.6 and applying the definition of the transition matrix as presented by expression 2.34, it is possible to obtain the following expression for the embedded transition operator:

$$\hat{T}(E,t)\,|k\rangle = \hat{V}_{eff}\,|\psi_P^+\rangle = \left(\hat{B}\hat{V} + \hat{B}\hat{G}\hat{G}_Q(E)\hat{G}\right)|\psi_P^+\rangle\,. \tag{12.9}$$

Projecting the previous equation onto a relative momentums state $|\mathbf{k}'\rangle$ and substituting the expression for $|\psi_P\rangle$ as presented in expression 12.8 into the previous relation, the following equation for the on-shell embedded transition matrix $T(\mathbf{k},\mathbf{k}',E)$ can be found:

$$\begin{aligned} T(E,\mathbf{k},\mathbf{k}',t) = {} & \langle\mathbf{k}|\hat{B}\hat{V}|\phi_P^+\rangle + \langle\mathbf{k}|\hat{B}\hat{G}\hat{G}_Q(E)\hat{G}|\phi_P^+\rangle + \langle\mathbf{k}|\hat{B}\hat{V}\hat{G}_P^e(E,t)\hat{B}\hat{G}\hat{G}_Q(E)\hat{G}|\psi_P^+\rangle \\ & + \langle\mathbf{k}|\hat{B}\hat{G}\hat{G}_Q(E)\hat{G}\hat{G}_P^e(E,t)\hat{B}\hat{G}\hat{G}_Q(E)\hat{G}|\psi_P^+\rangle\,. \end{aligned} \tag{12.10}$$

Solving equation 12.8 for $|\phi_P^+\rangle$, it is possible to rewrite the second term on the right hand side of expression 12.10, resulting in the following equivalent equation:

$$T(E,\mathbf{k},\mathbf{k}',t) = \langle\mathbf{k}|\hat{B}\hat{V}|\phi_P^+\rangle + \langle\mathbf{k}|\left(1 + \hat{B}\hat{V}\hat{G}_P^e(E,t)\right)\hat{B}\hat{G}\hat{G}_Q(E)\hat{G}|\psi_P^+\rangle\,. \tag{12.11}$$

The second term on the right hand side has been written into a suggestive form through the usage of the rounded brackets. A comparison between this bracketed term and equation 12.6 reveals that this term corresponds to the left-hand variant of expression 12.6. Therefore, it is possible to rewrite the previous equation into the following simplified form:

$$T(E,\mathbf{k},\mathbf{k}',t) = \langle\mathbf{k}|\hat{B}\hat{V}|\phi_P^+\rangle + \langle\phi_P^-|\hat{B}\hat{G}\hat{G}_Q(E)\hat{G}|\psi_P^+\rangle\,. \tag{12.12}$$

Next, upon using the same approximations as outlined in section 2.7, meaning that only a single bound state $|\phi_i\rangle$ is assumed to live in the closed channel subspace and the continuum states are neglected, it is possible to implement equation 2.41 into the previous expression, resulting in the following outcome:

$$T(E,\mathbf{k},\mathbf{k}',t) = \langle\mathbf{k}|\hat{B}\hat{V}|\phi_P^+\rangle + \frac{\langle\phi_P^-|\hat{B}\hat{G}|\phi_i\rangle\,\langle\phi_i|\hat{G}|\psi_P^+\rangle}{E-\nu_i}. \tag{12.13}$$

Comparing the previous expression to equation 2.47, the similarities between the embedded version of the transition matrix and the two-body transition matrix are now clearly visible. To be more specific, the two-body version of the transition matrix can be obtained from expression 12.13 in the vacuum limit, which amounts to replacing the Bose-enhancement operator with the identity operator and replacing the Hartree-Fock Hamiltonian operator with the kinetic energy operator.

Completely analogous to the method followed in chapter 4, it is possible to get rid of the explicit $|\psi_P^+\rangle$ dependency of the previous equation through the projection of expression 12.8 onto the state $\langle\phi_i|\,\hat{G}$. Upon carrying out this procedure and substituting the result into the previous equation, the following final general expression for the embedded transition matrix can be obtained:

$$T(E,\mathbf{k},\mathbf{k}',t) = \langle\mathbf{k}|\hat{B}\hat{V}|\phi_P^+\rangle + \frac{\langle\phi_P^-|\hat{B}\hat{G}|\phi_i\rangle\,\langle\phi_i|\hat{G}|\phi_P^+\rangle}{E-\nu_i-\langle\phi_i|\hat{G}\hat{G}_P^e(E,t)\hat{B}\hat{G}|\phi_i\rangle}. \tag{12.14}$$

As the previous equation only contains known terms, it is possible to follow the approach as outlined in chapter 4 in order to compute the embedded transition matrix which describes the scattering physics of the many-body system. In order to clarify the steps taken in the derivation of the embedded transition matrix, the components which have been indicated by different colors in equation 12.14 will be discussed in separate subsections.

12.2.1 Analysis of the uncoupled T-matrix term

The term which has been highlighted in purple in expression 12.14 represents the uncoupled part of the embedded two-channel T-matrix, as $\langle\mathbf{k}|\hat{B}\hat{V}|\phi_P^+\rangle = \langle\mathbf{k}|\hat{T}_{unc}(E,t)|\mathbf{k}'\rangle$. Using the definition of the T-matrix as presented in equation 2.33, this element can be calculated as follows:

$$\langle\mathbf{k}|\hat{T}_{unc}(E,t)|\mathbf{k}'\rangle = \langle\mathbf{k}|\hat{B}\hat{V}|\mathbf{k}'\rangle + \langle\mathbf{k}|\hat{B}\hat{V}\frac{1}{E-\hat{h}_{hf}}\hat{T}_{unc}(E,t)|\mathbf{k}'\rangle\,. \tag{12.15}$$

In order to simplify the analysis of the previous expression, the following operator $\tilde{T}_{unc}(E,t)$ is introduced:

$$\hat{T}_{unc}(E,t) = \hat{B}\tilde{T}_{unc}(E,t). \tag{12.16}$$

Upon implementing the previous expression into equation 12.15, the equivalent relation as presented below can be obtained:

$$(1+2\rho_{\mathbf{k}})\,\langle\mathbf{k}|\tilde{T}_{unc}(E,t)|\mathbf{k}'\rangle = (1+2\rho_{\mathbf{k}})\,\langle\mathbf{k}|\hat{V}|\mathbf{k}'\rangle + (1+2\rho_{\mathbf{k}})\,\langle\mathbf{k}|\hat{V}\frac{1}{E-\hat{h}_{hf}}\hat{B}\tilde{T}_{unc}(E,t)|\mathbf{k}'\rangle\,. \tag{12.17}$$

Dividing the previous expression by the Bose-enhancement term $(1+2\rho_{\mathbf{k}})$ and implementing the definition of the operators $\hat{B}$ and $\hat{V}$, equation 12.17 reduces to:

$$\langle\mathbf{k}|\tilde{T}_{unc}(E,t)|\mathbf{k}'\rangle = -\tilde{V}\,\langle\mathbf{k}|g\rangle\,\langle g|\mathbf{k}'\rangle - 4\pi\tilde{V}\,\langle\mathbf{k}|g\rangle\int_0^\Lambda \frac{(1+2\rho_{\mathbf{k}}'')k''^2}{E-h_{hf}^{red}(\mathbf{k}'')}\,\langle\mathbf{k}''|\tilde{T}_{unc}|\mathbf{k}'\rangle\,dk''. \tag{12.18}$$

Analogously to the outline followed in chapter 3, the embedded transition matrix can be expressed in the following separable form: $\tilde{T}_{unc}(E,t) = -\tilde{\tau}(E,t)\,|g\rangle\,\langle g|$. Using this form to rewrite the previous equation, the following equivalent expression can be obtained:

$$-\tilde{\tau}(E,t)g(\mathbf{k})g(\mathbf{k}') = -\tilde{V}g(\mathbf{k})g(\mathbf{k}') + 4\pi g(\mathbf{k})g(\mathbf{k}')\tilde{\tau}(E,t)\tilde{V}\int_0^\Lambda \frac{k''^2}{E-h_{hf}^{red}(\mathbf{k}'',t)}(1+2\rho_{\mathbf{k}''}(t))dk''. \tag{12.19}$$

Taking the vacuum limit of the previous equation, the expression for the $\tau(z)$ function as presented in equation 3.9 is rediscovered. Using this equivalence as a motivation, the embedded equivalent of the integral equation $\xi(z)$ as presented in equation 3.10 is now introduced:

$$\xi_{\rho}^{emb}(E,t) = \int_0^{\Lambda} \frac{k''^2}{E - 2h_{hf}(\mathbf{k}'',t)}(1 + 2\rho_{\mathbf{k}''}(t))dk''. \tag{12.20}$$

Contrary to equation 3.10, it is not possible to solve the previous equation analytically, as the expression is a function of the time-dependent parameters $\psi_a(t)$ and $\rho_{\mathbf{k}}(t)$, whose values needs to be extracted from many-body simulations. Substituting the expression for $\xi_{\rho}^{emb}(E,t)$ into equation 12.19, dividing by the form factors $g(k)g(k')$ and solving for the function $\tilde{\tau}(E,t)$, the following outcome can be recovered:

$$\tilde{\tau}(E,t) = \frac{\tilde{V}}{1 + 4\pi\tilde{V}\xi_{\rho}^{emb}(E,t)} \tag{12.21}$$

Using the relation between $\tilde{\tau}(E,t)$ and the operator $\tilde{T}(E,t)$ and applying the relation between $\tilde{T}_{unc}$ and $\hat{T}_{unc}$, the uncoupled embedded transition operator can be expressed as follows:

$$\hat{T}_{unc} = \frac{-\hat{B}\tilde{V}\,|g\rangle\,\langle g|}{1 + 4\pi\tilde{V}\xi_{\rho}^{emb}(E,t)}. \tag{12.22}$$

The projection of the previous equation onto the incoming and outgoing relative wave number states $|k\rangle$ and $|k'\rangle$ yields the following final expression for the uncoupled T-matrix part of equation 12.14:

$$T_{unc}(E,\mathbf{k},\mathbf{k}',t) = -(1 + 2\rho_{\mathbf{k}})\frac{\tilde{V}g(\mathbf{k})g(\mathbf{k}')}{1 + 4\pi\tilde{V}\xi_{emb}^{\rho}(E,t)}. \tag{12.23}$$

The result as presented in the previous expression can be directly substituted for the purple term of equation 12.14.

12.2.2 Finding an expression for $\langle\phi_P^-|\hat{B}\hat{G}|\phi_i\rangle\,\langle\phi_i|\hat{G}|\phi_P^+\rangle$

Whereas the investigation of the term highlighted in orange in equation 12.14 seems to be reminiscent of the analysis which has been performed in section 4.2, the difference between the left- and right-eigenvectors $|\phi_P^-\rangle$ and $|\phi_P^+\rangle$ and the presence of the Bose enhancement operator $\hat{B}$ in the highlighted term results in the fact that, contrary to the analysis as performed in section 4.2, the two different braket components both need to be analysed separately.

Using the relation $\hat{G}_P^e(E,t)\hat{B}\hat{V} = \hat{G}_P^{e,0}(E,t)\hat{T}_{unc}$, which has been previously applied in section 2.6, the left- and right eigenvectors, that are responsible for the symmetry breaking of the orange term in equation 12.14, can be expressed as follows:

$$\langle\phi_P^-| = \langle\mathbf{k}| + \langle\mathbf{k}|\,\hat{T}_{unc}(E,t)\frac{1}{E - \hat{h}_{hf}^{red}(t)} \tag{12.24}$$

$$|\phi_P^+\rangle = |\mathbf{k}'\rangle + \frac{1}{E - \hat{h}_{hf}^{red}(t)}\hat{T}_{unc}(E,t)\,|\mathbf{k}'\rangle \tag{12.25}$$

Expressing the uncoupled embedded transition operator in terms of $\hat{T}_{unc}(E,t) = -\hat{B}\tilde{\tau}(E,t)\,|g\rangle\,\langle g|$, as introduced in the previous section, the asymptotic solutions $|\phi_P^+\rangle$ and $|\phi_P^-\rangle$ can be rewritten into

the following equivalent form:

$$\langle \phi_P^- | = \langle \mathbf{k}| - \langle \mathbf{k}| \, \hat{B}\tilde{\tau}(E) \, |g\rangle \, \langle g| \, \frac{1}{E - \hat{h}_{hf}^{red}(t)}, \tag{12.26}$$

$$|\phi_P^+\rangle = |\mathbf{k}'\rangle - \frac{1}{E - \hat{h}_{hf}^{red}(t)} \hat{B}\tilde{\tau}(E) \, |g\rangle \, \langle g|\mathbf{k}'\rangle \, . \tag{12.27}$$

Having rewritten the asymptotic wave functions in terms of known operators and plane wave states, it is possible to express the orange term as presented in equation 12.14 as follows:

$$\langle \psi_P^- | \hat{B}\hat{G}|\phi_i\rangle \, \langle \phi_i|\hat{G}|\psi_P^+\rangle = \underbrace{\left(\langle \mathbf{k}|\hat{B}\hat{G}|\phi_i\rangle - \langle \mathbf{k}|\hat{B}\tilde{\tau}(E,t)|g\rangle \, \langle g| \frac{1}{E - \hat{h}_{hf}^{red}(t)} \hat{B}\hat{g}|\phi_i\rangle \right)}_{\text{A}} \cdot$$
$$\underbrace{\left(\langle \phi_i|\hat{G}|\mathbf{k}'\rangle - \langle \phi_i|\hat{G} \frac{1}{E - \hat{h}_{hf}^{red}(t)} \hat{B}\tilde{\tau}(E,t)|g\rangle \, \langle g|\mathbf{k}'\rangle \right)}_{\text{B}} \tag{12.28}$$

Due to the number of different terms which prevail in the previous expression, the equation has been split up into two parts, named part A and B which will be analysed separately in order to keep a manageable overview of the total analysis.

Proceeding with the analysis of part A as presented in the previous equation and explicitly working out the effect of the Bose enhancement operator, it is possible to obtain the following outcome:

$$A = (1 + 2\rho_{\mathbf{k}}) \left[\langle \mathbf{k}|\hat{G}|\phi_i\rangle - \tilde{\tau}(E,t) \, \langle \mathbf{k}|g\rangle \, \langle g| \frac{1}{E - \hat{h}_{hf}^{red}(t)} \hat{B}\hat{G}|\phi_i\rangle \right]. \tag{12.29}$$

Next, upon expanding the previous equation using normalized wave number states, the following equation can be recovered:

$$A = -(1 + 2\rho_{\mathbf{k}}) \, \langle \mathbf{k}|g\rangle \left[\int \beta \, \langle g|\mathbf{k}'\rangle \, \langle \mathbf{k}'|\phi_i\rangle \, d\mathbf{k}' \right. \tag{12.30}$$

$$\left. + \tilde{\tau}(E,t) \iiint \langle g|\mathbf{k}'\rangle \, \langle \mathbf{k}'| \frac{1}{E - \hat{h}_{hf}^{red}(t)} |\mathbf{k}''\rangle \, (1 + 2\rho_{\mathbf{k}''}) \, \langle \mathbf{k}''|g\rangle \, \beta \, \langle \mathbf{k}'''|\phi_i\rangle \, d\mathbf{k}' d\mathbf{k}'' d\mathbf{k}''' \right]. \tag{12.31}$$

The inspection of equation 12.30 reveals the presence of terms of the form $-\beta \, \langle \mathbf{k}|\phi_i\rangle$, which abide by the relations as presented by equations 11.7 and 11.8. Implementing these relations results in the following outcome:

$$A = -(1 + 2\rho_{\mathbf{k}}) \left[\langle \mathbf{k}|g\rangle \, \frac{G_1^*}{\sqrt{2}} - \tilde{\tau}(E,t) \, \langle \mathbf{k}|g\rangle \, \frac{G_1^*}{\sqrt{2}} \int |\langle g|\mathbf{k}'\rangle|^2 \frac{1}{E - h_{hf}^{red}(k',t)} d\mathbf{k}' \right]. \tag{12.32}$$

Recognizing the integral in the previous expression as the term $\xi_\rho^{emb}(E,t)$ which has been introduced in equation 12.20, the following final expression for the term A can be obtained:

$$= -\frac{G_1^*}{\sqrt{2}} (1 + 2\rho_{\mathbf{k}}) \, \langle \mathbf{k}|g\rangle \left[1 - 4\pi\tilde{\tau}(E,t) \xi_\rho^{emb}(E,t) \right]. \tag{12.33}$$

As the analysis for the part B as presented in equation 12.28 follows the same outline as the derivation of part A, the results of this analysis will be presented below without going into the details of the derivation:

$$B = -\frac{G_1}{\sqrt{2}} \, \langle g|\mathbf{k}'\rangle \left[1 - 4\pi\tilde{\tau}(E,t) \xi_\rho^{emb}(E,t) \right]. \tag{12.34}$$

Combining equations 12.33 and 12.34, the following final expression for the orange term as presented in equation 12.14 can be obtained:

$$\langle\phi_P^-|\hat{B}\hat{G}|\phi_i\rangle\,\langle\phi_i|\hat{G}|\phi_P^+\rangle = \frac{|G_1|^2}{2}\,\langle\mathbf{k}|g\rangle\,\langle g|\mathbf{k}'\rangle\left(1-4\pi\tilde{\tau}(E,t)\xi_\rho^{emb}(E,t)\right)^2. \tag{12.35}$$

The previous equation can be directly substituted into expression 12.28 in order to represent the numerator of the coupled part of the embedded transition matrix.

12.2.3 Analysis of the denominator of equation 12.14

In the analysis of the blue term in the denominator of equation 12.14, a difficulty which has previously been discussed in section 4.3 prevails. Similarly to the denominator of the two-body transition matrix, this term contains an open channel Green's operator which complicates the analysis. However, completely analogous to the procedure followed in section 4.3, it is possible to get rid of the dependence on the open channels Green's operator through the application of the following relation:

$$\begin{aligned}\langle\phi_i|\hat{G}\hat{G}_P^e(E,t)\hat{B}\hat{G}|\phi_i\rangle &= \langle\phi_i|\,\hat{G}\left[\frac{1}{E-\hat{h}_{hf}^{red}(t)}-\frac{1}{E-\hat{h}_{hf}^{red}(t)}\hat{B}\tilde{\tau}(E,t)\,|g\rangle\,\langle g|\,\frac{1}{E-\hat{h}_{hf}^{red}(t)}\right]\hat{B}\hat{G}\,|\phi_i\rangle \\ &= \underbrace{\langle\phi_i|\hat{G}\frac{1}{E-\hat{h}_{hf}^{red}(t)}\hat{B}\hat{G}|\phi_i\rangle}_{\text{C}} - \underbrace{\langle\phi_i|\frac{1}{E-\hat{h}_{hf}^{red}(t)}\hat{B}\tilde{\tau}(E,t)|g\rangle\,\langle g|\frac{1}{E-\hat{h}_{hf}^{red}(t)}\hat{B}\hat{G}|\phi_i\rangle}_{\text{D}}.\end{aligned} \tag{12.36}$$

Following the same method as applied in the previous section, equation 12.36 has been split-up into two parts in order to simplify the overall analysis. Investigating part C in more detail yields the following outcome:

$$\begin{aligned}C &= \langle\phi_i|\hat{G}\frac{1}{E-\hat{h}_{hf}^{red}(t)}\hat{B}\hat{G}|\phi_i\rangle\,, \\ &= \iiiint \langle\phi_i|\mathbf{k}'\rangle\,\langle\mathbf{k}'|g\rangle\,\beta\,\langle g|\mathbf{k}''\rangle\,\langle\mathbf{k}''|\frac{1}{E-\hat{h}_{hf}^{red}(t)}|\mathbf{k}'''\rangle\,(1+2\rho_{\mathbf{k}'''})\,\langle\mathbf{k}'''|g\rangle \\ &\qquad \beta\,\langle g|\mathbf{k}''''\rangle\,\langle\mathbf{k}''''|\phi_i\rangle\,d\mathbf{k}'d\mathbf{k}''d\mathbf{k}'''d\mathbf{k}.''''\end{aligned} \tag{12.37}$$

Once more, the application of the relations as presented in equation 11.7 and 11.8 prove useful in order to simplify the previous equation and to retrieve the following final expression for the term C:

$$\begin{aligned}C &= \frac{|G_1|^2}{2}\int|\langle g|\mathbf{k}'\rangle|^2\frac{1}{E-2h_{hf}(k,t')}(1+2\rho_{\mathbf{k}}')d\mathbf{k},' \\ &= 4\pi\frac{|G_1|^2}{2}\xi_\rho^{emb}(E,t).\end{aligned} \tag{12.38}$$

Having obtained a final expression for part C, the same approach can be applied in order to analyse the, slightly more complicated, part D. Due to the analogy in the derivation, only the final result is presented below:

$$D = \tilde{\tau}(E,t)(4\pi)^2\frac{|G_1|^2}{2}\xi_\rho^{emb}(E,t)^2. \tag{12.39}$$

Combining the previous expression with the outcome as presented in equation 12.38, it is possible to obtain the following final expression for the blue term in the denominator of expression 12.14:

$$\langle\phi_i|\frac{\hat{G}}{2}\hat{G}_P^e(E,t)\hat{B}\hat{G}|\phi_i\rangle = 4\pi\frac{|G|^2}{2}\xi_\rho^{emb}(E,t)\left(1-4\pi\tilde{\tau}(E,t)\xi_\rho^{emb}(E,t)\right). \tag{12.40}$$

12.2.4 Final expression for the embedded T-matrix

Having obtained the relevant expressions to rewrite equation 12.14 in the previous three subsections, the expression for the embedded transition matrix can be written into the following applicable form:

$$\begin{aligned} T(E,\mathbf{k},\mathbf{k}',t) =&(1+2\rho_{\mathbf{k}})\frac{-Vg(\mathbf{k})g(\mathbf{k}')}{1+4\pi V\xi^{\rho}_{emb}(E,t)} \\ &+\frac{\frac{|G_1|^2}{2}g(\mathbf{k})g(\mathbf{k}')\left(1-4\pi\tilde{\tau}(E,t)\xi^{emb}_{\rho}(E,t)\right)^2}{E-\nu-4\pi\frac{|G_1|^2}{2}\xi^{emb}_{\rho}(E,t)\left(1-4\pi\tilde{\tau}(E,t)\xi^{emb}_{\rho}(E,t)\right)}. \end{aligned} \tag{12.41}$$

Upon remembering that the potential interaction strength G_1 has been related to the factor g as introduced in appendix J and that this parameter has in turn been related to the system parameters such as the interaction strength β and the normalization factor X as outlined in equation J.15, the previous expression shows a remarkable similarity to the two-body transition matrix as presented in section 4.4. As a matter of fact, the comparison between the equation for the two-body transition matrix and the embedded version of the two-body transition matrix reveals that the embedded version reduces to the two-body transition matrix as presented in section 4.4 in the vacuum limit. Similarly to the analysis performed in chapter 11, this supports the validity of the derived many-body equations of motion.

12.3 The embedded dimer energy

Upon inspection of the pole of the coupled-channels part of the embedded transition matrix as presented in equation 12.41, the following expression for the embedded dimer energy $E_D(t)$ can be extracted:

$$E_D(t) = \nu + 2\pi|G|^2\xi^{emb}_{\rho}(E_D,t)\left(1+4\pi\tilde{\tau}(E_D,t)\xi^{emb}_{\rho}(E_D,t)\right). \tag{12.42}$$

Whereas the previous equation closely resembles the expression for the dimer energy as presented by equation 6.1, there is an important difference between these two expressions; being the explicit time dependence of the embedded dimer energy as presented in equation 12.43. This explicit time dependence, which was absent in the two-body dimer energy relation, not only means that the dimer energy will vary as a function of the time, but also means that the dimer energy cannot be calculated without the usage of numerical many-body simulation data of the population in the atomic condensate and the excited state population. Regardless of the explicit time-dependence and the dependence on numerical input data, it is still possible to follow the outline as presented in section 6.2 in order to rewrite the embedded dimer energy relation in terms of physical parameters, resulting in the following outcome:

$$\begin{aligned} E_D(t) =&\frac{-\hbar^2}{(a_s-a_{bg})mR^*}+\frac{2\hbar\Lambda}{\pi mR^*\left(1-\frac{2\Lambda a_{bg}}{\pi\hbar}\right)} \\ &+\frac{2\hbar\xi^{emb}_{\rho}(E_D,t)}{\pi m^2\left(1-\frac{2\Lambda a_{bg}}{\pi\hbar}\right)^2R^*}\left(1-\frac{\xi^{emb}_{\rho}(E_D,t)a_{bg}}{m\Lambda a_{bg}-\pi m\hbar/2+a_{bg}\xi^{emb}_{\rho}(E_D,t)}\right). \end{aligned} \tag{12.43}$$

In the vacuum limit, where $\xi^{emb}_{\rho}(E_D,t)\to\xi(E_D)$, with $\xi(E_D)$ defined as presented in equation 3.10, the previous equation reduces to the expression for the dimer energy as defined in equation 6.4. In order to gain more insight into the previous equation, we implement the information as presented

in section 1.4. As indicated in this section, the goal is to simulate a Bose-Einstein condensate at unitarity. Therefore, the simulation is initiated with all population contained in the atomic condensate. Furthermore, the system is quenched to unitarity. More details of this procedure will be outlined in the next chapter. However, for now it is enough to use the information that, at unitarity, the first term on the right hand side of the previous equation reduces to a value of zero. Furthermore, the initialization of the simulation with all population in the atomic condensate implies that the atomic excitation term $\rho_{\mathbf{k}}$ starts out with an initial value of zero. Using this information in the definition of the Hartree-Fock Hamiltonian as outlined in equation 12.2, this expression reduces to the following form:

$$h_{hf}^{red}(k) = E_{kin}^{red}(k) - 4\tilde{V}\theta\left(K - \frac{|k|}{2}\right)|\psi_a|^2. \tag{12.44}$$

The same relation has been found by V.E.Colussi [21]. As the volume in the many-body simulation will be set to equal a value of $1/n$, with n the atomic density, the second term on the right-hand side of the previous equation reduces to a value of $4Vn$, with $V = (2\pi)^3\tilde{V}$. Using this information, the expression for the integral equation $\xi_{\rho}^{emb}(E,t)$ reduces to the following form for $t = 0$:

$$\xi_{\rho}^{emb}(E,0) = \int_0^K \frac{k}{E - \frac{\hbar^2k^2}{m} + 4Vn}dk. \tag{12.45}$$

The previous expression for the integral equation $\xi_{\rho}^{emb}(E,t)$ is reminiscent of the integral equation as presented by expression 3.10. Upon mapping the momentum normalized expression for $\xi(z)$ as presented by equation 3.10 onto wave number space, and identifying the parameter z as $z = E-4Vn$, it becomes clear that the zero time limit of the embedded integral function $\xi_{\rho}^{emb}(E,t)$ corresponds to a *energy shifted* version of the two-body integral function $\xi(z)$. As V is defined to be positive and the dimer energy E_D is negative, the addition of the term $-4Vn$ to the dimer energy results in a shift of the energy towards a larger negative values. The effect of this energy shift on the embedded dimer energy will be investigated in more detail in the next chapter. As the many-body system is dynamic, the expression for the Hartree-Fock Hamiltonian as presented in equation 12.44 cannot be applied for times $t \neq 0$. Instead, its full form as presented by equation 12.2 has to be applied. Effectively, this means that the energy in the denominator of equation 12.45 is now shifted by the following amount:

$$E_{MF}(t) = -4V\left(\theta\left(K - \frac{|\mathbf{k}|}{2}\right)|\psi_a|^2 + \sum_{\mathbf{k}'}{}' \theta\left(K - \frac{|\mathbf{k}-\mathbf{k}'|}{2}\right)\rho_{\mathbf{k}'}\right). \tag{12.46}$$

The quantity $E_{MF}(t)$ which has been introduced in the previous equation is referred to as the *mean field shift*. An inspection of this equation reveals that, whereas it reduces to a value of $-4Vn$ for $t = 0$, the overall value of this function decreases as a function of the time as a small part of the population is drained to the molecular condensate. The magnitude of the change of the mean-field shift and its effect on the embedded dimer energy will be analysed in more detail in the next chapter. Having analysed the physical properties of the embedded dimer in more detail, the expression for the dimer energy as presented in equation 12.43 will be implemented numerically in order to investigate the embedded dimer energy for both Potassium-39 and Rubidium-85. The results of this analysis are presented in the next chapter.

12.4 Conclusion

In the first part of this chapter, the expression for the embedded transition matrix has been derived. Due to the analogy between the derivation of the two-body transition matrix and the embedded transition matrix, it has not been needed to introduce a new solving procedure. Instead, the steps taken in chapter 4 could be repeated for the many-body system. Applying these steps resulted in obtaining the transition matrix as presented in equation 12.41. In the vacuum limit, this expression reduces to the two-body transition matrix as presented in section 4.4. Similarly to the analysis as presented in the previous chapter, this supports the validity of the many-body model. Using the denominator of the embedded transition matrix, the expression for the embedded dimer energy could be extracted. Contrary to the dimer energy for the two-particle system, the embedded dimer energy is a function of the time, as it depends on the time dependent function $\xi_\rho^{emb}(E,t)$ as defined in equation 12.20. Furthermore, unlike the dimer energy in the two-body system, the embedded dimer is shifted towards more negative values by the mean field shift. The effect of the time dependence and the mean field shift on the embedded dimer energy will be analysed in more detail in the next chapter.

Chapter 13

Many-body coupled-channels simulations

Having analysed the equations of motion governing the many-body system in chapter 10 and having derived an expression for the embedded dimer energy in the previous chapter, this chapter will focus on the presentation of numerical results of the many-body simulation. The simulated model and the used input parameters will be presented in the first two sections of this chapter. After this, the Hartree-Fock-Bogoliubov equations will be applied in order to analyse the dynamics of a Bose-Einstein condensate consisting of either Potassium-39 and Rubidium-85. In this analysis, the calibrated values of the cut-off Λ which have introduced in chapter 6 will be implemented. Next, the embedded dimer energies of these two atomic species will be investigated. Furthermore, in order to inspect the effect of the resonance width on the observed embedded dimer energy, the resonance width parameter R^*, which is defined according to equation 5.27, will be varied. In order to gain an insight into the effect that this parameter has on the many-body system, the embedded dimer energy spectrum for Potassium-39 will be analysed for increasingly large values of the resonance strength parameter. Effectively this means that the resonance width is artificially reduced, without changing any other physical properties of the simulation, such as the background scattering length.

13.1 Input parameter values

In order to carry out the many-body simulations for Potassium-39 and Rubidium-85, the relevant experimental input parameter values have been extracted from an article by Chin et.al. [16]. Furthermore, the calibrated values of the momentum-space cut-off Λ as introduced in chapter 6 have been implemented in the simulations. An overview of this complete set of parameter values is presented in table 13.1.

Parameter	^{39}**K**	^{85}**Rb**	**Units**
R_{vdw}	64.61	82.1	a_0
$\bar{a}$	61.77	78.49	a_0
a_{bg}	-29	-443	a_0
m	38.9637	84.9	u
s_{res}	2.1	28	$-$
$\delta\mu$	1.5	-2.33	μ_B
B_0	402.4	155.04	G
Λ	0.46	0.6	$\hbar/R_{vdw}$

Table 13.1: Values of the system parameters for Potassium-39 and Rubidium-85 extracted from reference [16]. The parameters are expressed in units of the Bohr radius $a_0 = 5.29 \cdot 10^{-11}$m,in units of the atomic mass-unit $u = 1.6605402 \cdot 10^{-27}$kg and in units of the Bohr magnetron $\mu_B = 9.274009994 \cdot 10^{-24}$ J/T. The parameter s_{res} has been previously introduced in section 1.3.1.

Using the values that are presented in table 13.1 as a starting point, it is possible to derive the relevant input parameters which are used in the many-body simulations. An overview of these parameter values, and the equations which have been applied in order to obtain this data, is presented in table 13.2.

Parameter	**^{39}K**	**^{85}Rb**	**Units**	**Equations used**
R^*	29.41	2.80	a_0	**??**
ΔB	-51.7355	10.5101	G	5.27
$\tilde{\eta}$	$-1.18108 \cdot 10^{-53}$	$-3.06054 \cdot 10^{-53}$	m/(Js kg)	3.15
g_1	$1.36511 \cdot 10^{-38}$	$7.50495 \cdot 10^{-39}$	$\mathrm{J^2s^2/(kg\sqrt{m})}$	5.35 and J.16
ν	$1.52749 \cdot 10^{-26}$	$8.35291 \cdot 10^{-27}$	$\mathrm{Js^2/(m^2kg)}$	5.36

Table 13.2: Additionally derived input parameter values for the many-body equations of motion. The value of the parameter ν, with $\nu = \epsilon_Q + C$ is calculated for a system at unitarity, meaning that $B = B_0$.

The combination of the data as presented in tables 13.1 and 13.2 provides a complete set of input values for the many-body simulations and will be used throughout the remainder of this report.

13.2 The simulation model

As explained in section 1.1 and as performed in experiments [71, 72, 73], the value of the magnetic field B is changed in order to change the scattering length. In the simulation, the magnetic field is initiated at a value which is 1G removed from unitarity. Then, within a time of $t = 5\mu$s, the system is brought to unitarity. The initial value of the magnetic field has been chosen to be 1G removed from the resonance value as, for this value of the magnetic field, the system is in the weakly interacting regime and the condition as presented in equation 1.10 is abided by. Furthermore, the time rate at which the system reaches unitarity is chosen to be $t = 5\mu s$ due to the fact that this time is sufficiently small to beat three-body losses. In a Bose gas near unitarity, these three-body losses are important, as they scale with a^4 [44, 74]. Therefore, the system needs to be quenched to unitarity at a sufficiently high rate. Furthermore, following S.Musolino [75], the system is set to have an atomic density of $n = 2.77 \cdot 10^{18}$ m^{-3} for the Potassium-39 simulations and following V.E. Collusi [21] a value of $n = 4.00 \cdot 10^{18}$ m^{-3} for the Rubidium-85 simulations.

The modelled system initially purely consists of an atomic condensate. Starting out in this configuration means that the Bogoliubov- and the coherent state approximation which have been discussed in chapter 10 can be applied and the derived many-body equations of motions correctly represent the dynamics of the system. However, once the system is quenched to unitarity, the atomic condensate will be drained and the molecular condensate and excited state atoms can form [17]. Therefore, once applying a resonant magnetic field value, the applicability of the Bogoliubov- and coherent state approximation is limited to simulation values up to $t \approx 2t_n$, with t_n the Fermi time-scale[1]. This limiting value follows from the analysis as presented in appendix N and is in correspondence with the result as obtained by V.E. Colussi [6]. In order to clarify the simulation model as described above, a schematic representation of the followed sequence is presented in figure 13.1.

[1]This time scale will be discussed in more detail in the next section

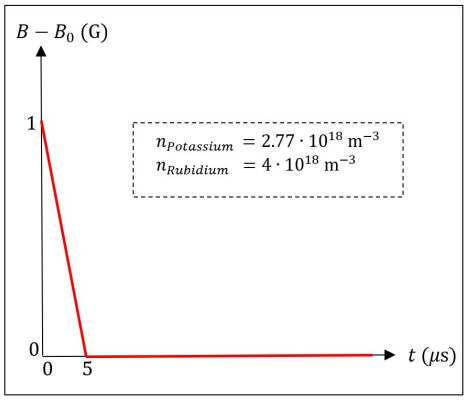

Figure 13.1: Schematic representation of the magnetic-field sequence in time used in the simulations for Potassium-39 and Rubidium-85.

13.3 Results: Dynamical evolution of the many-body system

Using the simulation set-up as outlined in the previous section and implementing the input parameters as presented in section 13.1, it is possible to use the many-body equations of motion in order to track the population distribution of the system as a function of the time. The results which will be presented in this will be rescaled in terms of the energy Fermi scale, which is defined as: $E_n = \hbar^2(6\pi n)^{2/3}/2m$, and the time Fermi scale, which is defined as $t_n = \hbar/E_n$ [74, 6]. This scale is used due to the fact that the *Universality hypothisis* hypothesises that, at unitarity, the density is the only remaining dominant length scale in the system [76]. This means that the gas should only be characterized by this parameter. Using these rescaling parameters, the results which have been obtained through the analysis of Rubidium-85 are presented in the following figure:

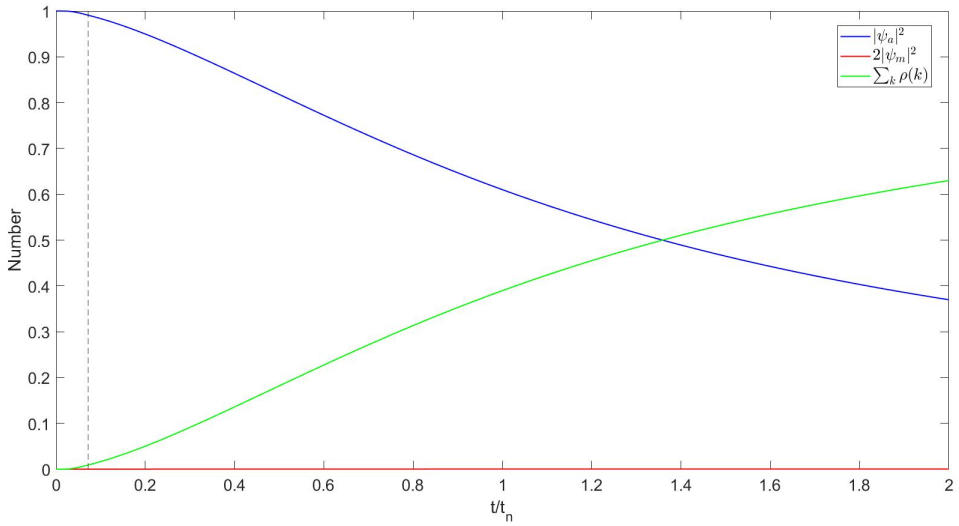

Figure 13.2: Population of Rubidium-85 as a function of the time t/t_n for the atomic condensate (blue line), the excited state atoms (green line) and the molecular condensate (red line). The dashed black line indicates where the system reaches unitarity.

One can see upon inspection of the previous figure, the atomic condensate is gradually depleted and the majority of the drained condensate atoms become excited state atoms. This can be understood upon inspection of the equation of motion of the atomic condensate as presented by equation 10.47. As indicated in this equation, the atomic condensate and the excited state atoms are coupled through the interaction with potential strength $\tilde{V}$. The observed quantum depletion of the atomic condenate is an interesting topic of research and is investigated both experimentally and theoretically [6, 77, 70].

Looking at the molecular condensate in more detail, it is clear that the population fraction in this state remains limited. To be more precise, the population fraction does not surpass a maximum value of 0.03% of the total population. This is a result of the *broad* character of the resonance. As one can see in table 13.2, the resonance strength parameter R^* equals a value of $R^* = 2.8\ a_0$ for Rubidium-85 [16]. In order to put this into perspective, this would correspond to a dimensionless value in the cut-off Λ of $\bar{R}^* \approx 0.02$, as presented in figure 9.3. As previously mentioned in the introduction, the broadness of the resonance indicates that the bound state effectively *lives* in the open channel and the two-channel system can effectively be reduced to a single channel system. This means that the closed channel contribution to the overall development of the many-body system is limited, as reflected by the small fraction of the population that occupies the molecular condensate.

Carrying out the same analysis for Potassium-39, a similar dynamical evolution of the many-body system can be observed. Due to the fact that no new physics emerges, the dynamical evolution of the Potassium-39 system is omitted from this section. It will instead be presented in figure 13.6 in the next section, with the goal to quantify the effect of the resonance width on the dynamical evolution of the Potassium-39 many-body system.

13.4 Results: the embedded dimer energy

Applying the same simulation model as presented in section 13.2, implementing the input parameters as outlined in section 13.1 and solving equation 12.43, the following results for the Rubidium-85 embedded dimer analysis can be obtained:

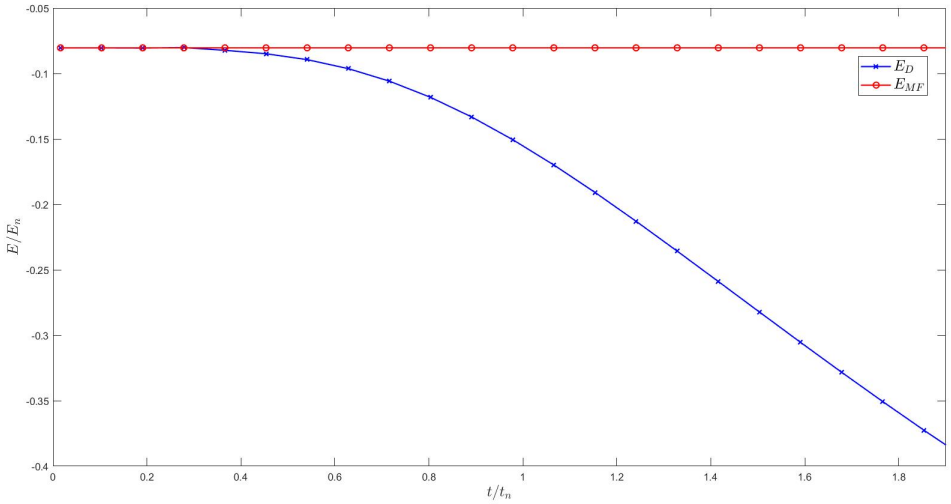

Figure 13.3: The embedded dimer energy (blue line) and the mean field energy shift (red line) of Rubidium-85 as a function of the time t/t_n. The time has been rescaled such that $t/t_n = 0$ corresponds to the completion of the quench to unitarity.

Upon inspection of the previous figure, it can be deduced that the dimer energy has been shifted towards a more negative value by an amount of $E_{MF}(t=0) = 4Vn$ immediately after the completion of the quench to unitarity. This observed energy shift is in correspondence with the expected behaviour as outlined in the previous chapter. However, as the system spends more time at unitarity, the binding energy starts to deviate from the mean field shift $E_{MF}(t)$ and decreases to form a more deeply bound state. This is a result of the depletion of the atomic condensate and the formation of atomic excitations as is indicated in figure 13.2. Due to the increase of the number of excited state atoms, the Bose enhancement term starts to increase in value. It is important to note that the increment in the Bose-enhancement factor is dependent on the relative momentum of the scattering particles. This dependency has been investigated by V.E. Colussi [6]. The result of this analysis is presented in figure 13.4.

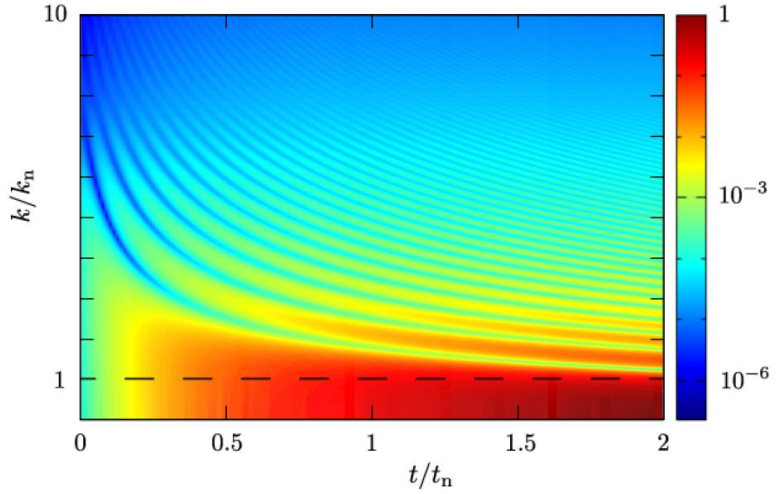

Figure 13.4: Density plot of the universal excitation density $\rho_{\mathbf{k}}$ as a function of the time spent at unitarity. The dashed line indicates the scale of the Fermi wavenumber k_n where the excitation population is most pronounced. This figure has been adapted from reference [6].

As can be seen upon inspection of the previous figure, states with a low relative wave number k become more populated than excited states with a high relative wave number k. This means that the interaction between atoms with a low relative wave number k is more enhanced than the interaction between atoms with a high relative wave number k. The correspondence between the results as presented by V.E. Colussi and the simulations as presented in this section can be verified through the comparison between the embedded dimer energy as presented in notes of V.E. Colussi [21] and the dimer energy as presented in figure 13.3. The correspondence between these results indicates the accordance between the simulations as performed by V.E.Colussi and the simulations as performed in this chapter.

Coming back to the effect that the increase in the excited state population $\rho_{\mathbf{k}}$ has on the Bose-enhancement factor, the inspection of the equation of motion of the anomalous density term as presented by equation 10.53 shows that the increase in the Bose enhancement term effectively increases the pairwise interaction strength between excited state atoms. This in turn effectively causes the embedded dimers to become more deeply bound. This effect is reflected by the blue curve in figure 13.3, which shows that the embedded dimer energy becomes more deeply bound and therefore moves away from the mean-field energy shift for increasing values of the simulation time.

Whereas the mean-field energy shift which is indicated by the red line in figure 13.2 seems to be constant on the scale of the figure, it is in fact changing as a function of the time. As presented

by equation 12.46, the value of the shift reduces as a function of the time due to the loss of atoms to the molecular condensate. However, as previously observed in figure 13.2, the broad character of the Rubidium-85 atomic species causes the depletion towards the molecular condensate to be limited. Therefore, the change in the mean-field shift $E_{MF}(t)$ as a function of the time remains limited. The effect of the resonance width on the time variation of the mean-field shift will be analysed in more detail in the next section.

Having analysed the embedded dimer energy for Rubidium-85, a similar analysis can be carried out for Potassium-39. This analysis will be presented in the next section, in combination with the artificial decrease in the resonance width ΔB in the many-body simulations.

13.5 Results: the effect of the Resonance width

As previously mentioned in the introduction, the effect of the resonance width is a desired topic of research, as the resonance width affects the importance of the closed channel subspace. Therefore, by analysing the embedded dimer energy for Potassium-39 and then subsequently increasing the value of the resonance strength parameter R^* whilst keeping the other input parameter for Potassium-39 as presented in table 6.1 constant, the effect of the decrease of the resonance width ΔB can be investigated. Carrying out this analysis, the results as presented in figure 13.5 can be obtained.

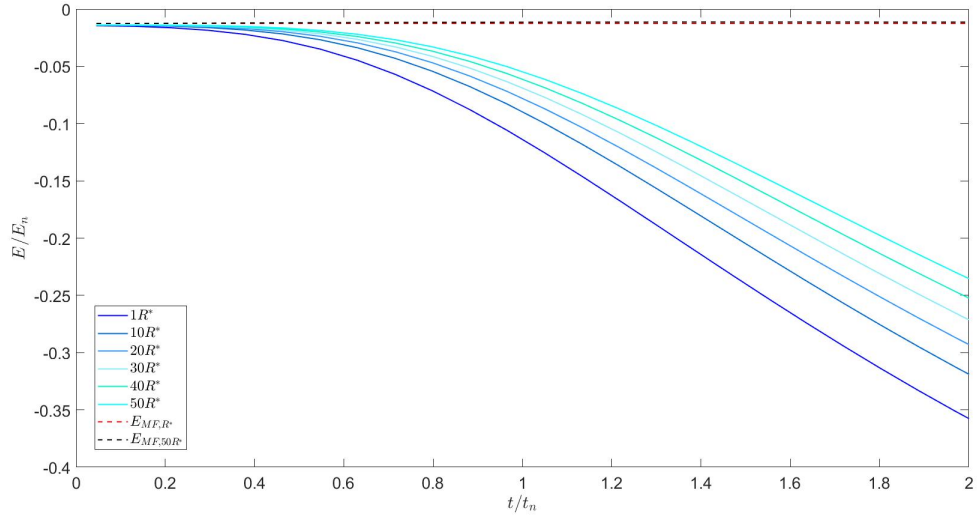

Figure 13.5: The embedded dimer energy E_D/E_n of Potassium-39 as a function of the time t/t_n for artificially increased values of the resonance strength parameter. The dotted lines indicate the mean-field shift of the original simulation and the simulation in which the resonance strength parameter has been increased by a factor of 50.

The inspection of figure 13.5 reveals that an increase of the resonance strength parameter R^* results in the embedded dimer energy being pushed upwards towards less deeply bound dimer energies. This is a result of the reduction of the Bose-enhancement factor for increasingly narrow resonances. In order to clarify this statement, the figure 13.6 can be used.

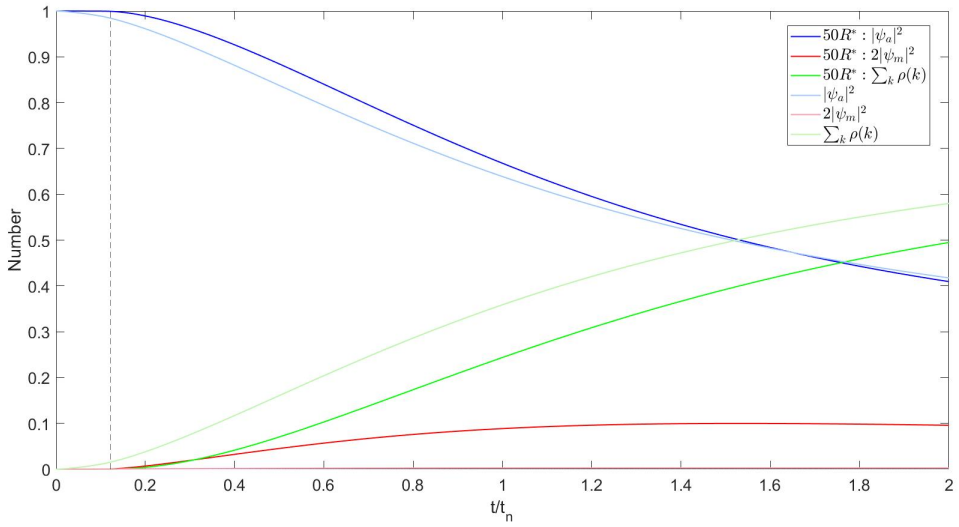

Figure 13.6: Same as figure 13.2, but for Potassium-39 using the resonance strength R^* as presented in table 6.1 (light lines) and for Potassium-39, using a 50 times larger value of the resonance strength R^* (darker lines).

As can be seen upon inspection of figure 13.6, the increase of the resonance strength parameter results in a decrease of the number of excited state atoms and an increase in the molecular condensate population. In order to put the increase of the resonance width into perspective, the multiplication of the resonance width by a factor 50 results in having increased the resonance width from an original dimensionless value of $\bar{R}^* \approx 0.21$ to a value of $\bar{R}^* \approx 10.5$. Figure 9.3 indicates that a value of $\bar{R}^* \approx 10.5$ corresponds to a narrow resonance whereas the original value corresponded to a broad resonance. As previously mentioned in the introduction, the increased amount of population in the molecular condensate for larger values of the resonance strength parameter signifies the increased importance of the closed channel for narrow resonances and the lack of the possibility to reduce the coupled-channels system to a single channel system for increasingly narrow resonances [7].

The observed decrease in the number of excited state atoms for narrow resonances causes the reduction of the Bose-enhancement factor. Due to this reduced value of this enhancement term, the effective increase in the pairwise interaction between atoms is limited. This means that the amount with which the embedded dimer energy is pushed downwards as a function of the time decreases, explaining the difference in the embedded dimer energies for various resonance width values as observed in figure 13.5. However, figure 13.6 also reveals that the increase in the molecular condensate fraction that is caused by the increase of the resonance strength parameter stagnates as the simulation time progresses. As the rate of the change of the population in the molecular condensate fraction decreases as the simulation progresses, the increase in the difference between the embedded dimer energies that is observed in figure 13.5 starts to halt. Therefore, whereas the dimer energies for various resonance strength parameters show an increasingly different development with respect to one another just after the simulation has started, the growth of the differences between the embedded dimer energies for various values of the resonance strength parameter is halted once the simulation time progresses.

Having discussed the effect of the resonance width on the Bose enhancement factor, and having related this effect to the observed change in the embedded dimer energy, the mean field shift $E_{MF}(t)$ is also expected to be influenced by a change in the resonance strength parameter. In order to analyse

the dependency of this quantity on the resonance width, the following figure can be analysed:

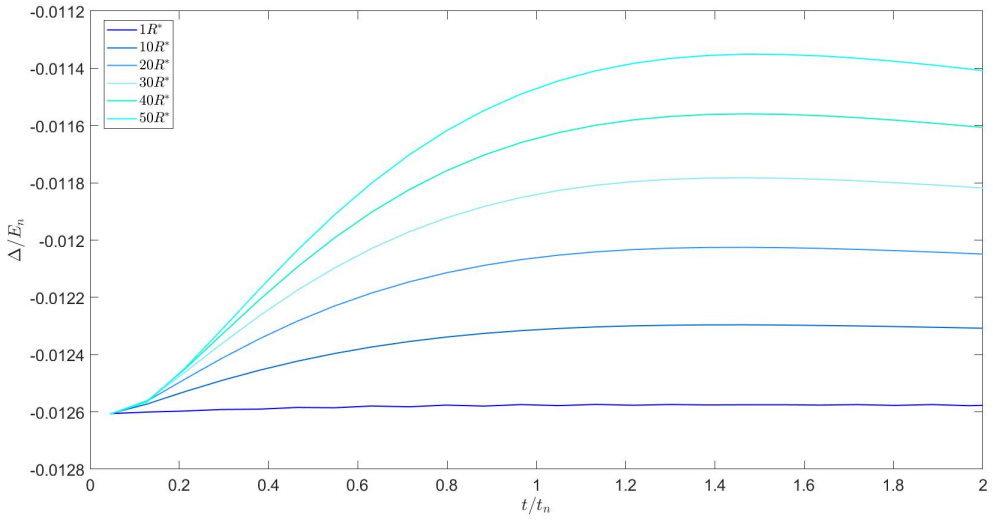

Figure 13.7: The mean field shift E_{MF}/E_n as a function of the time t/t_n for various values of the resonance strength parameter $R^*/R^*_{potassium}$.

Whereas figure 13.7 indicates the variation in the mean field shift as a result of the change of the resonance strength parameter, the magnitude of this parameter is small with respect to the change in the dimer energy. This results in the almost imperceptible change of the mean field shift as presented in figure 13.5. An analysis of the different values of the mean field shift as presented in figure 13.7 indicates that an increase of the resonance strength parameter by a factor of 50 can alter the mean field shift up to a difference of 9.5% with respect to the mean-field shift as calculated for Potassium-39 with the value of the resonance strength parameter as presented in table 6.1. This difference indicates that the resonance width is indeed affected by the change in the resonance width as expected, but that the magnitude of this change is negligibly small with respect to the observed change in the embedded dimer energy as presented in figure 13.5.

In order to analyse the effect of the resonance strength parameter on the embedded dimer as presented in figure 13.5 in more detail, the embedded dimer energy is plotted as a function of the dimensionless resonance strength parameter $\bar{R}^*$, similarly to the presentation that has been used to analyse the effect of the resonance strength parameter on the three-body parameter as displayed in figure 9.3. The results of this analysis are presented in figure 13.8.

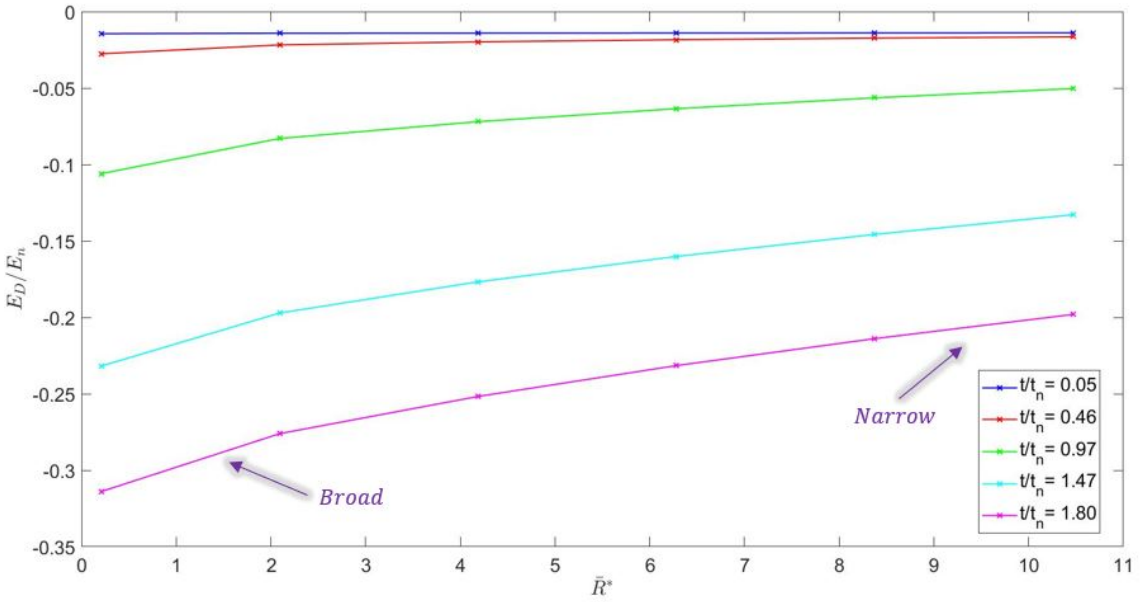

Figure 13.8: The dimer energy E_D/E_n as a function of the resonance strength parameter $\bar{R}^*$ for various values of the time spent at unitarity.

Both the previous figure and figure 13.5 indicate that at a time $t = 0$, the resonance width does not influence the embedded dimer energy. This is a result of the fact that the simulated model starts out with all population confined in the atomic condensate. This means that the mean field shift reduces to the constant value $E_{MF} = 4Vn$ independent of the used resonance strength parameter. However, once the system evolves, the difference between the embedded dimer energies for different values of the resonance strength parameter starts to increase. After spending a time of $t = 1.8t_n$ at unitarity, an increase of the resonance width from a value of $\bar{R}^* \approx 0.21$ to a value of $\bar{R}^* \approx 10.5$ results in an embedded dimer energy which differs from the original value by 37%. A more detailed analysis of the observed energy difference in the dimer as presented in appendix P reveals that a maximum energy difference of 53% is reached during the simulation. Analogously to the analysis of the mean field shift as a function of the time, this large difference indicates that the effect of the resonance width on the many-body simulations cannot be neglected. This means that, unlike broad resonances, it is not possible to simulate narrow resonances with a single channel model.

13.6 Conclusion

In this chapter, the dynamical evolution of the many-body system for both Potassium-39 and Rubidium-85 have been analysed. The analysis of Potassium-39 has been extended to include the inspection of the effect of the artificial increase of the resonance strength parameter R^* on the observed many-body dynamics. The details of the simulated model have been discussed in section 13.2. As explained in this section, the initial value of the magnetic field has been chosen to be removed 1G from the resonance value and the system is quenched to unitarity within 5 μs. Using this simulation model, the investigation of the dynamical evolution of the many-body system revealed the quantum depletion of the atomic condensate, similarly to the process observed in references [77, 70].

Continuing with the analysis of the embedded dimer energy as a function of the time in the second part of the chapter, the investigation revealed that the background gas causes a mean field shift of the dimer energy. This mean field shift pushes the dimer energy towards more deeply bound values

and decreases in magnitude upon an increase in the molecular condensate fraction. Furthermore, the observed shift of the dimer energy towards more deeply bound values for an increased simulation time has been contributed to the growing influence of the Bose enhancement term as a function of the time. After having analysed these many-body effects on the embedded dimer energies, the effect of the resonance strength parameter on the embedded dimer energy has been inspected. This analysis revealed that the dimer energy is pushed towards less deeply bound values upon an increase of the resonance strength parameter due to the increasingly large population fraction of the molecular condensate. The inspection of the embedded dimer energy and the mean field shift for various values of the resonance width as a function of the time indicated that the resonance width significantly affects the many-body physics. As mentioned in the previous section, this means that it is not possible to simulate narrow resonances with a single channel model. The deviation between the results as obtained through the analysis of broad- versus narrow resonances can be contributed to the increasing importance of the molecular condensate for narrow resonances and the decreasing value of the Bose-enhancement factor for narrow resonances.

Chapter 14

Conclusion

In this thesis, a coupled-channels approach has been applied in order to analyse two-body, three-body and many-body systems. A particular focus on the effect of the resonance width has taken a central stage in this investigation. In order to limit the complexity of the analysis, a separable potential has been used in this thesis. This separable potential has been analysed in momentum space and has been contributed a finite momentum-space cut-off in order to incorporate finite range effects in the studied interactions.

In the first part of this thesis, the Feshbach formalism has been implemented in order to obtain an expression for the two-body transition matrix. Using this transition matrix, the dimer energy of the two-body system has been analysed. As presented in section 6.1, the bound state energy, which lives in the closed channel subspace, becomes dressed due to the coupling between the open channel subspace and the closed channel subspace. The results as presented in figure 6.1 showed an increased deviation from the linear relation between the dimer energy and the asymptotic energy shift of the closed channel for an increased coupling between the two channels. As outlined in section 6.1, this is in correspondence with the expected behaviour of the scattering length as presented by equation 1.1 for increasingly broad resonances. Following this analysis, the expression for the dimer energy has been used in order to calibrate the value of the momentum space cut-off. In this calibration, input data obtained through the analysis of a full coupled-channels model has been used [45]. In doing so, physically realistic values for the momentum-space cut-off could be derived. These calibrated values have been implemented in the simulations of the many-body system.

In the second part of this thesis, three-body systems have been analysed. The Faddeev equations for three-body bound states have been used in this analysis and revealed that the off-shell equivalent of the two-body transition matrix could be used in the three-body analysis. Applying this information, it has been possible to obtain Efimov spectra for three-body systems with non-resonant open channel interactions. The recovered Efimov spectra showed the expected universal scaling behaviour that was outlined in section 1.3. As predicted, the ground-state Efimov trimer deviated from this universal scaling behaviour, due to the incorporation of a finite range into the model. Extracting the value of the three-body parameter $\bar{a}_0^-$ from the Efimov spectra for various values of the resonance strength parameter R^*, the remaining part of the three-body system analysis has focussed on the effect of the resonance width on the Efimov trimers. In correspondence with the expectation as outlined in subsection 1.3.1, a universal relation between the potential range and the three-body parameter has been obtained for broad resonances. Furthermore, the expected deviation from this universal relation for increasingly narrow resonances has also been observed. For narrow resonances, it has been possible to extract a linear relation between the three-body parameter and the resonance strength parameter R^*. This is in agreement with the behaviour as observed in other investigations [5, 7]. Physically, this result implies that the resonance strength parameter has replaced the range of the potential as the effective length scale that quantifies the interactions, with R^* much larger

than the potential range for narrow resonances.

Following the analysis of the few-body systems, the final part of this thesis has focussed on the investigation of the many-body system. In the investigation of this system, only particle correlations up to the second order have been incorporated. Using the Heisenberg equation of motion, the Hartree-Fock equations of motion, specific to the modelled coupled channels system, have been derived. In order to confirm the correspondence between the two-body equations and the many-body equations, the vacuum limit of the many-body equations of motion for the anomalous density term and the molecular condensate have been investigated in chapter 11. This analysis revealed that the equation of motion for the molecular condensate could successfully be related to the two-body closed channel wave function, whereas the anomalous density term could successfully be related to the non-zero relative momentum components of the open channel wave function. Next, the embedded analogue of the two-body transition matrix has been derived. This derivation showed many similarities with the derivation of the two-body transition matrix and, similarly to the two-body analysis, the expression for the embedded transition matrix has been used in order to derive an equation for the embedded dimer energy. Using the obtained equations, the many-body system has been analysed numerically. The results of this analysis have been presented in chapter 13. Both a system consisting out of Rubidium-85 atoms and a system consisting out of Potassium-39 atoms have been investigated. In all simulations, the many-body system was investigated at unitarity and initialized with all population contained in the atomic condensate. The investigation of the dynamical evolution of these many-body systems revealed the quantum depletion of the atomic condensate and the increase in the population of the excited state atoms for an increase in the simulation time. For broad resonances, the molecular condensate fraction remained small throughout the entire duration of the simulation. However, a decrease in the resonance width revealed an increase in the molecular condensate fraction. This is in correspondence with the expectation, as more narrow resonances imply the increased importance of the closed channel subspace in which the molecular condensate lives[4, 7].

After having analysed the dynamical evolution of the many-body simulations, the embedded dimer energy has been numerically investigated. Contrary to the two-body dimer energy, the embedded dimer energy changes as a function of the time. Immediately after the initialization of the simulations, the embedded dimer energy is pushed towards deeper bound values by the mean-field shift. As explained in chapter 12, this mean-field energy shift is a pure many-body effect and effectively redefines the two-body scattering continuum. A similar effect has been observed by V.E.Collusi for the single channel analysis of the embedded dimer energy for Rubidium-85 [21]. As the simulation time progresses, the embedded dimer energy is observed to be pushed down towards more negative energies. This means that the embedded dimers become more deeply bound. This dynamical evolution of the embedded dimer energy has been related to the Bose enhancement of the atomic excitations. As the dynamical evolution of the many-body system reveals an increase in the excited state population as a function of the simulation time, the equation of motion for the anomalous density term indicates an increase in the effective interaction strength between excited state atoms, due to the presence of background gas in the same wave number mode. This causes the embedded dimers to become more deeply bound.

In order to investigate the effect of the resonance width on the observed embedded dimer energy, the resonance strength parameter R^* has been artificially increased for the Potassium-39 simulation, whilst keeping all other input parameter values constant. This analysis revealed a reduction in the amount with which the embedded dimer energy is pushed towards more deeply bound values as a function of the simulation time. This observed change has been contributed to the decrease in the excited state population following the decrease of the resonance width. As a decrease in the excited state population corresponds to a decrease in the Bose enhancement factor, the effective interaction strength between the excited state atoms is increased to a lesser extend. This causes the

dimer energy to be less deeply bound for more narrow resonances. Due to the dynamic character of the embedded dimer energy, the observed differences between the embedded dimer energies for systems with distinct values of the resonance width is also time dependent, as indicated by figure 13.8. The investigation of the change between the embedded dimer energies for various values of the simulation time has revealed that the differences in the embedded dimer energies for narrow and broad resonances is substantial. This, similarly to the analysis of the three-body parameter, indicates the importance of the usage of a coupled-channels approach in order to be able to correctly describe narrow resonances.

14.1 Outlook

Whereas the simulated model has been successfully applied to a many-body system, there are still various options which could be interesting for further research. First of all, the modelled potential could be replaced by a more realistic potential, such as a potential with a van der Waals tail. Furthermore, in the analysis of the two-body interactions, higher order partial waves could be included since, as pointed out by reference [14], the effect of these higher order angular momentum terms can generally not be neglected. Furthermore, the coupled-channels model could be extended to include more than two channels, similarly to the approach as followed by T.M.Secker [20].

Apart from changes to the used model, there are also multiple additional factors that could be investigated using the current model. For example, the numerical analysis of the three-body system could be extended to include resonant open channel interactions. Furthermore, the many-body equations of motion could be extended to include third- and higher-order correlations. The inclusion of third order correlations would make it possible to study the Efimov trimers in an embedded environment, similarly to the analysis as presented in reference [6]. Another possibly interesting topic of further research would be the usage of an alternative scheme to quantify the resonance width of many-body systems. As outlined by Lun Ho.T et. al. [78], the product term $k_n R^*$, with k_n the Fermi wave number, analogous to the scale which has been used in section 13.3, could alternatively be used in order to quantify the width of a resonance. Effectively, this alternative approach relies on the fact that, even for large values of the resonance strength parameter R^*, the product $k_n R^*$, which corresponds to the second term of the effective range expansion as presented in equation 2.23 for narrow resonances [4], determines the deviation from the universal dimer binding energy relation as presented by equation 1.2. Therefore, if this product $k_n R^*$ remains small, despite the resonance strength parameter R^* being large, the universal relation for the dimer energy still holds. This means that this factor might offer an interesting alternative to study the effect of the resonance width on the many-body system, where the width of the resonance is now quantified by the energy scale $k_n R^*$.

Whereas it is clear that many possible options for further research exist, the theory as outlined in this thesis has presented a first step in the formation of a coupled-channels model which can be applied to the analysis of a many-body system. Therefore, continuing with the analysis of the physics of an ultra cold many-body system, we have managed to obtain some useful "*luggage*" that could be applied in further investigations.

Chapter 15

Technology assessment

Understanding the scattering physics taking place in ultra cold many-body systems is interesting due to possible applications of ultra cold systems in future technologies. For example, the options to use Bose-Einstein condensates to exploit superfluid phenomena [3, 9] and the possible application of Bose-Einstein as robust qubits [11, 12, 13] motivate the research into atomic interactions taking place in ultra cold gases. By following the bottom-up approach outlined in this thesis, it is possible to gain a more fundamental understanding of the underlying few-body physics that take place in a many-body system.

Apart from harnessing the properties of Bose-Einstein condensates to benefit on a technological level, the condensates also present a more fundamental theoretical interest. Due to the low temperatures of the condensates, they present excellent systems to analyse quantum effects, as the wave-like nature of atoms becomes more pronounced at lower temperatures. By using a coupled-channels approach in this thesis, it has furthermore become possible to analyse the dynamical evolution of a Bose-Einstein condensate which includes the possibility to form a molecular condensate fraction. Apart from this, by implementing a coupled-channels approach, both broad- and narrow resonances that exist in atomic species can be accurately modelled. Effectively, the model outlined in this thesis offers a relatively simple approach to analyse Bose-Einstein condensates numerically and to gain an insight into the atomic interactions taking place in these ultra cold systems.

Bibliography

[1] M. H. Anderson, J. R. Ensher, M. R. Matthews, C. E. Wieman, and E. A. Cornell. Observation of bose-einstein condensation in a dilute atomic vapor. *Science*, 269(5221):198–201, 1995.

[2] M.R. Andrews, C.G. Townsend, H.J. Miesner, D.S. Durfee, D.M. Kurn, and W. Ketterle. Observation of interference between two bose condensates. *Science*, 275, 1996.

[3] Biao Wu and Qian Niu. Superfluidity of boseeinstein condensate in an optical lattice: Landauzener tunnelling and dynamical instability. *New Journal of Physics*, 5(1):104, 2003.

[4] Pascal Naidon and Shimpei Endo. Efimov physics: a review. *Reports on Progress in Physics*, 80(5):056001, 2017.

[5] D. S. Petrov. Three-boson problem near a narrow feshbach resonance. *Phys. Rev. Lett.*, 93:143201, Sep 2004.

[6] V.E. Colussi, S. Musolino, and S.J.J.M.F Kokkelmans. Dynamical formation of the unitary bose gas. 2018.

[7] Sanjukta Roy, Manuele Landini, Andreas Trenkwalder, Giulia Semeghini, Giacomo Spagnolli, Andrea Simoni, Marco Fattori, Massimo Inguscio, and Giovanni Modugno. Test of the universality of the three-body efimov parameter at narrow feshbach resonances. *Phys. Rev. Lett.*, 111:053202, Aug 2013.

[8] A. Einstein. Quantum theory of the monoatomic ideal gas, 1925.

[9] J. R. Abo-Shaeer, C. Raman, J. M. Vogels, and W. Ketterle. Observation of vortex lattices in bose-einstein condensates. 292(5516):476–479, 2001.

[10] P.L. Barry and T. Phillips. A new form of matter ii. Webpage article, 2004.

[11] Hecht.T, B. Paredes, and J.I. Cirac. Quantum computation with bose-einstein condensates. Thesis, 2004.

[12] C. Monroe. Quantum information processing with atoms and photons. *Nature*, 416, 2002.

[13] Shlomo E. Sklarz and David J. Tannor. Loading a bose-einstein condensate onto an optical lattice: An application of optimal control theory to the nonlinear schrödinger equation. *Phys. Rev. A*, 66:053619, Nov 2002.

[14] Mestrom P.M.A. Efimov physics for non-separable finite-range interactions. Thesis, 2017.

[15] R.M. Kroeze. Finite range corrections to the universal e
mov spectrum. Thesis, 2016.

[16] Cheng Chin, Rudolf Grimm, Paul Julienne, and Eite Tiesinga. Feshbach resonances in ultracold gases. *Rev. Mod. Phys.*, 82:1225–1286, Apr 2010.

[17] C. Cohen-Tannoudji and D. Guery-Odelin. *Advances in Atomic Physics: An Overview*. World Scientific, 2011.

[18] V.N. Efimov. Energy levels arising from resonant two-body forces in a three-body system. *Physics Letters B*, 33(8):563 – 564, 1970.

[19] V.N. Efimov. Weakly bound states of three resonantly interacting particles. *Sov. J. Nucl. Phys.*, 12, 1971.

[20] T.M. Secker. T.m. secker is researching a full coupled-channels approach in which more than two channels are considered. this research is ongoing at the research group cqt at the technical university of eindhoven, 2018.

[21] Colussi V.E. Few-body bound states embedded in a quenched unitary bose-condensed gas. Unpublished notes, 2018.

[22] Thorsten Köhler, Krzysztof Góral, and Paul S. Julienne. Production of cold molecules via magnetically tunable feshbach resonances. *Rev. Mod. Phys.*, 78:1311–1361, Dec 2006.

[23] T. Kraemer, M. Mark, P. Waldburger, C. Chin, B. Engeser, A.D. Lange, K. Pilch, A. Jaakkola, H.C. Nagerl, and R. Grimm. Evidence for efimov quantum states in an ultracold gas of caesium atoms. *Nature*, 440, 2006.

[24] S. J. J. M. F. Kokkelmans, J. N. Milstein, M. L. Chiofalo, R. Walser, and M. J. Holland. Resonance superfluidity: Renormalization of resonance scattering theory. *Phys. Rev. A*, 65:053617, May 2002.

[25] Kokkelmans Servaas, Pivi Trm, and Klaus Sengstock. *FRONT MATTER*, chapter 4, pages i–vi. Imperial College Press, London, 2014.

[26] Herman Feshbach. Unified theory of nuclear reactions. *Annals of Physics*, 5(4):357 – 390, 1958.

[27] Chiara D'Errico, Matteo Zaccanti, Marco Fattori, Giacomo Roati, Massimo Inguscio, Giovanni Modugno, and Andrea Simoni. Feshbach resonances in ultracold 39 k. *New Journal of Physics*, 9(7):223, 2007.

[28] A.N. Mitra. Three-body problem with separable potentials: (i) bound states. *Nuclear Physics*, 32:529 – 542, 1962.

[29] M. Zaccanti, B. Deissler, C. DErrico, M. Fattori, M. Jona-Lasinio, S. Muller, G Roati, M. Inguscio, and G. Modugno. Observation of an efimiov spectrum in an atomic system. *Nature Physics*, 5, 2009.

[30] University of earth. https://www.laetusinpraesens.org/docs10s/entamind.php.

[31] Jia Wang, J. P. D'Incao, B. D. Esry, and Chris H. Greene. Origin of the three-body parameter universality in efimov physics. *Phys. Rev. Lett.*, 108:263001, Jun 2012.

[32] Eric Braaten and H.-W. Hammer. Universality in few-body systems with large scattering length. *Physics Reports*, 428(5):259 – 390, 2006.

[33] Alexander O. Gogolin, Christophe Mora, and Reinhold Egger. Analytical solution of the bosonic three-body problem. *Phys. Rev. Lett.*, 100:140404, Apr 2008.

[34] Yujun Wang, Jia Wang, J. P. D'Incao, and Chris H. Greene. Universal three-body parameter in heteronuclear atomic systems. *Phys. Rev. Lett.*, 109:243201, Dec 2012.

[35] R. Schmidt, S.P. Rath, and W. Zwerger. Efimov physics beyond universality. *The European Physical Journal B*, 85(11):386, Nov 2012.

[36] M. D. Barrett, J. A. Sauer, and M. S. Chapman. All-optical formation of an atomic bose-einstein condensate. *Phys. Rev. Lett.*, 87:010404, Jun 2001.

[37] M. W. Zwierlein, C. A. Stan, C. H. Schunck, S. M. F. Raupach, S. Gupta, Z. Hadzibabic, and W. Ketterle. Observation of bose-einstein condensation of molecules. *Phys. Rev. Lett.*, 91:250401, Dec 2003.

[38] A. Griffin. Bec and matter waves. Lecture notes, 2009.

[39] A. Griffin. Bose-einstein condensation of an ideal gas. Lecture notes, 2009.

[40] A.L. Fetter and J.D. Walecka. *Quantum Theory of Many-particle Systems.* Dover Books on Physics. Dover Publications, 2003.

[41] M. Evans. Section 5: Bose-einstein condensation. Lecture notes, 2009.

[42] W. Ketterle. What is bec? Group page introduction.

[43] Richard J. Fletcher, Alexander L. Gaunt, Nir Navon, Robert P. Smith, and Zoran Hadzibabic. Stability of a unitary bose gas. *Phys. Rev. Lett.*, 111:125303, Sep 2013.

[44] C. E. Klauss, D. L. Goldberger, E. A. Cornell, and D. S. Jin. Universal dynamics of a degenerate unitary bose gas. *Nature Physics*, 10, 2014.

[45] T.M. Secker. A mathematica file with data obtained from the analysis of the full coupled-channels model has been supplied by t.m. secker for potassium-39 and rubidium-85, 2018.

[46] L. D. Faddeev. Scattering theory for a three particle system. *Sov. Phys. JETP*, 12:1014–1019, 1961. [Zh. Eksp. Teor. Fiz.39,1459(1960)].

[47] J.R. Taylor. *Scattering Theory: The Quantum Theory of Nonrelativistic Collisions.* Dover Books on Engineering. Dover Publications, 2012.

[48] D.J. Griffiths. *Introduction to Quantum Mechanics.* Cambridge University Press, 2016.

[49] J.J. Sakurai and J. Napolitano. *Modern Quantum Mechanics.* Addison-Wesley, 2011.

[50] H. A. Bethe. Theory of the effective range in nuclear scattering. *Phys. Rev.*, 76:38–50, Jul 1949.

[51] John M. Blatt. On the neutron-proton force. *Phys. Rev.*, 74:92–96, Jul 1948.

[52] H. Murayama. Scattering theory i. Lecture notes.

[53] Herman Feshbach. A unified theory of nuclear reactions, ii. *Annals of Physics*, 281(1):519 – 546, 2000.

[54] S.W. Rienstra. Complex analysis, fourier analysis and asymptotic analysis of integrals. Lecture notes, 2017.

[55] Raphael D. Levine. Chemical dynamics. *International Journal of Chemical Kinetics*, 1(3):353–356.

[56] Goosen M. Universal relation between feshbach resonances and molecules. PhD thesis, 2011.

[57] A. J. Moerdijk, B. J. Verhaar, and A. Axelsson. Resonances in ultracold collisions of ^{6}Li, ^{7}Li, and ^{23}Na. *Phys. Rev. A*, 51:4852–4861, Jun 1995.

[58] G. F. Gribakin and V. V. Flambaum. Calculation of the scattering length in atomic collisions using the semiclassical approximation. *Phys. Rev. A*, 48:546–553, Jul 1993.

[59] Elster C. The 3n bound state. Lecture notes.

[60] W.H. Press, S.A. Teukolsky, W.T. Vetterling, and B.P. Flannery. *Numerical Recipes 3rd Edition: The Art of Scientific Computing.* Cambridge University Press, 2007.

[61] P. Dyke, S. E. Pollack, and R. G. Hulet. Finite-range corrections near a feshbach resonance and their role in the efimov effect. *Phys. Rev. A*, 88:023625, Aug 2013.

[62] S.R.P.G. Ripka, J.P. Blaizot, and G. Ripka. *Quantum Theory of Finite Systems*. Cambridge, MA, 1986.

[63] H. Murayama. Quantum field theory (a.k.a. second quantization). Lecture notes.

[64] Unknown. Gross-pitaevskii theory. Lecture powerpoint presentation.

[65] Robert Seiringer. Bose gases, boseeinstein condensation, and the bogoliubov approximation. *Journal of Mathematical Physics*, 55(7):075209, 2014.

[66] Colussi V.E. Beyond hartree-fock bogoliubov. Unpublished notes, 2018.

[67] C. Gerry, P. Knight, and P.L. Knight. *Introductory Quantum Optics*. Cambridge University Press, 2005.

[68] S. J. J. M. F. Kokkelmans and M. J. Holland. Ramsey fringes in a bose-einstein condensate between atoms and molecules. *Phys. Rev. Lett.*, 89:180401, Oct 2002.

[69] S. Musolino. Finite-range potential. Unpublished notes, 2017.

[70] M. Kira. Coherent quantum depletion of an interacting atom condensate. *Nature Communications*, 6, 2015.

[71] Ph. Courteille, R. S. Freeland, D. J. Heinzen, F. A. van Abeelen, and B. J. Verhaar. Observation of a feshbach resonance in cold atom scattering. *Phys. Rev. Lett.*, 81:69–72, Jul 1998.

[72] A. Marte, T. Volz, J. Schuster, S. Dürr, G. Rempe, E. G. M. van Kempen, and B. J. Verhaar. Feshbach resonances in rubidium 87: Precision measurement and analysis. *Phys. Rev. Lett.*, 89:283202, Dec 2002.

[73] R.A. Duine and H.T.C. Stoof. Atommolecule coherence in bose gases. *Physics Reports*, 396(3):115 – 195, 2004.

[74] A. G. Sykes, J. P. Corson, J. P. D'Incao, A. P. Koller, C. H. Greene, A. M. Rey, K. R. A. Hazzard, and J. L. Bohn. Quenching to unitarity: Quantum dynamics in a three-dimensional bose gas. *Phys. Rev. A*, 89:021601, Feb 2014.

[75] S. Musolino. Simulations for 39-k. Unpublished notes, 2018.

[76] Tin-Lun Ho. Universal thermodynamics of degenerate quantum gases in the unitarity limit. *Phys. Rev. Lett.*, 92:090402, Mar 2004.

[77] Raphael Lopes, Christoph Eigen, Nir Navon, David Clément, Robert P. Smith, and Zoran Hadzibabic. Quantum depletion of a homogeneous bose-einstein condensate. *Phys. Rev. Lett.*, 119:190404, Nov 2017.

[78] Tin-Lun Ho, Xiaoling Cui, and Weiran Li. Alternative route to strong interaction: Narrow feshbach resonance. *Phys. Rev. Lett.*, 108:250401, Jun 2012.

Appendix A

Derivation of equation 2.47

The goal of this appendix is to derive equation 2.47 using equation 2.46 as a starting point. Substituting the relation between the state $|\psi_P^+\rangle$ and the asymptotic solution $|\phi_P^+\rangle$ as presented in equation 2.43 into expression 2.46, the equation as presented below can be obtained:

$$\begin{aligned}\langle\chi_{out}|\hat{T}|\chi_{in}\rangle = &\langle\chi_{out}|\hat{V}_{PP}|\phi_P^+\rangle + \langle\chi_{out}|\hat{V}_{PP}\frac{1}{E^+-\hat{H}_{PP}}\hat{H}_{PQ}\frac{1}{E-\hat{H}_{QQ}}\hat{H}_{QP}|\psi_P^+\rangle \\ &+ \langle\chi_{in}|\hat{H}_{PQ}\frac{1}{E-\hat{H}_{QQ}}\hat{H}_{QP}|\phi_P^+\rangle \\ &+ \langle\chi_{in}|\hat{H}_{PQ}\frac{1}{E-\hat{H}_{QQ}}\hat{H}_{QP}\frac{1}{E^+-\hat{H}_{PP}}\hat{H}_{PQ}\frac{1}{E-\hat{H}_{QQ}}\hat{H}_{QP}|\psi_P^+\rangle \end{aligned} \tag{A.1}$$

Once more, applying equation 2.43 in order to rewrite the third term on the right hand side of the previous expression into terms of the wave function $|\psi_P\rangle$ and the plane wave state $|\chi_{in}\rangle$, the following equivalent form of the previous equation can be found:

$$\begin{aligned}\langle\chi_{out}|\hat{T}|\chi_{in}\rangle &= \langle\chi_{out}|\hat{V}_{PP}|\phi_P^+\rangle + \langle\chi_{out}|\hat{V}_{PP}\frac{1}{E^+-\hat{H}_{PP}}\hat{H}_{PQ}\frac{1}{E-\hat{H}_{QQ}}\hat{H}_{QP}|\psi_P^+\rangle \\ &\quad + \langle k|\hat{H}_{PQ}\frac{1}{E-\hat{H}_{QQ}}\hat{H}_{QP}|\psi_P^+\rangle \\ &= \langle\chi_{out}|\hat{V}_{PP}|\phi_P^+\rangle + \langle\chi_{in}|\left[1+\hat{V}_{PP}\frac{1}{E^+-\hat{H}_{PP}}\right]\hat{H}_{PQ}\frac{1}{E-\hat{H}_{QQ}}\hat{H}_{QP}|\psi_P^+\rangle \end{aligned} \tag{A.2}$$

A close inspection of the final form of the previous equation reveals the presence of the term $\langle\phi_P^-|$ as defined in equation 2.44. Using this definition, equation A.2 reduces to the form as presented below:

$$\langle\chi_{out}|\hat{T}|\chi_{in}\rangle = \langle\chi_{out}|\hat{V}_{PP}|\phi_P^+\rangle + \langle\phi_P^-|\hat{H}_{PQ}\frac{1}{E-\hat{H}_{QQ}}\hat{H}_{QP}|\psi_P^+\rangle \tag{A.3}$$

The previous equation matches equation 2.47. Therefore, the goal to derive this expression has been completed.

Appendix B

The normalization factor for the closed channel bound state

The goal of this appendix is to derive the expression for the factor X which needs to be implemented in the analysis of the coupled-channels system in order to normalize the bound state wave function $|\phi_Q\rangle$. Upon expanding the Green's function $G(E - H_{QQ})$ into bound states and $|\phi_{Q,n}\rangle$ and continuum states $|\phi(E)_Q\rangle$ and only keeping a single bound state $|\phi_Q\rangle$ in accordance with the Feshbach formalism as presented in section 2.7, the following normalization condition has to be abided by: $\langle\phi_Q|\phi_Q\rangle = 1$. The normalization constant ensuring that this condition is met, is named X'. Using this normalization constant and using the Lipmann-Schwinger equation for a bound state [49], the bound state can be expressed as follows:

$$X' \,|\tilde{\phi}_Q\rangle = X' \frac{1}{E - H_0} V \,|\tilde{\phi}_Q\rangle \,. \tag{B.1}$$

The $\sim$ symbol in equation B.1 indicates that the bound state $|\tilde{\phi}_Q\rangle$ is not net normalized. The normalized state will be denoted by $|\phi_Q\rangle$. Using this information, equation B.1 can be rewritten as follows:

$$|\phi_Q\rangle = X \frac{1}{\epsilon_Q - H_0} \,|g\rangle \,, \tag{B.2}$$

$$X = X' \frac{1}{\epsilon_Q - H_0} \,|g\rangle \,. \tag{B.3}$$

Using this information, the following expression for the normalization factor X, which is assumed to be positive and real can be obtained:

$$\begin{aligned}
\langle\phi_Q|\phi_Q\rangle &= \langle g|X \left(\frac{1}{\epsilon_Q - H_0}\right)^2 X|g\rangle = 1, \\
\langle\phi_Q|\phi_Q\rangle &= X^2 \iint \langle g|p'\rangle \,\langle p'| \left(\frac{1}{\epsilon_Q - H_0}\right)^2 |p\rangle \,\langle p|g\rangle \, d\vec{p}' \, d\vec{p}, \qquad \text{(B.4)} \\
X &= \sqrt{\frac{1}{4\pi \int_0^\Lambda \frac{p^2}{\left(\epsilon_Q - \frac{p^2}{2\mu}\right)^2} dp}}, \\
X &= \sqrt{\frac{1}{4\pi \left[-\frac{2\mu^2 \Lambda}{\Lambda^2 - 2\epsilon_Q \mu} - \frac{\sqrt{2}\mu^2 \,\mathrm{arctanh}\left[\frac{\Lambda}{\sqrt{2\mu\epsilon_Q}}\right]}{\sqrt{\mu\epsilon_Q}} \right]}}. \qquad \text{(B.5)}
\end{aligned}$$

Appendix C

Calculation of the form factor projected onto momentum space

The goal of this appendix is to derive an expression for the momentum space projection of the form factor $|g\rangle$. Using equation 3.6 and expanding the potential using spherical harmonics, the following relation can be obtained:

$$\langle \mathbf{p}'|V|\mathbf{p}\rangle = 4\pi \sum_{l=0}^{\infty} \sum_{m=-l}^{m=l} Y_l^m(\hat{p}) \bar{Y}_l^m(\hat{p'}) V_l(p,p'). \tag{C.1}$$

Simultaneously, the factor $\langle \mathbf{p}'|V|\mathbf{p}\rangle$ also needs to satisfy the relation as presented below:

$$\langle \mathbf{p}'|V|\mathbf{p}\rangle = -\eta \langle \mathbf{p}'|g\rangle \langle g|\mathbf{p}\rangle \tag{C.2}$$

Equating the previous two equations with one another, the following expression for the term $\langle \mathbf{p}|g\rangle$ can be obtained:

$$\begin{aligned} -\eta \langle \mathbf{p}'|g\rangle \langle g|\mathbf{p}\rangle &= -\eta g(\mathbf{p}) g(\mathbf{p}') 4\pi Y_0^0(\hat{p}) \bar{Y}_0^0(\hat{p'}) \\ \langle \mathbf{p}|g\rangle &= \sqrt{4\pi} \bar{Y}_0^0(\hat{p}) g(\mathbf{p}) \\ \langle \mathbf{p}|g\rangle &= \langle g|\mathbf{p}\rangle = g(\mathbf{p}) \end{aligned} \tag{C.3}$$

The factor $g(\mathbf{p})$ has been previously introduced in section 3.1.

Appendix D

The phase shift in terms of system parameters

In this appendix, the phase shift for a coupled-channels system with resonant- and non-resonant open channel interaction will be expressed in terms of system parameters. Using the relations between system parameters and physical parameters as presented in chapter 5, the following equivalent expressions to equations 5.32 and 5.33 can be obtained:

$$\delta_{0,nonres} = -ka_{bg} - \mathrm{Arg}\left[\frac{\hbar k^2}{8\pi^2\mu^2\beta^2(4\pi)^2X^2\xi^2(\epsilon_Q)\left[1-\frac{2\Lambda a_{bg}}{\pi\hbar}\right]^2}\right.$$
$$\left. -\frac{(\epsilon_Q+C)-2\mu\Lambda\left((4\pi)^3\beta^2X^2\xi(\epsilon_Q)^2\left[1-\frac{2a_{bg}\Lambda}{\pi\hbar}\right]\right)}{4\pi^2\mu\hbar\beta^2(4\pi)^2X^2\xi^2(\epsilon_Q)\left[1-\frac{2\Lambda a_{bg}}{\pi\hbar}\right]^2}+ik\right] \tag{D.1}$$

$$\delta_{0,res} = -\frac{\pi\hbar k}{2\Lambda} - \arctan\left[\frac{k\pi\hbar}{2\Lambda\left(8\pi\mu\Lambda\eta-1\right)}\right] - \mathrm{Arg}\left[\frac{\hbar k^2}{8\pi^2\mu^2\beta^2(4\pi)^2X^2\xi^2(\epsilon_Q)\left[1-\frac{2\Lambda a_{bg}}{\pi\hbar}\right]^2}\right.$$
$$\left. -\frac{(\epsilon_Q+C)-2\mu\Lambda\left((4\pi)^3\beta^2X^2\xi(\epsilon_Q)^2\left[1-\frac{2a_{bg}\Lambda}{\pi\hbar}\right]\right)}{4\pi^2\mu\hbar\beta^2(4\pi)^2X^2\xi^2(\epsilon_Q)\left[1-\frac{2\Lambda a_{bg}}{\pi\hbar}\right]^2}+\frac{ik}{1+\frac{ik\pi\hbar}{2\Lambda(8\pi\mu\Lambda\eta-1)}}\right] \tag{D.2}$$

Appendix E

Dimensionless in units of the cut-off and the mass

The parameters that are used to describe the Feshbach resonance of the contact-potential model with a cut-off Λ in momentum space can be made dimensionless in units of the cut-off Λ [1] and the mass of the interacting particles m, with $m = 2\mu$, resulting in the following dimensionless set of parameters:

$$\bar{k} = \frac{k\hbar}{\Lambda} \tag{E.1}$$

$$\bar{a} = \frac{a\Lambda}{\hbar} \tag{E.2}$$

$$\bar{\eta} = \eta \cdot (\Lambda m) \tag{E.3}$$

$$\bar{\beta} = \beta \cdot (\Lambda m) \tag{E.4}$$

$$\bar{\kappa} = \kappa \cdot (\Lambda m) \tag{E.5}$$

$$\bar{E} = \frac{mE}{\Lambda^2} \tag{E.6}$$

$$\bar{\xi} = \frac{\xi}{m\Lambda} \tag{E.7}$$

$$\bar{X}^2 = \frac{m^2 X^2}{\Lambda} \tag{E.8}$$

[1] The cut-off Λ has the following dimension: $[\Lambda] = \left[\frac{Js}{m}\right]$

Appendix F

The dimer energy as a function of the scattering length

For small values of the energy ($k \to 0$), it follows from equation 2.24 that the phase shift can be expressed in terms of the scattering length as follows:

$$\delta = -\arctan\left[-ka\right] \tag{F.1}$$

In order to study bound states ($E < 0$) the following real and positive parameter κ is introduced:

$$\kappa = \sqrt{\frac{-2\mu E}{\hbar^2}} \tag{F.2}$$

Upon inspection of the previous equation, it can be deduced that the parameter κ is related to the wave number k as follows: $\kappa = -ik$. As previously discussed in chapter 2, the scattering of a potential can solely affect the phase shift of the scattered wave. Therefore, a general solution to the radial Schrödinger equation $R(r)$ for bound states ($E < 0$) can be written as follows:

$$R(r) \propto \frac{e^{i(2\delta + kr)}}{r} + \frac{e^{-ikr}}{r} \tag{F.3}$$

The outgoing component that is present in the previous equation has been phase shifted. Comparing this phase shift term to the definition of the scattering matrix as presented in equation 2.22, the previous expression can be written into the following form:

$$R(r) \propto S(k)\frac{e^{ikr}}{r} + \frac{e^{-ikr}}{r} \tag{F.4}$$

The scattering matrix, which is present in the previous equation can similarly be written into the following form:

$$S(k) = e^{2i\delta} = \frac{1 + i\tan\left(\delta\right)}{1 - i\tan\left(\delta\right)} \tag{F.5}$$

Next, substituting equation F.1 into the previous expression results in the following analogous form of the S-matrix:

$$S(k) = \frac{1 - ika}{1 + ika} = \frac{1 + \kappa a}{1 - \kappa a} \tag{F.6}$$

Substituting this expression back into equation F.4 and using the re-normalizability of the wave function, the following expression can be obtained:

$$R(r) \propto \frac{e^{-\kappa r}}{r} + \frac{1-\kappa a}{1+\kappa a}\frac{e^{\kappa r}}{r} \tag{F.7}$$

In order for the previous equation to be normalizable, the factor $e^{\kappa r}$ needs to vanish, as this term blows up for large values of r. In order for this condition to be met, the value of κ can be found to equal the following value:

$$\kappa = \frac{1}{a} \tag{F.8}$$

Using the previous equation and applying the relation between κ and the energy as presented by expression F.2 results in the following expression:

$$E = \frac{-\hbar^2}{2\mu a^2} \tag{F.9}$$

The previous equation indicates that, for small values of the energy, the energy scales quadratically with the inverse scattering length.

Appendix G

Errors in the constant value cut-off calibration

In this appendix, the difference in percentage between the input data values and the obtained values for the Rubidium-85 and Potassium-39 calibrations will be presented.

G.1 Potassium-39

Analysing the difference between the input data values and the obtained values for the scattering length as obtained through the usage of equation 6.6 for various values of the cut-off Λ, the following figure can be obtained:

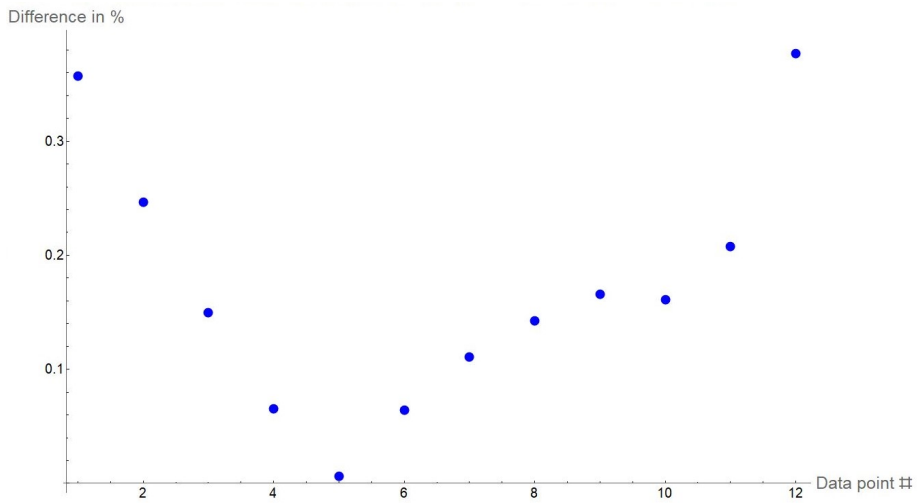

Figure G.1: The relative error % between the input data and the calculated data for various values of the cut-off Λ as a function of the data point index #.

G.2 Rubidium-85

Following the approach that has been used in the previous section, the following figure can be obtained for Rubidium-85:

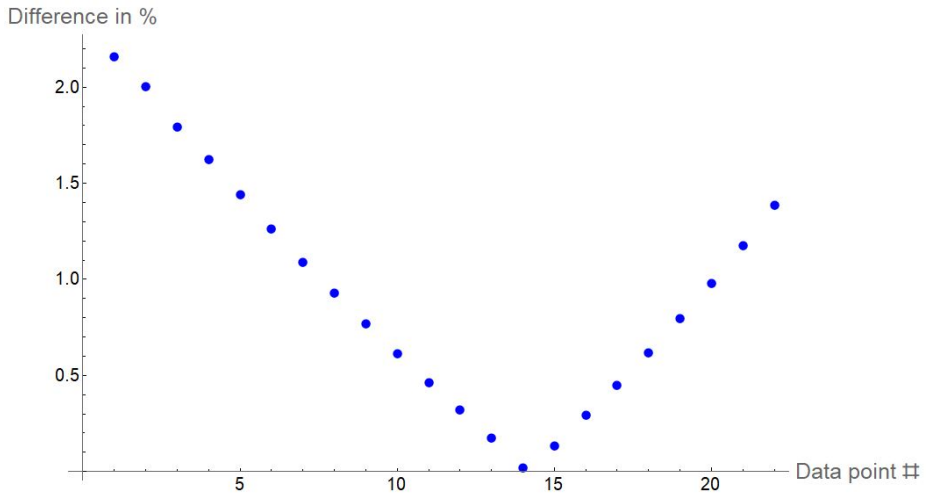

Figure G.2: The relative error % between the input data and the calculated data for various values of the cut-off Λ as a function of the data point index #.

Appendix H

Angular integration of the three-body equation

In this appendix, the angular integration of equation 7.18 will be carried out. Using spherical coordinates in order to carry out this integration, equation 7.18 can be rewritten into the following analoglous form:

$$\tilde{\psi}(\mathbf{q},E) = \iiint q'^2 dq' \sin(\theta) d\theta d\phi \frac{-2\tau_{coupled}\left(E - \frac{3}{8\mu}\mathbf{q}^2\right)}{E - \frac{1}{2\mu}\left(\mathbf{q}^2 + \mathbf{q}\cdot\mathbf{q}' + \mathbf{q}'^2\right)} g\left(\left|\mathbf{q} + \frac{1}{2}\mathbf{q}'\right|\right) g\left(\left|\mathbf{q}' + \frac{1}{2}\mathbf{q}\right|\right) \tilde{\psi}_0(\mathbf{q}',E) \tag{H.1}$$

Exploiting the fact that the integral is independent of the angle ϕ, this integration can be carried out in order to obtain the following equivalent expression:

$$\tilde{\psi}_0(q,E) = 2\pi \iint q'^2 dq' \sin(\theta) d\theta \frac{-2\tau_{coupled}\left(E - \frac{3}{8\mu}q^2\right)}{E - \frac{1}{2\mu}\left(q^2 + qq'\cos(\theta) + q'^2\right)} g\left(\left|\mathbf{q} + \frac{1}{2}\mathbf{q}'\right|\right) g\left(\left|\mathbf{q}' + \frac{1}{2}\mathbf{q}\right|\right) \tilde{\psi}_0(\mathbf{q}',E) \tag{H.2}$$

Using the definition of an inner product being: $\mathbf{q}\cdot\mathbf{q}' = qq'\cos(\theta)$ and introducing the variable $u = \cos(\theta)$, the previous equation can be rewritten as follows:

$$\tilde{\psi}_0(q,E) = -4\pi \iint dq' du \frac{q'^2 \tau_{coupled}\left(E - \frac{3}{8\mu}q^2\right)}{E - \frac{1}{2\mu}\left(q^2 + qq'u + q'^2\right)} g\left(\sqrt{\frac{1}{4}q^2 + q'^2 + uqq'}\right) g\left(\sqrt{\frac{1}{4}q'^2 + q^2 + uqq'}\right) \tilde{\psi}_0(q',E) \tag{H.3}$$

Appendix I

An Efimov spectrum for a positive background scattering length

Using the numerical implementation as discussed in chapter 8, it is possible to obtain Efimov spectra. Figure I.1 displays the Efimov spectrum for the dimensionless contact potential model for values of the parameters as indicated in the figure's description.

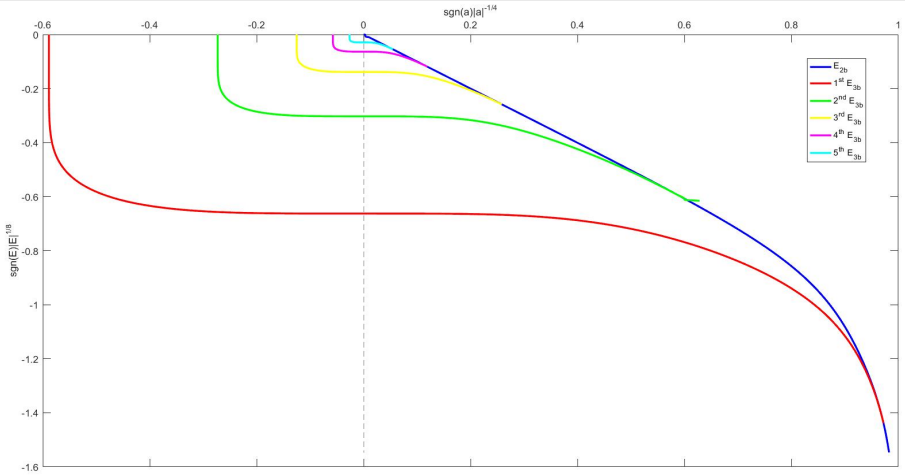

Figure I.1: Efimov spectrum for $\bar{a}_{bg} = 1$, $\bar{\kappa} = 8$, $\bar{\beta} = 0.5$.

Upon extracting values for $\bar{a}_n^-$ and $\bar{\kappa}_n^*$ from figure I.1, it is possible to determine whether the spectrum displays the universal scaling laws $\bar{a}_{n+1}^-/\bar{a}_n^- \approx 22.7$ and $\bar{a}_n^- \cdot \bar{\kappa}_n^* \approx -1.50763$. The results are summarized in the following table:

Efimov state n	$\bar{\mathbf{a}}_\mathbf{n}^-$	$\bar{\kappa}_\mathbf{n}^*$	$\bar{\mathbf{a}}_\mathbf{n+1}^-/\bar{\mathbf{a}}_\mathbf{n}^-$	$\bar{\mathbf{a}}_\mathbf{n}^- \cdot \bar{\kappa}_\mathbf{n}^*$
0	-8.34	0.1930	21.63	-1.6096
1	$-1.80 \cdot 10^2$	0.0084	22.57	-1.5120
2	$-4.07 \cdot 10^3$	$3.7 \cdot 10^{-4}$	22.69	-1.5059
3	$-9.24 \cdot 10^4$	$1.63 \cdot 10^{-5}$	22.67	-1.5061
4	$-2.09 \cdot 10^6$	$7.2 \cdot 10^{-7}$	–	-1.5048

As can be seen upon inspection of the data as presented in the previous table, the universal scaling laws which have been presented in section 1.3 can be observed. This indicates the applicability of the

model in the simulation of systems with small positive values of background scattering length. As mentioned in 9, the numerical model cannot be applied to systems with large positive values of the background scattering length, as the code does not inspect the presence of a pole in the uncoupled part of the transition matrix.

Appendix J

Derivation of many-body code parameters

The goal of this chapter is to derive an expression for the energy shift $\bar{\nu}_1$ between the collision continuum and the bound state and to derive an expression for the coupling constant $\bar{g}_1$. These constants are inspired by the method followed by S.Kokkelmans in reference [24], but are defined slightly differently. The parameters used in this appendix and the parameters as introduced by S.Kokkelmans are related as follows [1]:

$$\bar{g}_1^{used} = \sqrt{2}\bar{g}_1^{article} \tag{J.1}$$

J.1 Derivation of g1

Following the outline presented by S.Kokkelmans [24], in the case of a non-resonant open channel interaction, equation 5.13 can be expressed in terms of $\bar{g}_1$ and $\bar{\nu}_1$ as follows:

$$S(k) = e^{-2ika_{bg}}\left[1 - \frac{ik|\bar{g}_1|^2}{-\frac{4\pi\hbar^2}{m}\left(\bar{\nu}_1 - \frac{\hbar^2k^2}{m}\right) + \frac{ik}{2}|\bar{g}_1|^2}\right] \tag{J.2}$$

Using the fact that $m = 2\mu$ and upon going from an energy normalized state to a momentum normalized state, this equation can be rewritten as follows:

$$\begin{aligned}|\bar{g_1}|^2 &= \frac{4\pi\hbar^2}{km}\cdot 4\pi^2 m\hbar k\left|\langle\phi_P^+|H_{PQ}|\phi_Q\rangle\right|^2 \\ |\bar{g_1}|^2 &= 16\pi^3\hbar^3\left|\langle\phi_P^+|H_{PQ}|\phi_Q\rangle\right|^2 = 2(2\pi\hbar)^3\left|\langle\phi_P^+|H_{PQ}|\phi_Q\rangle\right|^2\end{aligned} \tag{J.3}$$

The change in normalization is well documented in the thesis of R.M.Kroeze [15] and textbook literature [49]. In the limit where $k \to 0$, the element $\left|\langle\phi_P^+|H_{PQ}|\phi_Q\rangle\right|^2$ that is present in equation J.3 reduces to $\left|\langle\psi_p^+(0)|H_{PQ}|\phi_Q\rangle\right|^2$. This expression is equivalent to the term $\langle\phi_P^-|\hat{H}_{PQ}|\phi_Q\rangle\langle\phi_Q|\hat{H}_{QP}|\phi_P^+\rangle$ which is present in equation 4.2 in the on-shell case in the limit $k \to 0$. This element has been previously analyzed in section 4.2. Upon applying the limit $k \to 0$ to equation 4.11, this results in

[1] Remember that the introduced strengths β and η are related to the parameter strengths g and V as introduced by S.Kokkelmans in reference [24] through $V = -(2\pi\hbar)^3\eta$ and $g = -(2\pi\hbar)^3\beta$.

the following expression:

$$\langle \phi_Q | H_{QP} | \phi_P(0) \rangle = -\beta(4\pi)^2 X \xi(\epsilon_Q) \left[\frac{1}{4\pi} - \tau(0)\zeta(0) \right] \tag{J.4}$$

Upon using equation 3.13 to extract the function for $\tau(0)$ and upon using equations **??** to extract information with respect to $\xi(\epsilon_Q)$ and $\zeta(0)$, expression J.4 can be rewritten as follows:

$$\langle \phi_Q | H_{QP} | \phi_P(0) \rangle = -\beta(4\pi)^2 X \xi(\epsilon_Q) \left[\frac{1}{4\pi} - \frac{\Lambda a_{bg}}{2\pi^2 \hbar} \right] = -4\pi\beta X \xi(\epsilon_Q) \left[1 - \frac{2\Lambda a_{bg}}{\pi\hbar} \right] \tag{J.5}$$

Upon substituting the expression as obtained in equation J.5 into equation J.3, the following expression for $|\bar{g}_1|^2$ can be obtained:

$$|\bar{g}_1|^2 = 2(2\pi\hbar)^3 \cdot (4\pi)^2 \beta^2 X^2 \xi(\epsilon_Q)^2 \left[1 - \frac{2\Lambda a_{bg}}{\pi\hbar} \right]^2 \tag{J.6}$$

In order to compare this expression to the expression for $|\bar{g}_1|^2$ as presented in equation 33 of reference [24], the parameter Γ that is present in this article will be introduced [2]:

$$\Gamma = \left(1 - \frac{2a_{bg}\Lambda}{\pi\hbar} \right)^{-1} \tag{J.7}$$

The factor Γ as presented in equation J.7 can be recognized in expression J.6, resulting in the following equivalent equation for $\bar{g}_1$:

$$|\bar{g}_1|^2 = 2(2\pi\hbar)^3 \cdot (4\pi)^2 \beta^2 X^2 \xi(\epsilon_Q)^2 \Gamma^{-2} \tag{J.8}$$

$$\bar{g}_1 = \pm\sqrt{2}(2\pi\hbar)^{3/2} 4\pi\beta X \xi(\epsilon_Q) \Gamma^{-1}$$

$$\bar{g}_1 = \pm\sqrt{2}(2\pi\hbar)^{3/2} 4\pi\beta X \xi(\epsilon_Q) \left[1 - \frac{2\Lambda a_{bg}}{\pi\hbar} \right] \tag{J.9}$$

In reference [24], $\bar{g}_1$ is defined as follows:

$$\bar{g}_1 = g_1 \Gamma^{-1} \tag{J.10}$$

The parameter $g_1(\mathbf{r})$ that is present in equation J.10 is defined as follows:

$$g_1(\mathbf{r}) = \sqrt{2} g(\mathbf{r}) \phi_i^Q(\mathbf{r}) = \sqrt{2} g \delta(\mathbf{r}) \phi_Q(\mathbf{r}) \tag{J.11}$$

Following the approach of section 3.1, $\langle p' | g\delta(\mathbf{r}) | p \rangle$ can be expressed as follows: $\langle p' | g\delta(\mathbf{r}) | p \rangle = -\beta g(p) g(p')$, with $\beta = -\frac{g}{(2\pi\hbar)^3}$. For a separable potential, the following operator can then be introduced: $\hat{V} = -\beta \left| g \right\rangle \left\langle g \right|$. Using this potential operator, $|g_1\rangle$ is now chosen to be defined as follows:

$$|g_1\rangle = -\sqrt{2}\beta \left| g \right\rangle \langle g | \phi_Q \rangle \tag{J.12}$$

Using equation B.2, the expression for $|g_1\rangle$ can be rewritten as follows:

$$|g_1\rangle = -\sqrt{2}\beta \left| g \right\rangle \langle g | X \frac{1}{\epsilon_Q - H_0} | g \rangle$$

$$|g_1\rangle = -4\pi\sqrt{2}\beta X \left| g \right\rangle \int_0^\Lambda \frac{p^2}{\epsilon_Q - \frac{p^2}{2\mu}} dp$$

$$|g_1\rangle = -4\pi\sqrt{2}\beta X \xi(\epsilon_Q) \left| g \right\rangle \tag{J.13}$$

[2] The factor K in the article corresponds to $K = \Lambda/\hbar$

Subsequently, using equation J.13, the parameter g_1, is defined as follows:

$$|g_1\rangle = \frac{g_1}{(2\pi\hbar)^{3/2}}|g\rangle \tag{J.14}$$

$$g_1 = -4\pi\beta X\xi(\epsilon_Q)(2\pi\hbar)^{3/2} \tag{J.15}$$

Upon substituting equation J.15 into equation J.10 and using the definition for Γ, the article expression matches the derived equation for $\bar{g}_1$ as presented in equation J.9 upon selecting the minus sign , meaning that $\bar{g}_1$ can properly be expressed as follows:

$$\bar{g}_1 = -\sqrt{2}(2\pi\hbar)^{3/2}4\pi\beta X\xi(\epsilon_Q)\left[1 - \frac{2\Lambda a_{bg}}{\pi\hbar}\right] \tag{J.16}$$

J.2 Derivation of nu1

Equation J.2 can be rewritten in a more suggestive form by multiplying the fraction by a factor of $\frac{m}{4\pi\hbar^2}$, resulting in the following outcome:

$$S(k) = e^{-2ika_{bg}}\left[1 - \frac{\left(\frac{m}{4\pi\hbar^2}\right)ik|\bar{g}_1|^2}{\frac{\hbar^2k^2}{m} - \bar{\nu}_1 + \left(\frac{m}{4\pi\hbar^2}\right)\frac{ik}{2}|\bar{g}_1|^2}\right] \tag{J.17}$$

Upon inspection of the denominator, it becomes clear that the first factor corresponds to the energy E. Using this information, it is possible to compare the denominator in equation J.2 to the denominator in equation 5.7, resulting in the following outcome:

$$E - \bar{\nu}_1 + \left(\frac{m}{4\pi\hbar^2}\right)\frac{ik}{2}|\bar{g}_1|^2 = E - (\epsilon_Q + C) - \langle\phi_Q|H_{QP}\frac{1}{E^+ - H_{PP}}H_{PQ}|\phi_Q\rangle \tag{J.18}$$

The factor $\bar{\nu}_1$ will now be defined as follows:

$$\bar{\nu}_1 = \epsilon_Q + C + \mathrm{Re}\left[\langle\phi_Q|H_{QP}\frac{1}{E^+ - H_{PP}}H_{PQ}|\phi_Q\rangle\right] \tag{J.19}$$

Upon selecting the real part from the expression for $\langle\phi_Q|H_{QP}\frac{1}{E^+-H_{PP}}H_{PQ}|\phi_Q\rangle$ as presented in section 4.3 in the limit $k \to 0$, equation J.19 can be rewritten as follows:

$$\bar{\nu}_1 = (\epsilon_Q + C) - 8\pi\mu\Lambda(4\pi)^2\beta^2X^2\xi(\epsilon_Q)^2\left[1 - \frac{2a_{bg}\Lambda}{\pi\hbar}\right] \tag{J.20}$$

It is possible to re-write equation J.20 in terms of $\bar{g}_1$ and g_1, resulting in the following outcome:

$$\begin{aligned}\bar{\nu}_1 &= \epsilon_Q + C - \frac{8\pi\mu\Lambda}{2(2\pi\hbar)^3}g_1\bar{g}_1 \\ \bar{\nu}_1 &= \epsilon_Q + C - \frac{m\Lambda}{4\pi^2\hbar^3}g_1\bar{g}_1\end{aligned} \tag{J.21}$$

In order to compare this to equation 34 of reference [24], the following factor α needs to be introduced:

$$\alpha = \frac{m\Lambda}{2\pi^2\hbar^3} \tag{J.22}$$

Using this parameter α, equation J.21 can be rewritten as follows:

$$\bar{\nu}_1 = \epsilon_Q + C - \frac{\alpha g_1 \bar{g}_1}{2} \tag{J.23}$$

Comparing this expression to equation 34 of reference [24], yields the following expression for ν_1:

$$\nu_1 = \epsilon_Q + C \tag{J.24}$$

Appendix K

Second quantization

K.1 One body operators and two body operators in second quantized form

In this appendix, the outline as presented by J.P. Blaizot and G.Ripka [62] is followed in order to derive the general expressions for a single-particle and a two-particle operator in second quantized form.

In general, the effect of a one-body operator $\hat{F}^{(i)}$ on N particles can be described as follows:

$$\hat{F}_N = \sum_i \hat{F}^{(i)}. \tag{K.1}$$

The single particle operator $\hat{F}^{(i)}$ can be expressed according to:

$$\hat{F}^{(i)} = \sum_{\alpha_i} \sum_{\beta_i} |\beta_i\rangle \langle\beta|\hat{F}^{(i)}|\alpha_i\rangle \langle\alpha_i| \,. \tag{K.2}$$

The states $|\alpha_i\rangle$ and $|\beta_i\rangle$ which were introduced here correspond to single particle states. Using the previous expression, the action of the single particle operator $\hat{F}^{(i)}$ on a product state of N particles, represented by $|\alpha_1\alpha_2..\alpha_i..\alpha_N\rangle$ can be expressed as:

$$\hat{F}^{(i)} = \sum_{\alpha_i} \sum_{\beta_i} |\beta_i\rangle \langle\beta_i|F^{(i)}|\alpha_i\rangle \langle\alpha_i|\alpha_1\alpha_2..\alpha_i..\alpha_N\rangle \,, \tag{K.3}$$

$$= |\alpha_1\rangle |\alpha_2\rangle .. |\alpha_{i-1}\rangle \left\{ \sum_{\beta_i} |\beta_i\rangle \langle\beta_i|F^{(i)}|\alpha_i\rangle \right\} |\alpha_{i+1}\rangle ... |\alpha_N\rangle \,, \tag{K.4}$$

$$= \sum_{\beta_i} \langle\beta_i|F^{(i)}|\alpha_i\rangle |\alpha_1\alpha_2..\alpha_{i-1}\beta_i\alpha_{i+1}...\alpha_N\rangle \,. \tag{K.5}$$

In order to extend from a single particle operator to a set of single particle operators that act on all N different particles, the procedure as described above has to be repeated N times for all different particles, resulting in the following expression:

$$\hat{F}^N = \sum_{i=1}^{N} \sum_{\alpha_i} \sum_{\beta_i} |\beta_i\rangle \langle\beta|F^{(i)}|\alpha_i\rangle \langle\alpha_i| \,. \tag{K.6}$$

Instead of using these operators $\hat{F}^N$ in which the particle index is relevant, it is possible to move to a space in which the operators acts on an enlarged Hilbert space in which each subspace corresponds to a fixed number of particles. This means that, instead of operating on a specific particle i, the operators will act on a space with a particular occupation number n_α. This space, known as Fock space, doesn't include the labeling of particles and hence leads to a simpler description of many particle states. The fact that this leads to a simpler description can be understood by realizing that the bosons which are investigated are indistinguishable. Therefore, the wave-function of the many-body system has to be symmetrized and the action on a specific particle i is rather unphysical, as it is not possible to distinguish this particular particle from the symmetrized wave-function.

The Fock space analogue of F^N acting on the extended Hilbert space with different numbers of particles N is defined as follows:

$$\hat{F} = \sum_\alpha \sum_\beta \langle \beta | F | \alpha \rangle \, \hat{a}^\dagger_\beta \hat{a}_\alpha. \tag{K.7}$$

In order to investigate the effect of this Fock space operator on the product state $|\alpha_1 \alpha_2 .. \alpha_i .. \alpha_N\rangle$, the product space is written in terms of a vacuum state $|0\rangle$ and creation operators, resulting in the following analogous form of the product state:

$$|\alpha_1 \alpha_2 .. \alpha_i .. \alpha_N\rangle = \hat{a}^\dagger_{\alpha_1} \hat{a}^\dagger_{\alpha_2} ... \hat{a}^\dagger_{\alpha_N} |0\rangle \, . \tag{K.8}$$

Using the previous expression, the effect of the application of the Fock space operator on the product state $|\alpha_1 \alpha_2 .. \alpha_i .. \alpha_N\rangle$ can be investigated:

$$\hat{F} |\alpha_1 \alpha_2 .. \alpha_i .. \alpha_N\rangle = \sum_\alpha \sum_\beta \langle \beta | F | \alpha \rangle \, \hat{a}^\dagger_\beta \hat{a}_\alpha \hat{a}^\dagger_{\alpha_1} \hat{a}^\dagger_{\alpha_2} ... \hat{a}^\dagger_{\alpha_N} |0\rangle \, , \tag{K.9}$$

$$= \left[\hat{F}, \hat{a}^\dagger_{\alpha_1}\right] \hat{a}^\dagger_{\alpha_2} ... \hat{a}^\dagger_{\alpha_N} |0\rangle + \hat{a}^\dagger_{\alpha_1} \left[\hat{F}, \hat{a}^\dagger_{\alpha_2}\right] ... \hat{a}^\dagger_{\alpha_N} |0\rangle + .. + \hat{a}^\dagger_{\alpha_1} .. \hat{a}^\dagger_{\alpha_{N-1}} \left[\hat{F}, \hat{a}^\dagger_{\alpha_N}\right] . \tag{K.10}$$

In order to simplify the previous expression, the commutation relation between $\hat{F}$ and a creation operator $\hat{a}^\dagger_\gamma$ has to be analysed. This analysis is presented below:

$$\left[\hat{F}, \hat{a}^\dagger_\gamma\right] = \sum_\alpha \sum_\beta , \langle \beta | F | \alpha \rangle \left[\hat{a}^\dagger_\beta \hat{a}_\alpha, \hat{a}^\dagger_\gamma\right] , \tag{K.11}$$

$$= \sum_\alpha \sum_\beta \langle \beta | F | \alpha \rangle \left(\hat{a}^\dagger_\beta \left[\hat{a}_\alpha, \hat{a}^\dagger_\gamma\right] + \left[\hat{a}^\dagger_\beta \hat{a}^\dagger_\gamma\right] \hat{a}_\alpha \right) , \tag{K.12}$$

$$= \sum_\beta \langle \beta | F | \gamma \rangle \, \hat{a}^\dagger_\beta \tag{K.13}$$

Using equation K.13, equation K.10 can be rewritten as:

$$\hat{F} |\alpha_1 \alpha_2 .. \alpha_i .. \alpha_N\rangle = \sum_{i=1}^{N} \sum_{\beta_i} \langle \beta_i | F | \alpha_i \rangle \, \hat{a}^\dagger_{\alpha_1} ... \hat{a}^\dagger_{\beta_i} ... \hat{a}^\dagger_{\alpha_N} |0\rangle \, . \tag{K.14}$$

Comparing the previous expression to equation K.5 indicates that the Fock space operator corresponds to $\sum_i^N \hat{F}^{(i)}$. Therefore, equation K.7 can be used in order to calculate n the single particle effects. This representation of the operator in Fock space in which creation and annihilation operators are used is known as the second-quantized form of a symmetric one-body operator.

An analogous method can be followed in order to express two-body operators in second quantized form, resulting in the following expression:

$$\hat{V} = \frac{1}{2} \sum_{\alpha,\beta,\gamma,\delta} \hat{a}^\dagger_\alpha \hat{a}^\dagger_\beta (\alpha\beta | V | \gamma\delta) \hat{a}_\delta \hat{a}_\gamma \tag{K.15}$$

Appendix L

Cumulant constraints

This appendix will present an overview of the general rules which the cumulant values have to abide by in order to yield non-zero values. The list of these constraints is presented below:

1. Single operator expectation values are zero for non-zero momenta.
   $\left(\left\langle \hat{a}_p^\dagger \right\rangle_c = \langle \hat{a}_p \rangle_c = 0 \quad \text{for} \quad p \neq 0\right)$
2. The total momentum of the sum of the annihilation operators has to equal the total momentum of the sum of the creation operators.
   $\left(\left\langle \hat{a}_{k_1}^\dagger .. \hat{a}_{k_n}^\dagger \hat{a}_{q_1} .. \hat{a}_{q_m} \right\rangle_c = 0 \quad \text{for} \quad \sum_{i=1}^{n} k_i \neq \sum_{j=1}^{m} q_j\right)$
3. Cumulant terms with only creation or annihilation operators are only non-zero if the sum of the momenta is zero.
   $\left(\langle \hat{a}_{p_1}^\dagger \hat{a}_{p_2}^\dagger \rangle_c = \langle \hat{a}_{p_1}^\dagger \hat{a}_{p_2}^\dagger \rangle_c = 0 \quad \text{for} \quad p_1 \neq -p_2\right)$
4. Cumulant terms are only non-zero for non-zero momenta
   $\left(\left\langle \hat{a}_0^\dagger \hat{a}_0 \right\rangle_c = \langle \hat{a}_0 \hat{a}_0 \rangle_c = \left\langle \hat{a}_0^\dagger \hat{a}_0^\dagger \right\rangle_c = \left\langle \hat{a}_0 \hat{a}_0^\dagger \right\rangle_c = 0\right)$.

Appendix M

Intermediate steps of many-body equation of motion calculations

This appendix contains a documentation of the intermediate steps which are taken in the derivation of the many-body equations of motion as presented in section 10.6.

M.1 The molecular condensate

In order to derive equation 10.42 starting from expression 10.36, the following steps have been taken:

$$
\begin{aligned}
i\hbar\frac{\partial}{\partial t}\hat{b}_{\mathbf{k}} &= \sum_{\mathbf{q}} \left(t^m_{\mathbf{q}} + \nu\right) \left(\left[\hat{b}_{\mathbf{k}}, \hat{b}^\dagger_{\mathbf{q}}\right] \hat{b}_{\mathbf{q}} + \hat{b}^\dagger_{\mathbf{q}} \left[\hat{b}_{\mathbf{k}}, \hat{b}_{\mathbf{q}}\right]\right) \\
&\quad - \frac{\tilde{G}}{2} \sum_{\mathbf{p},\mathbf{q}} \theta(K - |\mathbf{q}|) \left([\hat{b}_{\mathbf{k}}, \hat{b}^\dagger_2] \hat{a}_{\mathbf{p}+\mathbf{q}} \hat{a}_{\mathbf{p}-\mathbf{q}} + \hat{b}^\dagger_{2\mathbf{p}} [\hat{b}_{\mathbf{k}}, \hat{a}_{\mathbf{p}+\mathbf{q}}] \hat{a}_{\mathbf{p}-\mathbf{q}} + \hat{b}^\dagger_{2\mathbf{p}} \hat{a}_{\mathbf{p}+\mathbf{q}} [\hat{b}_{\mathbf{k}}, \hat{a}_{\mathbf{p}-\mathbf{q}}]\right) \\
&\quad - \frac{\tilde{G}}{2} \sum_{\mathbf{p},\mathbf{q}} \theta(K - |\mathbf{q}|) \left([\hat{b}_{\mathbf{k}}, \hat{b}_{2\mathbf{p}}] \hat{a}^\dagger_{\mathbf{p}+\mathbf{q}} \hat{a}^\dagger_{\mathbf{p}-\mathbf{q}} + \hat{b}_{2\mathbf{p}} [\hat{b}_{\mathbf{k}}, \hat{a}^\dagger_{\mathbf{p}+\mathbf{q}}] \hat{a}^\dagger_{\mathbf{p}-\mathbf{q}} + \hat{b}_{2\mathbf{p}} \hat{a}^\dagger_{\mathbf{p}+\mathbf{q}} [\hat{b}_{\mathbf{k}}, \hat{a}^\dagger_{\mathbf{p}-\mathbf{q}}]\right) \qquad \text{(M.1)} \\
&= \sum_{\mathbf{q}} \left(t^m_{\mathbf{q}} + \nu\right) \delta_{\mathbf{k},\mathbf{q}} \hat{b}_{\mathbf{q}} - \frac{\tilde{G}}{2} \sum_{\mathbf{p},\mathbf{q}} \theta(K - |\mathbf{q}|) \delta_{\mathbf{k},2\mathbf{p}} \hat{a}_{\mathbf{p}+\mathbf{q}} \hat{a}_{\mathbf{p}-\mathbf{q}} \\
&= \left(t^m_k + \nu\right) \hat{b}_{\mathbf{k}} - \frac{\tilde{G}}{2} \sum_{\mathbf{q}} \theta\left(K - |\mathbf{q}|\right) \hat{a}_{\mathbf{q}} \hat{a}_{-\mathbf{q}} \qquad \text{(M.2)}
\end{aligned}
$$

Equation M.2 corresponds to equation 10.42.

M.2 The atomic condensate

In order to derive equation 10.46 starting from equation 10.45, the following intermediate steps were taken:

$$\begin{aligned}
i\hbar\frac{\partial}{\partial t}\hat{a}_{\mathbf{k}} &= \left[\hat{a}_{\mathbf{k}}, \hat{H}\right] \\
&= \sum_{\mathbf{p}} t^a_{\mathbf{p}} \left(\left[\hat{a}_{\mathbf{k}}, \hat{a}^\dagger_{\mathbf{p}}\right]\hat{a}_{\mathbf{p}} + \hat{a}^\dagger_{\mathbf{p}}\left[\hat{a}_{\mathbf{k}}, \hat{a}_{\mathbf{p}}\right]\right) + \sum_{\mathbf{q}} \left(t^m_{\mathbf{q}} + \nu\right)\left(\left[\hat{a}_{\mathbf{k}}, \hat{b}^\dagger_{\mathbf{q}}\right]\hat{b}_{\mathbf{q}} + \hat{b}^\dagger_{\mathbf{q}}\left[\hat{a}_{\mathbf{k}}, \hat{b}_{\mathbf{q}}\right]\right) \\
&\quad - \frac{\tilde{V}}{2}\sum_{\mathbf{p'pq}} \theta\left(K - \frac{|\mathbf{p}-\mathbf{p'}+2\mathbf{q}|}{2}\right)\theta\left(K - \frac{|\mathbf{p}-\mathbf{p'}|}{2}\right)\left([\hat{a}_{\mathbf{k}}, \hat{a}^\dagger_{\mathbf{p}+\mathbf{q}}]\hat{a}^\dagger_{\mathbf{p'}-\mathbf{q}}\hat{a}_{\mathbf{p}}\hat{a}_{\mathbf{p'}} + \hat{a}^\dagger_{\mathbf{p}+\mathbf{q}}[\hat{a}_{\mathbf{k}}, \hat{a}^\dagger_{\mathbf{p'}-\mathbf{q}}]\hat{a}_{\mathbf{p}}\hat{a}_{\mathbf{p'}}\right) \\
&\quad - \frac{\tilde{V}}{2}\sum_{\mathbf{p'pq}} \theta\left(K - \frac{|\mathbf{p}-\mathbf{p'}+2\mathbf{q}|}{2}\right)\theta\left(K - \frac{|\mathbf{p}-\mathbf{p'}|}{2}\right)\left(\hat{a}^\dagger_{\mathbf{p}+\mathbf{q}}\hat{a}^\dagger_{\mathbf{p'}-\mathbf{q}}\left([\hat{a}_{\mathbf{k}}, \hat{a}_{\mathbf{p}}]\hat{a}_{\mathbf{p'}} + \hat{a}_{\mathbf{p}}[\hat{a}_{\mathbf{k}}, \hat{a}_{\mathbf{p'}}]\right)\right) \\
&\quad - \frac{\tilde{G}}{2}\sum_{\mathbf{p},\mathbf{q}} \theta(K - |\mathbf{q}|)\left([\hat{a}_{\mathbf{k}}, \hat{b}_{2\mathbf{p}}]\hat{a}^\dagger_{\mathbf{p}+\mathbf{q}}\hat{a}^\dagger_{\mathbf{p}-\mathbf{q}} + \hat{b}_{2\mathbf{p}}[\hat{a}_{\mathbf{k}}, \hat{a}^\dagger_{\mathbf{p}+\mathbf{q}}]\hat{a}^\dagger_{\mathbf{p}-\mathbf{q}} + \hat{b}_{2\mathbf{p}}\hat{a}^\dagger_{\mathbf{p}+\mathbf{q}}[\hat{a}_{\mathbf{k}}, \hat{a}^\dagger_{\mathbf{p}-\mathbf{q}}]\right)
\end{aligned} \tag{M.3}$$

$$\begin{aligned}
=& t^a_k\hat{a}_{\mathbf{k}} - \frac{\tilde{V}}{2}\sum_{\mathbf{p'p}} \theta\left(K - \frac{|2\mathbf{k}-\mathbf{p'}-\mathbf{p}|}{2}\right)\theta\left(K - \frac{|\mathbf{p}-\mathbf{p'}|}{2}\right)\left(\hat{a}^\dagger_{\mathbf{p'}+\mathbf{p}-\mathbf{k}}\hat{a}_{\mathbf{p}}\hat{a}_{\mathbf{p'}} + \hat{a}^\dagger_{\mathbf{p}+\mathbf{p'}-\mathbf{k}}\hat{a}_{\mathbf{p}}\hat{a}_{\mathbf{p'}}\right) \\
&\quad - \frac{\tilde{G}}{2}\sum_{\mathbf{p},\mathbf{q}} \theta\left(K - |\mathbf{q}|\right)\left(\hat{b}_{2\mathbf{p}}\hat{a}^\dagger_{\mathbf{p}-\mathbf{q}}\delta_{\mathbf{k},\mathbf{p}+\mathbf{q}} + \hat{b}_{2\mathbf{p}}\hat{a}^\dagger_{\mathbf{p}+\mathbf{q}}\delta_{\mathbf{k},\mathbf{p}-\mathbf{q}}\right) \\
=& t^a_{\mathbf{k}}\hat{a}_{\mathbf{k}} - \tilde{V}\sum_{\mathbf{p'p}} \theta\left(K - \frac{|2\mathbf{k}-\mathbf{p'}-\mathbf{p}|}{2}\right)\theta\left(K - \frac{|\mathbf{p}-\mathbf{p'}|}{2}\right)\hat{a}^\dagger_{\mathbf{p}+\mathbf{p'}-\mathbf{k}}\hat{a}_{\mathbf{p}}\hat{a}_{\mathbf{p'}} \\
&\quad - \tilde{G}\sum_{\mathbf{p}} \theta\left(K - |\mathbf{q}|\right)\hat{b}_{2\mathbf{q}}\hat{a}^\dagger_{2\mathbf{q}}
\end{aligned} \tag{M.4}$$

Furthermore, in the calculation of the expectation value of equation 10.46, the following cumulant expansion has been used:

$$\begin{aligned}
\left\langle \hat{a}^\dagger_{\mathbf{p}+\mathbf{p'}}\hat{a}_{\mathbf{p}}\hat{a}_{\mathbf{p'}}\right\rangle =& \left\langle \hat{a}^\dagger_{\mathbf{p}+\mathbf{p'}}\hat{a}_{\mathbf{p'}}\right\rangle_c \langle\hat{a}_{\mathbf{p}}\rangle_c + \langle\hat{a}_{\mathbf{p'}}\rangle_c \left\langle \hat{a}^\dagger_{\mathbf{p}+\mathbf{p'}}\hat{a}_{\mathbf{p}}\right\rangle_c + \left\langle \hat{a}^\dagger_{\mathbf{p'}+\mathbf{p}}\right\rangle_c \langle\hat{a}_{\mathbf{p'}}\hat{a}_{\mathbf{p}}\rangle_c \\
&+ \left\langle \hat{a}^\dagger_{\mathbf{p}+\mathbf{p'}}\right\rangle_c \langle\hat{a}_{\mathbf{p'}}\rangle_c \langle\hat{a}_{\mathbf{p}}\rangle_c
\end{aligned} \tag{M.5}$$

Applying the cumulant expansion as presented in equation 10.15 to the previous expression, it is possible to reduce the expression for $\left\langle \hat{a}^\dagger_{\mathbf{p}+\mathbf{p'}}\hat{a}_{\mathbf{p}}\hat{a}_{\mathbf{p'}}\right\rangle$ to the following form:

$$\begin{aligned}
\left\langle \hat{a}^\dagger_{\mathbf{p}+\mathbf{p'}}\hat{a}_{\mathbf{p}}\hat{a}_{\mathbf{p'}}\right\rangle &= 2\overbrace{\left\langle \hat{a}^\dagger_{\mathbf{p}}\hat{a}_{\mathbf{p}}\right\rangle_c}^{\mathbf{p}\neq 0}\psi_a + \psi^*_a\overbrace{\langle\hat{a}_{\mathbf{p}}\hat{a}_{-\mathbf{p}}\rangle_c}^{\mathbf{p}\neq 0} + |\psi_a|^2\psi_a \\
&= 2\rho_{\mathbf{p}}\psi_a + \psi^*_a\kappa_{\mathbf{p}} + |\psi_a|^2\psi_a
\end{aligned} \tag{M.6}$$

The previous equation can be used in order to obtain the atomic condensate equation of motion as presented by equation10.47.

M.3 The normal density

The terms describing the kinetic energy, the interactions between two atoms and the interactions between two atoms and a molecule will be analysed separately in the following subsections in order

to reduce equation 10.48 to equation 10.49. Next, the expectation value of equation 10.49 will be calculated in order to obtain the normal density equation of motion as presented in equation 10.50.

M.3.1 Analysis of atomic kinetic energy term

In order to analyse the term in the Heisenberg equation of motion for the normal density which describes the atomic kinetic energy, the following commutation relation has to be applied:

$$[AB, CD] = A\,[B, C]\,D + [A, C]\,BD + C\,[A, D]\,B + CA\,[B, D] \tag{M.7}$$

Applying this relation results in the following expression for the atomic kinetic energy term of the Hamiltonian:

$$\sum_{\mathbf{p}} t^a_{\mathbf{p}} \left[\hat{a}^\dagger_{\mathbf{k}}\hat{a}_{\mathbf{k}}, \hat{a}^\dagger_{\mathbf{p}}\hat{a}_{\mathbf{p}}\right] = \sum_{\mathbf{p}} t^a_{\mathbf{p}} \left(\hat{a}^\dagger_{\mathbf{k}}\left[\hat{a}_{\mathbf{k}}, \hat{a}^\dagger_{\mathbf{p}}\right]\hat{a}_{\mathbf{p}} + \left[\hat{a}^\dagger_{\mathbf{k}}, \hat{a}^\dagger_{\mathbf{p}}\right]\hat{a}_{\mathbf{k}}\hat{a}_{\mathbf{p}} + \hat{a}^\dagger_{\mathbf{p}}\left[\hat{a}^\dagger_{\mathbf{k}}, \hat{a}_{\mathbf{p}}\right]\hat{a}_{\mathbf{k}} + \hat{a}^\dagger_{\mathbf{p}}\hat{a}^\dagger_{\mathbf{k}}\left[\hat{a}_{\mathbf{k}}, \hat{a}_{\mathbf{p}}\right]\right) \tag{M.8}$$

Implementing equations 10.37 through 10.39, the previous expression can be reduced to the following form:

$$\sum_{\mathbf{p}} t^a_{\mathbf{p}} \left[\hat{a}^\dagger_{\mathbf{k}}\hat{a}_{\mathbf{k}}, \hat{a}^\dagger_{\mathbf{p}}\hat{a}_{\mathbf{p}}\right] = \sum_{\mathbf{p}} t^a_{\mathbf{p}} \left(\hat{a}^\dagger_{\mathbf{k}}\delta_{\mathbf{k},\mathbf{p}}\hat{a}_{\mathbf{p}} - \hat{a}^\dagger_{\mathbf{p}}\delta_{\mathbf{k},\mathbf{p}}\hat{a}_{\mathbf{k}}\right) = t^a_{\mathbf{k}}\left(\hat{a}^\dagger_{\mathbf{k}}\hat{a}_{\mathbf{k}} - \hat{a}^\dagger_{\mathbf{k}}\hat{a}_{\mathbf{k}}\right) = 0 \tag{M.9}$$

Equation M.9 indicates that the kinetic energy term as presented in equation 10.48 will not contribute to the equation of motion of the normal density term $\rho_{\mathbf{k}}$.

M.3.2 Analysis of atom-atom interaction term

In order to analyse the term in the Hamiltonian which describes the two-body interactions between atoms, the following commutation relation has to be applied:

$$\begin{aligned}[AB, CDEF] =& A\left([B, C]D + C[B, D]\right)EF + \left([A, C]D + C[A, D]\right)BEF \\ &+ CDA\left([B, E]F + E[B, F]\right) + CD\left([A, E]F + E[A, F]\right)B\end{aligned} \tag{M.10}$$

Using the previously introduced commutation relation results in obtaining the following expression for the term describing the atom-atom interactions in the Heisenberg equation of motion for the normal density term:

$$\begin{aligned}&-\frac{\tilde{V}}{2}\sum_{\mathbf{p'pq}}\theta\left(K - \frac{|\mathbf{p}-\mathbf{p'}+2\mathbf{q}|}{2}\right)\theta\left(K - \frac{|\mathbf{p}-\mathbf{p'}|}{2}\right)\Big\{\hat{a}^\dagger_{\mathbf{k}}\left([\hat{a}_{\mathbf{k}}, \hat{a}^\dagger_{\mathbf{p+q}}]\hat{a}^\dagger_{\mathbf{p'-q}} + a^\dagger_{\mathbf{p+q}}[\hat{a}_{\mathbf{k}}, \hat{a}^\dagger_{\mathbf{p'-q}}]\right)\hat{a}_{\mathbf{p}}\hat{a}_{\mathbf{p'}} \\ &+ \left([\hat{a}^\dagger_{\mathbf{k}}, \hat{a}^\dagger_{\mathbf{p+q}}]\hat{a}_{\mathbf{p}} + \hat{a}^\dagger_{\mathbf{p+q}}[\hat{a}^\dagger_{\mathbf{k}}, \hat{a}^\dagger_{\mathbf{p'-q}}]\right)\hat{a}_{\mathbf{k}}\hat{a}_{\mathbf{p}}\hat{a}_{\mathbf{p'}} + \hat{a}^\dagger_{\mathbf{p+q}}\hat{a}^\dagger_{\mathbf{p'-q}}\left([\hat{a}^\dagger_{\mathbf{}}\hat{a}_{\mathbf{p}}]\hat{a}_{\mathbf{p'}} + \hat{a}_{\mathbf{p}}[\hat{a}^\dagger_{\mathbf{k}}, \hat{a}_{\mathbf{p'}}]\right)\hat{a}_{\mathbf{k}} \\ &+ \hat{a}^\dagger_{\mathbf{p+q}}\hat{a}^\dagger_{\mathbf{p'-q}}\hat{a}^\dagger_{\mathbf{k}}\left([\hat{a}_{\mathbf{k}}, \hat{a}_{\mathbf{p}}]\hat{a}_{\mathbf{p'}} + \hat{a}_{\mathbf{p}}[\hat{a}_{\mathbf{k}}, \hat{a}_{\mathbf{p'}}]\right)\Big\}\end{aligned} \tag{M.11}$$

Applying the relations as presented in expressions 10.37 through 10.39, equation M.11 can be rewritten as follows:

$$\begin{aligned}&-\frac{\tilde{V}}{2}\sum_{\mathbf{p'pq}}\theta\left(K - \frac{|\mathbf{p}-\mathbf{p'}+2\mathbf{q}|}{2}\right)\theta\left(K - \frac{|\mathbf{p}-\mathbf{p'}|}{2}\right)\Big\{\hat{a}^\dagger_{\mathbf{k}}\delta_{\mathbf{k},\mathbf{p+q}}\hat{a}^\dagger_{\mathbf{p'-q}}\hat{a}_{\mathbf{p}}\hat{a}_{\mathbf{p'}} + \hat{a}^\dagger_{\mathbf{k}}\delta_{\mathbf{k},\mathbf{p'-q}}\hat{a}^\dagger_{\mathbf{p+q}}\hat{a}_{\mathbf{p}}\hat{a}_{\mathbf{p'}} \\ &- \hat{a}^\dagger_{\mathbf{p+q}}\hat{a}^\dagger_{\mathbf{p'-q}}\delta_{\mathbf{k},\mathbf{p}}\hat{a}_{\mathbf{p'}}\hat{a}_{\mathbf{k}} - \hat{a}^\dagger_{\mathbf{p+q}}\hat{a}^\dagger_{\mathbf{p'-q}}\hat{a}_{\mathbf{p}}\delta_{\mathbf{k},\mathbf{p'}}\hat{a}_{\mathbf{k}}\Big\}\end{aligned} \tag{M.12}$$

Using the freedom to relabel the dummy indices which are summed over in the previous expression, the second and the fourth term in the curly brackets are subjected to the following transformation: $\mathbf{p}' \rightarrow \mathbf{p}$ and $\mathbf{q} \rightarrow -\mathbf{q}$. Having applied these relabelling transformations, the previous expression reduces to the following form:

$$-\tilde{V}\sum_{\mathbf{p}'\mathbf{p}\mathbf{q}}\theta\left(K-\frac{|\mathbf{p}-\mathbf{p}'+2\mathbf{q}|}{2}\right)\theta\left(K-\frac{|\mathbf{p}-\mathbf{p}'|}{2}\right)\left(\delta_{\mathbf{k},\mathbf{p}+\mathbf{q}}\hat{a}^{\dagger}_{\mathbf{k}}\hat{a}^{\dagger}_{\mathbf{p}'-\mathbf{q}}\hat{a}_{\mathbf{p}}\hat{a}_{\mathbf{p}'}-\delta_{\mathbf{k},\mathbf{p}}\hat{a}^{\dagger}_{\mathbf{p}+\mathbf{q}}\hat{a}^{\dagger}_{\mathbf{p}'-\mathbf{q}}\hat{a}_{\mathbf{p}'}\hat{a}_{\mathbf{k}}\right) \tag{M.13}$$

Equation M.13 presents the form of the atom-atom interaction term which will be used in the analysis of the equation of motion for the normal density term $\rho_{\mathbf{k}}$.

M.3.3 Analysis of the atoms-molecule interaction term

In order to analyse the term in the Heisenberg equation of motion for the normal density term which describes the atoms-molecule interactions, the following commutation relation has to be applied:

$$[AB,CDE]=(A[B,C]+[A,C]B)\,DE+C\,([A,D]E+D[A,E])\,B+CA\,([B,D]E+D[B,E]) \tag{M.14}$$

Using the commutation relation as presented in the previous equation, the interaction term can be expressed as follows:

$$\begin{aligned}
&-\frac{\tilde{G}}{2}\sum_{\mathbf{p},\mathbf{q}}\theta\left(K-|\mathbf{q}|\right)\Big\{\left(\hat{a}^{\dagger}_{\mathbf{k}}[\hat{a}_{\mathbf{k}},\hat{b}^{\dagger}_{2\mathbf{p}}]+[\hat{a}^{\dagger}_{\mathbf{k}},\hat{b}^{\dagger}_{2\mathbf{p}}]\hat{a}_{\mathbf{k}}\right)\hat{a}_{\mathbf{p}+\mathbf{q}}\hat{a}_{\mathbf{p}-\mathbf{q}}+\hat{b}^{\dagger}_{2\mathbf{p}}\left([\hat{a}^{\dagger}_{\mathbf{k}},\hat{a}_{\mathbf{p}+\mathbf{q}}]\hat{a}_{\mathbf{p}-\mathbf{q}}+\hat{a}_{\mathbf{p}+\mathbf{q}}[\hat{a}^{\dagger}_{\mathbf{k}},\hat{a}_{\mathbf{p}-\mathbf{q}}]\right)\hat{a}_{\mathbf{k}}\\
&+\hat{b}^{\dagger}_{2\mathbf{p}}\hat{a}^{\dagger}_{\mathbf{k}}\left([\hat{a}_{\mathbf{k}},\hat{a}_{\mathbf{p}+\mathbf{q}}]\hat{a}_{\mathbf{p}-\mathbf{q}}+\hat{a}_{\mathbf{p}+\mathbf{q}}[\hat{a}_{\mathbf{k}},\hat{a}_{\mathbf{p}-\mathbf{q}}]\right)+\left(\hat{a}^{\dagger}_{\mathbf{k}}[\hat{a}_{\mathbf{k}},\hat{b}_{2\mathbf{p}}]+[\hat{a}^{\dagger}_{\mathbf{k}},\hat{b}_{2\mathbf{p}}]\hat{a}_{\mathbf{k}}\right)\hat{a}^{\dagger}_{\mathbf{p}+\mathbf{q}}\hat{a}^{\dagger}_{\mathbf{p}-\mathbf{q}}\\
&+\hat{b}_{2\mathbf{p}}\left([\hat{a}^{\dagger}_{\mathbf{k}},\hat{a}^{\dagger}_{\mathbf{p}+\mathbf{q}}]\hat{a}^{\dagger}_{\mathbf{p}-\mathbf{q}}+\hat{a}^{\dagger}_{\mathbf{p}+\mathbf{q}}[\hat{a}^{\dagger}_{\mathbf{k}},\hat{a}^{\dagger}_{\mathbf{p}-\mathbf{q}}]\right)\hat{a}_{\mathbf{k}}+\hat{b}_{2\mathbf{p}}\hat{a}^{\dagger}_{\mathbf{k}}\left([\hat{a}_{\mathbf{k}},\hat{a}^{\dagger}_{\mathbf{p}+\mathbf{q}}]\hat{a}^{\dagger}_{\mathbf{p}-\mathbf{q}}+\hat{a}^{\dagger}_{\mathbf{p}+\mathbf{q}}[\hat{a}_{\mathbf{k}},\hat{a}^{\dagger}_{\mathbf{p}-\mathbf{q}}]\right)\Big\}
\end{aligned} \tag{M.15}$$

Applying equations 10.37 through 10.39 and using the knowledge that the molecular operator $\hat{b}$ acts on a different subspace from the atomic operator $\hat{a}$, the previous expression can be rewritten as follows:

$$-\frac{\tilde{G}}{2}\sum_{\mathbf{p},\mathbf{q}}\theta\left(K-|\mathbf{q}|\right)\Big\{\hat{b}_{2\mathbf{p}}\hat{a}^{\dagger}_{\mathbf{k}}\hat{a}^{\dagger}_{\mathbf{p}-\mathbf{q}}\delta_{\mathbf{k},\mathbf{p}+\mathbf{q}}+\hat{b}_{2\mathbf{p}}\hat{a}^{\dagger}_{\mathbf{k}}\hat{a}^{\dagger}_{\mathbf{p}+\mathbf{q}}\delta_{\mathbf{k},\mathbf{p}-\mathbf{q}}-\hat{b}^{\dagger}_{2\mathbf{p}}\hat{a}_{\mathbf{p}-\mathbf{q}}\hat{a}_{\mathbf{k}}\delta_{\mathbf{k},\mathbf{p}+\mathbf{q}}-\hat{b}^{\dagger}_{2\mathbf{p}}\hat{a}_{\mathbf{p}+\mathbf{q}}\hat{a}_{\mathbf{k}}\delta_{\mathbf{k},\mathbf{p}-\mathbf{q}}\Big\} \tag{M.16}$$

Using the freedom to re-index dummy variables, the second and the fourth term between the curly brackets in the previous expression are relabelled through replacing the factor $\mathbf{q}$ with $-\mathbf{q}$. This results in the following equivalent expression:

$$-\tilde{G}\sum_{\mathbf{p},\mathbf{q}}\theta\left(K-|\mathbf{q}|\right)\left(\hat{b}_{2\mathbf{p}}\hat{a}^{\dagger}_{\mathbf{k}}\hat{a}^{\dagger}_{\mathbf{p}-\mathbf{q}}\delta_{\mathbf{k},\mathbf{p}+\mathbf{q}}-\hat{b}^{\dagger}_{2\mathbf{p}}\hat{a}_{\mathbf{p}-\mathbf{q}}\hat{a}_{\mathbf{k}}\delta_{\mathbf{k},\mathbf{p}+\mathbf{q}}\right) \tag{M.17}$$

Equation M.17 represents the form of the term describing the interactions between two atoms and a molecule which will be used in the analysis of the equation of motion for the normal density term $\rho_{\mathbf{k}}$.

M.3.4 The equation of motion for $\hat{a}_k^\dagger \hat{a}_k$

Implementing equations M.9 , M.13 and M.17, expression 10.48 can be rewritten as follows:

$$
\begin{aligned}
&i\hbar\frac{\partial}{\partial t}\left(\hat{a}_{\mathbf{k}}^\dagger\hat{a}_{\mathbf{k}}\right) = \\
&-\tilde{V}\sum_{\mathbf{p'pq}}\theta\left(K-\frac{|\mathbf{p}-\mathbf{p'}+2\mathbf{q}|}{2}\right)\theta\left(K-\frac{|\mathbf{p}-\mathbf{p'}|}{2}\right)\left(\delta_{\mathbf{k},\mathbf{p+q}}\hat{a}_{\mathbf{k}}^\dagger\hat{a}_{\mathbf{p'-q}}^\dagger\hat{a}_{\mathbf{p}}\hat{a}_{\mathbf{p'}}-\delta_{\mathbf{k},\mathbf{p}}\hat{a}_{\mathbf{p+q}}^\dagger\hat{a}_{\mathbf{p'-q}}^\dagger\hat{a}_{\mathbf{p'}}\hat{a}_{\mathbf{k}}\right)\\
&-\tilde{G}\sum_{\mathbf{p,q}}\theta\left(K-|\mathbf{q}|\right)\left(\hat{b}_{2\mathbf{p}}\hat{a}_{\mathbf{k}}^\dagger\hat{a}_{\mathbf{p-q}}^\dagger\delta_{\mathbf{k},\mathbf{p+q}}-\hat{b}_{2\mathbf{p}}^\dagger\hat{a}_{\mathbf{p-q}}\hat{a}_{\mathbf{k}}\delta_{\mathbf{k},\mathbf{p+q}}\right)
\end{aligned}
\tag{M.18}
$$

Explicitly writing out the effect of the delta-functions which are present in the previous equation, results in the following equivalent expression:

$$
\begin{aligned}
i\hbar\frac{\partial}{\partial t}\left(\hat{a}_{\mathbf{k}}^\dagger\hat{a}_{\mathbf{k}}\right) = &-\tilde{V}\sum_{\mathbf{p'q}}\theta\left(K-\frac{|\mathbf{k}-\mathbf{p'}+\mathbf{q}|}{2}\right)\theta\left(K-\frac{|\mathbf{k}-\mathbf{p'}-\mathbf{q}|}{2}\right)\left(\hat{a}_{\mathbf{k}}^\dagger\hat{a}_{\mathbf{p'-q}}^\dagger\hat{a}_{\mathbf{k-q}}\hat{a}_{\mathbf{p'}}\right)\\
&+\tilde{V}\sum_{\mathbf{p'q}}\theta\left(K-\frac{|\mathbf{k}-\mathbf{p'}+2\mathbf{q}|}{2}\right)\theta\left(K-\frac{|\mathbf{k}-\mathbf{p'}|}{2}\right)\left(\hat{a}_{\mathbf{k+q}}^\dagger\hat{a}_{\mathbf{p'-q}}^\dagger\hat{a}_{\mathbf{p'}}\hat{a}_{\mathbf{k}}\right)\\
&-\tilde{G}\sum_{\mathbf{q}}\theta\left(K-|\mathbf{q}|\right)\left(\hat{b}_{2\mathbf{k-2q}}\hat{a}_{\mathbf{k}}^\dagger\hat{a}_{\mathbf{k-2q}}^\dagger-\hat{b}_{2\mathbf{k-2q}}^\dagger\hat{a}_{\mathbf{k-2q}}\hat{a}_{\mathbf{k}}\right)
\end{aligned}
\tag{M.19}
$$

M.3.5 Cumulant expansions of expectation values

In order to obtain the equation of motion for the normal density $\rho_{\mathbf{k}}$, equation 10.49 indicates that the following expectation values have to be computed:

1. $\left\langle \hat{a}_{\mathbf{k}}^\dagger\hat{a}_{\mathbf{p'-q}}^\dagger\hat{a}_{\mathbf{k-q}}\hat{a}_{\mathbf{p'}}\right\rangle$
2. $\left\langle \hat{a}_{\mathbf{k+q}}^\dagger\hat{a}_{\mathbf{p'-q}}^\dagger\hat{a}_{\mathbf{p'}}\hat{a}_{\mathbf{k}}\right\rangle$
3. $\left\langle \hat{b}_{2\mathbf{k-2q}}\hat{a}_{\mathbf{k}}^\dagger\hat{a}_{\mathbf{k-2q}}^\dagger\right\rangle$
4. $\left\langle \hat{b}_{2\mathbf{k-2q}}^\dagger\hat{a}_{\mathbf{k-2q}}\hat{a}_{\mathbf{k}}\right\rangle$

Similarly to the method as applied in the calculation of the equation of motion for atomic condensate wave-function, the expectation values will be analysed through the application of a cumulant expansion, which is truncated at the third order, meaning cumulants of three operators or more are neglected. Using this information, the expectation values as presented above can be rewritten as follows:

1. $\left\langle \hat{a}_{\mathbf{k}}^\dagger\hat{a}_{\mathbf{p'-q}}^\dagger\hat{a}_{\mathbf{k-q}}\hat{a}_{\mathbf{p'}}\right\rangle =$

$$
\begin{aligned}
&\left\langle \hat{a}_{\mathbf{k}}^\dagger\right\rangle_c\left\langle \hat{a}_{\mathbf{p'-q}}^\dagger\right\rangle_c\langle\hat{a}_{\mathbf{k-q}}\rangle_c\langle\hat{a}_{\mathbf{p'}}\rangle_c+\left\langle \hat{a}_{\mathbf{k}}^\dagger\hat{a}_{\mathbf{p'-q}}^\dagger\right\rangle_c\langle\hat{a}_{\mathbf{k-q}}\rangle_c\langle\hat{a}_{\mathbf{p'}}\rangle_c\\
&+\left\langle \hat{a}_{\mathbf{k}}^\dagger\hat{a}_{\mathbf{p'-q}}^\dagger\right\rangle_c\langle\hat{a}_{\mathbf{k-q}}\hat{a}_{\mathbf{p'}}\rangle_c+\left\langle \hat{a}_{\mathbf{k}}^\dagger\hat{a}_{\mathbf{k-q}}\right\rangle_c\left\langle \hat{a}_{\mathbf{p'-q}}^\dagger\right\rangle_c\langle\hat{a}_{\mathbf{p'}}\rangle_c\\
&+\left\langle \hat{a}_{\mathbf{k}}^\dagger\hat{a}_{\mathbf{k-q}}\right\rangle_c\left\langle \hat{a}_{\mathbf{p'-q}}^\dagger\hat{a}_{\mathbf{p'}}\right\rangle_c+\left\langle \hat{a}_{\mathbf{k}}^\dagger\hat{a}_{\mathbf{p'}}\right\rangle_c\left\langle \hat{a}_{\mathbf{p'-q}}^\dagger\right\rangle_c\langle\hat{a}_{\mathbf{k-q}}\rangle_c\\
&+\left\langle \hat{a}_{\mathbf{k}}^\dagger\hat{a}_{\mathbf{p'}}\right\rangle_c\left\langle \hat{a}_{\mathbf{p'-q}}^\dagger\hat{a}_{\mathbf{k-q}}\right\rangle_c+\left\langle \hat{a}_{\mathbf{p'-q}}^\dagger\hat{a}_{\mathbf{k-q}}\right\rangle_c\left\langle \hat{a}_{\mathbf{k}}^\dagger\right\rangle_c\langle\hat{a}_{\mathbf{p'}}\rangle_c\\
&+\left\langle \hat{a}_{\mathbf{p'-q}}^\dagger\hat{a}_{\mathbf{p'}}\right\rangle_c\left\langle \hat{a}_{\mathbf{k}}^\dagger\right\rangle_c\langle\hat{a}_{\mathbf{k-q}}\rangle_c+\langle\hat{a}_{\mathbf{k-q}}\hat{a}_{\mathbf{p'}}\rangle_c\left\langle \hat{a}_{\mathbf{p'-q}}^\dagger\right\rangle_c\left\langle \hat{a}_{\mathbf{k}}^\dagger\right\rangle_c
\end{aligned}
\tag{M.20}
$$

2. $\left\langle \hat{a}^\dagger_{\mathbf{k+q}} \hat{a}^\dagger_{\mathbf{p'-q}} \hat{a}_{\mathbf{p'}} \hat{a}_{\mathbf{k}} \right\rangle =$

$$\begin{aligned}
&\left\langle \hat{a}^\dagger_{\mathbf{k+q}} \right\rangle_c \left\langle \hat{a}^\dagger_{\mathbf{p'-q}} \right\rangle_c \langle \hat{a}_{\mathbf{k-q}} \rangle_c \langle \hat{a}_{\mathbf{p'}} \rangle_c + \left\langle \hat{a}^\dagger_{\mathbf{k+q}} \hat{a}^\dagger_{\mathbf{p'-q}} \right\rangle_c \langle \hat{a}_{\mathbf{k-q}} \rangle_c \langle \hat{a}_{\mathbf{p'}} \rangle_c \\
&+ \left\langle \hat{a}^\dagger_{\mathbf{k+q}} \hat{a}^\dagger_{\mathbf{p'-q}} \right\rangle_c \langle \hat{a}_{\mathbf{k-q}} \hat{a}_{\mathbf{p'}} \rangle_c + \left\langle \hat{a}^\dagger_{\mathbf{k+q}} \hat{a}_{\mathbf{k-q}} \right\rangle_c \left\langle \hat{a}^\dagger_{\mathbf{p'-q}} \right\rangle_c \langle \hat{a}_{\mathbf{p'}} \rangle_c \\
&+ \left\langle \hat{a}^\dagger_{\mathbf{k+q}} \hat{a}_{\mathbf{k-q}} \right\rangle_c \left\langle \hat{a}^\dagger_{\mathbf{p'-q}} \hat{a}_{\mathbf{p'}} \right\rangle_c + \left\langle \hat{a}^\dagger_{\mathbf{k+q}} \hat{a}_{\mathbf{p'}} \right\rangle_c \left\langle \hat{a}^\dagger_{\mathbf{p'-q}} \right\rangle_c \langle \hat{a}_{\mathbf{k-q}} \rangle_c \\
&+ \left\langle \hat{a}^\dagger_{\mathbf{k+q}} \hat{a}_{\mathbf{p'}} \right\rangle_c \left\langle \hat{a}^\dagger_{\mathbf{p'-q}} \hat{a}_{\mathbf{k-q}} \right\rangle_c + \left\langle \hat{a}^\dagger_{\mathbf{p'-q}} \hat{a}_{\mathbf{k-q}} \right\rangle_c \left\langle \hat{a}^\dagger_{\mathbf{k+q}} \right\rangle_c \langle \hat{a}_{\mathbf{p'}} \rangle_c \\
&+ \left\langle \hat{a}^\dagger_{\mathbf{p'-q}} \hat{a}_{\mathbf{p'}} \right\rangle_c \left\langle \hat{a}^\dagger_{\mathbf{k+q}} \right\rangle_c \langle \hat{a}_{\mathbf{k-q}} \rangle_c + \langle \hat{a}_{\mathbf{k-q}} \hat{a}_{\mathbf{p'}} \rangle_c \left\langle \hat{a}^\dagger_{\mathbf{p'-q}} \right\rangle_c \left\langle \hat{a}^\dagger_{\mathbf{k+q}} \right\rangle_c
\end{aligned} \tag{M.21}$$

3. $\left\langle \hat{b}_{\mathbf{2k-2q}} \hat{a}^\dagger_{\mathbf{k}} \hat{a}^\dagger_{\mathbf{k-2q}} \right\rangle =$

$$\begin{aligned}
&\left\langle \hat{b}_{\mathbf{2k-2q}} \right\rangle_c \left\langle \hat{a}^\dagger_{\mathbf{k}} \right\rangle_c \left\langle \hat{a}^\dagger_{\mathbf{k-2q}} \right\rangle_c + \left\langle \hat{b}_{\mathbf{2k-2q}} \hat{a}^\dagger_{\mathbf{k}} \right\rangle_c \left\langle \hat{a}^\dagger_{\mathbf{k-2q}} \right\rangle_c + \left\langle \hat{b}_{\mathbf{2k-2q}} \hat{a}^\dagger_{\mathbf{k-2q}} \right\rangle_c \left\langle \hat{a}^\dagger_{\mathbf{k}} \right\rangle_c \\
&+ \left\langle \hat{a}^\dagger_{\mathbf{k}} \hat{a}^\dagger_{\mathbf{k-2q}} \right\rangle_c \left\langle \hat{b}_{\mathbf{2k-2q}} \right\rangle_c
\end{aligned} \tag{M.22}$$

4. $\left\langle \hat{b}^\dagger_{\mathbf{2k-2q}} \hat{a}_{\mathbf{k-2q}} \hat{a}_{\mathbf{k}} \right\rangle =$

$$\begin{aligned}
&\left\langle \hat{b}^\dagger_{\mathbf{2k-2q}} \right\rangle_c \langle \hat{a}_{\mathbf{k}} \rangle_c \langle \hat{a}_{\mathbf{k-2q}} \rangle_c + \left\langle \hat{b}^\dagger_{\mathbf{2k-2q}} \hat{a}_{\mathbf{k}} \right\rangle_c \langle \hat{a}_{\mathbf{k-2q}} \rangle_c + \left\langle \hat{b}^\dagger_{\mathbf{2k-2q}} \hat{a}_{\mathbf{k-2q}} \right\rangle_c \langle \hat{a}_{\mathbf{k}} \rangle_c \\
&+ \langle \hat{a}_{\mathbf{k}} \hat{a}_{\mathbf{k-2q}} \rangle_c \left\langle \hat{b}^\dagger_{\mathbf{2k-2q}} \right\rangle_c
\end{aligned} \tag{M.23}$$

In order to simplify the previous expressions for the expectation values, the constraints which apply to the cumulant values as listed in appendix L have to be applied [1]. Applying these constraints, the previous expressions for the expectation values can be simplified to the following form:

$$\begin{aligned}
\left\langle \hat{a}^\dagger_{\mathbf{k}} \hat{a}^\dagger_{\mathbf{p'-q}} \hat{a}_{\mathbf{k-q}} \hat{a}_{\mathbf{p'}} \right\rangle &= \left\langle \hat{a}^\dagger_{\mathbf{k}} \hat{a}_{\mathbf{k}} \right\rangle_c \left\langle \hat{a}^\dagger_{\mathbf{p'}} \hat{a}_{\mathbf{p'}} \right\rangle_c \delta_{\mathbf{q},0} + \left\langle \hat{a}^\dagger_{\mathbf{k}} \hat{a}_{\mathbf{k}} \right\rangle_c \left\langle \hat{a}^\dagger_{\mathbf{k-q}} \hat{a}_{\mathbf{k-q}} \right\rangle_c \delta_{\mathbf{p'},\mathbf{k}} \\
&+ \left\langle \hat{a}^\dagger_{\mathbf{k}} \hat{a}_{\mathbf{k}} \right\rangle_c \left\langle \hat{a}^\dagger_0 \right\rangle_c \langle \hat{a}_0 \rangle_c \delta_{\mathbf{q},0} \delta_{\mathbf{p'},0} + \left\langle \hat{a}^\dagger_{\mathbf{k}} \hat{a}_{\mathbf{k}} \right\rangle_c \left\langle \hat{a}^\dagger_0 \right\rangle_c \langle \hat{a}_0 \rangle_c \delta_{\mathbf{q},\mathbf{k}} \delta_{\mathbf{p'},\mathbf{k}} \\
&+ \left\langle \hat{a}^\dagger_{\mathbf{k}} \hat{a}^\dagger_{-\mathbf{k}} \right\rangle_c \langle \hat{a}_{\mathbf{p'}} \hat{a}_{-\mathbf{p'}} \rangle_c \delta_{\mathbf{k},-(\mathbf{p'-q})} + \left\langle \hat{a}^\dagger_{\mathbf{k}} \hat{a}^\dagger_{-\mathbf{k}} \right\rangle_c \langle \hat{a}_0 \rangle_c \langle \hat{a}_0 \rangle_c \delta_{\mathbf{q},\mathbf{k}} \delta_{\mathbf{p'},\mathbf{k}}
\end{aligned} \tag{M.24}$$

$$\begin{aligned}
\left\langle \hat{a}^\dagger_{\mathbf{k+q}} \hat{a}^\dagger_{\mathbf{p'-q}} \hat{a}_{\mathbf{p'}} \hat{a}_{\mathbf{k}} \right\rangle &= \left\langle \hat{a}^\dagger_{\mathbf{k+q}} \hat{a}^\dagger_{-\mathbf{k-q}} \right\rangle_c \langle \hat{a}_{-\mathbf{k}} \hat{a}_{\mathbf{k}} \rangle_c \delta_{\mathbf{p'},\mathbf{k}} + \left\langle \hat{a}^\dagger_{\mathbf{k+q}} \hat{a}_{\mathbf{k+q}} \right\rangle_c \left\langle \hat{a}^\dagger_{\mathbf{k}} \hat{a}_{\mathbf{k}} \right\rangle_c \delta_{\mathbf{p'},\mathbf{k+q}} \\
&+ \left\langle \hat{a}^\dagger_{\mathbf{k}} \hat{a}_{\mathbf{k}} \right\rangle_c \left\langle \hat{a}^\dagger_{\mathbf{p'}} \hat{a}_{\mathbf{p'}} \right\rangle_c \delta_{\mathbf{q},0} + \left\langle \hat{a}^\dagger_{\mathbf{k}} \hat{a}_{\mathbf{k}} \right\rangle_c \left\langle \hat{a}^\dagger_0 \right\rangle_c \langle \hat{a}_0 \rangle_c \delta_{\mathbf{p'},0} \delta_{\mathbf{q},0} \\
&+ \left\langle \hat{a}^\dagger_0 \right\rangle_c \left\langle \hat{a}^\dagger_0 \right\rangle_c \langle \hat{a}_{-\mathbf{k}} \hat{a}_{\mathbf{k}} \rangle_c \delta_{\mathbf{q},-\mathbf{k}} \delta_{\mathbf{q},\mathbf{p'}} + \left\langle \hat{a}^\dagger_0 \right\rangle_c \langle \hat{a}_0 \rangle_c \left\langle \hat{a}^\dagger_{\mathbf{k}} \hat{a}_{\mathbf{k}} \right\rangle_c \delta_{\mathbf{q},-\mathbf{k}} \delta_{\mathbf{p'},0}
\end{aligned} \tag{M.25}$$

$$\left\langle \hat{b}_{\mathbf{2k-2q}} \hat{a}^\dagger_{\mathbf{k}} \hat{a}^\dagger_{\mathbf{k-2q}} \right\rangle = \left\langle \hat{b}_0 \right\rangle_c \left\langle \hat{a}^\dagger_{\mathbf{k}} \hat{a}^\dagger_{-\mathbf{k}} \right\rangle \delta_{\mathbf{q},\mathbf{k}} \tag{M.26}$$

$$\left\langle \hat{b}^\dagger_{\mathbf{2k-2q}} \hat{a}_{\mathbf{k-2q}} \hat{a}_{\mathbf{k}} \right\rangle = \left\langle \hat{b}^\dagger_0 \right\rangle_c \langle \hat{a}_{\mathbf{k}} \hat{a}_{-\mathbf{k}} \rangle \, \delta_{\mathbf{q},\mathbf{k}} \tag{M.27}$$

[1] Furthermore, the value of $\mathbf{k}$ is set to equal a non-zero value as we want to investigate the equation of motion for $\rho_{\mathbf{k}}$ with $\mathbf{k} \neq 0$

M.3.6 The equation of motion for the normal density term $\rho_{\mathbf{k}} = \left\langle \hat{a}_k^\dagger \hat{a}_k \right\rangle$

Using the previous four equations, implementing the third constraint as presented in appendix L and applying equation 10.49, the following equation of motion for the normal density term $\rho_{\mathbf{k}} = \left\langle \hat{a}_{\mathbf{k}}^\dagger \hat{a}_{\mathbf{k}} \right\rangle$ can be derived:

$$\begin{aligned} i\hbar \frac{\partial}{\partial t} \left\langle \hat{a}_{\mathbf{k}}^\dagger \hat{a}_{\mathbf{k}} \right\rangle =& \tilde{V} \sum_{\mathbf{p}'}{}' \theta\left(K - |\mathbf{k}|\right) \theta\left(K - |\mathbf{p}'|\right) \left[\left\langle \hat{a}_{\mathbf{k}}^\dagger \hat{a}_{-\mathbf{k}}^\dagger \right\rangle_c \left\langle \hat{a}_{\mathbf{p}'} \hat{a}_{-\mathbf{p}'} \right\rangle_c - \left\langle \hat{a}_{\mathbf{k}} \hat{a}_{-\mathbf{k}} \right\rangle_c \left\langle \hat{a}_{\mathbf{p}'}^\dagger \hat{a}_{-\mathbf{p}'}^\dagger \right\rangle_c \right] \\ &+ \tilde{V} \theta\left(K - |\mathbf{k}|\right) \left[\left\langle \hat{a}_{\mathbf{k}}^\dagger \hat{a}_{-\mathbf{k}}^\dagger \right\rangle_c \psi_a^2 - \left\langle \hat{a}_{\mathbf{k}} \hat{a}_{-\mathbf{k}} \right\rangle_c \psi_a^{*^2} \right] \\ &+ g\theta\left(K - |\mathbf{k}|\right) \left[\left\langle \hat{a}_{\mathbf{k}}^\dagger \hat{a}_{-\mathbf{k}}^\dagger \right\rangle_c \psi_m - \left\langle \hat{a}_{\mathbf{k}} \hat{a}_{-\mathbf{k}} \right\rangle_c \psi_m^* \right] \end{aligned} \tag{M.28}$$

The previous equation corresponds to the equation of motion for the normal density term as presented in expression 10.50.

M.4 The anomalous density

The terms describing the kinetic energy, the interactions between two atoms and the interaction between two atoms and a molecule will be analysed separately in the following subsections in order to reduce equation 10.51 to equation M.32. Next, the expectation value of this equation will be analysed in order to obtain the equation of motion of the anomalous density term as presented in equation **??**.

M.4.1 Analysis of the atomic kinetic energy term

In order to analyse the term representing the atomic kinetic energy as presented in equation 10.51, the commutation relation as presented in equation M.7 can be applied, resulting in the following outcome:

$$\begin{aligned} \sum_{\mathbf{p}} t_{\mathbf{p}}^a \left[\hat{a}_{-\mathbf{k}} \hat{a}_{\mathbf{k}}, \hat{a}_{\mathbf{p}}^\dagger \hat{a}_{\mathbf{p}} \right] =& \sum_{\mathbf{p}} t_{\mathbf{p}}^a \left\{ \hat{a}_{-\mathbf{k}} [\hat{a}_{\mathbf{k}}, \hat{a}_{\mathbf{p}}^\dagger] \hat{a}_{\mathbf{p}} + [\hat{a}_{-\mathbf{k}}, \hat{a}_{\mathbf{p}}^\dagger] \hat{a}_{\mathbf{k}} \hat{a}_{\mathbf{p}} + \hat{a}_{\mathbf{p}}^\dagger \hat{a}_{-\mathbf{k}} [\hat{a}_{\mathbf{k}}, \hat{a}_{\mathbf{p}}] + \hat{a}_{\mathbf{p}}^\dagger [\hat{a}_{-\mathbf{k}}, \hat{a}_{\mathbf{p}}] \hat{a}_{\mathbf{k}} \right\} \\ & \sum_{\mathbf{p}} t_{\mathbf{p}}^a \left\{ \hat{a}_{-\mathbf{k}} \hat{a}_{\mathbf{p}} \delta_{\mathbf{k},\mathbf{p}} + \hat{a}_{\mathbf{k}} \hat{a}_{\mathbf{p}} \delta_{-\mathbf{k},\mathbf{p}} \right\} \\ =& \left(t_{\mathbf{k}}^a + t_{-\mathbf{k}}^a \right) \hat{a}_{\mathbf{k}} \hat{a}_{-\mathbf{k}} \end{aligned} \tag{M.29}$$

Equation M.29 represents the form of the term describing the atomic kinetic energy which will be used in the analysis of the equation of motion for the anomalous density term $\kappa_{\mathbf{k}}$.

M.4.2 Analysis of the atom-atom interaction term

In order to analyse the term representing the atom-atom interactions as presented in equation 10.51, the commutation relation as presented in equation M.10 can be applied, resulting in the following

outcome:

$$-\frac{\tilde{V}}{2}\sum_{\mathbf{p'pq}}\theta\left(K-\frac{|\mathbf{p}-\mathbf{p'}+2\mathbf{q}|}{2}\right)\theta\left(K-\frac{|\mathbf{p}-\mathbf{p'}|}{2}\right)\left[\hat{a}_{-\mathbf{k}}\hat{a}_{\mathbf{k}},\hat{a}^{\dagger}_{\mathbf{p}+\mathbf{q}}\hat{a}^{\dagger}_{\mathbf{p'}-\mathbf{q}}\hat{a}_{\mathbf{p}}\hat{a}_{\mathbf{p'}}\right]$$

$$\begin{aligned}
&=-\frac{\tilde{V}}{2}\sum_{\mathbf{p'pq}}\theta\left(K-\frac{|\mathbf{p}-\mathbf{p'}+2\mathbf{q}|}{2}\right)\theta\left(K-\frac{|\mathbf{p}-\mathbf{p'}|}{2}\right)\Big\{\hat{a}_{-\mathbf{k}}\left([\hat{a}_{\mathbf{k}},\hat{a}^{\dagger}_{\mathbf{p}+\mathbf{q}}]\hat{a}^{\dagger}_{\mathbf{p'}-\mathbf{q}}+\hat{a}^{\dagger}_{\mathbf{p}+\mathbf{q}}[\hat{a}_{\mathbf{k}},\hat{a}^{\dagger}_{\mathbf{p'}-\mathbf{q}}]\right)\hat{a}_{\mathbf{p}}\hat{a}_{\mathbf{p'}}\\
&+\left([\hat{a}_{-\mathbf{k}},\hat{a}^{\dagger}_{\mathbf{p}+\mathbf{q}}]\hat{a}^{\dagger}_{\mathbf{p'}-\mathbf{q}}+\hat{a}^{\dagger}_{\mathbf{p}+\mathbf{q}}[\hat{a}_{-\mathbf{k}},\hat{a}^{\dagger}_{\mathbf{p'}-\mathbf{q}}]\right)\hat{a}_{\mathbf{k}}\hat{a}_{\mathbf{p}}\hat{a}_{\mathbf{p'}}+\hat{a}^{\dagger}_{\mathbf{p}+\mathbf{q}}\hat{a}^{\dagger}_{\mathbf{p'}-\mathbf{q}}\hat{a}_{-\mathbf{k}}\left([\hat{a}_{\mathbf{k}},\hat{a}_{\mathbf{p}}]\hat{a}_{\mathbf{p'}}\hat{a}_{\mathbf{p}}[\hat{a}_{\mathbf{k}},\hat{a}_{\mathbf{p'}}]\right)\\
&+\hat{a}^{\dagger}_{\mathbf{p}+\mathbf{q}}\hat{a}^{\dagger}_{\mathbf{p'}-\mathbf{q}}\left([\hat{a}_{-\mathbf{k}},\hat{a}_{\mathbf{p}}]\hat{a}_{\mathbf{p'}}+\hat{a}_{\mathbf{p}}[\hat{a}_{-\mathbf{k}},\hat{a}_{\mathbf{p'}}]\right)\Big\}
\end{aligned}$$

$$\begin{aligned}
&=-\frac{\tilde{V}}{2}\sum_{\mathbf{p'pq}}\theta\left(K-\frac{|\mathbf{p}-\mathbf{p'}+2\mathbf{q}|}{2}\right)\theta\left(K-\frac{|\mathbf{p}-\mathbf{p'}|}{2}\right)\Big\{\hat{a}_{-\mathbf{k}}\hat{a}^{\dagger}_{\mathbf{p'}-\mathbf{q}}\hat{a}_{\mathbf{p}}\hat{a}_{\mathbf{p'}}\delta_{\mathbf{k},\mathbf{p}+\mathbf{q}}\\
&+\hat{a}_{-\mathbf{k}}\hat{a}^{\dagger}_{\mathbf{p}+\mathbf{q}}\hat{a}_{\mathbf{p}}\hat{a}_{\mathbf{p'}}\delta_{\mathbf{k},\mathbf{p'}-\mathbf{q}}+\hat{a}^{\dagger}_{\mathbf{p'}-\mathbf{q}}\hat{a}_{\mathbf{k}}\hat{a}_{\mathbf{p}}\hat{a}_{\mathbf{p'}}\delta_{-\mathbf{k},\mathbf{p}+\mathbf{q}}+\hat{a}^{\dagger}_{\mathbf{p}+\mathbf{q}}\hat{a}_{\mathbf{k}}\hat{a}_{\mathbf{p}}\hat{a}_{\mathbf{p'}}\delta_{-\mathbf{k},\mathbf{p'}-\mathbf{q}}\Big\}
\end{aligned}$$

$$\begin{aligned}
&=-\tilde{V}\sum_{\mathbf{p'q}}\theta\left(K-\frac{|\mathbf{k}-\mathbf{p'}+\mathbf{q}|}{2}\right)\theta\left(K-\frac{|\mathbf{k}-\mathbf{q}-\mathbf{p'}|}{2}\right)\hat{a}_{-\mathbf{k}}\hat{a}^{\dagger}_{\mathbf{p'}-\mathbf{q}}\hat{a}_{\mathbf{k}-\mathbf{q}}\hat{a}_{\mathbf{p'}}\\
&-\tilde{V}\sum_{\mathbf{p'q}}\theta\left(K-\frac{|-\mathbf{k}-\mathbf{p'}+\mathbf{q}|}{2}\right)\theta\left(K-\frac{|-\mathbf{k}-\mathbf{q}-\mathbf{p'}|}{2}\right)\hat{a}^{\dagger}_{\mathbf{p'}-\mathbf{q}}\hat{a}_{\mathbf{k}}\hat{a}_{-\mathbf{k}-\mathbf{q}}\hat{a}_{\mathbf{p'}} \qquad \text{(M.30)}
\end{aligned}$$

Equation M.30 presents the form of the atom-atom interaction term which will be used in the analysis of the equation of motion for the anomalous density term $\kappa_{\mathbf{k}}$.

M.4.3 Analysis of the atoms-molecule interaction term

Similarly to the procedure followed in the analysis of the normal density term, the commutation relation as presented in equation M.14 has to be applied in order to analyse the interaction term between two atoms and a single molecule. Applying this commutation relation, results in the following outcome:

$$\begin{aligned}
&-\frac{\tilde{G}}{2}\sum_{\mathbf{p},\mathbf{q}}\theta\left(K-|\mathbf{q}|\right)\left([\hat{a}_{-\mathbf{k}}\hat{a}_{\mathbf{k}},\hat{b}^{\dagger}_{2\mathbf{p}}\hat{a}_{\mathbf{p}+\mathbf{q}}\hat{a}_{\mathbf{p}-\mathbf{q}}]+[\hat{a}_{-\mathbf{k}}\hat{a}_{\mathbf{k}},\hat{b}_{2\mathbf{p}}\hat{a}^{\dagger}_{\mathbf{p}+\mathbf{q}}\hat{a}^{\dagger}_{\mathbf{p}-\mathbf{q}}]\right)\\
&=-\frac{\tilde{G}}{2}\sum_{\mathbf{p},\mathbf{q}}\theta\left(K-|\mathbf{q}|\right)\Big\{\left(\hat{a}_{-\mathbf{k}}[\hat{a}_{\mathbf{k}},\hat{b}^{\dagger}_{2\mathbf{p}}]+[\hat{a}_{-\mathbf{k}},\hat{b}^{\dagger}_{2\mathbf{p}}]\hat{a}_{\mathbf{k}}\right)\hat{a}_{\mathbf{p}+\mathbf{q}}\hat{a}_{\mathbf{p}-\mathbf{q}}+\hat{b}^{\dagger}_{2\mathbf{p}}\left([\hat{a}_{-\mathbf{k}},\hat{a}_{\mathbf{p}+\mathbf{q}}]\hat{a}_{\mathbf{p}-\mathbf{q}}+\hat{a}_{\mathbf{p}+\mathbf{q}}[\hat{a}_{-\mathbf{k}},\hat{a}_{\mathbf{p}-\mathbf{q}}]\right)\hat{a}_{\mathbf{k}}\\
&+\hat{b}^{\dagger}_{2\mathbf{p}}\hat{a}_{-\mathbf{k}}\left([\hat{a}_{\mathbf{k}},\hat{a}_{\mathbf{p}+\mathbf{q}}]\hat{a}_{\mathbf{p}-\mathbf{q}}+\hat{a}_{\mathbf{p}+\mathbf{q}}[\hat{a}_{\mathbf{k}},\hat{a}_{\mathbf{p}-\mathbf{q}}]\right)+\left(\hat{a}_{-\mathbf{k}}[\hat{a}_{\mathbf{k}},\hat{b}_{2\mathbf{p}}]+[\hat{a}_{-\mathbf{k}},\hat{b}_{2\mathbf{p}}]\hat{a}_{\mathbf{k}}\right)\hat{a}^{\dagger}_{\mathbf{p}+\mathbf{q}}\hat{a}^{\dagger}_{\mathbf{p}-\mathbf{q}}\\
&+\hat{b}_{2\mathbf{p}}\left([\hat{a}_{-\mathbf{k}},\hat{a}^{\dagger}_{\mathbf{p}+\mathbf{q}}]\hat{a}^{\dagger}_{\mathbf{p}-\mathbf{q}}+\hat{a}^{\dagger}_{\mathbf{p}+\mathbf{q}}[\hat{a}_{-\mathbf{k}},\hat{a}^{\dagger}_{\mathbf{p}-\mathbf{q}}]\right)\hat{a}_{\mathbf{k}}+\hat{b}_{2\mathbf{p}}\hat{a}_{-\mathbf{k}}\left([\hat{a}_{\mathbf{k}},\hat{a}^{\dagger}_{\mathbf{p}+\mathbf{q}}]\hat{a}^{\dagger}_{\mathbf{p}-\mathbf{q}}+\hat{a}^{\dagger}_{\mathbf{p}+\mathbf{q}}[\hat{a}_{\mathbf{k}},\hat{a}^{\dagger}_{\mathbf{p}-\mathbf{q}}]\right)\Big\}\\
&=-\frac{\tilde{G}}{2}\sum_{\mathbf{p},\mathbf{q}}\theta\left(K-|\mathbf{q}|\right)\Big\{\hat{b}_{2\mathbf{p}}\hat{a}^{\dagger}_{\mathbf{p}-\mathbf{q}}\hat{a}_{\mathbf{k}}\delta_{-\mathbf{k},\mathbf{p}+\mathbf{q}}+\hat{b}_{2\mathbf{p}}\hat{a}^{\dagger}_{\mathbf{p}+\mathbf{q}}\hat{a}_{\mathbf{k}}\delta_{-\mathbf{k},\mathbf{p}-\mathbf{q}}+\hat{b}_{2\mathbf{p}}\hat{a}_{-\mathbf{k}}\hat{a}^{\dagger}_{\mathbf{p}-\mathbf{q}}\delta_{\mathbf{k},\mathbf{p}+\mathbf{q}}+\hat{b}_{2\mathbf{p}}\hat{a}_{-\mathbf{k}}\hat{a}^{\dagger}_{\mathbf{p}+\mathbf{q}}\delta_{\mathbf{k},\mathbf{p}-\mathbf{q}}\Big\}\\
&=-\tilde{G}\sum_{\mathbf{q}}\theta\left(K-|\mathbf{q}|\right)\hat{b}_{2\mathbf{q}-2\mathbf{k}}\hat{a}^{\dagger}_{2\mathbf{q}-\mathbf{k}}\hat{a}_{\mathbf{k}}+\tilde{G}\sum_{\mathbf{q}}\theta\left(K-|\mathbf{q}|\right)\hat{b}_{2\mathbf{k}+2\mathbf{q}}\hat{a}_{-\mathbf{k}}\hat{a}^{\dagger}_{\mathbf{k}+2\mathbf{q}} \qquad \text{(M.31)}
\end{aligned}$$

Equation M.31 presents the form of the atoms-molecule interaction term which will be used in the analysis of the equation of motion for the anomalous density term $\kappa_{\mathbf{k}}$.

M.4.4 The equation of motion for $\hat{a}_{-k}\hat{a}_k$

Implementing equations M.29, M.30 and M.31, equation 10.51 can be rewritten as follows:

$$\begin{aligned}
i\hbar\frac{\partial}{\partial t}\left(\hat{a}_{-\mathbf{k}}\hat{a}_{\mathbf{k}}\right) &= \left(t^a_{\mathbf{k}} + t^a_{-\mathbf{k}}\right)\hat{a}_{\mathbf{k}}\hat{a}_{-\mathbf{k}} \\
&- \tilde{V}\sum_{\mathbf{p'q}}\theta\left(K - \frac{|\mathbf{k}-\mathbf{p'}+\mathbf{q}|}{2}\right)\theta\left(K - \frac{|\mathbf{k}-\mathbf{q}-\mathbf{p'}|}{2}\right)\hat{a}_{-\mathbf{k}}\hat{a}^\dagger_{\mathbf{p'}-\mathbf{q}}\hat{a}_{\mathbf{k}-\mathbf{q}}\hat{a}_{\mathbf{p'}} \\
&- \tilde{V}\sum_{\mathbf{p'q}}\theta\left(K - \frac{|-\mathbf{k}-\mathbf{p'}+\mathbf{q}|}{2}\right)\theta\left(K - \frac{|-\mathbf{k}-\mathbf{q}-\mathbf{p'}|}{2}\right)\hat{a}^\dagger_{\mathbf{p'}-\mathbf{q}}\hat{a}_{\mathbf{k}}\hat{a}_{-\mathbf{k}-\mathbf{q}}\hat{a}_{\mathbf{p'}} \\
&- \tilde{G}\sum_{\mathbf{q}}\theta\left(K - |\mathbf{q}|\right)\hat{b}_{2\mathbf{q}-2\mathbf{k}}\hat{a}^\dagger_{2\mathbf{q}-\mathbf{k}}\hat{a}_{\mathbf{k}} + \tilde{G}\sum_{\mathbf{q}}\theta\left(K - |\mathbf{q}|\right)\hat{b}_{2\mathbf{k}+2\mathbf{q}}\hat{a}_{-\mathbf{k}}\hat{a}^\dagger_{\mathbf{k}+2\mathbf{q}}
\end{aligned} \tag{M.32}$$

Similarly to the approach which was used in order to obtain the equation of motion for the normal density term $\rho_{\mathbf{k}}$, a cumulant expansion method will be used in order to obtain the equation of motion for the anomalous density term $\kappa_{\mathbf{k}}$ starting from equation M.32. The cumulant expansion of the expectation values needed to compute the equation of motion for the anomalous density term will be presented in the following subsection.

M.4.5 Cumulant expansion of expectation values

In order to obtain the equation of motion for the anomalous density term $\kappa_{\mathbf{k}}$, equation M.32 indicates that the following expectation values have to be analysed:

1. $\left\langle \hat{a}_{-\mathbf{k}}\hat{a}^\dagger_{\mathbf{p'}-\mathbf{q}}\hat{a}_{\mathbf{k}-\mathbf{q}}\hat{a}_{\mathbf{p'}}\right\rangle_c$
2. $\left\langle \hat{a}^\dagger_{\mathbf{p'}-\mathbf{q}}\hat{a}_{\mathbf{k}}\hat{a}_{-\mathbf{k}-\mathbf{q}}\hat{a}_{\mathbf{p'}}\right\rangle_c$
3. $\left\langle \hat{b}_{2\mathbf{k}+2\mathbf{q}}\hat{a}_{-\mathbf{k}}\hat{a}^\dagger_{\mathbf{k}+2\mathbf{q}}\right\rangle_c$
4. $\left\langle \hat{b}_{2\mathbf{q}-2\mathbf{k}}\hat{a}^\dagger_{2\mathbf{q}-\mathbf{k}}\hat{a}_{\mathbf{k}}\right\rangle_c$

Analogous to the method followed in subsection M.3.5, keeping the constraints as presented in appendix L in mind, the following expressions for the four expectation values as presented above can be obtained:

$$\begin{aligned}
\left\langle \hat{a}_{-\mathbf{k}}\hat{a}^\dagger_{\mathbf{p'}-\mathbf{q}}\hat{a}_{\mathbf{k}-\mathbf{q}}\hat{a}_{\mathbf{p'}}\right\rangle_c &= \left\langle \hat{a}_{-\mathbf{k}}\hat{a}^\dagger_{-\mathbf{k}}\right\rangle_c\left\langle \hat{a}_{\mathbf{p'}}\hat{a}_{-\mathbf{p'}}\right\rangle_c\delta_{-\mathbf{k},\mathbf{p'}-\mathbf{q}} + \left\langle \hat{a}_{-\mathbf{k}}\hat{a}_{\mathbf{k}}\right\rangle_c\left\langle \hat{a}^\dagger_{\mathbf{p'}}\hat{a}_{\mathbf{p'}}\right\rangle_c\delta_{\mathbf{q},0} \\
&+ \left\langle \hat{a}_{\mathbf{k}}\hat{a}_{-\mathbf{k}}\right\rangle_c\left\langle \hat{a}^\dagger_{\mathbf{k}-\mathbf{q}}\hat{a}_{\mathbf{k}-\mathbf{q}}\right\rangle_c\delta_{\mathbf{p'},\mathbf{k}} + \left\langle \hat{a}_{-\mathbf{k}}\hat{a}^\dagger_{-\mathbf{k}}\right\rangle_c\left\langle \hat{a}_0\right\rangle_c\left\langle \hat{a}_0\right\rangle_c\delta_{\mathbf{k},\mathbf{q}}\delta_{\mathbf{p'},0} \\
&+ \left\langle \hat{a}_{\mathbf{k}}\hat{a}_{-\mathbf{k}}\right\rangle_c\left\langle \hat{a}^\dagger_0\right\rangle_c\left\langle \hat{a}_0\right\rangle_c\delta_{\mathbf{q},0}\delta_{\mathbf{p'},0} + \left\langle \hat{a}_{\mathbf{k}}\hat{a}_{-\mathbf{k}}\right\rangle_c\left\langle \hat{a}^\dagger_0\right\rangle_c\left\langle \hat{a}_0\right\rangle_c\delta_{\mathbf{k},\mathbf{p'}}\delta_{\mathbf{k},\mathbf{q}}
\end{aligned} \tag{M.33}$$

$$\begin{aligned}
\left\langle \hat{a}^\dagger_{\mathbf{p'}-\mathbf{q}}\hat{a}_{\mathbf{k}}\hat{a}_{-\mathbf{k}-\mathbf{q}}\hat{a}_{\mathbf{p'}}\right\rangle_c &= \left\langle \hat{a}^\dagger_{\mathbf{k}}\hat{a}_{\mathbf{k}}\right\rangle_c\left\langle \hat{a}_{\mathbf{p'}}\hat{a}_{-\mathbf{p'}}\right\rangle_c\delta_{\mathbf{k},\mathbf{p'}-\mathbf{q}} + \left\langle \hat{a}_{\mathbf{k}}\hat{a}_{-\mathbf{k}}\right\rangle_c\left\langle \hat{a}^\dagger_{\mathbf{p'}}\hat{a}_{\mathbf{p'}}\right\rangle_c\delta_{\mathbf{q},0} \\
&+ \left\langle \hat{a}_{\mathbf{k}}\hat{a}_{-\mathbf{k}}\right\rangle_c\left\langle \hat{a}^\dagger_{-\mathbf{k}-\mathbf{q}}\hat{a}_{-\mathbf{k}-\mathbf{q}}\right\rangle_c\delta_{\mathbf{p'},-\mathbf{k}} + \left\langle \hat{a}^\dagger_{\mathbf{k}}\hat{a}_{\mathbf{k}}\right\rangle_c\left\langle \hat{a}_0\right\rangle_c\left\langle \hat{a}_0\right\rangle_c\delta_{-\mathbf{k},\mathbf{q}}\delta_{\mathbf{p'},0} \\
&+ \left\langle \hat{a}_{\mathbf{k}}\hat{a}_{-\mathbf{k}}\right\rangle_c\left\langle \hat{a}^\dagger_0\right\rangle_c\left\langle \hat{a}_0\right\rangle_c\delta_{\mathbf{q},0}\delta_{\mathbf{p'},0} + \left\langle \hat{a}_{\mathbf{k}}\hat{a}_{-\mathbf{k}}\right\rangle_c\left\langle \hat{a}^\dagger_0\right\rangle_c\left\langle \hat{a}_0\right\rangle_c\delta_{-\mathbf{k},\mathbf{p'}}\delta_{-\mathbf{k},\mathbf{q}}
\end{aligned} \tag{M.34}$$

$$\left\langle \hat{b}_{2\mathbf{k}+2\mathbf{q}}\hat{a}_{-\mathbf{k}}\hat{a}^\dagger_{\mathbf{k}+2\mathbf{q}}\right\rangle_c = \left\langle \hat{b}_0\right\rangle_c\left\langle \hat{a}_{-\mathbf{k}}\hat{a}^\dagger_{-\mathbf{k}}\right\rangle_c\delta_{\mathbf{q},-\mathbf{k}} \tag{M.35}$$

$$\left\langle \hat{b}_{2\mathbf{q}-2\mathbf{k}}\hat{a}^\dagger_{2\mathbf{q}-\mathbf{k}}\hat{a}_{\mathbf{k}}\right\rangle_c = \left\langle \hat{b}_0\right\rangle_c\left\langle \hat{a}^\dagger_{\mathbf{k}}\hat{a}_{\mathbf{k}}\right\rangle_c\delta_{\mathbf{q},\mathbf{k}} \tag{M.36}$$

M.4.6 The equation of motion for the anomalous density term $\kappa_{\mathbf{k}} = \langle \hat{a}_k \hat{a}_{-k} \rangle$

Using the previous four equations, implementing the third constraint as presented in appendix L and applying equation M.32, the following equation of motion for the anomalous density term $\kappa_{\mathbf{k}} = \langle \hat{a}_{-\mathbf{k}} \hat{a}_{\mathbf{k}} \rangle$ can be obtained:

$$
\begin{aligned}
i\hbar \frac{\partial}{\partial t} \langle \hat{a}_{-\mathbf{k}} \hat{a}_{\mathbf{k}} \rangle &= 2t^a_{\mathbf{k}} \langle \hat{a}_{\mathbf{k}} \hat{a}_{-\mathbf{k}} \rangle_c \\
&\quad - 2\tilde{V} \sum_{\mathbf{p}'}{}' \left[\theta\left(K - \frac{|\mathbf{k} - \mathbf{p}'|}{2} \right) + \theta\left(K - \frac{|-\mathbf{k} - \mathbf{p}'|}{2} \right) \right] \langle \hat{a}_{-\mathbf{k}} \hat{a}_{\mathbf{k}} \rangle_c \left\langle \hat{a}^\dagger_{\mathbf{p}'} \hat{a}_{\mathbf{p}'} \right\rangle_c \\
&\quad - \tilde{V} \sum_{\mathbf{p}'}{}' \theta\left(K - |\mathbf{k}|\right) \theta\left(K - |\mathbf{p}'|\right) \left[\left\langle \hat{a}_{-\mathbf{k}} \hat{a}^\dagger_{-\mathbf{k}} \right\rangle_c + \left\langle \hat{a}^\dagger_{\mathbf{k}} \hat{a}_{\mathbf{k}} \right\rangle_c \right] \langle \hat{a}_{-\mathbf{p}'} \hat{a}_{\mathbf{p}'} \rangle_c \\
&\quad - 4\tilde{V} \theta\left(\mathbf{k} - \frac{|\mathbf{k}|}{2} \right) \langle \hat{a}_{\mathbf{k}} \hat{a}_{-\mathbf{k}} \rangle_c |\psi_a|^2 - \tilde{V} \theta\left(K - |\mathbf{k}|\right) \psi_a^2 \left[\left\langle \hat{a}_{-\mathbf{k}} \hat{a}^\dagger_{-\mathbf{k}} \right\rangle_c + \left\langle \hat{a}^\dagger_{\mathbf{k}} \hat{a}_{\mathbf{k}} \right\rangle_c \right] \\
&\quad - \tilde{G} \theta\left(K - |\mathbf{k}|\right) \psi_m \left[\left\langle \hat{a}^\dagger_{\mathbf{k}} \hat{a}_{\mathbf{k}} \right\rangle_c + \left\langle \hat{a}_{-\mathbf{k}} \hat{a}^\dagger_{-\mathbf{k}} \right\rangle_c \right] \\
&= 2t^a_{\mathbf{k}} \kappa_{\mathbf{k}} - 2\tilde{V} \sum_{\mathbf{p}'}{}' \left[\theta\left(K - \frac{|\mathbf{k} - \mathbf{p}'|}{2} \right) + \theta\left(K - \frac{|-\mathbf{k} - \mathbf{p}'|}{2} \right) \right] \kappa_{\mathbf{k}} \rho_{\mathbf{p}'} \\
&\quad - \tilde{V} \sum_{\mathbf{p}'}{}' \theta\left(K - |\mathbf{k}|\right) \theta\left(K - |\mathbf{p}'|\right) \left[1 + 2\rho_{\mathbf{k}} \right] \kappa_{\mathbf{p}'} \\
&\quad - 4\tilde{V} \theta\left(K - \frac{|\mathbf{k}|}{2} \right) \kappa_{\mathbf{k}} |\psi_a|^2 - \tilde{V} \theta\left(K - |\mathbf{k}|\right) \psi_a^2 \left[1 + 2\rho_{\mathbf{k}} \right] \\
&\quad - \tilde{G} \theta\left(K - |\mathbf{k}|\right) \psi_m \left[1 + 2\rho_{\mathbf{k}} \right]
\end{aligned}
\tag{M.37}
$$

The previous equation corresponds to the equation of motion for the anomalous density term as presented in expression 10.53.

Appendix N

Maximum simulation time many-body numerics

As presented in chapter 10, the many-body equations have been derived under the Bogoliubov- and coherent state approximation. In order to be able to use these approximations, the ground state needs to be macroscopically occupied. This means that the number of particles in the condensate N_0 approaches the total number of particles N. Therefore, we can make the following (approximative) identification:

$$N = N_0 \tag{N.1}$$

However, if the number of excited state particles starts to increase, the previous expression is no longer a valid representation of the total number of particles. Instead, the equation needs to be altered to the following form:

$$N = N_0 + \sum_{k}{}' \rho_{\mathbf{k}} + N_m, \tag{N.2}$$

where N_m represents the number of particles in the molecular condensate, which remains small compared to the number of excited state atoms $\sum_k{}' \rho_{\mathbf{k}}$ [1]. If the second term on the right hand side of the previous equation starts to increase to the point where one of the excited state modes $\rho_{\mathbf{k}}$ reaches a value of $\rho_{\mathbf{k}}/N \approx 1$, the Bogoliubov approximation and the coherent state approximation are no longer valid. This is a result of the fact that it is no longer possible to neglect the first order cumulant of the excited state population $\langle a \rangle_{c,\mathbf{k}\neq 0}$ as these values do no longer represent small fluctuations to the condensate expectation value $\langle \hat{a}_0 \rangle_c$.

In order to identify the point where the point $\rho_{\mathbf{k}\neq 0}/N \approx 1$ is reached and the used approximations break down, the excited state population $\rho_{\mathbf{k}}$ is plotted a function of the wave number k for various values of the time spent at unitarity. The results of this analysis for Potassium-39 and Rubidium-85 are presented in the following two sections.

[1] This can be seen in figure 13.2.

N.1 Maximum time at unitarity for Potassium-39

Using the simulation model as presented in section 13.2 and implementing the input parameter values for Potassium-39 as introduced in section 13.1, the following figure can be obtained:

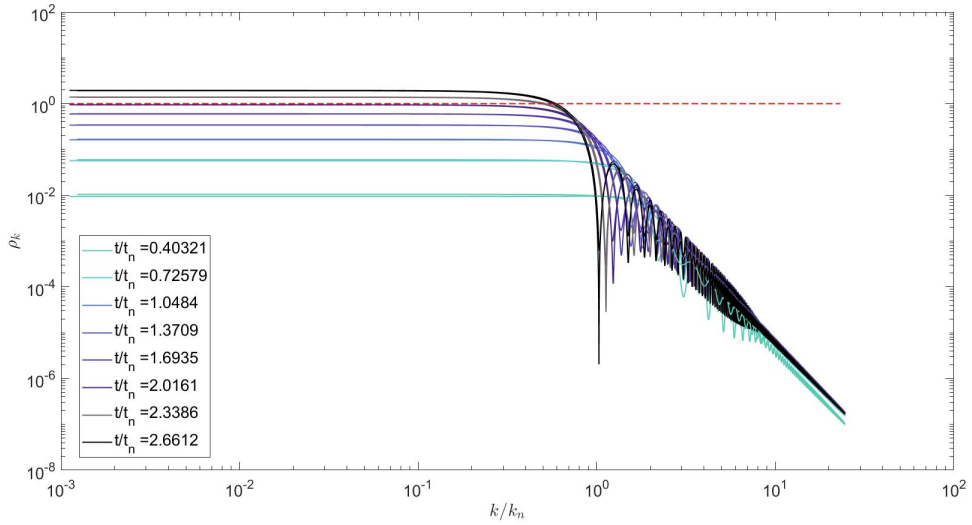

Figure N.1: Evolution of the excited state population $\rho_{\mathbf{k}}$ as a function of the relative momentum k. Different lines indicate different times spent at unitarity. The red line signifies the point where the derived many-body equations no longer properly represent the system.

As can be seen upon inspection of the previous figure, the validity of the simulated model breaks down after spending a time of $t \approx 2t_n$ at unitarity. Therefore, in order to obtain valid results, the simulations in this report will not surpass a time of $t = 2t_n$ after quenching the system to unitarity. The limiting value of the time $t = 2t_n$ is in correspondence with the results as presented in reference [75].

N.2 Maximum time at unitarity for Rubidium-85

Similarly to the procedure followed in the previous section, the following figure can be obtained for Rubidium-85:

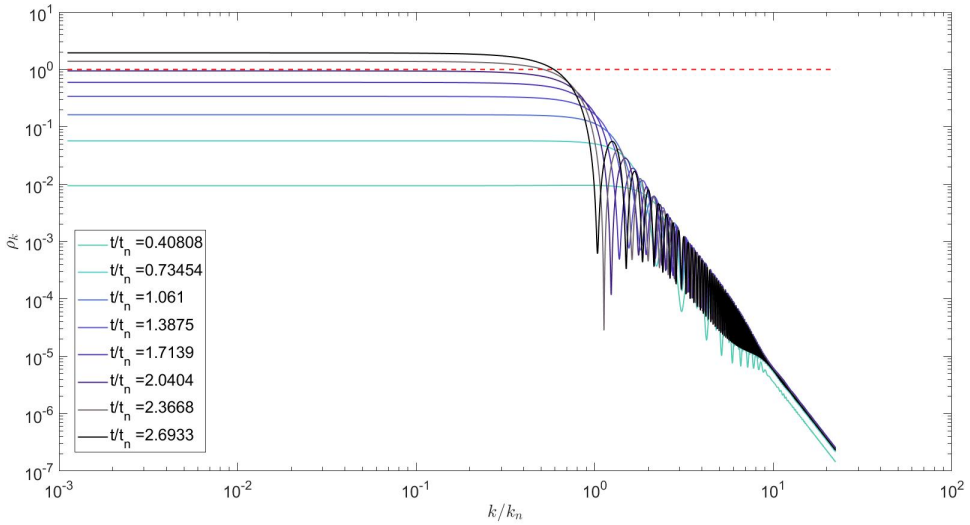

Figure N.2: Evolution of the excited state population $\rho_{\mathbf{k}}$ as a function of the relative momentum k. Different lines indicate different times spent at unitarity. The red line signifies the point where the derived many-body equations no longer properly represent the system.

Similar to the value obtained for the Potassium-39 analysis, the previous figure reveals the breakdown of the simulation model beyond values of $t \approx 2t_n$. This value is consistent with the value observed by V.E. Colussi [6].

Appendix O

Right versus Left Eigenvectors

Analogously to the defintion of the set of right eigenvectors as presented in matrix equation 12.3, the systems left eigenvectors can be expressed as follows:

$$E\begin{pmatrix}\langle\psi_P^L| & \langle\psi_Q^L|\end{pmatrix} = \begin{pmatrix}\langle\psi_P^L| & \langle\psi_Q^L|\end{pmatrix}\begin{pmatrix}\hat{h}_{hf}+\hat{B}\hat{V} & \hat{B}\hat{g}\\ \hat{g} & \hat{H}_{QQ}\end{pmatrix} \tag{O.1}$$

Similarly to the procedure followed in chapter 11, the open channel component is projected onto a momentum state $|k\rangle$ resulting in the following equation for the left eigenvector $\phi_a^L(k)$:

$$\begin{aligned}
E\phi_a^L(k) &= \langle\psi_P^L|(\hat{h}_{hf}+\hat{B}\hat{V}|k\rangle + \langle\psi_Q^L|\hat{g}|k\rangle\\
E\phi_a^L(k) &= 2h_{hf}(k)\phi_a^L + V\sum_{k'}\phi_a^L(k')\left(1+2\rho_{\mathbf{k}'}\right)\langle k'|g\rangle\langle g|k\rangle + \sum_{k'} g\langle\psi_Q^L|\phi_i\rangle\langle\phi_i|k'\rangle\langle k'|g\rangle\langle g|k\rangle\\
E\phi_a^L(k) &= 2h_{hf}(k)\phi_a^L + V\sum_{k'}\phi_a^L(k')\left(1+2\rho_{\mathbf{k}'}\right)\langle k'|g\rangle\langle g|k\rangle + \sum_{k'}\sqrt{2}\phi_m\frac{g(k')}{\sqrt{2}}\langle k'|g\rangle\langle g|k\rangle\\
E\phi_a^L(k) &= 2h_{hf}(k)\phi_a^L + V\sum_{k'}\phi_a^L(k')\left(1+2\rho_{\mathbf{k}'}\right)\langle k'|g\rangle\langle g|k\rangle + g\phi_m\langle g|k\rangle
\end{aligned} \tag{O.2}$$

Apart from the inspection of the open channel component, the closed channel component is projected onto a bound state $|\phi_i\rangle$, similarly to the procedure followed in chapter 11, resulting in the following outcome:

$$\begin{aligned}
E\langle\phi_Q^L|\phi_i\rangle &= \langle\psi_P^L|\hat{B}\hat{g}|\phi_i\rangle + \langle\psi_Q^L|\hat{H}_{QQ}|\phi_i\rangle\\
\sqrt{2}E\phi_m^L &= \sum_{k,k'} g(1+2\rho_{\mathbf{k}'})\langle\psi_P^L|k'\rangle\langle k'|g\rangle\langle g|k\rangle\langle k|\phi_i\rangle + \sqrt{2}\nu\phi_m^L\\
\sqrt{2}E\phi_m^L &= \sum_{k,k'}(1+2\rho_{\mathbf{k}'})\phi_a^L(k)\langle k'|g\rangle\langle g|k\rangle\frac{g(k)}{\sqrt{2}} + \sqrt{2}\nu\phi_m^L\\
E\phi_m^L &= \frac{g}{2}\sum_{k'}(1+2\rho_{\mathbf{k}'})\phi_a^L(k')\langle k'|g\rangle + \nu\phi_m^L
\end{aligned} \tag{O.3}$$

Having obtained the set of equations for the left eigenvectors, the following comparison between the left eigenvectors and the right eigenvectors can be made:

Eigenvector	**Open channel component**
Left	$2h_{hf}(k)\phi_a^L + V\sum_{k'}\phi_a^L(k')\left(1+2\rho_{\mathbf{k}'}\right)\langle k'\|g\rangle\langle g\|k\rangle + \frac{g}{2}\phi_m^L\langle g\|k\rangle$
Right	$2h_{hf}(k)\phi_a^R + \left(1+2\rho_{\mathbf{k}}\right)V\sum_{k'}\phi_a^R(k')\langle k'\|g\rangle\langle g\|k\rangle + g\phi_m^R\langle g\|k\rangle$

Eigenvector	**Closed channel component**
Left	$\frac{g}{2}\sum_{k'}(1+2\rho_{\mathbf{k}'})\phi_a^L(k')\langle k'\|g\rangle + \nu\phi_m^L$
Right	$\frac{g}{2}\sum_{k'}\phi_a^R(k')\langle g\|k'\rangle + \nu\phi_m^R$

Upon inspection of the previous tables, the following relations between the right and left eigenvectors can be obtained:

$$\phi_a^L(k) = \frac{\phi_a^R(k)}{1+2\rho_{\mathbf{k}}} \tag{O.4}$$

$$\phi_m^L = \phi_m^R \tag{O.5}$$

The molecular eigenvectors are identical, due to the fact that the interaction between molecules has been neglected in the system. Therefore, there is no Bose enhancement term in the equation of motion of the molecular condensate. Upon taking the vacuum limit of the previous two equations, the discrepancy between the left- and the right eigenvectors disappears. This is consistent with the symmetry of the many-body Hamiltonian 12.3 in the vacuum limit, as in this limit, the bose-enhancement operator $\hat{B}$ reduces to a value of unity.

Appendix P

Embedded dimer energy difference for various resonance widths

Presented below is the difference in the computed embedded dimer energies compared to the original Potassium-39 simulation for various values of R^* as a function of the time spent at unitarity. The figure below has been obtained using the same input data which has been used in order to obtain figure 13.5.

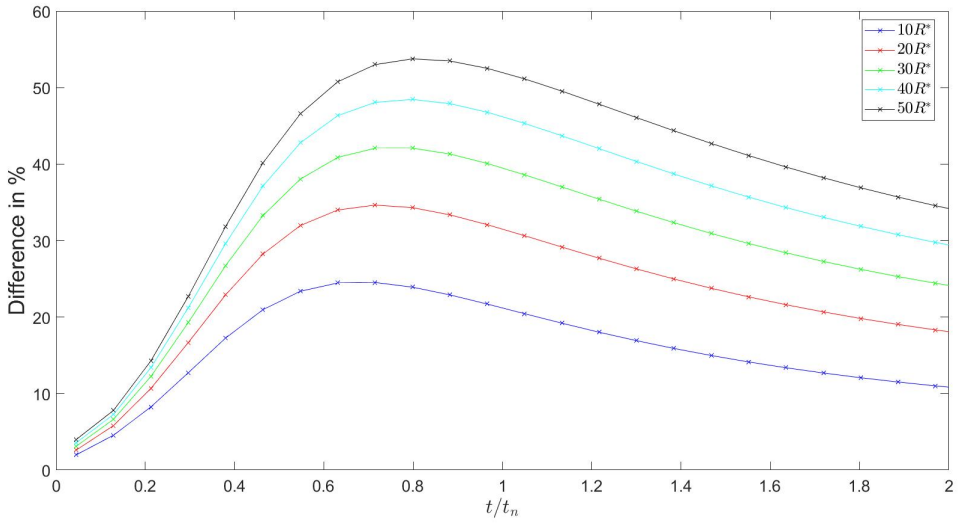

Figure P.1: Difference in percentage of embedded dimer energies for various values of the resonance strength parameterresonance strength parameter as a function of the time spent at unitarity.